

**DESIGN OF MULTIMODAL DEGRADABLE HYDROGELS FOR
CONTROLLED THERAPEUTIC DELIVERY**

by

Prathamesh Madhav Kharkar

A dissertation submitted to the Faculty of the University of Delaware in partial fulfillment of the requirements for the degree of Doctor of Philosophy in Materials Science and Engineering

Spring 2016

© 2016 P.M. Kharkar
All Rights Reserved

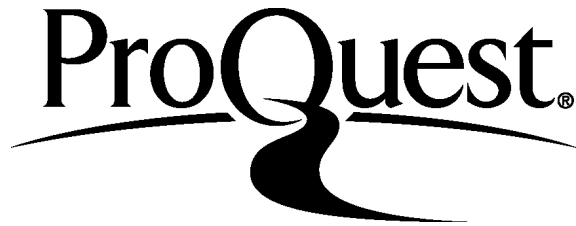
ProQuest Number: 10156481

All rights reserved

INFORMATION TO ALL USERS

The quality of this reproduction is dependent upon the quality of the copy submitted.

In the unlikely event that the author did not send a complete manuscript and there are missing pages, these will be noted. Also, if material had to be removed, a note will indicate the deletion.



ProQuest 10156481

Published by ProQuest LLC (2016). Copyright of the Dissertation is held by the Author.

All rights reserved.

This work is protected against unauthorized copying under Title 17, United States Code
Microform Edition © ProQuest LLC.

ProQuest LLC.
789 East Eisenhower Parkway
P.O. Box 1346
Ann Arbor, MI 48106 - 1346

**DESIGN OF MULTIMODAL DEGRADABLE HYDROGELS FOR
CONTROLLED THERAPEUTIC DELIVERY**

by

Prathamesh Madhav Kharkar

Approved:

Darrin J. Pochan, Ph.D.

Chair of the Department of Materials Science and Engineering

Approved:

Babatunde A. Ogunnaike, Ph.D.

Dean of the College of College of Engineering

Approved:

Ann L. Ardis, Ph.D.

Senior Vice Provost for Graduate and Professional Education

I certify that I have read this dissertation and that in my opinion it meets the academic and professional standard required by the University as a dissertation for the degree of Doctor of Philosophy.

Signed:

April M. Kloxin, Ph.D.
Professor in charge of dissertation

I certify that I have read this dissertation and that in my opinion it meets the academic and professional standard required by the University as a dissertation for the degree of Doctor of Philosophy.

Signed:

Kristi L. Kiick, Ph.D.
Professor in charge of dissertation

I certify that I have read this dissertation and that in my opinion it meets the academic and professional standard required by the University as a dissertation for the degree of Doctor of Philosophy.

Signed:

Darrin J. Pochan, Ph.D.
Member of dissertation committee

I certify that I have read this dissertation and that in my opinion it meets the academic and professional standard required by the University as a dissertation for the degree of Doctor of Philosophy.

Signed:

Xinqiao Jia, Ph.D.
Member of dissertation committee

ACKNOWLEDGMENTS

Many people have contributed significantly to the work contained in this thesis and I am forever grateful for their help and guidance. I would like to express my sincere gratitude to my PhD advisors, thesis committee members, lab members, collaborators, friends, and family for their help and support during this doctoral study.

TABLE OF CONTENTS

LIST OF TABLES	x
LIST OF FIGURES	xi
ABSTRACT	xxv

Chapter

1	DESIGNING DEGRADABLE HYDROGELS FOR THERAPEUTIC DELIVERY	1
1.1	Introduction	1
1.2	Design Criteria	3
1.2.1	Biocompatibility	4
1.2.2	Mild Crosslinking Reactions	6
1.2.3	Mechanical Properties	6
1.2.4	Controlled Degradation	7
1.2.5	Mass Transport	8
1.3	Drug Release Mechanism.....	9
1.4	Materials for Hydrogel Preparation.....	11
1.4.1	Hydrogels from Natural Polymers.....	13
1.4.1.1	Hyaluronic Acid	13
1.4.1.2	Chitosan.....	16
1.4.1.3	Heparin.....	17
1.4.1.4	Alginate.....	19
1.4.1.5	Other Natural Polymers.....	20
1.4.2	Hydrogels from Synthetic Polymers	20
1.4.2.1	Poly(ethylene glycol).....	20
1.4.2.2	Poly(vinyl alcohol).....	22
1.4.2.3	Other Synthetic Polymers.....	23
1.5	Material Functionalization for Hydrogel Formation.....	26

1.5.1	Chemically Crosslinked Hydrogels.....	27
1.5.1.1	Radical Polymerization	27
1.5.1.2	Click Chemistry.....	29
1.5.1.2.1	Azide-alkyne Cycloadditions	31
1.5.1.2.2	Diels-Alder Reactions	32
1.5.1.2.3	Thiol-ene Reactions.....	34
1.5.1.2.4	Oxime Reactions	36
1.5.1.2.5	Schiff Base Crosslinking Reactions	37
1.5.2	Physically Crosslinked Hydrogels.....	38
1.6	Engineering Degradation.....	41
1.6.1.1	Controlling Degradation Rates	42
1.6.1.2	Modes of Degradation	44
1.6.1.2.1	Enzymatic Degradation	47
1.6.1.2.2	Hydrolytic Degradation	49
1.6.1.2.3	Reversible Click Reactions.....	50
1.6.1.2.4	Light-mediated Degradation.....	51
1.7	Delivery of Bioactive Cargo in Hydrogels.....	53
1.7.1	Small Molecular Drug and Therapeutic Peptide Delivery	53
1.7.2	Therapeutic Protein Delivery	60
1.8	Dissertation Summary	68
2	DUALLY DEGRADABLE CLICK HYDROGELS FOR CONTROLLED DEGRADATION AND PROTEIN RELEASE.....	70
2.1	Introduction	70
2.2	Materials and Methods	73
2.2.1	Materials	73
2.2.2	Synthesis of Mercaptoacid-based PEG-thiols	74
2.2.3	Gelation Time and Rheology Characterization	76
2.2.4	Hydrogel Degradation Characterization.....	77
2.2.5	Volumetric Swelling and Mesh Size Calculations	77
2.2.6	Protein Release	78
2.2.7	Statistical Analysis	79
2.3	Results and Discussion.....	79

2.3.1	Hydrogel Compositions for Control of Degradation.....	79
2.3.2	Consistent Hydrogel Formation	81
2.3.3	Degradation in a Reducing Microenvironment	84
2.3.4	Influence of GSH Concentration on Hydrogel Degradation	88
2.3.5	Degradation Kinetics.....	91
2.3.6	Controlled Release of a Model Protein	93
2.4	Conclusion.....	97
2.5	Acknowledgements	98
2.6	Supporting Information	99
2.6.1	Degradation Kinetics.....	101
2.6.2	Cumulative Protein Release	105
2.6.3	Mesh Size Calculation.....	106
2.6.4	Effective Diffusion Coefficient Calculation.....	107
3	DESIGN OF THIOL- AND LIGHT-SENSITIVE DEGRADABLE HYDROGELS USING MICHAEL-TYPE ADDITION REACTIONS	108
3.1	Introduction	108
3.2	Design and Synthesis of Building Blocks with Different Degradable Functional Groups	112
3.3	Hydrogel Formation and Tunable Mechanical Properties	116
3.4	Degradation in Response to Exogenous and Endogenous Stimuli.....	119
3.5	Degradation Mediated Release of Model Cargo Nanobeads	125
3.6	Conclusion.....	128
3.7	Acknowledgement.....	129
3.8	Supporting Information	129
3.8.1	Materials	129
3.8.2	Organic Synthesis and Polymer Modification.....	130
3.8.2.1	Mercaptophenylacetic Acid-based Aryl Thiol-end Functionalized PEG (PEG-MPA).....	130
3.8.2.2	Ethyl 4-(4-acetyl-2-methoxyphenoxy)butanoate (II) .	131
3.8.2.3	Ethyl 4-(4-acetyl-2-methoxy-5- nitrophenoxy)butanoate (III)	132
3.8.2.4	Ethyl 4-(4-(1-hydroxyethyl)-2-methoxy-5- nitrophenoxy)butanoate (IV)	132
3.8.2.5	4-(4-(1-hydroxyethyl)-2-methoxy-5- nitrophenoxy)butanoic acid (V)	133
3.8.2.6	Hydroxyl End-functionalized Photodegradable PEG Intermediate (pII).....	133

3.8.2.7	Carboxyl End-functionalized Photodegradable PEG Intermediate (pIII)	134
3.8.2.8	Maleimide End-functionalized Photodegradable PEG (pIV).....	134
3.8.3	Hydrogel Formation and Rheological Characterization.....	135
3.8.4	Mesh Size Calculations	136
3.8.5	Absorbance of Photodegradable PEG Macromonomer	138
3.8.6	Degradation Monitored using Oscillatory Rheometry	139
3.8.7	Degradation Kinetics	141
3.8.8	Degradation Monitored Using Hydrogel Volume	143
3.8.9	Calculating Light Attenuation	145
3.8.10	Cargo Release.....	145
3.8.11	Statistical Analysis	147
4	DEGRADABLE HEPARIN-POLY(ETHYLENE GLYCOL) HYDROGELS FOR BIOLOGICS DELIVERY	148
4.1	Introduction	148
4.2	Materials and Methods	151
4.2.1	Materials	151
4.2.2	Synthesis of Aryl-thiol End Functionalized PEG.....	151
4.2.3	Synthesis of Maleimide Functionalized Heparin	152
4.2.4	Synthesis of Aryl-thiol End Functionalized Photodegradable PEG.....	153
4.2.5	Hydrogel Formation and Rheological Characterization.....	153
4.2.6	Hydrogel Degradation	154
4.2.7	Fibroblast Growth Factor (FGF-2) Release.....	155
4.2.8	Cell Culture	155
4.2.9	Serum Stripping.....	156
4.2.10	Proliferation Assay	156
4.2.11	Statistical Analysis	157
4.3	Results and Discussion.....	158
4.3.1	Synthesis of Monomers	158
4.3.2	Michael-type Crosslinking to Form Hydrogels.....	163
4.3.3	Stimuli-responsive Hydrogel Degradation	165
4.3.4	Growth Factor Release	171
4.3.5	Bioactivity of Released Growth Factor	173
4.4	Conclusion.....	177
4.5	Acknowledgement.....	177

4.6	Supporting Information	178
5	CONCLUSION AND FUTURE DIRECTIONS	181
	REFERENCES	185
Appendix		
	LICENSES FOR COPYRIGHTED MATERIAL	227

LIST OF TABLES

Table 1.1 Selecting materials for hydrogel preparation. Comparison of natural and synthetic polymers typically used for preparation of cell compatible hydrogels.	13
Table 1.2 Click reactions for hydrogel for hydrogel formation. Comparison of important click reactions typically used for formation of cell compatible hydrogels	30
Table 2.1: D2ER hydrogel degradation kinetics	103
Table 3.1 Degradation kinetics of multimodal degradable hydrogels	125
Table 3.2 Mechanical properties of hydrogels	135

LIST OF FIGURES

- Figure 1.1 Design considerations.** The design of hydrogels for orthogonal property control in cellular microenvironments is dictated by the biocompatibility, crosslinking in presence of cells or proteins, mechanical properties, degradability, mass transport properties, and target microenvironment. 4
- Figure 1.2 Therapeutic loading and release mechanisms from hydrogel-based delivery vehicles.** Hydrogels can be formed *in vitro* or *in vivo* for therapeutic delivery applications. Stoichiometric reaction between functional groups on multiarm poly(ethylene glycol) (PEG) macromers functionalized with specific alkenes or thiols, respectively, has been reported, producing thiol–ene hydrogels with nearly ideal network structure (shown here); these are of growing interest for delivery applications toward providing a well defined and predictable mesh size. However, macromolecules of varied length and functionality, both of synthetic and natural origin and decorated with various alkenes or thiols. Engineering of material structure and chemistry provide handles for controlling release profiles. **(A)** For example, therapeutics frequently have been encapsulated within the hydrogel network, where the cargo is entrapped if the average pore size (e.g., mesh size) of the hydrogel is smaller than the drug; degradation of the network, which increases mesh size, controls release. **(B)** Small molecule drugs or peptides, which can be difficult to entrap within hydrophilic highly-swollen hydrogels, have been tethered to the network and released upon tether cleavage (or complete network degradation); here, cleavage by a cell-secreted enzyme is depicted. **(C)** Ligands for a therapeutic of interest also have been incorporated within hydrogels for controlling retention and release by affinity binding; reversible binding of the ligand dictated by k_{on}/k_{off} determines the fraction of bound/free therapeutic, where diffusion of the free species (or matrix degradation) controls release. These therapeutic loading and release mechanisms can be used in different combinations than those depicted here and have been used in hydrogels for drug delivery applications. 11
- Figure 1.3 Range of natural and synthetic polymer building blocks.** Molecular structures of typical polymer repeat units used for preparation of cell

compatible hydrogels: (A) hyaluronic acid, (B) chitosan, (C) heparin, (D) alginate, (E) linear poly(ethylene glycol) (PEG), (F) four-arm PEG, (G) poly(ethylene glycol)-*b*-poly(propylene oxide)-*b*-poly(ethylene glycol) (PEG-PPO-PEG), (H) poly(lactic acid-*co*-glycolic acid)-*b*-poly(ethylene glycol)-*b*-poly(lactic acid-*co*-glycolic acid) (PLGA-PEG-PLGA), and (I) poly(vinyl alcohol). 15

Figure 1.4 Chemical functional groups for hydrogel formation. A wide range of functional groups is available for either hydrogel formation or modification post-polymerization. Functional group selection depends on several factors related to the application of interest, including the desired initiation mechanism, the specificity, and speed of the reaction, and the stability of the resulting bond under various solution conditions. 26

Figure 1.5 Degradation strategies. Chemically crosslinked hydrogels can be degraded via cleavage of (A) the polymer backbone, (B) crosslinker or (C) pendant group depending upon the chemistry used for hydrogel formation (choice of polymer, crosslinker, and crosslinking mechanism). 45

Figure 1.6 Selection of labile groups to control degradation rates. Chemically crosslinked hydrogels can be engineered to degrade at a preprogrammed, cell-dictated, or user-defined rate with varying degrees of spatiotemporal control 47

Figure 1.7 Controlled release of small molecular weight drugs and therapeutic peptides. (A) Dexamethasone (Dex) was covalently conjugated to the backbone of the hydrogel network using a thiol-functionalized MMP-sensitive peptide linker (KCGPQG↓IAGQCK). In the presence of cell-secreted MMP, the dexamethasone fragment (closed circle) was released and bioactive as demonstrated by enhanced alkaline phosphate (ALP) activity of encapsulated stem cells compared to the negative control (open circle, peptide sequence with substitution of *D*-isoleucine [QG(d-)I] making the linker MMP-insensitive and non-degradable). Adapted from Yang *et al.* ³⁰⁴ with permission from Elsevier publishing. Copyright (2012). (B) Furan-functionalized peptide (integrin-binding RGDS) was incorporated in thiol-maleimide hydrogels by a Diels-Alder reaction with excess maleimides. The release of peptide was controlled by a retro Diels-Alder reaction, which increases in rate with elevated temperature as demonstrated by the increasing fraction of peptide released at 37, 60, and 80 °C. Adapted from Koehler *et al.* ³⁰⁹ with permission from ACS

publishing. Copyright (2013). **(C)** Toward promoting angiogenesis, a vascular endothelial growth factor mimetic peptide (Qk) was tethered to a non-degradable thiol–ene hydrogel using an MMP-cleavage linker, and temporal control of Qk release was achieved *in vitro* and *in vivo* by changing the MMP2-susceptible peptide tether (FL = Qk-PES↓LRAG-C-G, SL = Qk-VPLS↓LYSG-C-G). * $p < 0.05$; &: $p < 0.01$, #: $p < 0.0001$ compared to buffer alone for each respective time point. Adapted from van Hove *et al.*³¹⁰ with permission from Wiley publishing. Copyright (2015). 58

Figure 1.8. Controlled release of therapeutic proteins **(A)** Proteins of various sizes were released from PEG-based hydrolytically-degradable thiol-vinyl sulfone hydrogels. Lysozyme, the smallest protein, was released in less than 24 hours, whereas Ig, the largest protein, was released upon complete gel degradation. Adapted from Zustiak and Leach³¹⁹ with permission from Wiley. **(B)** The growth factor VEGF was loaded into microspheres containing a peptide-based ligand derived from VEGF receptor 2 (VBP). VEGF was bound and released from the microspheres containing the VEGF receptor mimic, whereas microspheres containing a scrambled inert sequence exhibited a low level of release corresponding with random diffusion of VEGF into and out of the microspheres. Adapted from Impellitteri *et al.*³²¹ with permission from Elsevier. **(C)** Lysozyme was exposed to free radicals in conditions mimicking that of photoinitiated thiol–ene hydrogel polymerization. Higher radical concentrations would result from higher photoinitiator concentrations (10 mM), as compared to lower photoinitiator concentrations (0.1 mM), and from increased exposure time to light (plotted on x-axis). Increasing radical exposure decreased the bioactivity of lysozyme, indicating the importance of minimizing protein exposure to free radicals during gel formation. Bioactivity was increased upon introduction of reactive thiol and norbornene functional groups, supporting the protective effect of thiol–ene chemistry during hydrogel formation relative to acrylate homopolymerization (data not shown). Adapted from McCall and Anseth³²³ with permission from ACS Publishing. **(D)** FITC-labeled ovalbumin was released from thiol-functionalized ethoxylated polyol ester/PEG-diacrylate based hydrogels of different compositions. By changing the ratio of the macromers within the hydrogel, the rate of release and the overall release profiles were tuned over a wide range of timescales. Adapted from Langer and coworkers³²⁴ with permission from Wiley. 64

- Figure 2.1 **Functionalization of 4-arm PEG.** Schematic of the synthesis of thiol-functionalized PEG. (a: Toluene, PTSA, $\sim 110^{\circ}\text{C}$)..... 74
- Figure 2.2 **Hydrogel formation via click reaction.** Degradable PEG hydrogels were synthesized by Michael type addition reaction between thiol functionalized 4-arm PEG (PEG-4-SH) and maleimide functionalized linear PEG (PEG-2-MI). The thiol-functionalized macromers were synthesized by esterification of PEG using two different mercaptoacids (Scheme 1). The identity of the thiol was varied to tune the degradability of the hydrogels (**Control**: no degradable groups; **D1E**: one degradable group per crosslink (i.e., ester linkage); and **D2ER**: two degradable groups per crosslink (i.e., ester and reducing environment susceptible click = linkages). 81
- Figure 2.3 **Modulus evolution during hydrogel formation.** (A) Time-sweep measurements on an oscillatory rheometer were utilized to monitor hydrogel formation (**D2ER** hydrogel shown). Although formation of a gel is clearly observed, samples polymerize too quickly for measurement of the gel point with rheometry. To estimate the time to initial gelation, the tube-tilt method was utilized (inset images), where faster gelation was observed for **D2ER** (~ 20 s) as compared to **Control** (~ 40 s) and **D1E** (~ 35 s) hydrogels. For better visual assessment, Allura Red AC dye was added to the precursor solution (0.5 mg/ml) for tube-tilt measurements. (B) Irrespective of the identity of the thiol used for the hydrogel formation, the storage moduli for all three hydrogels post-gelation were statistically similar, indicating similar structural and mechanical properties. The data shown illustrate the mean ($n = 3$), with error bars showing the standard error. 82
- Figure 2.4 **Multimode hydrogel degradation.** Schematic of the click bond cleavage and thiol exchange reaction of thioether succinimide linkages under a glutathione (GSH) reducing microenvironment and by ester hydrolysis. The **D1E** hydrogels can only undergo degradation by ester hydrolysis. **D2ER** hydrogels can undergo degradation by ester hydrolysis and by thiol exchange reactions, owing to the presence of arylthiol-based thioether succinimide linkages. Owing to the lack of degradable functional groups, control hydrogels do not degrade in aqueous reducing microenvironments. The rate and extent of the click bond cleavage depends on the Michael donor reactivity and thiol pK_a 85
- Figure 2.5 **Hydrogel degradation in reducing microenvironment by cleavage of click bonds.** Degradation of the hydrogel in a thiol-rich reducing

microenvironment (10 mM GSH) was studied by monitoring **(A)** the storage modulus and **(B)** % volumetric swelling at discrete time points. All compositions exhibit an initial change in properties over 24 h as equilibrium swelling occurs. Due to the presence of the arylthiol-based thioether succinimide crosslinks, D2ER hydrogels exhibited rapid bulk degradation by click cleavage and thiol exchange reactions. The arrow indicates the time point when reverse gelation was observed. D1E and Control hydrogels were relatively stable during the experimental time frame due to the absence of GSH-sensitive crosslinks. The data shown illustrate the mean ($n = 6$), with error bars showing the standard error. 87

Figure 2.6 Influence of GSH concentration on hydrogel degradation. The effect of GSH concentration (0, 0.01, and 10 mM) on D2ER hydrogel degradation was studied by analyzing A) the decrease in the storage modulus, and B) the % volumetric swelling. The dependence of the decrease in moduli on GSH concentration indicates that the click cleavage and thiol exchange reaction is the dominant degradation mechanism for the D2ER hydrogels. The increase in volumetric swelling as a function of time before the reverse gel point confirms bulk degradation of hydrogels. The arrow indicates the time point when reverse gelation was observed for the 10 mM GSH condition. The data shown illustrate the mean ($n = 6$), with error bars showing the standard error. 89

Figure 2.7 Reducing environment-dependent degradation kinetics. **(A)** D2ER hydrogels exhibited first order degradation kinetics in a strong reducing microenvironment (10 mM GSH), whereas limited degradation is observed in a thiol-lacking microenvironment (0 mM GSH), owing to the slow rate of ester hydrolysis. Data point for 0 mM GSH at 2880 minutes was identified as a significant outlier (Grubb's test, $p < 0.05$) and hence omitted during regression analysis. **(B)** D2ER hydrogels followed second order reaction kinetics in a weak reducing microenvironment (0.01 mM GSH). Later time points were omitted during the regression analysis, due to large standard error, which can be attributed to experimental limitations when handling soft, more liquid-like degraded gels. As a whole, this study highlights the dependence of hydrogel degradation on GSH concentration. The data shown illustrate the mean ($n = 6$), with error bars showing the standard error. Black line indicates the linear fit using regression analysis. Blue and red lines indicate 95% confidence and prediction bands. 91

Figure 2.8 Protein release in a reducing microenvironment. (A) Release of a fluorescently-labeled model cargo protein, bovine serum albumin (BSA-488), was monitored using fluorometry. The arrow indicates the time point when reverse gelation (complete gel dissolution) was observed for the **D2ER** hydrogel. While some protein is initially released from all compositions upon gel equilibrium swelling, release from the **Control** and **D1E** hydrogels after this is minimal, owing to no or slow hydrolytic degradation, respectively, over the time course of the experiment. Substantial, statistical differences ($p < 0.05$ for time points after complete hydrogel degradation) in protein release are observed as the **D2ER** hydrogel rapidly degrades by the click cleavage and thiol-mediated exchange mechanism in addition to hydrolytic degradation. Differences in the release profile of BSA-488 from **D2ER**, **D1E**, and **Control** hydrogels highlight that the delivery of cargo molecules is controlled by hydrogel degradation. The data shown illustrate the mean ($n = 6$), with error bars showing the standard error. (B) SDS-PAGE analysis of released protein. Lane 1: protein ladder; Lane 2: free BSA-488; Lane 3: free BSA-488 suspended in reducing microenvironment (10 mM GSH/PBS) with hydrogel precursor solution; Lane 4, 5, 6: supernatant after protein release from **Control**, **D1E**, and **D2ER** hydrogel, respectively. No major differences in the locations of the free BSA and released BSA band are observed, confirming that the protein remained intact during encapsulation and release. Further, analysis of the band intensity by densitometry further supports the relative amounts of protein released from each gel composition as determined by fluorescence (**Control**: ~33%; **D1E**: ~36%; and **D2ER**: ~90%). 95

Figure 2.9 Functionalization of PEG. A) Reaction schematic for mercaptoacid esterification of PEG. ^1H NMR spectra for 4-arm PEG functionalized with B) 3-mercaptopropionic acid and C) 4-mercaptophenylacetic acid. The functionality was calculated using the integration area of the proton (labeled b) neighboring the ester linkage (functionality: MP = 92%, MPA = 90%). 99

Figure 2.10 Potential side reactions. Hydrogel precursor solutions can undergo (A) disulfide formation and (B) maleimide ring hydrolysis, which can impact the effective stoichiometry of available SH:MI groups for hydrogel formation. (C) Thioether succinimides can undergo ring hydrolysis, making the thioether succinimide linkage unavailable for thiol exchange reactions. However, the rate of ring opening is significantly slower as compared the thiol exchange (order of

magnitude different). In addition, ring hydrolysis does not result in breaking of crosslinks and subsequent hydrogel degradation. 100

Figure 2.11 Stability of Control and D1E hydrogels under non-reducing and reducing microenvironment. The effect of local microenvironment (0 and 10 mM GSH) on **(A) Control** and **(B) D1E** hydrogel was studied by monitoring the decrease in storage modulus at discrete time points. The initial decrease in moduli for **Control** and **D1E** in 0 mM GSH and 10 mM GSH can be attributed to equilibrium swelling. **D1E** hydrogels, compared to the **Control**, show a relatively larger decrease in moduli, confirming their slow degradation due to hydrolysis. Overall, these data indicate that there were no significant changes in moduli for reducing vs. non-reducing conditions for **Control** and **D1E** hydrogels at respective time points. The data shown illustrate the mean ($n = 6$), with error bars showing the standard error. 101

Figure 2.12 Regression analysis for Control hydrogel. Changes in mechanical properties were studied by monitoring storage moduli of **Control** hydrogels suspended under A) non-reducing and B) reducing conditions. The initial decrease in normalized moduli can be attributed to equilibrium swelling. The regression analysis was carried out for timepoints after ~24 hours. The linearity of data points with limited slope (slope with standard error for non-reducing condition = $6.64 \times 10^{-6} \pm 5.24 \times 10^{-6}$ and for reducing condition = $8.53 \times 10^{-6} \pm 6.06 \times 10^{-6}$) indicates that the **Control** hydrogels were stable under both conditions (i.e., no degradation). The data shown illustrate the mean ($n = 6$), with error bars showing the standard error. Initial time points till 1440 minutes were excluded in regression analysis due to initial swelling causing decrease in moduli. Black line indicates linear fit. Blue and red lines indicate 95% confidence and prediction bands. 104

Figure 2.13 Regression analysis for D1E hydrogel. Changes in mechanical properties were studied by monitoring storage moduli of **D1E** hydrogel suspended under A) non-reducing and B) reducing conditions. The initial decrease in normalized moduli can be attributed to equilibrium swelling. The regression analysis was carried out for timepoints after ~24 hours. The linearity of degradation curve with slope indicates that the **D1E** hydrogels showed degradation due to ester hydrolysis (slope with standard error for reducing condition = $4.09 \times 10^{-5} \pm 8.12 \times 10^{-6}$ and non-reducing condition = $2.58 \times 10^{-5} \pm 6.71 \times 10^{-6}$). Comparison of rate of degradation based on regression analysis and slope values for **D1E** and **Control** using Student's t-test indicated statistically significant differences highlighting role of ester

linkages in degradation of **DIE** hydrogels. The data shown illustrate the mean ($n = 6$), with error bars showing the standard error. Initial time points till 1440 minutes were excluded in regression analysis due to initial swelling causing decrease in moduli. Black line indicates linear fit. Blue and red lines indicate 95% confidence and prediction bands. Values for coefficient of determination for non-reducing and reducing conditions were found to be 0.86 and 0.79 respectively. 105

Figure 3.1 Multimodal degradable hydrogel formation and degradation. (A) Multimodal degradable hydrogels were formed by reacting maleimide and thiol end functionalized four-arm poly(ethylene glycol) macromolecular precursors using (B) a Michael-type addition reaction. (C) An *o*-nitrobenzyl ether based photodegradable functional group that undergoes irreversible cleavage upon irradiation with UV, visible, or two-photon IR light were incorporated into the backbone of the network, providing externally-triggered, rapid degradation of thick hydrogels by surface erosion. (D) Presence of arylthiol based thioether succinimide linkages allowed responsive, bulk degradation by retro Michael-type reaction, where thiol exchange with exogenous glutathione (GSH) present in a reducing microenvironment leads to irreversible cleavage. (E) Ester linkages were incorporated within both macromolecular precursors for bulk degradation of hydrogels by hydrolysis over longer timescales. 111

Figure 3.2 Synthetic route for preparing a macromolecular crosslinking agent functionalized with photodegradable maleimide. Reagents and conditions are as follows: *a*) DIPEA, HATU in DMF under Ar; *b*) Succinic anhydride, DMAP in DMF under Ar at 50 °C; and *c*) N-(2-aminoethyl) maleimide, TFA, DIPEA, HATU in DMF under Ar. 114

Figure 3.3 Rheological characterization of hydrogels (A) Hydrogel formation was monitored by dynamic time sweep measurements using an oscillatory rheometer, where all measurements were performed within the linear viscoelastic regime (representative data for 5 wt% hydrogel shown). (B) Polymer concentration was varied to achieve a range of moduli and corresponding mesh sizes (see Fig. S3.4), and the impact on crosslinking time was assessed. With increased polymer concentration, the crosslink density increased resulting in increased storage modulus and lowered gelation time. The data shown illustrate the mean ($n \geq 3$) with error bars showing the standard error. 118

Figure 3.4 Degradation of multimodal degradable hydrogels. Degradation of hydrogels in response to different stimuli was studied by monitoring

the storage modulus as a function of time. **(A)** Hydrogels exhibited a rapid decrease in the modulus in response to externally applied, low doses of light (10 mW/cm^2 at 365 nm , 30 sec pulse, closed symbols), and **(B)** complete degradation is observed after ~ 4.5 minutes of continuous exposure. The negative control hydrogels, which lack a photolabile group, show no significant change in modulus over time in response to the same light exposure (open symbols). The hydrogels also were responsive to low intensity visible light (10 mW/cm^2 at 400 to 500 nm , continuous irradiation, inset). **(C)** In a thiol-rich reducing microenvironment like that observed in tumors (ca. 10 mM GSH), a decrease in the modulus of the multimodal degradable hydrogel (closed symbols) was observed, indicating responsive degradation due to reversible click and thiol exchange reactions of aryl thiol based thioether succinimide linkages with GSH under reducing conditions. Complete degradation is observed in approximately 2 days. **(D)** In an aqueous microenvironment (phosphate buffer), the multimodal degradable hydrogel exhibited slower degradation due to hydrolysis of ester linkages with complete degradation in approximately 4 days (closed symbols). The negative control (no degradable groups), after initial swelling, was relatively stable during the experimental time frame (open symbols). The data shown illustrate the mean ($n \geq 3$) with error bars showing the standard error..... 122

Figure 3.5 Degradation-mediated release of cargo. Fluorescent nanobeads (diameter $\sim 100 \text{ nm}$) were encapsulated as a model cargo within the multimodal degradable hydrogel during formation. Since the diameter of cargo molecules is ~ 10 times larger than the mesh size, we hypothesized that the release would be controlled by degradation of the hydrogel. Hydrogel samples that were incubated in a reducing microenvironment (10 mM GSH) showed burst release of nanobeads upon hydrogel dissolution (e.g., reverse gelation). When irradiated with pulses of light (10 mW/cm^2 at 365 nm periodically for 10 minute intervals), the hydrogel exhibited surface erosion (Fig. S6), owing to light attenuation within these thick hydrogels (height $\sim 1.8 \text{ mm}$), and the release of nanobeads correlated with this light-mediated surface erosion of the hydrogels. The data shown illustrate the mean ($n \geq 3$) with error bars showing the standard error..... 126

Figure 3.6 Synthesis of PEG-MPA. 4-arm PEG was reacted with 4-mercaptophenylacetic acid (MPA) to yield aryl thiol end-functionalized PEG (a: Toluene, PTSA, $\sim 110^\circ\text{C}$)..... 130

- Figure 3.7 Synthetic route for preparing small molecule photolabile precursor.** Reagents and conditions are as follows: *a*) ethyl-4-bromobutyrate, potassium carbonate in DMF; *b*) nitric acid (69.3% w/w); *c*) sodium borohydride in ethanol at 38 °C; and *d*), potassium hydroxide in water:THF (1:1). Each chemical compound is numbered for its identification in experimental procedures. 131
- Figure 3.8 Rheological characterization under the linear viscoelastic regime.** (A) Frequency and (B) strain sweep data was used to determine the linear viscoelastic regime for subsequent rheological characterization (representative data for a 5 wt% gel sample shown). Representative dynamic time sweep measurements for (C) 2 wt% and (D) 3.5 wt% are shown..... 136
- Figure 3.9 Influence of polymer concentration on PEG hydrogel mesh size.** Estimated value of the mesh size decreased with increase in the polymer concentration, which can be attributed to the resulting increase in the crosslink density per the theory of rubber elasticity. The data shown illustrate the mean ($n \geq 3$) with error bars showing the standard error..... 137
- Figure 3.10 Molar absorptivity of the photolabile moiety on the photodegradable macromer.** The nitrobenzyl ether based photolabile moiety absorbs 365 nm UV light strongly compared to 400 to 500 nm visible light wavelengths. 138
- Figure 3.11 Structural differences between the (A) multimode degradable and (B) nondegradable negative control hydrogels.** Nondegradable hydrogels (negative control) were prepared by reacting maleimide end functionalized PEG with the alkyl thiol end-functionalized four-arm PEG. The resulting hydrogels thus did not contain any degradable or chemically susceptible functional groups within the backbone structure, as compared with multimode degradable hydrogels. 140
- Figure 3.12 Regression analysis for degradation of multimode degradable hydrogels.** Multimode degradable hydrogels exhibited first order degradation kinetics in response to the (A) aqueous microenvironment (PBS buffer) with a rate constant of $6.84 \times 10^{-4} \text{ min}^{-1}$, (B) reducing microenvironment (10 mM GSH) with a rate constant of $1.56 \times 10^{-3} \text{ min}^{-1}$, and applied light (10 mW/cm²) at (C) 365 nm with a rate constant of $3.03 \times 10^{-1} \text{ min}^{-1}$ and (D) 400 to 500 nm with a rate constant of $2.20 \times 10^{-2} \text{ min}^{-1}$. The data shown illustrate the mean ($n \geq 3$) with error bars showing the standard error. The black line indicates the linear fit using regression analysis. Blue (long dashes) and red

lines (short dashes) indicate 95% confidence and prediction intervals, respectively..... 143

Figure 3.13 Light-mediated surface erosion of hydrogels. (A) Schematic showing surface erosion of the hydrogel upon application of light (10 mW/cm² at 365 nm). (B) Multimode degradable hydrogels exhibit a continuous decrease in the normalized volume (closed circle symbols) compared with the negative control (open circle symbols), indicating surface erosion due to degradation of the hydrogel with continuous externally-applied light. The changes in volume are associated with (C) the changes in the height of hydrogel samples, where a continuous decrease in the height with limited changes in diameter are observed, suggesting surface erosion is the prominent mode of degradation of the multimode hydrogel samples upon irradiation (open symbols = negative control and closed symbols = multimode degradable gels; triangle = diameter; circles = height). The data shown illustrate the mean (n ≥ 3) with error bars showing the standard error. 144

Figure 3.14 Degradation-mediated release of cargo in response to hydrolytic degradation. Encapsulated nanobeads were released after 4 days (5760 minutes) upon complete dissolution of the hydrogel owing to bulk degradation by ester hydrolysis. The data shown illustrate the mean (n ≥ 5) with error bars showing the standard error. 147

Figure 4.1 Polymeric building blocks for hydrogel formation. Reducing microenvironment sensitive hydrogels were formed by reacting aryl-thiol end functionalized poly(ethylene glycol) macromolecular precursor (PEG-4-MPA) with maleimide-end functionalized PEG (PEG-2-MI) and maleimide functionalized low molecular heparin (Heparin-MI) via Michael-type reaction under aqueous microenvironment. Low molecular weight proteins such as growth factors, cytokine, and immunomodulatory agents can be incorporated within hydrogel network during the hydrogel formation. 159

Figure 4.2 Synthesis of aryl-thiol (PEG-4-MPA). Reagents and conditions are as follows: (a) NaI, H₂O₂ in EtOAc; (b) DIPEA, HATU in DMF under Ar; (c) TCEP in DI water followed by dialysis against acidified water. 160

Figure 4.3 Synthesis of maleimide-functionalized heparin (heparin-MI). (a) EDC, HOBt, AEM in AEM buffer 161

Figure 4.4 Synthesis of photodegradable aryl thiol. Reagents and conditions are as follows: (a) DIPEA, HATU in DMF under Ar; (b) 20% (v/v)

piperidine in DMF; (c) DIPEA, HATU in DMF under Ar; (d) TCEP in DI water followed by dialysis against acidified water. 162

Figure 4.5 Rheological characterization during hydrogel formation. Oscillatory rheology (A) time sweep and (B) frequency sweep data for 7.5 wt% PEG-heparin hydrogels. Crossover point between storage and loss modulus was not observed in time sweep measurement due to rapid hydrogel formation. The data shown illustrate the mean ($n \geq 3$) with error bars showing the standard error. 164

Figure 4.6 Hydrogel degradation pathways (A) Aryl-thiol based succinimide thioether linkage can exchange thiol in solution to form a relatively stable alkyl-thiol (i.e., cysteine) based succinimide thioether linkage resulting in hydrogel degradation. (B) *o*-nitrobenzyl ether moiety undergoes irreversible photoisomerization yielding respective ketone and amide under cytocompatible light doses. 165

Figure 4.7 Hydrogel degradation in reducing microenvironment. (A) Hydrogels underwent degradation via retro-Michael and subsequent thiol exchange reaction with similar rate constants ($p = 1$) when incubated with biologically relevant alkyl thiols such as glutathione (GSH), dithiothreitol (DTT), and cysteine (CYS). (B) The rate of degradation was found to be dependent on glutathione concentration. At high reducing microenvironment (10 mM) that is found in intracellular compartment and carcinoma tissues, the rate of degradation was an order of magnitude faster compared to lower reducing microenvironment concentration proving promising approach for reducing-microenvironment sensitive drug delivery carriers. (C) By varying ratio of alkyl to aryl thiol, the number of degradable crosslinked was varied between 33% to 100% degradable hydrogels, which in turned controlled the rate of bulk degradation. The degradation half-life was found to be ~ 2550 minutes and ~ 635 minutes for 66% and 100% degradable hydrogels respectively, where as 33% hydrogel did not undergo complete degradation. The data shown illustrate the mean ($n \geq 6$) with error bars showing the standard error. 169

Figure 4.8 Light-mediated degradation. (A) Photodegradable MPA-based hydrogels undergo degradation in response to externally applied light (365 nm, 10 mW/cm²). (B) Photodegradation kinetics were evaluated in a linear region between 6 to 16 minutes yielding photodegradation rate constant of 0.12 min⁻¹. The data shown illustrate the mean ($n \geq 3$) with error bars showing the standard error. 171

- Figure 4.9 Degradation mediated release of biologics.** Release of small molecular weight protein, FGF-2 (fibroblast growth factor) was monitored in vitro using immunochemical assay. The release of FGF-2 in reducing microenvironment (PBS buffer containing 10 mM GSH) that is found at carcinoma tissues was compared with non-reducing microenvironment (PBS buffer). Hydrogels show minimal burst release under the non-reducing microenvironment. In contrast, under the reducing microenvironment FGF-2 was released rapidly, with approximately ~40% of cargo getting released before complete erosion, and ~80-95% of cargo getting released once complete hydrogel degradation (i.e. reverse gelation) was observed. The data shown illustrate the mean ($n \geq 4$) with error bars showing the standard error. 173
- Figure 4.10 Bioactive FGF-2 promotes cell proliferation.** Bioactivity of released FGF-2 from PEG-heparin hydrogels was studied using adventitial fibroblast (AFs) proliferation assay since the FGF-2 is known to promote proliferation of AFs. Released FGF-2 from reducing microenvironment and non-reducing microenvironment was added to in vitro cell culture and proliferating cell nuclei were labeled with Alexa Fluor 555 (red) using EdU assay. Released FGF-2 demonstrated similar effect on cell proliferation compared to pristine FGF-2 added at a similar concentration (positive control) indicating that the protein bioactivity was not affected during encapsulation and subsequent release process. 174
- Figure 4.11 Quantification of cell proliferation.** FGF-2 released from reducing microenvironment had similar bioactivity as that of the positive control (i.e. pristine FGF-2). However, released FGF-2 from reducing microenvironment showed significant difference compared to negative control (i.e., no FGF-2) and non-reducing condition. The data shown illustrate the mean ($n \geq 4$) with error bars showing the standard error. * indicate p value < 0.05 176
- Figure 4.12 $^1\text{H-NMR}$ spectrum for four-arm aryl-thiol functionalized PEG MPA.** Functionality was calculated based on the integration of the aromatic proton (labeled as b and c), in this case, 88%. 178
- Figure 4.13 $^1\text{H-NMR}$ spectrum for maleimide functionalized heparin.** Functionality was calculated based on the integration of the maleimide ring protons, in this case, $f \sim 2.2$ 179
- Figure 4.14 $^1\text{H-NMR}$ spectrum for four-arm aryl-thiol functionalized photodegradable PEG MPA.** Functionality was calculated based on

the integration of the aromatic proton (labeled as u and v), in this case,
78%..... 180

ABSTRACT

Hydrogels are of growing interest for the delivery of therapeutics to specific sites in the body. For localized drug delivery, hydrophilic polymeric precursors often are laden with bioactive moieties and then directly injected to the site of interest for in situ gel formation. The release of physically entrapped cargo is dictated by Fickian diffusion, degradation of the drug carrier, or a combination of both. The goal of this work was to design and characterize degradable hydrogel formulations that are responsive to multiple biologically relevant stimuli for degradation-mediated delivery of cargo molecules such as therapeutic proteins, growth factors, and immunomodulatory agents.

We began by demonstrating the use of cleavable click linkages formed by Michael-type addition reactions in conjunction with hydrolytically cleavable functionalities for the degradation of injectable hydrogels by endogenous stimuli for controlled protein release. Specifically, the reaction between maleimides and thiols was utilized for hydrogel formation, where thiol selection dictates the degradability of the resulting linkage under thiol-rich reducing conditions. Relevant microenvironments where degradation would occur in vivo include those rich in glutathione (GSH), a tripeptide that is found at elevated concentrations in carcinoma tissues. Degradation of the hydrogels was monitored with rheometry and volumetric swelling measurements. Arylthiol-based thioether succinimide linkages underwent degradation via click cleavage and thiol exchange reaction in the presence of GSH and via ester hydrolysis, whereas alkylthiol-based thioether succinimide linkages only

undergo degradation by only ester hydrolysis. The resulting control over the degradation rate within a reducing microenvironment resulted in ~2.5 fold differences in the release profile of the model protein, a fluorescently-labeled bovine serum albumin, from dually degradable hydrogels compared to non-degradable hydrogels, where the thiol exchange reaction facilitated rapid and responsive protein release in the presence of GSH.

A photolabile o-nitrobenzyl ether group (o-NB) was subsequently incorporated within the PEG-based, gel-forming monomers to demonstrate cargo release triggered by exogenous stimuli for patient-specific therapies. Upon the application of cytocompatible doses of light, the photolabile o-NB linkage underwent irreversible cleavage yielding ketone and carboxylic acid-based cleavage products. Hydrogel degradation kinetics was characterized in response to externally applied cytocompatible light or GSH in aqueous microenvironments. By incorporating a photodegradable o-nitrobenzyl ether group, a thiol-sensitive succinimide thioether linkage, and ester linkages within the hydrogels, we demonstrated unique control over degradation via surface erosion or bulk degradation mechanisms, respectively, with degradation rate constants ranging from $\sim 10^{-1} \text{ min}^{-1}$ to $\sim 10^{-4} \text{ min}^{-1}$. As a proof of concept, the controlled release of nanobeads from the hydrogel was demonstrated in a preprogrammed and stimuli-responsive fashion.

The multimodal degradable hydrogels were then investigated for the local controlled release of small molecular weight proteins, which are of interest for regulating various cellular functions and fates in vivo. Low molecular weight heparin, a highly sulfated polysaccharide was incorporated within the hydrogel network by Michael-type reaction due to its affinity with biologics such as growth factors and

immunomodulatory proteins. Incorporation of reduction-sensitive linkages resulted in ~2.3 fold differences in the release profile of fibroblast growth factor-2 (FGF-2) in the presence of GSH compared to non-reducing microenvironment. Bioactivity of released FGF-2 was comparable to pristine FGF-2, indicating the ability of the hydrogel to retain bioactivity of cargo molecules during encapsulation and release. Further, preliminary in vivo studies demonstrated control over hydrogel degradation by varying % degradable contents. Collectively, this research developed injectable hydrogels that are responsive to various endogenous and exogenous stimuli, establishing a platform for stimuli-responsive drug delivery carriers.

Chapter 1

DESIGNING DEGRADABLE HYDROGELS FOR THERAPEUTIC DELIVERY

1.1 Introduction

Significant advancements have been made in the last decade to develop new therapeutics with the potential to improve the treatment of a variety of diseases, from small molecular weight hydrophilic and hydrophobic drugs to larger peptides and biologics (e.g., therapeutic proteins and antibodies). In particular, biologics have been a major area of growth for the pharmaceutical industry with the worldwide sales of biologics exceeding \$92 billion in 2009.¹ Despite this increasing demand, costs of drug development and production remain high.²⁻³ Delivery of therapeutics at a controlled rate to a targeted site affords opportunities to both improve treatment efficacy and reduce total treatment costs. However, successful development of drug carriers with appropriate therapeutic retention and release characteristics for clinical use remains a challenge and an area of active research. Tremendous progress has been made in the design of novel drug carriers, including liposomes,⁴⁻⁵ nanoparticles,⁶⁻⁸ polymersomes,⁹⁻¹¹ dendrimers,¹²⁻¹³ microparticles,¹⁴⁻¹⁵ and hydrogels,¹⁶⁻¹⁷ with improved efficacy, prolonged drug action *in vivo*, reduced drug toxicity, and decreased drug-associated costs. Among these drug carriers, hydrogels have emerged as promising delivery vehicles, especially for biologics, owing to their high cargo loading efficiency and their ability to retain cargo bioactivity.¹⁸

Hydrogels, or hydrophilic polymer networks that imbibe and retain large amounts of water, have been fabricated for controlled release applications using a range of natural and synthetic polymers as their base building blocks. Due to their inherent biocompatibility and bioactivity, natural polymers, such as hyaluronic acid,¹⁹ chitosan,²⁰ heparin,²¹ silk,²² and alginate,²³ often provide synergistic interactions with cargo molecules and with cells *in vivo*. On the other hand, synthetic biocompatible polymers, including poly(ethylene glycol) (PEG) and poly(vinyl alcohol) (PVA), generally offer greater flexibility for chemical modification, improved tunability over mechanical properties, facile incorporation of degradable functional groups, and limited batch-to-batch variation.¹⁸ Control over the formation of these hydrogels is essential for delivery applications since the connectivity (e.g., crosslink density) and mechanical properties of the network dictate mass transport and therapeutic release. For example, increasing the crosslink density decreases the distance between crosslinks in the hydrogel (i.e., mesh size), often resulting in a decreased initial burst of cargo.²⁴⁻²⁵

Hydrogels have been formed by *i*) physical crosslinking (i.e., non-covalent interactions), including ionic, electrostatic, or hydrophobic interactions between the polymeric macromers, or *ii*) chemical crosslinking by reactive functional groups to form covalent linkages.²⁶ Physically crosslinked hydrogels offer advantages for injectable formulations, including dynamic crosslinks for gel dissolution and therapeutic release, shear thinning for injection, and *in situ* formation without initiators or catalysts.²⁷ However, covalently crosslinked hydrogels provide better control over crosslink density and allow easier incorporation of labile functional groups for stimuli-responsive degradability of and release from the delivery vehicle.²⁸ Amongst covalent

crosslinking chemistries, click reactions, including copper-free azide–alkyne cycloadditions, Diels-Alder, thiol–ene, and oxime reactions, are attractive for therapeutic delivery applications due to their fast reaction kinetics under mild conditions, permitting rapid formation *in situ* in the presence of cargo molecules and tissues.^{26, 29-30}

In this chapter, we aim to provide a comprehensive survey of hydrogels and to overview seminal and recent works utilizing these chemistries that are degradable, orthogonal, or both to permit controlled release for therapeutic cargo molecules. Providing criteria and context for controlling properties in the presence of biologics, we will summarize (i) natural and synthetic polymers that are commonly employed as the hydrogel base (ii) reactive functional groups for hydrogel formation, and (iii) degradable moieties for temporal evolution of physical or biochemical properties. We subsequently overview how chemically crosslinked hydrogels have been used for delivery of small molecular weight drugs, therapeutic peptides, and proteins.

1.2 Design Criteria

Hydrogels that permit orthogonal control of multiple properties in the cell microenvironment must meet a number of biological and physical design criteria that are dictated by the intended application (**Fig. 1.1**). For example, hydrogels for three-dimensional (3D) cell culture or delivery must be crosslinked in presence of cells while maintaining cell viability; additionally, they need to mimic critical aspects of the natural ECM, such as mechanical support and degradation, to enable appropriate and desired cellular functions, such as proliferation and protein secretion.³¹⁻³³ In this section, we will address these challenges and provide perspective on key design

criteria for producing cell-compatible hydrogels with properties that can be orthogonally controlled both in space and in time.

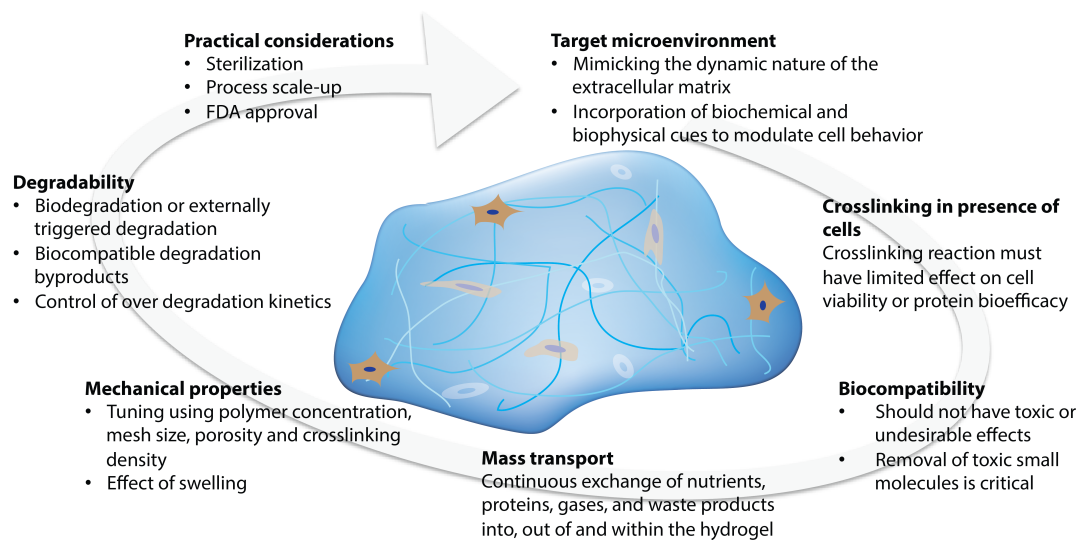


Figure 1.1 Design considerations. The design of hydrogels for orthogonal property control in cellular microenvironments is dictated by the biocompatibility, crosslinking in presence of cells or proteins, mechanical properties, degradability, mass transport properties, and target microenvironment.

1.2.1 Biocompatibility

Biocompatibility is the first, and perhaps the most critical, parameter when considering the application of hydrogels in the cellular microenvironment. Biocompatibility is defined as the ability of a biomaterial to perform its desired function without eliciting any undesirable local or systemic side effects.³⁴ The hydrogel must be immunocompatible and not elicit a significant inflammatory response for use within *in vivo* microenvironments. Various naturally derived polymers (e.g., polysaccharides such as hyaluronic acid) and a few synthetic polymers (e.g., polyethylene glycol) have demonstrated adequate biocompatibility. Removal of

small molecules used or generated during hydrogel fabrication (such as unreacted monomer, initiator, and crosslinkers) is essential to consider during material design, as such molecules can be toxic to host cells both *in vivo* and *in vitro*. For example, unreacted maleimides, which are widely used in Michael-type addition reactions, are highly potent neurotoxins;³⁵ similarly, photoinitiators, such as 2,2-dimethoxy-2-phenyl-acetophenone used frequently in free-radical polymerization, can be cytotoxic.³⁶

In addition, the hydrogel or its base components need to be simple to sterilize and should not undergo any significant functional changes during sterilization. Further, hydrogels for implantation also need to meet appropriate regulatory body (i.e., FDA, EPA) guidelines. Synthetic polymers, such as PEG, PLGA, and PLA, and natural polymers, such as alginate, collagen and fibrin, have been approved for specific clinical applications by the FDA. Kim and Wright recently investigated use of FDA-approved DuraSeal™, a PEG based hydrogel used as a sealant for human spinal fluid leaks.³⁷ In a clinical trial with a total of 158 patients, it was found that DuraSeal™ spinal sealant had a significantly higher rate of intraoperative watertight dural closure (100%) compared to the control (i.e., treated with traditional methods, 65%). In addition, no significant statistical differences were seen in postoperative infection and healing between PEG hydrogel and the control group. Overall, the PEG hydrogel spinal sealant system was found to be an efficient and safe adjunct to suturing for watertight dural repair. Such biocompatible and clinically tested hydrogels (i.e., DuraSeal™, Evolence®, TachoSil™, Tisseel Artiss™, Tegagel™), which are commercially available, cost effective, easy to use and have a stable shelf life (ranging from 6 months to 36 months) along with well defined *in vivo* stability, hold potential

for bioengineering applications, such as wound healing, tissue engineering, 3D cell culture and vascular surgeries.³⁸

1.2.2 Mild Crosslinking Reactions

The ability to form hydrogels in the presence of cells and cargo molecules is critical for creating three-dimensional, controlled microenvironments *in vitro* and offers several advantages *in vivo*, including the ability to mold the gel to the shape of the defect site and delivery in a minimally invasive way. The chemical transformations involved in hydrogel formation, however, can be damaging to cells, and such effects must be considered for both *in vitro* and *in vivo* microenvironments. For example, free radicals can cause damage to cell membranes or detrimental loss of the pericellular matrix during cell isolation and encapsulation.³⁹⁻⁴⁰ Sudden localized changes in temperature, pH, and free radicals during gelation also can affect the activity of cargo molecules (e.g., oxidation of protein) or cell function or viability.⁴¹ However, the incorporation of cells in pre-formed hydrogels is often restricted, since the average mesh size of most hydrogels is much smaller than a cell's diameter; consequently, cells often are introduced within liquid hydrogel precursor solutions.⁴² By selecting an appropriate gelation mechanism, cells can be encapsulated in hydrogels without significantly altering their viability or activity.⁴³⁻⁴⁵ Different chemistries for hydrogel formation in the presence of cells and their cytocompatibility will be discussed in detail.

1.2.3 Mechanical Properties

The success of cell-compatible hydrogels in a given bioengineering application is usually coupled with achieving appropriate mechanical properties. For example,

tissue formation can depend on the mechanical properties of the hydrogel scaffold (e.g., load bearing capability until cells have produced their own functional ECM);⁴⁶⁻⁴⁷ in cell-encapsulation applications, control of the mechanical properties of the hydrogel can determine the therapeutic efficacy of the transplanted cells.⁴⁸ It is well accepted that these effects are the result of the mechanical properties of the hydrogel substrate influencing cellular responses, including cell migration, proliferation, and differentiation; for example, the seminal work of Discher and coworkers demonstrated that stem cell lineage specification depends on optimal outside-in signaling of hydrogel matrix elasticity.⁴⁹⁻⁵⁰ Polymer concentration, the stoichiometry of reactive groups, and crosslinking density are all commonly used to tune the mechanical properties of cell-compatible hydrogels and accordingly to control the cellular microenvironment.⁵¹⁻⁵³

1.2.4 Controlled Degradation

Cell-compatible hydrogels can be designed to degrade via ester hydrolysis, enzymatic hydrolysis, photolytic cleavage or a combination of these mechanisms with varying degrees of control and desired degradation rates depending on the application. In tissue engineering applications, degradation provides space for proliferating cells and allows infiltration of blood vessels.⁵⁴⁻⁵⁵ In controlled 3D cell culture applications, degradation can enable cell proliferation, migration, and synthetic matrix remodeling to better mimic the native ECM and understand *in vivo* cell behaviors.⁵⁶ In controlled drug and gene delivery applications, degradation permits spatiotemporal control of the release of cargo molecules.¹⁸ Release kinetics are dictated primarily by surface erosion or bulk degradation rates when the hydrogel mesh size is smaller than the hydrodynamic radius of the cargo molecule, and by diffusion when mesh size is larger

than the hydrodynamic radius of cargo molecule. For example, Hennink and coworkers demonstrated zero-order release of entrapped proteins from β -cyclodextrin and cholesterol-derivatized PEG hydrogels,⁵⁷ in which the protein release was controlled by surface erosion and dissolution. Ideally, degradation kinetics are well controlled and stable, and the generated byproducts from degradation are biocompatible without eliciting any potential side effects, such as cytotoxicity, inflammation, or immunological or foreign body responses. An optimum balance between degradability and mechanical properties, such as elastic modulus and matrix integrity, is vital to ensure the proper functionality of the hydrogel within the desired timespan.

1.2.5 Mass Transport

Appropriate mass transport properties, matching those of native tissues, are essential for many bioengineering applications. In tissue engineering and cell encapsulation, continuous exchange of nutrients, proteins, gases (i.e., O₂ and CO₂) and waste products into, out of, or within the hydrogel is vital for survival and proliferation of encapsulated cells. For controlled delivery of bioactive cargo (i.e., therapeutics, proteins) where initial burst is undesirable, restricted free diffusion is essential. Hydrogel matrix permeability is thus an important design parameter, given that mass transport in these materials is controlled primarily by diffusion. The permeability of the scaffold is also correlated with the mechanical properties of the hydrogel network and its swelling properties, and as expected, variation in the permeability is a widely employed strategy for controlling cargo release.⁵⁸⁻⁶⁰ For a comprehensive review of the mass transport and diffusivity of bioactive molecules

through hydrogel, readers are referred to reviews by Peppas and coworkers,^{32, 61} and Lin and Metters.⁶²

1.3 Drug Release Mechanism

Strategies for incorporation of therapeutics into hydrogels generally fall into three categories: (1) encapsulation, where therapeutics are entrapped within the crosslinks of the polymer network (**Fig. 1.2 A**); (2) tethering, where drugs of interest are covalently bound to the polymer network (**Fig. 1.2 B**); and (3) affinity binding, where hydrophobic, ionic, or peptide interactions are utilized to retain therapeutics within the hydrogel network ⁶³ (**Fig. 1.2 C**). To design effective drug delivery vehicles, these strategies are combined with appropriate release mechanisms to suit the application of interest; several examples are shown in the right hand column of **Fig. 1.2**. The release of therapeutics entrapped within or tethered to the matrix can be controlled by *i*) Fickian diffusion, *ii*) degradation of tethered linkages in response to relevant biological stimuli, or *iii*) combinations of both. With affinity binding, a ligand is added to the hydrogel with affinity for therapeutic(s) of interest. In this way, release is controlled by the reversible binding of the ligand to the therapeutic in combination with diffusion of the free species or matrix degradation. The binding kinetics between bound and free therapeutic often are described by association and dissociation constants indicating how quickly binding and dissociation occur (k_{on} and k_{off} , respectively).⁶⁴

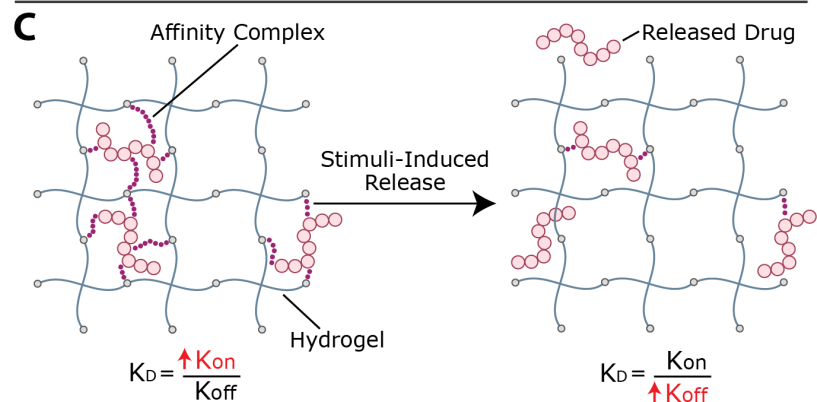
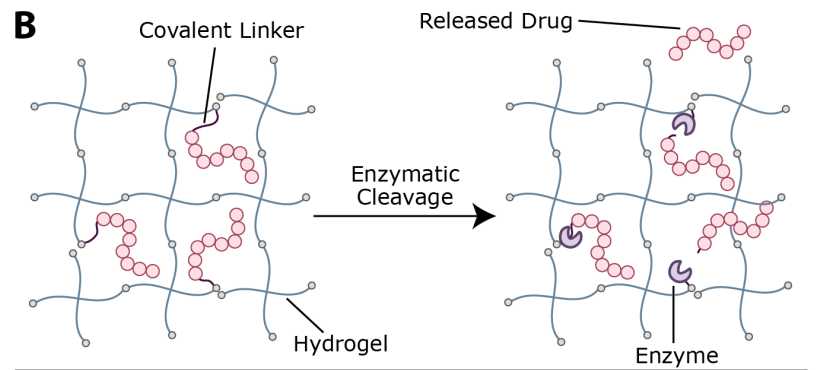
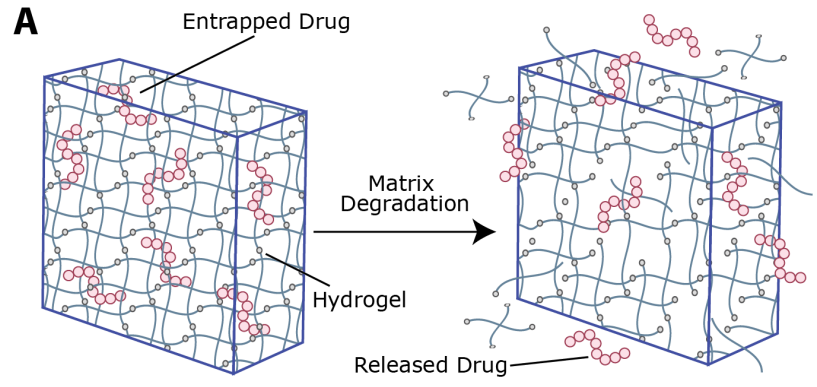


Figure Legend			
	Drug		Covalent Bond
	Hydrogel		Enzyme
	Affinity Complex		

Figure 1.2 Therapeutic loading and release mechanisms from hydrogel-based delivery vehicles. Hydrogels can be formed *in vitro* or *in vivo* for therapeutic delivery applications. Stoichiometric reaction between functional groups on multiarm poly(ethylene glycol) (PEG) macromers functionalized with specific alkenes or thiols, respectively, has been reported, producing thiol–ene hydrogels with nearly ideal network structure (shown here); these are of growing interest for delivery applications toward providing a well defined and predictable mesh size. However, macromolecules of varied length and functionality, both of synthetic and natural origin and decorated with various alkenes or thiols. Engineering of material structure and chemistry provide handles for controlling release profiles. **(A)** For example, therapeutics frequently have been encapsulated within the hydrogel network, where the cargo is entrapped if the average pore size (e.g., mesh size) of the hydrogel is smaller than the drug; degradation of the network, which increases mesh size, controls release. **(B)** Small molecule drugs or peptides, which can be difficult to entrap within hydrophilic highly-swollen hydrogels, have been tethered to the network and released upon tether cleavage (or complete network degradation); here, cleavage by a cell-secreted enzyme is depicted. **(C)** Ligands for a therapeutic of interest also have been incorporated within hydrogels for controlling retention and release by affinity binding; reversible binding of the ligand dictated by k_{on}/k_{off} determines the fraction of bound/free therapeutic, where diffusion of the free species (or matrix degradation) controls release. These therapeutic loading and release mechanisms can be used in different combinations than those depicted here and have been used in hydrogels for drug delivery applications.

1.4 Materials for Hydrogel Preparation

Cell-compatible hydrogels have been prepared using a variety of polymeric materials, which can be divided broadly into two categories according to their origin: natural or synthetic.³¹ Natural polymers such as polysaccharides serve as ideal building blocks for preparing hydrogels that can mimic aspects of the structural and biological properties of the cellular microenvironment. For instance, proteoglycans are one of the vital components of articular cartilage, and use of glycosaminoglycan (GAG) hydrogels, such as those based on hyaluronic acid or chitosan, as a scaffold

can be useful for cartilage tissue engineering.⁶⁵ Moreover, as shown in **Table 1.1**, the mechanical properties, water content, and inherent chain flexibility of polysaccharide-based hydrogels help to mimic the natural ECM. In addition, such polymers can be degraded by naturally occurring cell-secreted enzymes in the cellular microenvironment, mimicking the dynamic nature of the ECM. Further, the specific cell-surface receptors for polysaccharides are known and have been extensively studied. For example, in the case of hyaluronic acid (HA), a non-sulfated glycosaminoglycan found in the ECM, both cluster of differentiation (CD) 44 and the receptor for hyaluronan-mediated motility (RHAMM) are known to enable cell adhesion and proliferation on HA.⁶⁶ However, limited tunability of degradation kinetics, relatively poor mechanical properties, batch-to-batch variations from manufacturers, or potential immunogenic reactions can restrict the application of natural polymer based hydrogels.⁶⁷ Synthetic polymers afford tunable mechanical properties and a large scope of chemical modification, including the introduction of degradable or biochemical moieties. Commercial availability, coupled with great flexibility in the working range of pH, ionic strength, and chemical conditions, make synthetic polymers excellent candidates for hydrogel preparation. However, purely synthetic materials often exhibit inferior biocompatibility and biodegradability in comparison to naturally derived materials, which may limit their use in applications where targeted and specific biological activity is desired. Hence, many combinations of natural and synthetic polymers have been studied for developing hydrogels with orthogonal property control in the cellular microenvironment. In this section, we will limit the discussion to several widely used natural and synthetic polymer building blocks used in controlled microenvironments.

Table 1.1 Selecting materials for hydrogel preparation. Comparison of natural and synthetic polymers typically used for preparation of cell compatible hydrogels.

Feature/function	Natural polymers	Synthetic polymers
Biocompatibility	Polymer dependent	Polymer dependent
Bioactivity (i.e. cell specific receptor)	Possible	Limited
Inherent biodegradability	✓✓	✓
Tunability of degradation kinetics	✓	✓✓
Degradation byproducts	Biocompatible	Potentially harmful
Flexibility for chemical modification	✓	✓✓
Flexibility of working range (i.e. pH and ionic strength)	✓	✓✓
Tuning of mechanical properties	✓	✓✓
Commercial availability	✓	✓✓
Batch to batch variations	Likely	Controlled

1.4.1 Hydrogels from Natural Polymers

1.4.1.1 Hyaluronic Acid

Hyaluronate or HA is a non-sulfated GAG in the ECM that is distributed throughout connective, epithelial, and neural tissues. This GAG is composed of alternating disaccharide units of D-glucuronic acid and N-acetyl-D-glucosamine linked together with β -1,4 and β -1,3 glycosidic bonds (**Fig. 1.3**).⁶⁸ HA is inherently biocompatible and non-immunogenic and degrades in the presence of hyaluronidase as well as in the presence of reactive oxygen species. HA is a critical component of the ECM and plays an important role in various biological processes, including wound

healing, angiogenesis, and activation of various signaling pathways that direct cell adhesion, cytoskeletal rearrangement, migration, proliferation, and differentiation.^{19, 69-71} Although concerns over batch-to-batch variation and the possibility of contamination with endotoxins and pathogenic factors persist, recent developments in recombinant technology have significantly improved the quality of commercially-available HA.⁷²⁻⁷³ However, the rapid degradation of HA in the presence of hyaluronidase can hinder its usefulness in certain applications. For example, approximately one-third of the typical fifteen grams of HA found in a human is degraded and re-synthesized daily.⁷⁴ Limited control over HA degradation kinetics (i.e., rapid degradation) can lead to precipitate changes in mechanical properties, such as hydrogel stiffness, which may be undesirable in certain bioengineering applications.

HA can be modified with thiols, haloacetates, dihydrazides, aldehydes, or carbodiimide functional groups to allow crosslinking into hydrogels.⁷⁵ HA-based hydrogels have shown excellent potential for biomedical engineering applications, such as tissue engineering,⁷⁶⁻⁷⁸ valve regeneration,⁷⁹⁻⁸⁰ controlled delivery,⁸¹⁻⁸⁴ and controlling stem cell behavior.⁸⁵⁻⁸⁶ For example, Jia and coworkers synthesized HA- and heparin-based spherical hydrogel particles with an inverse emulsion polymerization, creating inherently bioactive delivery vehicles (due to inductive role of HA in chondrogenesis) for controlled growth factor (BMP-2) release.⁸⁷ Additionally, Elia et al. used HA-based degradable hydrogels embedded within electrospun silk for sustained release of encapsulated cargo molecules (anti-inflammatory steroid drugs and proteins) over 45 to 400 minutes.⁸⁴ Such approaches that utilize simple fabrication techniques and tuning of release kinetics make HA hydrogels attractive candidates for tissue regeneration and sustained therapeutic

1.4.1.2 Chitosan

Chitosan, the deacetylated derivative of chitin, is a linear polycationic polysaccharide composed of randomly distributed β -(1-4)-linked D-glucosamine and N-acetyl-D-glucosamine (**Fig. 1.3**). The structural units of chitosan are similar to those of GAGs of the ECM.⁸⁹ It can be degraded by various mechanisms, including surface erosion, enzymatic degradation through chitosanase and lysozyme, and dissolution.⁹⁰ By using appropriate crosslinking chemistries and densities, the degradation kinetics can be tuned. The inherent properties of chitosan, such as excellent cytocompatibility, biodegradation, minimal foreign body response, and antimicrobial properties, make chitosan-based hydrogels attractive candidates for engineering applications, including wound-healing, bioactive molecule delivery and soft tissue engineering.

The large number of accessible hydroxyl and amine groups in chitosan provide numerous possibilities to create hydrogels via chemical crosslinking.⁹¹ These functional groups can react with many bifunctional small molecule crosslinkers, such as glutaraldehyde, formaldehyde, genepin, diethyl squarate and diacrylate, to form chemically crosslinked hydrogels.²⁰ In addition, incorporation of new functionalities along backbone chain (i.e., those susceptible to the Schiff base reaction, disulfide bonding or Michael-type additions) can be used for *in situ* gel formation. Chitosan-based hydrogels can be used for the controlled delivery of drugs,^{20, 92} proteins,⁹² and growth factors⁹³ as well as the encapsulation of living cells,⁹³⁻⁹⁴ the controlled differentiation of stem cells,⁹⁵⁻⁹⁶ and applications in tissue engineering.⁹⁷⁻¹⁰⁰ For example, Bellamkonda and coworkers recently reported chitosan-based photocrosslinkable, degradable hydrogels for neural tissue engineering application¹⁰⁰ Chitosan was functionalized with amino-ethyl methacrylate for network formation via photoinitiated radical polymerization. The cytocompatible hydrogel enhanced

differentiation of primary cortical neurons by ~30% and enhanced dorsal root ganglia neurite extension by about two-fold in 3D *in vitro* studies, as compared to an agarose-based hydrogel control. In principle, such hydrogels additionally can be used to control cell behavior and lineage specific differentiation by incorporation of growth factors since the gel formation chemistry does not alter the active end groups on chitosan, which allow bioactive molecule binding.

1.4.1.3 Heparin

Heparin is a heterogeneous GAG, consisting of α -L-iduronic acid, β -D-glucuronic acid, and α -D-glucosamine residues (**Fig. 1.3**). Heparin has the highest negative charge density of any known biological macromolecule giving rise to ionic interactions with bioactive molecules such as proteins, growth factors, and cytokines.¹⁰¹⁻¹⁰² Such noncovalent interactions of heparin in many cases serve not only to sequester the proteins, but also to control their biological activity (e.g., enhancing cell receptor affinity).¹⁰¹ Heparin and heparan sulfate mediate number of biological interactions, such as cell adhesion, cell proliferation, or cell surface binding of lipase and other proteins that are critical in developmental processes, blood coagulation, angiogenesis, viral invasion, and tumor metastasis.¹⁰³ Moreover, heparin and heparan sulfate protect proteins from degradation, regulate protein transport through basement membranes, and mediate internalization of proteins.¹⁰⁴ However, potential adverse effects of heparin, an potent anticoagulant include bleeding, thrombocytopenia, osteoporosis, alopecia, and priapism, and are related to this wide variety of biological activities.¹⁰⁵⁻¹⁰⁷ Such undesirable effects may limit the use of heparin in certain *in vivo* applications.

Physically and chemically crosslinked heparin-based hydrogels have been employed for the investigation of cell function and fate,¹⁰⁸⁻¹¹¹ cell encapsulation,¹¹²⁻¹¹⁵ and controlled bioactive molecule delivery.^{51, 116-118} For instance, Kiick and coworkers used heparin-based hydrogels to modulate cell response in a 2D *in vitro* experiment.¹⁰⁸ To modulate cell adhesion and response, hydrogels with different moduli were prepared using the Michael addition reaction between combinations of maleimide-functionalized heparin, thiol functionalized PEG and maleimide functionalized PEG. Such systems, with the ability to tune biochemical and mechanical properties, make heparin based hydrogels promising candidates for controlling adventitial fibroblast remodeling of blood vessels. In another example, Tae and coworkers took advantage of heparin-based hydrogels to stably bind fibrinogen and collagen type I on a hydrogel surface using heparin binding affinity by physisorption.¹¹⁰ The hydrogels were prepared by a Michael-type addition reaction using thiolated heparin and PEG diacrylate. The significant physisorption of proteins on the heparin hydrogel, as compared to a control PEG hydrogel, led to enhanced fibroblast adhesion and proliferation. Such approaches can be used to adhere cells on selective heparin hydrogel surfaces for applications such as biosensors, cell culture, and tissue engineering. Additionally, Werner and coworkers recently reported use of heparin-based hydrogels for cell replacement therapies in the neurodegenerative diseases.¹¹¹ By tuning the mechanical and biological properties of the PEG-heparin hydrogels, neural stem cell differentiation and axo-dendritic outgrowth were modulated. *In vivo* stability and excellent histocompatibility make such hydrogel systems attractive candidates for neuronal cell replacement therapies. For a comprehensive overview of

heparin hydrogels, readers are referred to a recent book chapter by McGann and Kiick.¹⁰¹

1.4.1.4 Alginate

Alginate is a hydrophilic, cationic polysaccharide consisting of (1-4)-linked β -D-mannuronate (M) and its C-5 epimer α -L-guluronate (G) residues (**Fig. 1.3**). It is obtained from brown algae, and depending upon the algae source, it may consist of blocks of similar or strictly alternating residues. Alginate-based hydrogels are biocompatible and undergo physical gelation in the presence of divalent cations. Despite these advantages, the uncontrolled degradation of physically crosslinked alginate hydrogels upon the loss of divalent cations can hinder their stability. Covalent crosslinking with various crosslinkers, such as adipic acid dihydrazide and lysine, can be employed to overcome this uncontrolled degradation. A lack of cell-specific interactions, however, can limit the use of alginate hydrogels in bioengineering applications; an attractive approach to induce bioactivity for cell culture is by covalent incorporation of bioactive ligands such as RGD-containing peptides. An additional challenge for alginate hydrogels *in vivo* is that the alginate macromolecule itself is difficult to break down under physiological conditions, and the molecular weight of released alginate strands is typically above the renal clearance threshold.¹¹⁹⁻¹²⁰ However, partially oxidized alginate, which undergoes biodegradation, can be utilized to overcome these limitations.¹²¹

Alginate-based hydrogels have been used for in drug delivery,¹²²⁻¹²⁴ tissue engineering,¹²⁵⁻¹²⁷ wound healing,¹²⁸⁻¹³⁰ cell encapsulation,¹³¹⁻¹³² and as adhesion barriers.¹³³ For instance, recently Kim et al. employed alginate-based hydrogels for delivering differentiated adipogenic cells for adipose tissue engineering.¹²⁷ Oxidized

alginate (susceptible to hydrolysis) was coupled with an adhesion peptide and crosslinked with calcium sulfate to encapsulate cells *in vivo*. The injected cell-laden hydrogels led to the formation of soft, semitransparent adipose tissue after 10 weeks in male nude mice highlighting the ability of degradable alginate hydrogels to deliver cells and generate living tissue via a minimally invasive injection.

1.4.1.5 Other Natural Polymers

Discussion of natural polymers for hydrogel preparation in this section mainly has been limited to HA, chitosan, heparin, alginate, and fibrin, owing to scope of the article. However, other natural polymers, such as collagen, gelatin, chondroitin sulfate, agarose, carrageenan, dextran, and silk, have been utilized for variety of bioengineering applications, including cartilage, neural, spinal cord, skin and vocal cord tissue engineering as well as therapeutic and controlled delivery. Readers are directed to recent reviews by Slaughter et al.³² for collagen based hydrogels, Vlierberghe et al.¹³⁴ for collagen, gelatin, and chondroitin sulfate based hydrogels, Perale et al.¹³⁵ for alginate and collagen based hydrogels, and Kaplan and coworkers¹³⁶⁻¹³⁷ for silk based hydrogels.

1.4.2 Hydrogels from Synthetic Polymers

1.4.2.1 Poly(ethylene glycol)

Poly(ethylene glycol) (PEG), also known as poly(ethylene oxide) (PEO) or poly(oxyethylene) (POE) depending upon the molecular weight of the polymer, is the hydrophilic non-degradable polymer of ethylene oxide (**Fig. 1.3**). It lacks any protein binding sites, and due to its hydrophilic and uncharged structure, it

forms highly hydrated layers that restrict protein adsorption.¹³⁸ The excellent biocompatibility and low toxicity of PEG-based hydrogels make them ideal candidates for various biomedical applications, and PEG-containing formulations have been approved by the FDA for several medical applications, including use as laxatives, solvents in liquid formulations, conjugates to therapeutic proteins, and lubricants.¹³⁹⁻¹⁴¹ Acute, short and long-term toxicology of PEG with oral, intraperitoneal and intravenous administration routes have been thoroughly reviewed.¹⁴²⁻¹⁴³ Low molecular weight PEGs ($M_w < 1$ kDa) can be oxidized *in vivo* into toxic diacids and hydroxyl acid metabolites,¹⁴⁴ but high molecular weight PEGs ($M_w > 5$ kDa) show little or no metabolism.¹⁴²

PEG macromolecules can be functionalized easily via its hydroxyl end groups to yield numerous homofunctional or heterofunctional terminal groups, including thiols,¹⁴⁵ vinyl sulfones,¹⁴⁶ maleimides,^{51, 147} acrylates¹⁴⁸⁻¹⁴⁹ allyls,¹⁵⁰ and norbornenes.¹⁵¹⁻¹⁵² The PEG hydrogels have been widely used as blank slates for the presentation of biophysical and biochemical cues in tissue engineering,¹⁵³⁻¹⁵⁶ cell encapsulation,¹⁵⁷⁻¹⁵⁹ controlled stem cell differentiation,¹⁶⁰⁻¹⁶² and bioactive molecule delivery applications.^{154, 163-165} For a comprehensive overview of PEG hydrogels, readers are referred to recent reviews by Lin and Anseth¹⁸ for controlled delivery applications and by Papavasiliou et al.¹⁶⁶ for tissue engineering applications.

A large number of PEG copolymers have been utilized for drug delivery, such as non-biodegradable triblocks of PEG and polypropylene oxide (PPO) (PEG-*b*-PPO-*b*-PEG, Pluronics™) and hydrolytically degradable block polymers of PEG, polylactic acid (PLA), and polylactic acid-co-glycolic acid (PLGA), as shown in Fig. 3G. For example, H. Chang et al. investigated the effect on an active form of an antitumor

drug, topotecan (TPT), which was encapsulated in an amphiphilic PEGA-PEG-PLGA hydrogel matrix for controlled release.¹⁶⁷ Due to the increased pK_a of the carboxylate groups as a result of the hydrophobic interactions between the amphiphilic polymer matrix and TPT, the active form content of TPT was increased by about 40%, as compared to free TPT in PBS solution under physiological conditions. Further, the release was sustained for 5 days with only a mild initial burst release.

1.4.2.2 Poly(vinyl alcohol)

Poly(vinyl alcohol) (PVA), as shown in **Fig. 1.3**, is commercially obtained by partial or complete hydrolysis of poly(vinyl acetate). The extent of hydrolysis and the molecular weight of the macromolecule can be used to tune its hydrophilicity and solubility, and the pendant hydroxyl groups can act as biomolecule attachment sites. Due to its low protein adsorption and excellent biocompatibility, PVA has been used in soft contact lenses, eye drops, tissue adhesion barriers, and cartilage replacement applications.¹⁶⁸ For a comprehensive overview of PVA hydrogels in biomaterial applications, readers are referred to recent reviews by Baker et al.¹⁶⁸ and Alves et al.¹⁶⁹

PVA-based hydrogels can be formed by chemical crosslinking using various chemistries, such as click chemistry,¹⁷⁰⁻¹⁷¹ radical polymerization,¹⁷²⁻¹⁷⁴ and Schiff base reaction.¹⁷⁵⁻¹⁷⁶ The hydrogels also can be formed by physical crosslinking via methods such as cryogenic gelation and hydrogen bonding,¹⁷⁷⁻¹⁷⁹ and PVA hydrogels formed via these methods have been successfully used for tissue engineering and regenerative medicine applications.^{178, 180-182} For instance, Samal et al. prepared hybrid hydrogels consisting of PVA, chitosan, and multiwalled carbon nanotubes (MWCNT) by the physical freeze-drying method.¹⁷⁸ The incorporation of MWCNT improved the mechanical strength, structural coherence, and electrical conductivity of the hydrogel

matrix and could influence cell behavior due to biophysical and electrostimulating cues. The hydrogel matrix showed excellent biocompatibility while retaining the inherent properties of PVA, chitosan, and MWCNT, indicating its potential for biomedical applications.

1.4.2.3 Other Synthetic Polymers

Poly(hydroxyethyl) methacrylate (PHEMA), a hydrophilic, water-stable polymer, was the base material for one of the first hydrogels to be successfully used for ophthalmic applications (e.g., contact lenses).¹⁸³ While PHEMA hydrogels are stable under physiological conditions, their controlled degradation can be achieved by incorporation of hydrolytically or enzymatically cleavable linkages, such as polycaprolactone,¹⁸⁴⁻¹⁸⁵ and collagenase-cleavable peptide sequences¹⁸⁶⁻¹⁸⁷. Another poly(acrylate) derivative, poly(N-isopropylacrylamide) (PNIPAAm), a thermoresponsive polymer with lower critical solution temperature (LCST) of approximately 32 °C, has been utilized for preparing responsive hydrogels for tissue engineering and drug delivery applications.¹⁸⁸⁻¹⁹⁰ For a comprehensive review of strategies to improve the thermosensitivity of PNIPAAm hydrogels, readers are referred to a review by Zhang et al.¹⁹¹

Polyphosphazene, an organometallic polymer with a phosphorous-nitrogen backbone and organic side groups, can degrade under physiological conditions into nontoxic molecules, such as H₃PO₄ and NH₄⁺. The inorganic backbone undergoes hydrolytic degradation, where the rate of degradation is dictated by the side chain structures.¹⁹² Polyphosphazene hydrogels can be prepared via physical crosslinking (i.e., ionic interaction using divalent ions), or chemical crosslinking via glucosyl or glyceryl side groups.¹⁹³ Readers are referred to a recent review by Allcock for a

comprehensive review of polyphosphazene;¹⁹⁴ but we note here that polyphosphazene based hydrogels have been used for bioactive molecule delivery and drug delivery.¹⁹⁵⁻

196

Polyesters, such as PLA, polyglycolic acid (PGA), and polycaprolactone (PCL), also have been used for the preparation of cell-compatible hydrogels. Polyester-based polymers offer inherent biodegradability due to ester hydrolysis under physiological conditions. Thus, using combinations of polyesters with other synthetic or natural polymers, the rate of hydrogel degradation can be tuned as per application requirements. For a comprehensive overview of polyester-based hydrogels, readers are referred to a review by Tomas and coworkers.¹⁹⁷

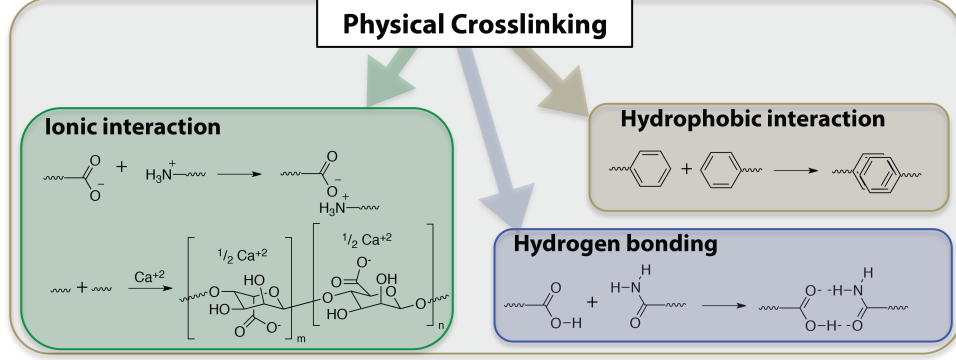
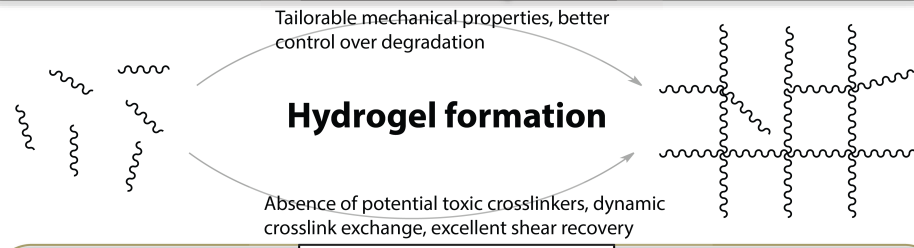
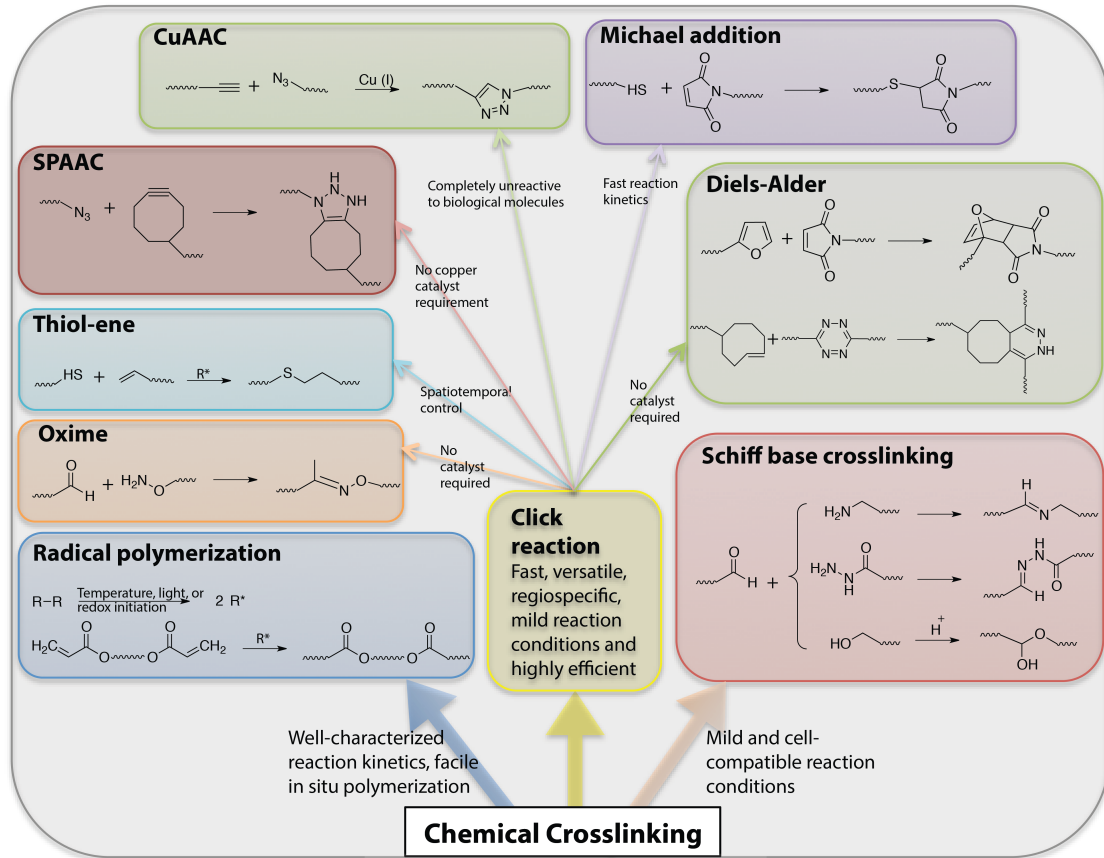


Figure 1.4 Chemical functional groups for hydrogel formation. A wide range of functional groups is available for either hydrogel formation or modification post-polymerization. Functional group selection depends on several factors related to the application of interest, including the desired initiation mechanism, the specificity, and speed of the reaction, and the stability of the resulting bond under various solution conditions.

1.5 Material Functionalization for Hydrogel Formation

The stable crosslinking of hydrogels is essential to prevent uncontrolled dissolution of macromolecular chains in aqueous cellular microenvironments. Numerous chemical and physical crosslinking strategies have been utilized for the preparation of cell-compatible hydrogels (**Fig. 1.4**). Chemical crosslinking strategies covalently couple reactive functional groups for hydrogel formation using chain or step growth reactions, including free radical chain polymerization, click reactions, reactions of Schiff bases, and carbodiimide-mediated activation reactions. Physical crosslinking strategies utilize non-covalent interactions between functional groups, such as ionic interactions, electrostatic interactions, hydrogen bonding, crystallization, hydrophobic interactions, and protein interactions.

The crosslink concentration, or density, dictates various physical properties of hydrogels, including elasticity, diffusivity, water content, and mesh size. In addition, the degree of crosslinking influences the hydrogel degradation rate, and hence, precise control over hydrogel crosslinking is highly desirable. Further, for control of the properties of the cell microenvironment, hydrogel formation in the presence of cells or proteins is often required, and it is thus essential to choose a cytocompatible crosslinking method for preparing these applications.

1.5.1 Chemically Crosslinked Hydrogels

1.5.1.1 Radical Polymerization

Radical polymerization involves the formation of free radicals via decomposition of an initiator by light, temperature, or redox reaction.¹⁹⁸ The successive reaction of multifunctional free radical building blocks leads to the formation of a polymer network. Free radicals can be used to initiate hydrogel formation by different polymerization mechanisms: chain growth, step growth, or mixed mode (a combination of chain and step) polymerization.¹⁹⁹ Hydrogel formation by free radical polymerization offers advantages such as well-characterized reaction kinetics and facile *in situ* polymerization in presence of cells with spatiotemporal control.²⁰⁰ However, free radicals can be transferred to proteins, affecting their bioactivity, or transferred to biomolecules present in the ECM, affecting cell viability.^{41, 201} These exothermic reactions also can cause a local increase in temperature,²⁰² where temperature rise must be minimized to maintain cell viability and function. Despite these challenges, free radical polymerization via chain growth mechanisms is a well-established method for cell encapsulation; however, the heterogeneous nature of the chain polymerization mechanism leads to a distribution of polymer chain molecular weights and thus molecular-level inhomogeneity within the network. Inhomogeneity in network can dramatically reduce the mechanical strength of hydrogels.²⁰³ The widespread use of free radical chain polymerization for hydrogel formation partly arises from the availability of many hydrophilic meth(acrylate)-functionalized building blocks. Historically, radical polymerization of hydroxyethyl methacrylate (HEMA) using ethylene dimethacrylate (EDMA) as a crosslinker was extensively studied for commercial-scale manufacturing of flexible contact lenses.¹⁸³

A large number of macromolecules, such as HA,^{79, 204-206} chitosan,^{195, 207} and PEG,²⁰⁷⁻²⁰⁸ are easily functionalized with vinyl end groups and can undergo radical polymerization to form hydrogels in presence of appropriate initiators. For example, Morelli and Chiellini functionalized Ulvan, a sulfated polysaccharide from green seaweed, with methacryloyl group.²⁰⁹ The biocompatible hydrogel network was formed via radical polymerization using UV irradiation in the presence of methacrylic anhydride or glycidyl methacrylate.

A significant advantage of radical polymerization methods is that, when used in conjunction with a photoinitiator, they can provide spatiotemporal control over hydrogel formation and *in situ* properties.^{36, 210} For instance, Guvendiren and Burdick demonstrated short and long-term cellular response to a dynamic microenvironment using methacrylated hyaluronic acid.²¹⁰ The methacrylated HA was crosslinked with a dithiol via the Michael-type addition, creating a low modulus hydrogel, and subsequently via free radical chain polymerization of the remaining methacrylates, increasing the crosslink density and modulus of the hydrogel at time points of interest. Human mesenchymal stem cells (hMSCs) that were cultured on these hydrogel substrates spread from cell areas of ~ 500 to $3,000 \mu\text{m}^2$ and exhibited greater traction over a timescale of hours during stiffening (with E increasing from 3 to 30 kPa). The cell response to matrix stiffening was found to vary over 2 weeks in culture; an increased population of terminally differentiating hMSCs was present over time and was no longer responsive to variations in the mechanical properties of the hydrogel.

Alternatives such as controlled chain polymerization have been employed for hydrogel preparation to provide more control of hydrogel properties;²¹¹⁻²¹³ however, potential cytotoxicity of the unremoved metal catalysts employed during these

methods can restrict their use in the cell microenvironment. Free radical step growth polymerization recently has emerged as an alternative hydrogel formation strategy that provides a more homogeneous network structure and enables spatiotemporal control of hydrogel formation;²¹⁴ recent developments in this area (e.g., thiol–ene click reactions) will be discussed.

1.5.1.2 Click Chemistry

Click reactions, broadly defined, are a class of reactions that are fast, versatile, regiospecific, and highly efficient.²⁹ Click reactions usually yield a single product, leaving no reaction byproducts, and occur under mild conditions. After the introduction of click reactions by Sharpless,²⁹ the copper (I)-catalyzed azide-alkyne cycloaddition (CuAAC) has been widely used for the facile synthesis of new molecules, polymers, and hydrogels.²¹⁵ Over the past decade, several reactions have been observed to have ‘click’ reaction attributes while not requiring a metal catalyst, including the radical addition of thiols to select alkenes and alkynes, Michael-type addition of thiols to maleimides, Diels-Alder reactions between dienes and dienophiles, and oxime reactions between aminooxy groups and aldehydes or ketones (**Table 1.2**).²¹⁶ Click reactions are attractive tools for synthesizing cell-compatible hydrogels, which can be used for controlled cell culture, tissue engineering, and controlled release applications.²¹⁷⁻²²⁰ Advantages such as fast reaction kinetics, high regio- and chemo-selectivity, mild reaction conditions, and facile tuning of structural and mechanical properties using stoichiometry make click reactions highly useful for synthesizing cell-compatible hydrogels.^{171, 221-222}

Table 1.2 Click reactions for hydrogel for hydrogel formation. Comparison of important click reactions typically used for formation of cell compatible hydrogels

Click reactions	Reacting functional groups	Reaction conditions ²²²	Key features	Applications
CuAAC	azide and alkyne	pH 4-12, reaction time <1 h, Cu catalyst required	bioorthogonal reversible difficulties with complete removal of cytotoxic Cu	cell encapsulation and delivery, ²¹⁸ drug delivery, ²²³⁻²²⁴ 2D cell culture ²²⁵
SPAAC	cyclooctyne and azide	pH 7.4, reaction time <1 h	no catalyst required	cell encapsulation, ²²⁶⁻²²⁷ 3D cell culture ^{217, 219}
Diels-Alder	conjugated diene and substituted alkene	pH 5.5-6.5, reaction time <8 h	no catalyst required longer reaction time than most of the other click reactions	cell encapsulation and release, ³⁰ controlled cargo delivery ²²⁸
Inverse electron demand Diels-Alder	dienophile and diene	pH 7.4, reaction time <5 min	faster rate of reaction than many other Cu-free click reactions no catalyst required	live cell imaging, ²²⁹ drug targeting ²³⁰ , cell surface protein labeling ²³¹
Thiol-ene	thiol and unsaturated functional group (radical mediated)	pH 6-8, reaction time <1 h	spatiotemporal control possible with select chemistries and using a photoinitiator	cell encapsulation, ¹⁵¹⁻¹⁵² degradable 3D cell culture ^{149, 232}
Michael addition	thiol and α,β -unsaturated carbonyl group	pH 6-8, reaction time <30 min	no catalyst required reversible	cell encapsulation, ^{159, 162, 233} controlled cargo delivery ^{51, 234}
Oxime	aminoxy and aldehyde/ ketone	pH 6-8, reaction time <30 min	no catalyst required	cell encapsulation, ²³⁵ protein immobilization ²³⁶

1.5.1.2.1 Azide-alkyne Cycloadditions

Copper (I)-catalyzed azide-alkyne cycloadditions (CuAAC) unite two unsaturated reactants, azides and alkynes, to form triazoles.²³⁷ CuAAC click reactions have been extensively used for crosslinking both natural²²³⁻²²⁵ and synthetic^{171, 218, 238} polymer-based hydrogels. One advantage of this class of reactions is that both azides and alkynes are almost completely unreactive toward biological molecules.²³⁹ Their limitations include alkyne homocoupling, difficulties removing residual heavy metal catalyst, and the biocompatibility of the resulting 1,2,3-triazoles. In particular, use of toxic and unstable Cu catalysts can limit applicability in cellular microenvironments. Nevertheless, Piluso et al. recently reported the preparation of HA-based hydrogels via CuAAC click crosslinking of alkyne-functionalized HA.²²⁵ The elastic modulus of the resulting HA hydrogels was tuned between 0.5 to 4 kPa by varying the stoichiometry, length, and rigidity of an azide-functionalized crosslinker. In this case, limited toxicity was observed with L292 cells encapsulated in these hydrogels, indicating their potential as biomaterials.

Copper-free strain-promoted azide-alkyne cycloaddition (SPAAC) reactions have emerged to address issues with copper toxicity in biological systems.²⁴⁰ Ring strain, as well as electron-withdrawing fluorine substituents in some cases, promotes rapid reaction of cyclooctynes with azides in the absence of the Cu catalyst.²⁴¹ Owing to the absence of the catalyst, SPAAC click chemistry has been used to crosslink hydrogels in the presence of cells to form controlled cellular microenvironments.^{217, 219, 226-227} For instance, Zheng et al. reported use of a SPAAC strategy to create hydrogels by functionalizing PEG with 4-dibenzocyclooctynol.²²⁶ The versatility and biocompatibility of this strategy allowed hMSC encapsulation, maintaining their viability as assessed using a live-dead imaging-based cytotoxicity assay (~90%

viability after 24h). In a broader context, such an approach can be useful for cell delivery, in which cells are hypersensitive to presence of Cu during crosslinking. In another example, DeForest et al. used SPAAC click chemistry for hydrogel formation followed by a thiol-ene reaction for photoaddition of three-dimensional biochemical patterns with micrometer scale resolution and in the presence of fibroblasts (>90% viability at post 24 h encapsulation).²¹⁹ Specifically, an enzymatically degradable peptide sequence was incorporated into the hydrogel via SPAAC reaction, and the adhesion ligand was incorporated in the hydrogel network via cytocompatible thiol-ene photolithographic patterning. The cells selectively adhered to regions in which the RGD motif was presented and subsequently degraded the hydrogel matrix through cleavage of the enzymatically degradable linker, leading to localized cell proliferation. In principle, such approaches can be used to study cell behavior in spatiotemporally controlled 3D microenvironments.

1.5.1.2.2 Diels-Alder Reactions

The Diels-Alder (DA) reaction is a well-established solution-based reaction that has also been utilized for hydrogel formation. DA reactions involve addition of conjugated dienes to substituted alkenes to form substituted cyclohexenes.^{216, 242} The efficient and facile DA reaction occurs under mild reaction conditions and does not require an initiator, which is advantageous for crosslinking hydrogels in the presence of cells. However, the reactions are slow, which could be a limitation in certain applications. The DA reaction has been utilized for the preparation of various hydrogels for bioengineering applications.^{30, 228, 243}

Shoichet and coworkers recently demonstrated the use of a Diels-Alder click reaction to create stable and biocompatible hyaluronic acid hydrogels.³⁰ The

carboxylic acid group of HA was reacted with furfurylamine to create furan-functionalized HA, and the modified HA was crosslinked with a maleimide PEG crosslinker to form a hydrogel. The mechanical and degradation properties of these hydrogels were modulated using the furan to maleimide molar ratio. *In vitro* studies with a cancer cell line, MDA-MB-231, demonstrated the cytocompatibility of these Diels-Alder HA-PEG hydrogels, and a high level of cell viability was maintained over 2 weeks (>98%, live-dead assay after 14 days). Using a similar approach, Marra and coworkers prepared HA-based hydrogels for controlled release application.²²⁸ HA was functionalized with either a maleimide or a furan group and crosslinked in PBS at 37 °C within ~ 40 minutes. Insulin (negatively charged) or lysozyme (positively charged) were encapsulated as model proteins within these HA-based hydrogels. The release profiles showed slight or no burst release depending upon the protein, owing to electrostatic interactions. In addition, the hydrogels were cytocompatible and maintained the viability of the entrapped cells. Taken together, these recent examples indicate that the Diels-Alder crosslinking for creating cell-compatible hydrogels is a promising strategy for soft tissue engineering, regenerative medicine and controlled release applications.

Fox and coworkers created an inverse-electron-demand Diels-Alder reaction, reacting a trans-cyclooctene with dipyridyltetrazine.²⁴⁴ As compare to any other Cu-free click reaction, the rate of this reaction was an order of magnitude higher ($k = 10^3 \text{ M}^{-1} \text{ s}^{-1}$).²⁴¹ Using a similar approach, reactions of tetrazines with other alkenes such as norbornene²²⁹ and cyclobutene²³⁰ have also been reported. In principle, such reactions could be valuable for crosslinking cell-compatible hydrogels. Additionally, inverse-

electron-demand Diels-Alder reaction has been used for cell surface protein labeling indicating their bioorthogonality.²³¹

1.5.1.2.3 Thiol-ene Reactions

Thiol-ene reactions typically involve reaction of thiols with unsaturated functional groups, such as unactivated alkenes, maleimides, acrylates, and norbornenes. Thiol-ene reactions can proceed by free radical addition, Michael-type nucleophilic addition, or a combination of these mechanisms depending on the reaction conditions. Thiol-ene reactions share many attributes with classical click reactions: thiol-ene reactions proceed rapidly under mild conditions, have high orthogonality, yield a single regioselective product, and do not yield any byproducts. Hence, reactions that proceed by either mechanism are commonly referred as thiol-ene click reactions. For a comprehensive review of thiol-ene click reactions, readers are referred to recent reviews Hoyle et al.²⁴⁵ and Kade et al.²⁴⁶

Gress et al. were the first to identify the radical-mediated thiol-ene reaction as a click reaction.²⁴⁷ This radical-mediated thiol-ene coupling has since emerged as a highly attractive reaction for hydrogel formation and modification due to its high efficiency, ease of photoinitiation, and orthogonality with numerous functional groups.^{245, 248} The reaction offers advantages, such as spatiotemporal control over crosslinking and the possibility of conducting crosslinking in the presence of cells. Rydholm et al. reported the use of thiol-acrylate mixed mode free radical photopolymerization for the formation of hydrolytically degradable PEG hydrogels.¹⁴⁹ The mechanical properties and degradation profiles were modulated with thiol concentration. Use of photoinitiation enables controlled polymerization both spatially and temporally. In addition, thiols and acrylates also can photopolymerize in absence

of a photoinitiator, which could prove useful for *in situ* crosslinking in the presence of cells.²⁴⁵

Fairbanks et al. have utilized a thiol-norbornene reaction to synthesize enzymatically degradable PEG hydrogels.¹⁵¹ Four-arm PEG was functionalized with norbornene end groups, and thiol-containing chymotrypsin- or MMP-degradable peptides were used for crosslinking. The step-growth mechanism ensured homogeneity in the resulting hydrogel network, and the crosslinking reaction did not significantly affect the viability of encapsulated hMSCs. Shih and Lin have recently shown the hydrolytic degradability of similar thiol-norbornene PEG hydrogels via ester hydrolysis under neutral or mildly basic conditions.²³² Taken together, degradation properties of these hydrogels can be modulated with the degree of crosslinking and the crosslinking peptide sequence, making them promising for tissue engineering applications in which fine control over degradation is desired.¹⁵²

Nucleophilic Michael-type addition reactions between thiols and electron deficient 'ene's, such as maleimides, methacrylates, α,β -unsaturated ketones, acrylonitrile, and crotonates, are another type of thiol-ene click reaction. Due to the mild reaction conditions, numerous hydrogels have been prepared via Michael-type addition in the presence of cells without significantly altering cell viability.^{159, 162, 233-234, 249} For example, Phelps et al. used 4-arm PEG macromers functionalized with maleimide end groups and dithiol-containing protease-cleavable peptides to form hydrogels.¹⁵⁹ The mechanical properties of the hydrogels were modulated using appropriate polymer concentrations to mimic the modulus of the native ECM. Further, these PEG hydrogels maintained cell viability during gel formation and promoted the spreading of encapsulated C2C12 cells. Kiick and coworkers have employed Michael-

type additions crosslinking the production of a variety of hydrogels. In one example, polypeptide-PEG hybrid hydrogels were produced via the reaction of the cysteine (CYS) residues of the polypeptide with vinyl sulfone (VS) functionalized PEG.²³³ Resilin-like polypeptides (RLP) were employed owing to the outstanding elastomeric properties of natural resilin for cardiovascular tissue engineering application, and to provide bioactivity to inherently inert PEG hydrogels. Depending upon the molecular weight of the RLP and the stoichiometric ratio (CYS:VS), the storage modulus of the hydrogel was modulated from $G \sim 2.6$ kPa to 12 kPa. Encapsulated AoAFs adopted a spread morphology over 7 days and maintained their viability within *in vitro* culture in these hydrogels. These recent examples demonstrate the versatility of Michael-type addition reactions to crosslink hydrogels in presence of cells for soft tissue and cardiovascular tissue engineering.

1.5.1.2.4 Oxime Reactions

Oxime reactions between aminoxy and aldehyde or ketone functional groups have recently been classified as click reactions owing to their fast reaction kinetics, orthogonality to various functional groups found in the cell microenvironment, and lack of catalyst. Recently, Grover et al. utilized oxime click reactions to synthesize cytocompatible PEG hydrogels.²³⁵ Eight-arm PEG was functionalized with aminoxy groups and crosslinked with glutaraldehyde. By varying the polymer concentration and stoichiometric ratio of aminoxy to aldehyde, hydrogel mechanical properties and water content were modulated. This click reaction permitted encapsulation of murine MSCs, maintaining cell viability and metabolic activity. However, glutaraldehyde has been observed to undergo various structural rearrangements in solution depending on the pH, influencing the reaction mechanisms and potentially influencing the ‘click’

nature of this reaction.²⁵⁰ Maynard and coworkers used oxime click reaction and CuAAC to immobilize different proteins in PEG-hydrogel constructs.²³⁶ PEG was functionalized with aminoxy and alkyne groups in order to conjugate ketoamide-myoglobin and azide-modified ubiquitin as model proteins for surface patterning. While the orthogonality of these two reactions is clear, many proteins and cells present free amines in solutions, such as hydrophilic lysines along the backbone of ECM proteins and growth factors; consequently, the specificity of the oxime reaction for orthogonal gel formation should be evaluated based on the protein and application of interest. In principle such an approach can be extended for numerous possible combinations of proteins in adjacent regions of a single plane or in multilayer constructs to modulate cell behavior.

1.5.1.2.5 Schiff Base Crosslinking Reactions

Schiff base crosslinking involves the reaction of macromolecules containing alcohol, amine, or hydrazide functionalities with aldehydes to form a hydrogel network. Due to the mild reaction conditions, this strategy has been utilized to prepare cell-compatible hydrogels for cell encapsulation and controlled drug delivery applications.^{76, 251} For example, Tan et al. synthesized N-succinyl-chitosan by introduction of succinyl groups at the N-position of the glucosamine units and also prepared hyaluronic acid with aldehyde functionality via cis-diol bond cleavage.⁷⁶ The chitosan-HA hydrogel was prepared with Schiff base linkages and exhibited a gelation time of ~1-4 minutes. The hydrogel supported cell adhesion, and encapsulated bovine articular chondrocytes were found to have regular spherical morphology, indicating the potential of this chemistry for tissue engineering applications. While a promising tool, many proteins present hydrophilic free amines (e.g., lysines) or alcohols (e.g.,

serine and tyrosine) in solution, as discussed with oxime reactions; the specificity of Schiff base crosslinking for orthogonal gel formation should be examined on based on the desired application.

1.5.2 Physically Crosslinked Hydrogels

Noncovalent interactions, such as ionic interactions, crystallization, hydrophobic interactions, electrostatic interactions, hydrogen bonding, or combinations of these, can be used for physically crosslinking macromolecules to obtain cell-compatible hydrogels.²⁵²⁻²⁵⁹ Self-assembled amphiphilic block polymers, proteins, peptides, and polypeptides typically form hydrogels via physical crosslinking.^{133, 260-263} Physically crosslinked hydrogels afford simple network formation, without the use of any potentially toxic chemical crosslinkers or initiators. In addition, their dynamic crosslink exchange, shear-thinning flow, and excellent shear recovery can be attractive for use as injectable hydrogels for therapeutic delivery.^{133, 258} However, potential limitations include insufficient mechanical strength for some applications due to the weakness of the physical interactions and limited control over their degradation rates, presenting possible challenges for controlled cell culture. Here, physical crosslinking methods used to design cell-compatible hydrogels from ‘off the shelf’ polymers (e.g., alginate, PVA), block copolymers, and peptide/proteins are discussed along with potential applications for orthogonal property control in cellular microenvironments.

Ionic interactions have been extensively used to physically crosslink commercially available polysaccharides, such as alginate and chitosan, to form hydrogels.²⁵⁵⁻²⁵⁷ The use of ionic interactions offers the possibility of biodegradation since ionic species present in cellular microenvironments can competitively bind,

leading to dissociation of the hydrogel network. Matyash et al. used physical crosslinking with divalent cations such as Ca^{2+} to prepare alginate-based hydrogels that were biocompatible and facilitated neurite outgrowth.²⁵⁷ Hydrogels can also be created by the formation of crystallites, which act as physical crosslinks for network formation. As in the example above, PVA can form a highly elastic hydrogel when subjected to a freeze-thawing process to form crystallites, and such hydrogels have been used for various bioengineering applications, such as controlled drug delivery.^{177, 252, 259} For example, Abdel-Mottaleb et al. used three cycles of freeze-thawing to prepare PVA hydrogels for topical delivery of Fluconazole within the dermal microenvironment.²⁵² The hydrogels were stable up to 6 months and effective in the topical treatment of skin infections.

Multiblock copolymers or graft copolymers can also be physically crosslinked for hydrogel formation. For example, Hunt et al. developed hydrogels with tunable physical and chemical properties using ionic coacervation upon mixing of two ABA triblock polymers, poly(allyl glycidyl ether-*b*-ethylene glycol-*b*-allyl glycidyl ether) with an oppositely charged poly(allyl glycidyl ether)-block.²⁵⁴ Non-covalent interactions of the positively charged (ammonium and guanidinium) and negatively charged (sulfonate, carboxylate) ABA triblock copolymers resulted in the formation of polymer-dense coacervate domains leading to network formation. The ionic interactions were efficient, specific, and sensitive to polymer concentration, pH and presence of salt. Such approach highlights the use of ionic interactions for preparing highly tunable and dynamic physically crosslinked hydrogels with superior mechanical properties and ease of synthesis, which can be potentially used as 3D cell scaffolds.

Polypeptides and proteins represent another important class of biocompatible polymers that can be physically crosslinked upon the formation of secondary structures (i.e., α -helix and β -sheet) that drive intermolecular association. Peptide based hydrogels have been synthesized for potential applications in controlled release, 3D cell culture, and tissue regeneration.^{133, 261, 264-267} For example, Yan et al. recently prepared β -hairpin peptide-based hydrogels via self-assembly for osteoblast encapsulation.¹³³ The effect of shear flow on the preformed, injectable β -hairpin hydrogel was investigated. The gel that was directly in contact with the syringe wall experienced a velocity gradient, while the central, plug-flow region experienced little to no shear. The study demonstrated that the shear thinning of preformed hydrogels did not significantly affect encapsulated cell viability. Further, Heilshorn and coworkers used tryptophan and proline-rich peptide domains for preparing materials mixing-induced, two component hydrogels (MITCH) for effective encapsulation of cells within 3D hydrogels.²⁶⁶ In addition to peptide-peptide interactions, specific peptide-polysaccharide interactions also can be utilized for physically crosslinking hydrogels.²⁶⁸

Kiick and coworkers employed noncovalent interactions between heparin-modified PEG polymers and a heparin-binding growth factor (VEGF) to create bioresponsive hydrogels.²⁶⁹ The VEGF-LMWH interactions were confirmed by the increase in hydrogel modulus by addition of VEGF to PEG-LMWH ($G'(\omega) > 10$ Pa in presence of VEGF, ~ 1 Pa in absence of VEGF) measured using optical tweezer microrheology. The hydrogels significantly eroded after day 4, and released approximately 80% of VEGF by day 10 in presence of VEGFR-2 (a VEGF receptor), as compared to PBS ($\sim 30\%$ release over same time period). The released VEGF was

bioactive, and the hydrogels were biocompatible, as confirmed by *in vitro* experiments (cell proliferation assay and live-dead staining respectively). VEGF-LMWH interactions were further studied for their cell-responsive nature employing two different cell types: porcine aortic endothelial (PAE) cells overexpressing VEGFR-2 and PAE cells that were not equipped with VEGFR-2 transcript.²⁷⁰ The hydrogels were eroded by day 4, and VEGF release was greater in presence of VEGFR-2 expressing cells. Such physically crosslinked hydrogels offer novel targeting strategies depending upon cell surface receptor-ligand interactions and could be used for sustained and targeted delivery of VEGF to promote angiogenesis.

1.6 Engineering Degradation

Many cellular processes are influenced by spatiotemporal changes in the cell microenvironment. In hydrogel microenvironments, temporal control of matrix properties is easily achieved through selective incorporation of degradable moieties, enabling examination of how property changes influence cell function and fate. Additionally, as discussed in earlier, controlled degradation of hydrogels is highly desirable for biomedical applications, including soft tissue engineering to promote cell secretory properties and enable tissue elaboration and therapeutic delivery to allow tunable, controlled release locally or systemically. Degradation can be achieved by forming hydrogels with degradable polymer backbones, degradable crosslinks, degradable pendant groups, or reversible non-covalent interactions. This section will focus on degradation kinetics and modes of degradation.

1.6.1.1 Controlling Degradation Rates

The desired rate of network degradation is dictated by the final application of cell-compatible hydrogels. For controlled release of bioactive molecules, rapid degradation can lead to an initial burst or rapid release of cargo, generating large bioactive molecule concentrations which may be desirable, out of a biologically-relevant range, or even toxic depending on the application. For tissue engineering scaffolds and controlled cell culture applications, degradation affects the hydrogel crosslink density and mechanics and hence cell behavior,²⁷¹ where ideally the rate of degradation should match the rate of new tissue formation. To control degradation and the temporal properties of the cell microenvironment, hydrogel degradation rates can be tuned by careful selection of network chemistries, degradation kinetics, and network connectivity, which influence crosslink density and mass loss. A brief overview of the general ‘handles’ for modulating degradation is provided here.

Degradation rates are influenced by the chemical nature of the polymer network backbone chain. The number and type of degradable linkages and the local environment surrounding the degradable moieties alter cleavage kinetics. For example, groups present along the polymer backbone or its side chains such as esters, succinimide–thioether linkages, and nitrobenzyl ethers can be degraded via hydrolytic,²⁷²⁻²⁷⁴ via retro-Michael reaction^{249, 275} and photolytic^{145, 276-277} degradation mechanisms, respectively. The covalent bond cleavage kinetics will influence the overall rate of hydrogel degradation. For example, Jo et al. studied the effect of adjacent charged amino acids on the hydrolysis rate of ester bonds and the resulting degradation rate of PEG acrylates modified with cysteine-containing oligopeptides.²⁷⁸ The positively charged arginine caused a six-fold increase in ester hydrolysis, as

compared to negatively charged aspartic acid, and similarly release of covalently linked bovine serum albumin (BSA) was influenced by the rate of degradation.

Hydrogel degradation rates can be tuned by optimizing network connectivity and mesh size. Increased crosslinking density typically leads to smaller mesh size, increased modulus, and slower degradation, owing to an increased number of cleavable bonds that must be broken for network mass loss and erosion.³¹ Decreased mesh size also can limit accessibility of the degradable moiety within the hydrogel to larger molecules, such as enzymes, owing to a reduced diffusion rate.¹⁶⁴ In such cases, release of cargo molecules will be slower as well due to hindered diffusion.

Encapsulated cells, cell secreted enzymes, and growth media can influence degradation rates for chemically or physically crosslinked hydrogels.²⁷⁹⁻²⁸⁰ Additionally, the degradation products can influence cell proliferation and differentiation. For instance, Lampe et al. studied the effect of degradable macromer content on neural cell metabolic activity, proliferation and differentiation using PEG and poly(lactic acid) copolymer based hydrogels.²⁸¹ It was found that the neural cell survival, proliferation and metabolic functions immediately after encapsulation were improved in hydrogels prepared with increasing degradable macromer content, suggesting a beneficial impact of lactic acid released during degradation.

Degradation rates can be investigated using bulk property measurements, such as the *in vitro* monitoring of hydrogel swelling, mass loss, mechanical properties, or solubilization or the *in vivo* imaging and analysis of implanted materials. Hydrogel degradation rate also can be studied by monitoring direct bond cleavage or monitoring degradation products (i.e., uronic acid release due to HA degradation).²⁸² Methods for

assessing hydrogel degradation rates are well covered within a recent review by Peppas et al.³¹

1.6.1.2 Modes of Degradation

Hydrogels can degrade through surface erosion, bulk degradation, or a combination of the two depending upon the type and number of degradable linkages. At high crosslinking density, restricted diffusion of water and enzyme may preferentially lead to surface erosion. Bulk degradation, typically observed in hydrogels owing to their high water content and relatively high diffusivity, occurs when cleavable groups present throughout the bulk as well as on surface degrade simultaneously.

Physically crosslinked hydrogels can degrade by processes that reverse the gelation mechanism or disturb the non-covalent interactions of the crosslinks. For example, calcium crosslinked alginate hydrogels are known to degrade *in vitro* due to ion-exchange processes between Ca^{+2} ions, present within hydrogel network, and Na^{+} ions of buffered solutions.¹²⁰ Further, stereocomplexed hydrogels formed using amphiphilic copolymers of PLA and PEG can be degraded by disruption of the aggregate packing.²⁸³

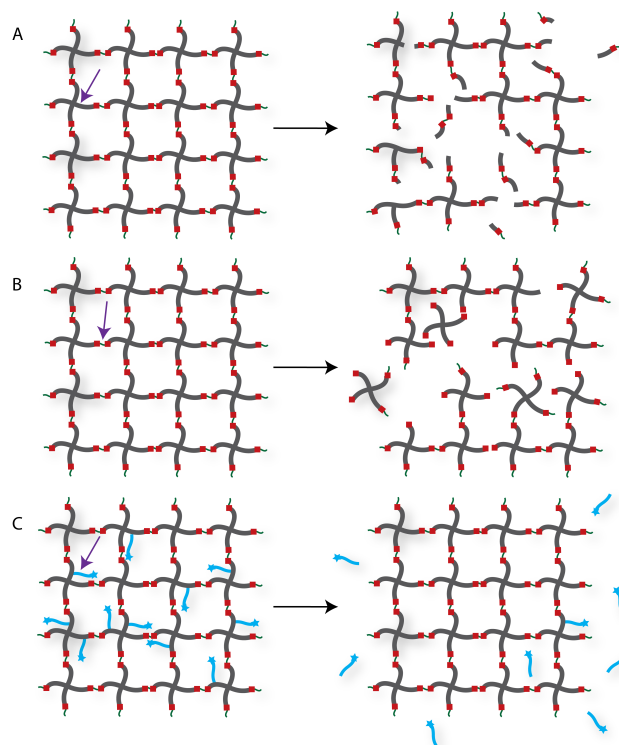


Figure 1.5 Degradation strategies. Chemically crosslinked hydrogels can be degraded via cleavage of (A) the polymer backbone, (B) crosslinker or (C) pendant group depending upon the chemistry used for hydrogel formation (choice of polymer, crosslinker, and crosslinking mechanism).

Chemically crosslinked hydrogels can be degraded via several mechanisms, including cleavage of the backbone chain, crosslinker, or pendant groups (**Fig. 1.5**). Hydrogels prepared using polymers with degradable functional groups within the backbone chain are degraded into smaller segments of the original polymer depending upon the location of the degradable groups. A large number of hydrogels include degradable crosslinkers, such as peptides, proteins, or polymers that contain chemically labile moieties. Such hydrogel networks degrade into high molecular weight polymer backbone chains and degradation products from the crosslinker.

Polymer chains also can be end-capped with degradable functional groups followed by the addition of reactive functionalities, thus creating crosslinkable degradable macromers. After crosslinking and degradation, the hydrogel network is degraded into the components that comprise the polymer network backbone; for example, in the case of PEG-PLA diacrylate hydrogels, the degradation products are PEG, polyacrylate, and lactic acid. Chemically crosslinked hydrogels often are degraded through hydrolysis, enzymatic cleavage, reversible click reactions, or photolytic degradation (**Fig. 1.6**). To engineer hydrogel degradability, it is essential to understand the types of cleavable groups and modes of degradation, their byproducts, and factors affecting degradation rates. These modes of degradation are briefly discussed below with respect to their use in cell-compatible hydrogels.

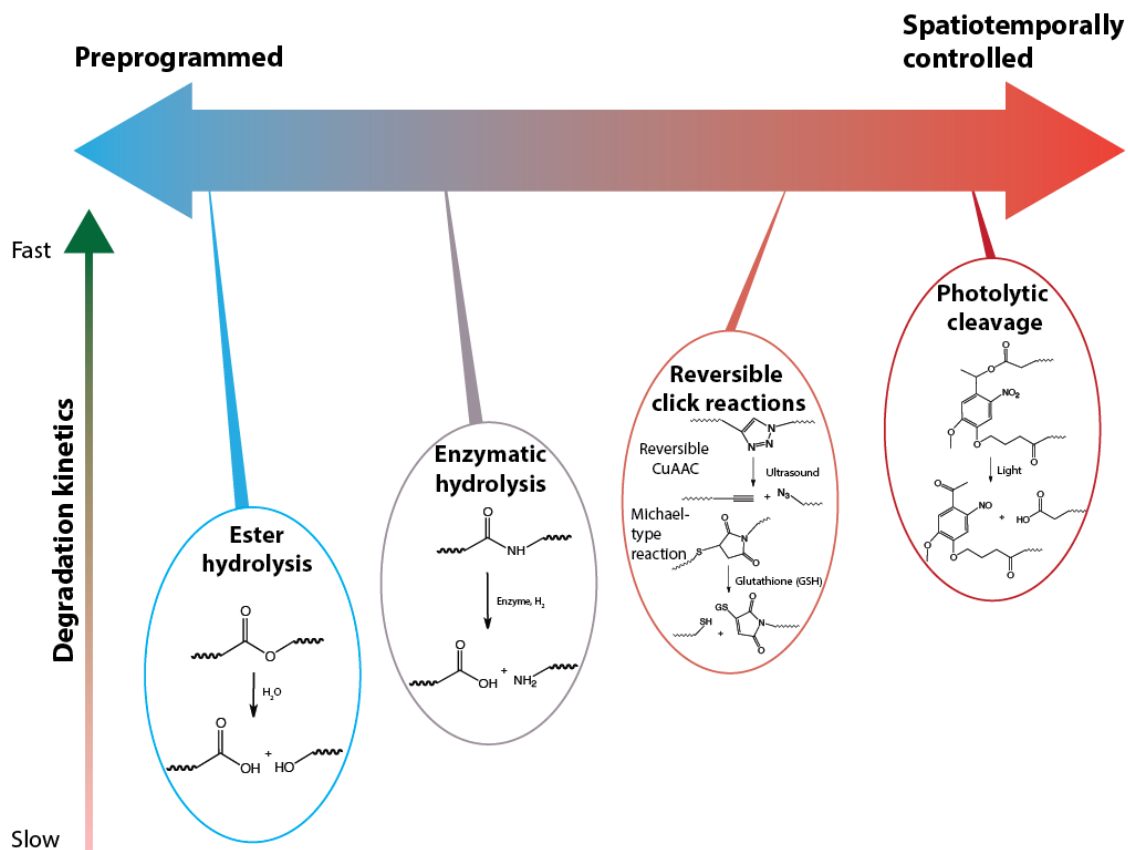


Figure 1.6 Selection of labile groups to control degradation rates. Chemically crosslinked hydrogels can be engineered to degrade at a preprogrammed, cell-dictated, or user-defined rate with varying degrees of spatiotemporal control

1.6.1.2.1 Enzymatic Degradation

Cell-mediated enzymatic cleavage is of particular importance for the degradation of hydrogels composed of natural polymers, proteins, or peptide linkages. For instance, Kane and coworkers incorporated alginate-loaded PLGA microspheres in an alginate hydrogel.²⁸⁴ The rate of hydrogel degradation was tuned by the activity of alginate released from microspheres, as mammalian cells do not produce alginate.

Further, these degradable alginate hydrogels enhanced neural progenitor cell expansion rates *in vitro* as compared to control non-degradable hydrogels.

Enzymatically degradable hydrogels also have been utilized for targeted drug delivery since the concentration of enzyme is dependent upon cell and tissue types, enabling local triggered drug release. For instance, the concentration of hyaluronidase is known to be substantially higher in various carcinomas,²⁸⁵ and enzymatically-degradable HA-based hydrogels can be used as site-specific therapeutic delivery vehicles. HA-based hydrogels degrade in the presence of hyaluronidase, a family of enzymes that catalyze the hydrolysis of C-O, C-N and C-C bonds. Lee et al. prepared a HA-tyramine based injectable hydrogel for protein delivery in which the release of the cargo molecule was partially dependent on hydrogel degradation via hyaluronidase.²⁸² Approximately 70% of the activity of released lysozyme, a model cargo protein, was retained *in vitro*. In principle, such an approach can be used for sustained, local therapeutic protein release to inhibit tumor growth.

Parameters such as pH, local ionic strength, enzyme concentration, and temperature may change degradation profiles due to their influence on the specificity of enzyme-substrate complex formation. The crosslinking density and pore size of the hydrogel also can influence the hydrogel degradation rate. For instance, Aimetti et al. reported use of a human neutrophil elastase (HNE) sensitive peptide for crosslinking PEG hydrogels using thiol-ene photopolymerization.¹⁶⁴ The gels were engineered to degrade via surface erosion by limiting diffusion of HNE inside the hydrogel network via a high crosslink density and small mesh size; upon erosion, a physically entrapped protein was released. Surface degradation was investigated using mass loss and swelling ratio measurements, and the release of the model encapsulated protein, BSA,

was modulated by changing peptide k_{cat} values with amino acid substitutions, HNE concentration, and peptide crosslinker concentration.

Incorporation of protein- or peptide-based linkages, which are susceptible to proteases as noted in the example above, is a powerful way to control hydrogel degradation both synthetically and *in situ*.^{152, 164, 286-288} For instance, Patterson and Hubbell prepared PEG hydrogels with protease-sensitive peptides through Michael-type addition reactions.²⁸⁶ When incubated with MMP1 and MMP2, the hydrogel samples degraded via enzymatic hydrolysis with variable rates depending upon the peptide sequence used (MMP1 $k_{cat} \sim 0.1$ to 7.9 sec^{-1} , MMP2 $\sim k_{cat} 0.30$ to 5.6 sec^{-1}). Encapsulated fibroblasts showed increased spreading and proliferation when cultured in three-dimensions within hydrogels crosslinked using more rapidly degrading peptides. The results highlighted the possibility of engineering hydrogel degradability in response to specific MMPs that are overexpressed in relevant cell type(s) of interest. For example, endothelial cells predominantly express MMP-2 and MMP-9,²⁸⁹ and thus MMP-2 and MMP-9 sensitive hydrogels can be used to promote endothelial cell invasion for angiogenesis. Further, enzymatically degradable hydrogels have been employed for wound healing²⁹⁰⁻²⁹¹ and bone regeneration.^{286, 292}

1.6.1.2.2 Hydrolytic Degradation

A myriad of synthetic hydrogels have been engineered to degrade through hydrolysis of ester linkages within the network backbone or crosslinker, where ester cleavage produces a carboxylic acid and an alcohol. In hydrolytically degradable hydrogels, crosslinking density, local pH, and polymer network chemistry, including backbone molecular weight, crystallinity, and hydrophobicity, influence the degradation rate. Recently, Zhang et al. reported use of a biodegradable triblock

copolymer poly(ϵ -caprolactone-co-lactide)-*b*-poly(ethylene glycol)-*b*-poly(ϵ -caprolactone-co-lactide) hydrogel as a post-operative intestinal adhesion barrier.²⁷² The hydrogel retained its integrity for approximately 6 weeks *in vivo* and eventually degraded by ester hydrolysis without significant cytotoxicity. Patenaude and Hoare synthesized hydrolytically degradable thermoresponsive hydrogel using aldehyde and hydrazide functionalized PNIPAAm.²⁹³ The rate of hydrolysis of the hydrazone linkages in acidic microenvironment varied from 2 to 6 hours, leading to complete degradation of cell-compatible hydrogels, and extrapolation of kinetic data predicted degradation on the order of several months under physiological conditions.

1.6.1.2.3 Reversible Click Reactions

Click chemistries offer several advantages in hydrogel network formation as discussed earlier; however, the application of reversible click reactions as a simple approach to engineer degradability near physiological conditions has been restricted. Baldwin and Kiick recently reported use of a retro click reaction to engineer the degradation rates of heparin-functionalized hydrogels prepared using thiol-based Michael-type addition reactions between multifunctional PEG thiols and maleimide-modified heparin.^{249, 275} Differences in the pK_a of the mercaptoacids used to functionalize PEG led to differences in hydrogel degradation rate within a reducing environment (i.e., in the presence of glutathione), owing to differential retro Michael-type cleavage rates of the succinimide–thioether linkage; the more rapid equilibration of an aryl thioether succinimide product with its reactant aryl-thiol modified PEGs and maleimide-functionalized heparin resulted in the capture of the liberated maleimide by the exogenous glutathione (GSH). The choice of mercaptoacid also was used to control the release of bioactive molecules *in vitro*. The intracellular concentration of

GSH, a tripeptide of glutamic acid, cysteine, and glycine, is known to be significantly higher than the extracellular concentration,²⁹⁴ and the GSH content of carcinoma cells also is elevated, owing to the role of GSH in regulating mutagenic mechanisms, DNA synthesis, and growth.²⁹⁵⁻²⁹⁶ Since the rate of degradation and release of cargo molecules from these gels depend upon the local reducing environment, this degradation strategy is promising for intracellular or site-specific controlled drug delivery.

Another exciting class of reversible click reactions is retro Diels-Alder cycloreversion, which can be an attractive tool to modulate hydrogel degradation. Early examples of incorporating this reversible reaction chemistry within the crosslinks of hydrogels exhibited significant network degradation at temperatures above 60 °C, potentially limiting their translation into controlled cell microenvironments.^{242, 297} However, recent work incorporating furan-functionalized pendant peptides within PEG-maleimide-based hydrogels demonstrates controlled release of these peptide tethers under physiological conditions.²⁹⁸ While higher temperatures (up to 80°C) increased release, physiological temperature was adequate for significant tether release (~ 40%), and dexamethasone released by this mechanism was shown to promote osteogenic differentiation of encapsulated hMSCs.²⁹⁸ This class of reversible click reactions is promising for predictable, tunable control of cell microenvironment properties.

1.6.1.2.4 Light-mediated Degradation

Photolabile monomers and polymers engineered to cleave under cytocompatible irradiation conditions allow spatiotemporal control of hydrogel degradation and *in situ* property tuning.²⁹⁹ Anseth and coworkers developed

photodegradable hydrogels for cell culture by creating an acrylated nitrobenzyl ether-derived moiety with a pendant carboxylic acid that could be attached to poly(ethylene glycol) (PEG)-bis-amine or amine-terminated peptides to create a photocleavable cross-linking diacrylate macromer (PEG-diPDA) or a photoreleasable pendant peptide tether, respectively.²⁰⁷ The PEG-diPDA hydrogels degraded when irradiated with cytocompatible doses of long wavelength UV, visible, or two-photon IR light (365, 405, and 740 nm, respectively), enabling precise control over hydrogel degradation profiles *in situ*. Hydrogel photodegradation and the corresponding change in crosslink density led to an increase in the mesh size and decrease in the polymer density surrounding the cells, promoting encapsulated hMSC spreading as compared to non-irradiated control hydrogels.²⁷⁶ In addition, photolabile RGDS containing hydrogels were found to influence the integrin expression on the surface of cells, where temporal modulation enhanced hMSC differentiation. Griffin and Kasko recently incorporated *o*-nitrobenzyl groups with varying cleavage kinetics within the backbone of PEG hydrogels (Fig. 13).²⁷⁷ The hydrogels were formed using redox polymerization in presence of hMSCs and were selectively photodegraded to release specific stem cell population. Such an approach can be used for cell encapsulation and on-demand release of therapeutic cells for regenerative medicine and wound healing applications.

In a complementary light-mediated approach, Anseth and coworkers used photoinitiators to degrade disulfide-bonded PEG hydrogels.¹⁴⁵ When irradiated, the photoinitiator created free radicals through heterolytic decomposition, attacking the disulfide bonds and resulting in hydrogel degradation. In principle, this photoinitiated disulfide bond degradation could be conducted in the presence of cells in conjunction with cytocompatible disulfide gel formation.³⁰⁰ Almutairi and coworkers recently

reported synthesis of polymer containing a pendant photocleavable group, 4-bromo7-hydroxycoumarin (Bhc).³⁰¹ Upon photolysis with cell and tissue compatible near infrared irradiation, the polymer undergoes a triggered cascade of cyclization reactions, leading to degradation of the polymer backbone with potential applications for controlled release *in vivo* within deep tissues.

1.7 Delivery of Bioactive Cargo in Hydrogels

1.7.1 Small Molecular Drug and Therapeutic Peptide Delivery

PEG hydrogels have been developed to control the release of small molecular drugs by rational design and control of hydrogel mesh size.³⁰²⁻³⁰⁴ However, controlled delivery of small cargo molecules using PEG hydrogels faces two major challenges: maintaining precise control over the mesh size during equilibrium swelling and incorporating hydrophobic drugs within highly hydrophilic hydrogels. In this section, we will highlight recent advances in material chemistry for the delivery of small molecular weight drugs and therapeutic peptides.

Swelling of the hydrogels has been controlled by careful selection of macromers. For example, the hydrophilicity of PEG is increased by increasing the number of repeating units of ethylene glycol (e.g., increasing chain length). However, to control the swelling of hydrogels and thus control hydrogel mesh size, an optimum balance between hydrophilic and hydrophobic content is needed. By selecting low molecular weight macromer precursors, hydrogel syneresis can be achieved, a process by which water is lost after formation reducing the hydrogel mesh size. With this approach, Langer and coworkers reported the synthesis of PEG-based thiol-ene hydrogels that can undergo syneresis in physiological conditions, reducing gel volume

by ~40%. They utilized these materials for the controlled release of methylprednisolone sodium succinate (MPSS), a glucocorticoid prodrug with anti-inflammatory and immunosuppressant properties.³⁰² Hydrogels were prepared using acrylate end-functionalized PEG and a commercially available trifunctional thiol macromer (ethoxylated trimethylolpropane tri-3-mercaptopropionate). Incorporation of MPSS within the hydrogel suppressed the rate of hydrolysis of the ester linkage between methylprednisolone and succinate groups ($k = 3.12 \pm 0.10 \times 10^{-3} \text{ h}^{-1}$ encapsulated as compared to $k = 5.98 \pm 0.50 \times 10^{-3} \text{ h}^{-1}$ in PBS), demonstrating how hydrogels can increase therapeutic stability. Sustained release of MPSS was achieved over ~20 days independent of the initial drug loading concentration, providing an opportunity to change the drug concentration based on individual patients' needs without changing the drug carrier volume.

Incorporation of small molecular hydrophobic drugs within hydrogels presents additional challenges owing to their limited water solubility. Introduction of hydrophobic units within the hydrogel network have been used to improve drug-loading efficiency and influence the swelling behavior of the hydrogels. For example, Harth and coworkers reported polycarbonate-based thiol-ene hydrogels for sustained delivery of paclitaxel, a chemotherapeutic drug used to treat ovarian and breast cancer.³⁰³ To incorporate the hydrophobic drug and optimize its residence time in the hydrogel-based drug carrier, polycarbonate was incorporated within the hydrogel as an additional hydrophobic backbone component. A three component system (polycarbonate, poly(ethylene oxide), and semi-branched polyglycidols) was used to optimize the balance between hydrophilicity and hydrophobicity, controlling hydrogel swelling behavior and drug release kinetics. Hydrogels that undergo ester hydrolysis

were formed using light-mediated thiol–ene reactions by reacting allyl-functionalized polycarbonates with linear thiol-functionalized poly(ethylene oxide). Paclitaxel was encapsulated within the network during hydrogel formation with high loading efficiency (>98%), and release of ~7% to ~30% of the drug was observed over 7 days depending on initial hydrogel swelling.

As noted earlier, control over release kinetics also can be achieved by covalently conjugating the drug molecule to the hydrogel backbone. The rate of release of cargo molecules in such cases depends on the rate of degradation of the covalent linkage between the drug and the network. Covalently-linked drug molecules can have preprogrammed drug release kinetics (e.g., different numbers of hydrolytically degradable ester linkages with known rates of hydrolysis)³⁰⁵⁻³⁰⁶ or can cleave in response to the local microenvironment; both approaches have been used in drug delivery systems. For example, Anseth and coworkers reported the use of thiol–ene click hydrogels for cell-mediated delivery of dexamethasone (Dex), an anti-inflammatory and immunosuppressant steroid drug (**Fig. 1.7**).³⁰⁴ Dex was covalently linked to a peptide crosslinker (KCGPQGIAGQCK), which was susceptible to enzymatic cleavage by MMPs secreted by cells within tissues. The hydrogels were formed by reacting norbornene end-functionalized PEG with the thiol groups of MMP-degradable peptide crosslinkers and the release of Dex was controlled by cleavage of tethers. Since Dex is known to promote osteogenic differentiation of human mesenchymal stem cells (hMSCs), released Dex bioactivity was monitored by measuring hMSC alkaline phosphatase (ALP) activity, a marker of early osteogenic differentiation.³⁰⁷ hMSCs encapsulated within hydrogels containing Dex-conjugated MMP-degradable peptide showed a significant increase in ALP activity compared to

hydrogels containing Dex conjugated to a non-degradable linker, demonstrating both the release and bioactivity of Dex. While such an approach can be translated to deliver other small molecules using thiol–ene hydrogels, the biological activity of drugs or released drug fragments may change substantially after conjugation and release from the network.³⁰⁸ For each drug of interest, tests must be run to ensure the conjugated and released drug retains its desired biological activity.

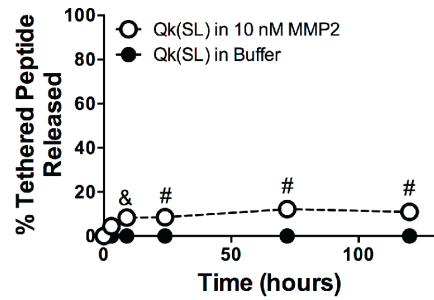
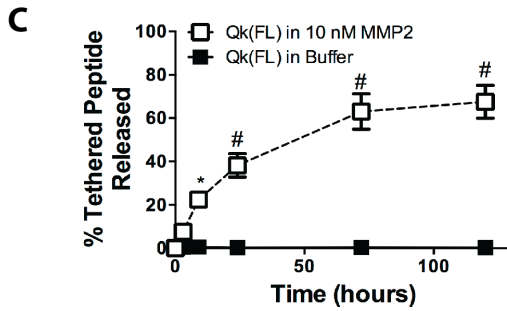
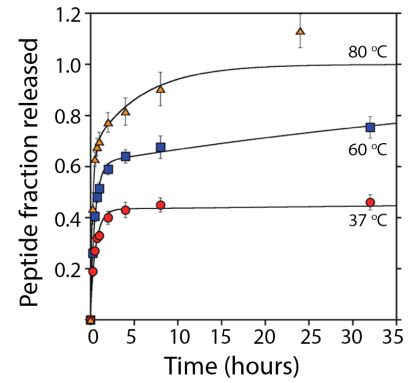
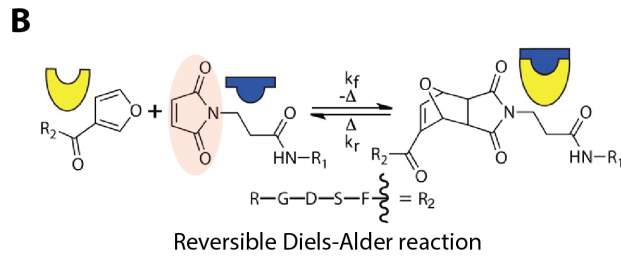
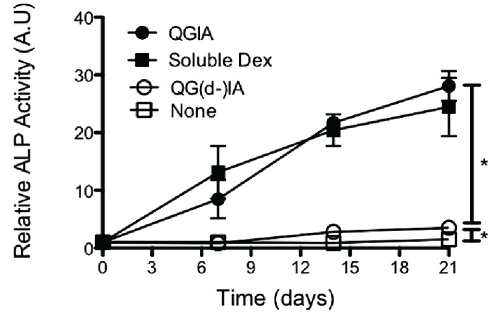
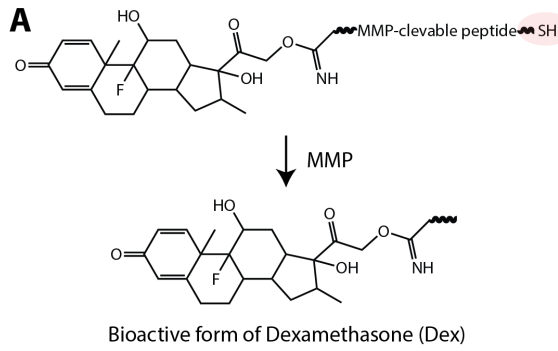


Figure 1.7 Controlled release of small molecular weight drugs and therapeutic peptides. (A) Dexamethasone (Dex) was covalently conjugated to the backbone of the hydrogel network using a thiol-functionalized MMP-sensitive peptide linker (KCGPQG↓IAGQCK). In the presence of cell-secreted MMP, the dexamethasone fragment (closed circle) was released and bioactive as demonstrated by enhanced alkaline phosphate (ALP) activity of encapsulated stem cells compared to the negative control (open circle, peptide sequence with substitution of *D*-isoleucine [QG(d-I)] making the linker MMP-insensitive and non-degradable). Adapted from Yang *et al.*³⁰⁴ with permission from Elsevier publishing. Copyright (2012). (B) Furan-functionalized peptide (integrin-binding RGDS) was incorporated in thiol-maleimide hydrogels by a Diels-Alder reaction with excess maleimides. The release of peptide was controlled by a retro Diels-Alder reaction, which increases in rate with elevated temperature as demonstrated by the increasing fraction of peptide released at 37, 60, and 80 °C. Adapted from Koehler *et al.*³⁰⁹ with permission from ACS publishing. Copyright (2013). (C) Toward promoting angiogenesis, a vascular endothelial growth factor mimetic peptide (Qk) was tethered to a non-degradable thiol-ene hydrogel using an MMP-cleavage linker, and temporal control of Qk release was achieved *in vitro* and *in vivo* by changing the MMP2-susceptible peptide tether (FL = Qk-PES↓LRAG-C-G, SL = Qk-VPLS↓LYSG-C-G). * $p < 0.05$; &: $p < 0.01$, #: $p < 0.0001$ compared to buffer alone for each respective time point. Adapted from van Hove *et al.*³¹⁰ with permission from Wiley publishing. Copyright (2015).

In the last decade, with significant advances in solid-phase synthesis and recombinant DNA technology, FDA-approved, peptide-based drugs have gained substantial importance for the treatment of human diseases.³¹¹⁻³¹² For example, peptide formulations such as cilengitide, taltirelin hydrate, and ziconotide acetate are in clinical trials for treating diseases associated with the central nervous system (i.e., spinocerebellar degeneration, ataxia, and severe chronic pain).³¹³ Thiol-ene hydrogels have been used to deliver therapeutic peptides owing to their ability to maintain the bioactivity of cargo peptides and the ease of peptide encapsulation by facile crosslinking chemistries.^{309, 314} Recently, Wang *et al.* demonstrated the release of a

fluorescently-labeled library of different model peptide.³¹⁴ Hydrogels were formed using a combination of a thiol-containing protein (ubiquitin-like domain tetramer of SATB1 with cysteine residues) and PEG-maleimide via a Michael-type crosslinking reaction. Controlled release of model peptide drugs (~50 to 80% release) was achieved within approximately 24 hours, depending on the protein-peptide affinity interactions (i.e., higher binding affinity peptide released more slowly). In another example, Koehler *et al.* reported the release of a covalently-linked peptide (integrin-binding RGDS) by reversible Diels-Alder reactions (**Fig. 1.7B**).³⁰⁹ PEG-based hydrogels were formed using thiol-maleimide chemistry, and temperature sensitive Diels-Alder linkages were used to conjugate the bioactive peptide functionalized with furan groups by reaction with excess maleimide groups. The release rate of peptide was tuned by incorporation of different numbers of maleimide tethering sites (varied by incorporation of the monofunctional thiol) in the hydrogels: ~45 to 60% of peptide was released by 35 hours depending on the number of maleimide tethering sites, and the percent release could be further varied with changes in local temperature (i.e., ~40% cargo released at 37°C and ~70% cargo released at 60°C). In another example, Benoit and coworkers reported thiol-ene hydrogels to control release of Qk, a proangiogenic peptide mimic of vascular endothelial growth factor using tissue-specific enzymatic activity.³¹⁰ Qk was tethered to the hydrogel using enzymatically cleavable linkers, and variation in k_{cat}/K_M provided temporal control over release kinetics (i.e., ~70% release was achieved using the sequence [Qk-PESLRAG-C-G] whereas only ~15% release was achieved using the sequence [Qk-VPLSLYSG-C-G], **Fig. 1.7C**). These examples highlight approaches and methods for the design of hydrogels to deliver peptide-based therapeutics.

1.7.2 Therapeutic Protein Delivery

Protein therapeutics are in development to treat cancer, autoimmune diseases, protein deficiencies, and infectious diseases.³¹⁵ The complexity of proteins allows them to complete tasks that small molecules cannot easily achieve, such as catalyzing an enzymatic reaction or inhibiting a biological process in a specific manner.⁴¹ For example, the antibody rituximab binds specifically to CD20, a cell-surface glycoprotein on B-cells, and has been approved to treat non-Hodgkin's lymphoma.³¹⁶ However, their complexity leads to additional challenges, as protein structure must be maintained and proteolytic degradation must be avoided until the protein achieves the desired therapeutic effect either locally or systemically.⁴¹ Controlled release of therapeutic proteins from hydrogels offers the potential to maintain potent concentrations over extended periods of time and to limit premature degradation before the therapeutic reaches its desired target.³¹⁷

As with small molecule drugs, the mesh size of hydrogel-based delivery vehicles is an important consideration; however, the mesh sizes of typical synthetic hydrogels and the size of therapeutic proteins are often on the same scale (approximately 1-10 nm). As a result, the protein often is encapsulated within the network and released by diffusion. If the protein size is smaller than the mesh size of the hydrogel, the protein can diffuse out of the hydrogel, usually at a slower rate than protein diffusion through water (and slower than uninhibited diffusion throughout the body). If the protein size is larger than the mesh size of the hydrogel, the protein is trapped until released by hydrogel degradation or a stimulus-triggered change in mesh size. Both approaches have proven useful depending on the desired time scale for therapeutic release as noted in examples below. In many cases, model proteins of different sizes, such as lysozyme (14 kDa) or BSA (66 kDa), are used. While these are

useful and inexpensive models for protein release experiments, it is important to note that the bioactivity of therapeutic proteins might be compromised during loading or release from hydrogel delivery vehicles, and the compatibility of the hydrogel with a specific therapeutic protein of interest needs to be verified for each application.

PEG-based hydrogels are some of the most common types used in controlled release of therapeutic proteins. For example, Buwalda *et al.* crosslinked 8-arm PEG-poly(L-lactide)-acrylate block copolymers with multifunctional PEG-thiols by Michael addition for encapsulation and release of the model proteins lysozyme and albumin.³¹⁸ Protein diffusion out of the hydrogel was slowed relative to diffusion in water and took place on time scales of days to weeks, demonstrating controlled release. Zustiak and Leach used an entirely PEG-based network formed by thiol-vinyl sulfone chemistry with hydrolytically degradable ester bonds for controlled protein release.³¹⁹ Lysozyme encapsulated in the hydrogel diffused out within 18 hours, but the largest protein encapsulated, immunoglobulin, remained in the gel until complete hydrogel degradation at one week (**Fig. 1.8**). In both of these cases, the diffusion rate was tuned by changing the number of ester bonds present in the network, affecting the degradation rate of the hydrogel and protein release.

While Michael-type reactions have enabled successful encapsulation and release of model proteins, gel formation in these systems begins upon mixing of all components. In contrast, photopolymerization allows for spatial and temporal control of polymerization, enabling the use of photolithography and micromolding for the formation of macroscale hydrogel geometries and microscale particles.³²⁰ Impellitteri *et al.* used a photopolymerized PEG-based thiol-norbornene reaction to encapsulate vascular endothelial growth factor (VEGF) in hydrogel microspheres containing a

peptide mimic of the VEGF receptor (RTELNVGIDFNWEYP), serving as an affinity binding sequence that mediated VEGF release.³²¹⁻³²² The microspheres were formed in a water-in-water emulsion: one phase contained 4-arm PEG-norbornene, PEG-dithiol, and 0.5% w/w of the photoinitiator Irgacure 2959; the other phase contained 40 kDa dextran. The PEG macromers were crosslinked into stable microspheres by irradiation (low dose of UV light, 4 mW/cm² for 8 minutes). Released VEGF was shown to be bioactive by its enhancement of human umbilical vein endothelial cell proliferation *in vitro*. (Fig. 1.8).

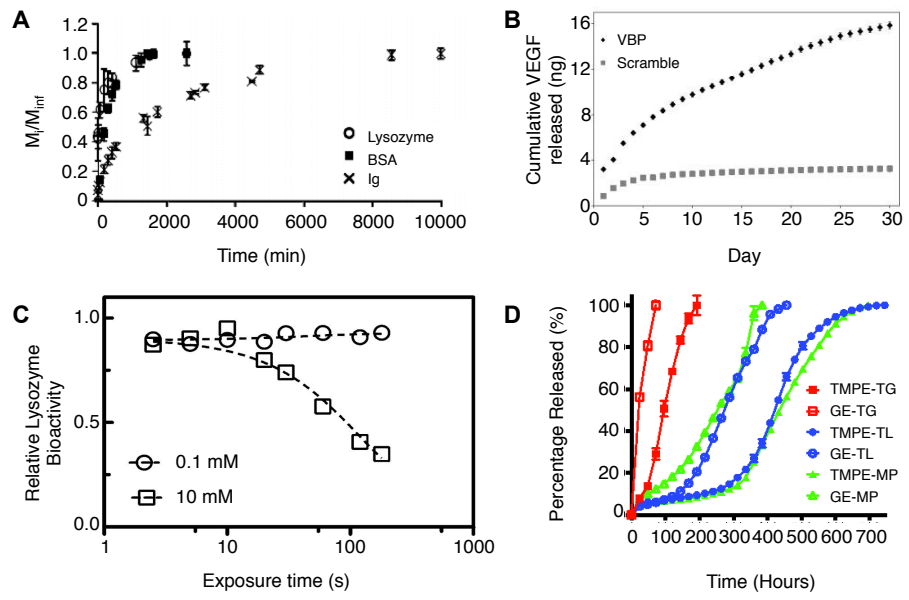


Figure 1.8. Controlled release of therapeutic proteins (A) Proteins of various sizes were released from PEG-based hydrolytically-degradable thiol-vinyl sulfone hydrogels. Lysozyme, the smallest protein, was released in less than 24 hours, whereas Ig, the largest protein, was released upon complete gel degradation. Adapted from Zustiak and Leach³¹⁹ with permission from Wiley. (B) The growth factor VEGF was loaded into microspheres containing a peptide-based ligand derived from VEGF receptor 2 (VBP). VEGF was bound and released from the microspheres containing the VEGF receptor mimic, whereas microspheres containing a scrambled inert sequence exhibited a low level of release corresponding with random diffusion of VEGF into and out of the microspheres. Adapted from Impellitteri *et al.*³²¹ with permission from Elsevier. (C) Lysozyme was exposed to free radicals in conditions mimicking that of photoinitiated thiol-ene hydrogel polymerization. Higher radical concentrations would result from higher photoinitiator concentrations (10 mM), as compared to lower photoinitiator concentrations (0.1 mM), and from increased exposure time to light (plotted on x-axis). Increasing radical exposure decreased the bioactivity of lysozyme, indicating the importance of minimizing protein exposure to free radicals during gel formation. Bioactivity was increased upon introduction of reactive thiol and norbornene functional groups, supporting the protective effect of thiol-ene chemistry during hydrogel formation relative to acrylate homopolymerization (data not shown). Adapted from McCall and Anseth³²³ with permission from ACS Publishing. (D) FITC-labeled ovalbumin was released from thiol-functionalized ethoxylated polyol ester/PEG-diacrylate based hydrogels of different compositions. By changing the ratio of the macromers within the hydrogel, the rate of release and the overall release profiles were tuned over a wide range of timescales. Adapted from Langer and coworkers³²⁴ with permission from Wiley.

McCall and Anseth compared the efficacy of photoinitiated thiol-norbornene or acrylate only reactions for the encapsulation of a model protein lysozyme within PEG-based hydrogels.³²³ At equal functional group concentrations (40 mM acrylate or 40 mM norbornene with 40 mM thiol) and the same photoinitiator concentration (1 mM LAP, 10 mW/cm² at 365 nm for <5 min), the rapid thiol-norbornene system maintained a higher level of lysozyme activity after encapsulation and release than the

slower (oxygen-inhibited) acrylate-based chain-growth system. This result was attributed to the protective effect of thiol–ene chemistry during hydrogel formation, which may limit the overall protein exposure to damaging free radicals in the gel-forming solution compared to acrylate homopolymerization (**Fig. 1.8**).

Hydrogel degradation rates can be engineered to respond to microenvironment conditions (e.g., enzymes, reducing conditions, pH), allowing triggered release of a protein therapeutic. For example, PEG-based hydrogels formed by thiol-norbornene photopolymerization with cysteine-functionalized, enzyme-sensitive peptide crosslinks were developed and used for protein release by Anseth and coworkers.¹⁶⁴ The crosslinks contained a sequence (CGAAPVRGGGGC) that degrades in the presence of human neutrophil elastase (HNE), an enzyme upregulated at the site of inflammatory disease and injury.³²⁵ The model protein BSA was released from these hydrogels upon the application of human neutrophil elastase.¹⁶⁴ Notably, no protein release was observed in the absence of the enzyme, demonstrating that the protein release was controlled by the degradation of the hydrogel in the presence of HNE.

In an alternative approach to localized protein release, Kharkar *et al.* formed PEG-based hydrogels sensitive to glutathione, which is elevated in tumors, using thiol-maleimide chemistry.³²⁶⁻³²⁷ Hydrogels encapsulating BSA were formed with PEG-maleimide and PEG functionalized with different thiols that influenced hydrogel degradability. Approximately 40% of BSA was released from all compositions as a result of initial swelling; however, when the thiol-containing macromer contained an electron-withdrawing aryl group (PEG-4-mercaptophenylacetic acid), an additional 50% of the BSA was released in the presence of 10 mM glutathione over the course of 7 days. Negligible additional release was observed over 7 days for the compositions

that were glutathione-insensitive, collectively demonstrating promise for tailoring protein release within tumor microenvironments.

While PEG-based materials are often commercially available and a number of them are FDA-approved,³²⁸ there is a limit to the tunability one can achieve simply by varying the end groups and functionality of PEG-based monomers. Langer and coworkers synthesized a library of thiol-functionalized ethoxylated polyol esters and reacted them with PEG-diacrylate to form a library of hydrogels with highly tailorable rates of degradation.³²⁴ By changing the thiol composition of the hydrogel from 100% thioglycolate-functionalized ethoxylated polyol ester to 100% thiolactate-functionalized ethoxylated polyol ester, the time for complete hydrogel degradation was varied from ~ 12 days to ~ 38 days. The release of many model macromolecules (3, 10, 20, and 40 kDa FITC-dextrans; FITC-labeled ovalbumin; and Alexa Fluor 647 IgG) was controlled by changing the chemical identity of the polyol esters and by using multiple polyol esters within a single hydrogel. For example, FITC-labeled ovalbumin was released from the hydrogel over the course of ~ 4 days to ~ 25 days, depending on which of the six thiol-containing polyol esters was used to form the hydrogel (**Fig. 1.8**). In a follow-up work, trehalose, a disaccharide known for its protein-stabilizing properties, was incorporated within these hydrogels.³²⁹ Trehalose diacrylate was mixed with PEG-diacrylate at various ratios and reacted with thiol-functionalized polyol esters for a total of 25 wt% polymer in the final hydrogel. When 100% of the acrylate groups came from trehalose (i.e., 0% from PEG-diacrylate), nearly 100% of active horseradish peroxidase encapsulated in the gel was recovered within ~ 4 days. In contrast, when 6.25% of the acrylate groups came from trehalose (i.e., 93.75% from PEG-diacrylate), less than 3% of the horseradish peroxidase was

recovered in active form within ~ 12 days. Covalent incorporation of trehalose also maintained the activity of two other model proteins, glucose oxidase and α -chymotrypsin. Although the mechanism of trehalose-mediated protein stabilization is not fully understood, trehalose is produced by many plants and animals in response to osmotic, high temperature, and other stresses, and it is thought to stabilize proteins by making protein unfolding more thermodynamically unfavorable.³³⁰ This concept may motivate additional approaches for stabilization of proteins in hydrogels.

Natural polymers and their derivatives also have been used to make hydrogels for protein release. For instance, Peng *et al.* reacted dextran-maleimide with thiol-containing azobenzene to form a photo-responsive dextran hydrogel.³³¹ The cis/trans isomerization of azobenzene was used to release green fluorescent protein in a light-responsive manner (100 W at 365 nm). Beyond model proteins, hyaluronic acid-based hydrogels have been used to deliver two growth factors, stromal cell-derived factor-1 (SDF-1) and BMP-2, to promote hMSC infiltration and differentiation for bone regeneration in an animal model.³³² These hydrogels were formed *in situ* by a Michael-type reaction between hyaluronic acid-maleimide, a dithiol MMP-degradable peptide (GCRDVPMSMRGGDRCG), and a thiol-functionalized RGD peptide (GCGYGRGDSPG). Limited release of these growth factors occurred by diffusion, but in the presence of the enzyme collagenase, the gel crosslinks were degraded and growth factors were released from the hydrogel. Complete degradation was observed within 9 days with 1 U ml⁻¹ collagenase and within 4 days with 2 U ml⁻² collagenase. Toward modulating myofibroblast activities and tissue regeneration after myocardial infarction, Burdick and coworkers also created injectable, MMP-degradable, hyaluronic acid-based hydrogel for delivery a recombinant tissue inhibitor of MMPs

(rTIMP-3).³³³ The hydrogel was formed by conjugating a thiol- and hydrazide-functionalized MMP-degradable peptide (GGRMSMPV) to maleimide-functionalized hyaluronic acid. The hydrazide-functionalized MMP-degradable hyaluronic acid macromer was then reacted with aldehyde-functionalized hyaluronic acid to form a hydrogel *in situ* upon injection. Additionally, aldehyde-functionalized dextran sulphate was incorporated into the hydrogel to sequester encapsulated rTIMP-3 through electrostatic interactions. The hydrogel/TIMP-3 construct was delivered to a region of MMP overexpression in a porcine myocardial infarction model, resulting in significantly reduced MMP activity and adverse left ventricular remodeling. The study demonstrated the ability to locally release an MMP-inhibitor as needed in response to MMP-overexpressing pathologies.

1.8 Dissertation Summary

This dissertation reports the design of multimodal hydrogels that are responsive to biologically relevant endogenous and exogenous stimuli for delivery of cargo molecules such as therapeutic proteins, growth factors, and immunomodulatory agents. This introduction, **Chapter 1**, reviewed several topics important to this project including design criteria, material for hydrogel preparation, hydrogel crosslinking chemistries, degradable chemistries, and present drug delivery technologies. In **Chapter 2**, we focused on design of the hydrogels that are responsive to endogenous stimuli: thiol-rich reducing microenvironment that is found in carcinoma tissue and aqueous microenvironment. Incorporation of aryl thiol based succinimide thioether along with ester linkages demonstrated degradation via retro-Michael and subsequent thiol exchange reaction and ester hydrolysis, respectively. **Chapter 3** will introduce incorporation of *o*-nitrobenzyl ether based functional groups within polymeric

monomers for hydrogel formation. Hydrogel degradation kinetics in response to externally applied cytocompatible light, reducing conditions, and hydrolysis were characterized, and degradation of the gel was controlled over multiple time scales from seconds to days. In **Chapter 4**, a novel PEG-heparin hydrogels for delivery of low molecular weight proteins is demonstrated via receptor-host interaction and degradation-mediated controlled release. **Chapter 5** will conclude this doctoral dissertation by summarizing major discoveries for increasing our understanding of degradable chemistries to tune the rate of degradation and cargo release.

Chapter 2

DUALLY DEGRADABLE CLICK HYDROGELS FOR CONTROLLED DEGRADATION AND PROTEIN RELEASE

2.1 Introduction

Click reactions have garnered significant interest in the broader areas of materials science and bioconjugation owing to their fast reaction kinetics, high regioselectivity, and efficient reaction yields, all under mild conditions.^{29, 215, 222, 334} Many click chemistries have been applied to the production of materials, including the traditional azide-alkyne, Diels-Alder, Michael addition, thiol-ene, and oxime reactions.^{26, 222} In particular, click reactions that do not require a catalyst or initiator and are free of byproducts, such as the reaction of maleimides and thiols, are useful for biological applications owing to their cytocompatibility in the presence of proteins, cells, or tissues.³³⁵⁻³³⁶ Utilizing these reactions, injectable hydrogels can be easily created as delivery vehicles for therapeutics, particles, or cells.^{51, 249, 314} In this application, temporal changes in material properties caused by degradation allow the controlled release of therapeutics, the elaboration of secreted matrix by encapsulated or infiltrating cells, or the spreading, migration, and release of encapsulated cells.^{156, 337-338}

Cleavage of the click linkages provides an attractive and relatively cost-effective approach to incorporate degradability without the use of more complex components, such as degradable peptides or proteins. Recent studies have demonstrated the degradability of click crosslinks under mechanical³³⁹⁻³⁴⁰ and

thermal^{309, 341} stresses; however, such reaction conditions can limit the translation of these approaches into clinical applications owing to the limited cytocompatibility of their associated stimuli. Overcoming this limitation, Baldwin and Kiick have recently introduced thiol-maleimide click reactions in solution and within PEG-heparin hydrogels that are sensitive to reducing microenvironments found *in vivo*.^{249, 275} Opportunities to exploit these strategies for controlled delivery of encapsulated cargo molecules, however, have not yet been demonstrated.

Despite recent technological advances, the delivery of therapeutic proteins (e.g., Trastuzumab, Bevacizumab, Rituximab) and small molecule drugs (e.g., Fluorouracil, Paclitaxel) remains a major challenge in the treatment of many diseases, including cancer.³⁴² In approaches for cancer treatment, delivery to the site of a tumor is critical for therapeutic success and minimization of side effects.³⁴³ Injectable hydrogel-based drug carriers offer advantages for these applications, enabling the efficient encapsulation of cargo molecules while maintaining bioactivity for localized delivery at a preprogrammed rate or responsive manner.^{32, 41, 344-345} Depending on the cargo molecule of interest, the rate of release can be controlled by diffusion, degradation, affinity, or a combination of these mechanisms through hydrogel design. Degradation-mediated release is a versatile approach for the temporally controlled delivery of numerous payloads, from hydrophilic proteins to small molecules caged within nanoparticles, without chemical modification of the therapeutic, which can affect drug efficacy and clinical translation.^{164, 346-347} Several strategies have been employed to incorporate degradability within the hydrogel by inclusion of labile crosslinks, including esters,^{274, 348} photolabile groups,^{207, 276, 349} and enzyme-sensitive linkers.^{164, 286} As will be elaborated below, linkers that are sensitive to reductants are

attractive and simple for controlled release in cancerous tissues, which have elevated levels of sulfur-containing compounds.³⁵⁰

Accordingly, reduction-sensitive disulfide linkages have been widely used for intracellular delivery of DNA, siRNA, proteins, and therapeutic drugs.³⁵¹⁻³⁵⁵ These strategies rely on rapid destabilization of the drug carrier due to reduction of disulfide bonds in the presence of glutathione (GSH) tripeptides, one of the major sulfur-containing compounds found at elevated levels within cancerous tissues and cells.³⁵⁶⁻³⁵⁷ Since the intracellular concentration of GSH (ca. 0.5 mM to 10 mM) is 100 to 1000 times higher than the extracellular concentration (ca. 0.001 mM to 0.02 mM), efficient intracellular delivery of cargo molecules has been achieved using disulfide chemistry.^{295, 358} However, the rapid rate of degradation of disulfide linkages provides limited control over material degradation and cargo release, and GSH-sensitive linkers that permit controlled extracellular delivery over days to weeks thus have been less explored. In addition, since the concentration of GSH is higher in carcinoma tissues than in healthy tissues due to abnormal proliferative activities of cancer cells,^{356-357, 359} reducing sensitive chemistries incorporated within drug delivery carriers offer great potential for localized cancer treatment. To address this need and opportunity, we present reducing microenvironment-sensitive hydrogels that undergo tunable degradation on the order of days to weeks for controlled protein delivery, demonstrating the broad utility of the click bond cleavage and thiol exchange reaction as a general strategy not only to control degradation but also to control the release of cargo molecules locally from a bioinert delivery vehicle.

Specifically, we describe the development of multimode, degradable poly(ethylene glycol) (PEG) hydrogels using Michael-type addition and exchange

reactions by incorporation of select thioether succinimide crosslinks. These hydrogels are composed of multifunctional PEG crosslinked using thiol-maleimide click chemistry and can undergo degradation by two mechanisms: i) cleavage of click linkages and thiol exchange reactions in the presence of GSH and ii) ester hydrolysis. To achieve this, multiarm PEG macromers were functionalized with different mercaptoacids and reacted with maleimide-functionalized PEG, creating hydrogels that degrade by either hydrolytic *or* hydrolytic and thiol-exchange mechanisms. Hydrogel degradation was monitored in physiologically-relevant GSH microenvironments via oscillatory rheometry and volumetric swelling measurements to assess the degradation kinetics. The ability to incorporate and selectively release a cargo molecule was investigated by monitoring, via fluorescence spectroscopy, the release of bovine serum albumin (BSA) as a model protein. The ability to precisely control hydrogel degradation and thus the release profile of cargo molecules using cleavage of click linkages offers exciting avenues for designing biomaterials for drug delivery and tissue engineering applications.

2.2 Materials and Methods

2.2.1 Materials

4-arm hydroxyl-functionalized poly(ethylene glycol) (PEG-4-OH, 10000 g mol⁻¹), 4-arm thiol-functionalized PEG (PEG-4-SH, 10000 g mol⁻¹), and linear maleimide-functionalized PEG (PEG-2-MI, 5000 g mol⁻¹) were purchased from JenKem Technology USA Inc. (Allen, TX). 3-Mercaptopropionic acid (MP), 4-mercaptophenylacetic acid (MPA), p-toluenesulfonic acid monohydrate (PTSA), triethylamine (TEA), dithiothreitol (DTT), and glutathione (GSH) were purchased

from Sigma-Aldrich (St. Louis, MO). Trifluoroacetic acid (TFA) and all solvents were obtained from Fisher Scientific (Pittsburgh, PA). Bovine serum albumin labeled with Alexa Fluor 488 (BSA-488) was purchased from Life Technologies (Grand Island, NY). All commercially available reagents were used as received without further purification unless otherwise noted.

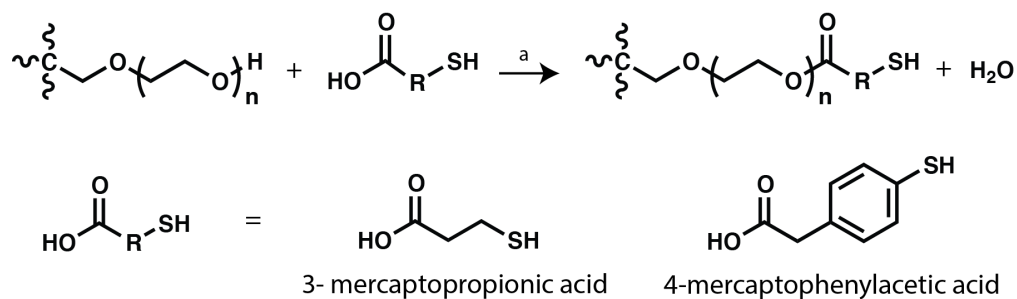


Figure 2.1 **Functionalization of 4-arm PEG.** Schematic of the synthesis of thiol-functionalized PEG. (a: Toluene, PTSA, $\sim 110^\circ\text{C}$)

2.2.2 Synthesis of Mercaptoacid-based PEG-thiols

PEG was modified with MP or MPA functional groups based on modified versions of previously published protocols.^{51, 249} Briefly, PEG-4-OH (0.1 mmol), mercaptoacid (4 mmol), PTSA (0.04 mmol), and toluene (20 mL) were added to an oven-dried round-bottom flask equipped with a reflux condenser. The reaction setup was purged with nitrogen under room temperature. The reaction (**Fig. 2.1**) was heated to reflux (110°C) and stirred for 48 hours, and generated water was collected by using a Dean-Stark trap. Upon completion, the reaction was cooled to room temperature, and the functionalized PEG precipitated three times in ethyl ether. The product was recovered by vacuum filtration and rinsed with 2-propanol followed by hexane. The dried polymer product (1 equiv) was reduced in toluene using DTT (1 equiv) and TEA

(1 equiv) for 5 hours, under inert atmosphere. The finished reaction was acidified with TFA (1.1 equiv), and the polymer was again precipitated in ethyl ether and recovered by filtration. Subsequently, the polymer was dissolved in methanol, and the mixture was filtered through a 0.22 μm filter followed by precipitation in 2-propanol and vacuum filtration. The solid product was rinsed with copious amounts of 2-propanol and hexane. The final dried polymer was obtained by removal of residual solvents under reduced pressure. The degree of thiol functionalization of the polymer was characterized via ^1H NMR spectroscopy, using a Bruker AV 400 NMR spectrometer (Bruker Daltonics, Billerica, MA) with CDCl_3 as the solvent and TMS as the reference.

PEG-4-MP

The general procedure for synthesis of PEG-thiol was followed using MP as the mercaptoacid to yield PEG-4-MP. The final polymer was obtained as a white solid (0.6 g, 74% yield). The functionality was estimated to be 92% based on integration of the proton neighboring the ester linkage relative to the PEG backbone protons. (**Fig. S1 B**). ^1H NMR (400 MHz, CDCl_3) δ : 4.28 (8H, t), 3.90-3.35 (900H, bs), 2.82-2.62 (16H, m), 1.68 (4H, t).

PEG-4-MPA

The general procedure for synthesis of PEG-thiol was followed using MPA as the mercaptoacid to yield PEG-4-MPA. The final polymer was obtained as a white solid (0.54 g, 66% yield). The functionality was estimated to be 90% based on integration of the proton neighboring the ester linkage relative to the PEG backbone protons (**Fig. S1**

C). ^1H NMR (400 MHz, CDCl_3) δ : 7.24-7.08(16H, m), 4.24 (8H, t), 3.90-3.35 (900H, bs), 3.42-3.39 (4H, s).

2.2.3 Gelation Time and Rheology Characterization

Hydrogel precursor solutions were prepared by dissolution of thiol- and maleimide-functionalized PEG (5% w/w) in citric acid buffer (pH 5) and phosphate-buffered saline (pH 7.4), respectively. Slightly acidic conditions allowed tuning of the gelation time (i.e., increased gelation time) due to the reduced nucleophilicity of thiolate species under acidic conditions,^{249, 360} these polymerization conditions previously have been shown to be effective for use in cell/protein studies in vitro.³⁶¹ Gelation time was studied qualitatively using the tube inversion method. Briefly, the hydrogel precursor solutions were mixed (100 μL) and immediately pipetted into a glass vial. In five-second intervals, vials were inverted to observe if the solution flowed. The timepoint at which the solution did not flow was recorded as the gelation time.

For rheological studies, the hydrogels were formed directly on the rheometer (AR-G2, TA instruments, USA) by mixing the precursor solutions (1:1 maleimide:thiol molar ratio resulting in 5 % w/w hydrogels), immediately pipetting onto a Peltier plate at 25 $^{\circ}\text{C}$, and commencing measurements (120 μm gap). Gelation at room temperature ensured that the gelation time was sufficiently slow to allow good mixing of precursor solutions on the Peltier plate prior to gelation. This also allowed the gels to form homogeneously so that all gels had similar moduli prior to protein release experiments. The gelation time and final shear modulus of the hydrogel were determined using rheometry experiments. Frequency sweeps were performed to determine the linear viscoelastic regime (0.01 to 10 % strain at 6 rad/s). Using a 20-

mm diameter parallel plate geometry, time-sweep measurements were obtained within the linear viscoelastic regime (1 % constant strain mode at a frequency of 6 rad/s) at 25 °C.

2.2.4 Hydrogel Degradation Characterization

For hydrogel degradation studies, polymer precursor solutions (5% w/w) were mixed in a 1:1 maleimide:thiol molar ratio and pipetted into a cylindrical mold (diameter = 4.6 mm, thickness = 1.8 mm). The solutions were allowed to gel for two hours at room temperature to ensure maximum possible crosslink density was achieved for all samples. The rheological data showed that once the gels have been formed (i.e., stable storage moduli is achieved at 30 min), the moduli remain consistent through 2 hours. The resulting hydrogels were washed with PBS and incubated, at room temperature, in 5 mL of PBS buffer (pH 7.4) containing GSH (0 mM, 0.01 mM or 10 mM) over the experimental time period. The pH of the buffer after GSH addition was adjusted to a pH of 7 by addition of 0.1 M sodium hydroxide. Degradation was monitored by measuring volumetric swelling and shear modulus. For the shear modulus measurements, time sweeps were performed within the linear viscoelastic regime for each sample (2 rad/s, 2% strain, and 0.25 N normal force in order to prevent hydrogel slip).

2.2.5 Volumetric Swelling and Mesh Size Calculations

Hydrogel discs (diameter = 4.6 mm, thickness = 1.8 mm) were placed in PBS buffer with 0 mM, 0.01 mM, or 10 mM GSH at room temperature and gently rocked. Samples were removed at respective time points, and the diameters of hydrogels were measured using a Vernier caliper, whereas the height was determined using the

rheometer gap values. Volume of the hydrogel at each time points was determined based on measured diameter and height and assuming cylindrical geometry. The % volumetric swelling at each time point was calculated by normalizing to the volume of the gel immediately after formation (day 0 before equilibrating with PBS).

2.2.6 Protein Release

For protein release experiments, polymer precursor solutions (5% w/w) were mixed in a 1:1 maleimide:thiol molar ratio along with BSA-488 (loading concentration 1.2 mg/ml) and added to a cylindrical mold (diameter = 4.6 mm, thickness = 1.8mm). The solutions were allowed to gel for two hours at room temperature. Hydrogel discs were immediately washed with PBS thrice to remove any non-encapsulated BSA-488 and then gently rocked at room temperature in 5 mL of PBS buffer with GSH (10 mM). The amount of BSA-488 present in the hydrogel was calculated by subtracting the amount of BSA-488 released during wash steps from the amount of BSA-488 that was initially loaded into the gel. At each time point, a 100- μ L aliquot of the sink solution was removed for protein release measurements and replaced by 100 μ L of fresh GSH in PBS. The released BSA-488 was quantified by fluorescence measurements using a microplate reader (Synergy H4, BioTek Inc., Winooski, VT) taking into account the cumulative sample dilution due to removal and addition of fresh GSH in PBS at each time point measurement (see Supporting Information). To estimate the concentration of released BSA-488, a calibration curve for the fluorescence of BSA-488 as a function of its concentration was acquired. The release of the BSA was monitored via SDS-PAGE analysis of the solutions removed at each timepoint; 7 μ L of sink solution containing released protein was loaded onto a standard sodium dodecyl sulfate-polyacrylamide gel electrophoresis (SDS-PAGE) for

analysis. The concentration of protein in each band was quantified with densitometry analysis using the gel analysis function in ImageJ (version 1.46).

2.2.7 Statistical Analysis

Results are expressed as mean \pm standard error of mean (SEM) unless otherwise specified. Monomer synthesis reactions were performed in duplicate. Hydrogel formation experiments were performed in triplicate. Degradation and protein release studies were performed in duplicate with 3 hydrogels per condition at each experimental time point. Statistical comparisons were based on analysis of variance (ANOVA) and $p < 0.05$ was considered statistically significant.

2.3 Results and Discussion

2.3.1 Hydrogel Compositions for Control of Degradation

Many natural and synthetic polymers have been used for hydrogel formation, with polymer selection partly dictated by the application of interest.²⁶ PEG-based hydrogels are well suited for drug delivery applications owing to their biocompatibility, lack of protein binding sites, and the ease of engineering their properties.¹⁸ The facile functionalization of the hydroxyl end groups of PEG allows the incorporation of different chemical functionalities for hydrogel formation in the presence of proteins and cells *and* for controlled degradation. Exploiting these advantages, PEG-OH was functionalized with alkyl (MP) and aryl (MPA) based mercaptoacids utilizing established protocols.^{51, 249} These thiol end groups act as nucleophiles and react rapidly with maleimide functional groups to form crosslinks by a Michael-type addition reaction. Michael-type addition reactions are highly efficient and versatile reactions that occur under physiological conditions without byproducts

and have been used to crosslink cytocompatible hydrogels.^{159, 234, 362} Here, the composition of the hydrogel was varied to enable microenvironment-controlled degradation and protein release (**Fig. 2.2**). PEG-4SH-based hydrogels (**Control**), which contain water stable ether bonds, served as a non-degradable control owing to lack of any degradable functional groups. Owing to the presence of ester linkages, MP-based hydrogels (one degradable group, **D1E**) undergo ester hydrolysis, whereas the MPA-based hydrogels (two degradable groups, **D2ER**) undergo ester hydrolysis and click bond cleavage and thiol exchange reactions.

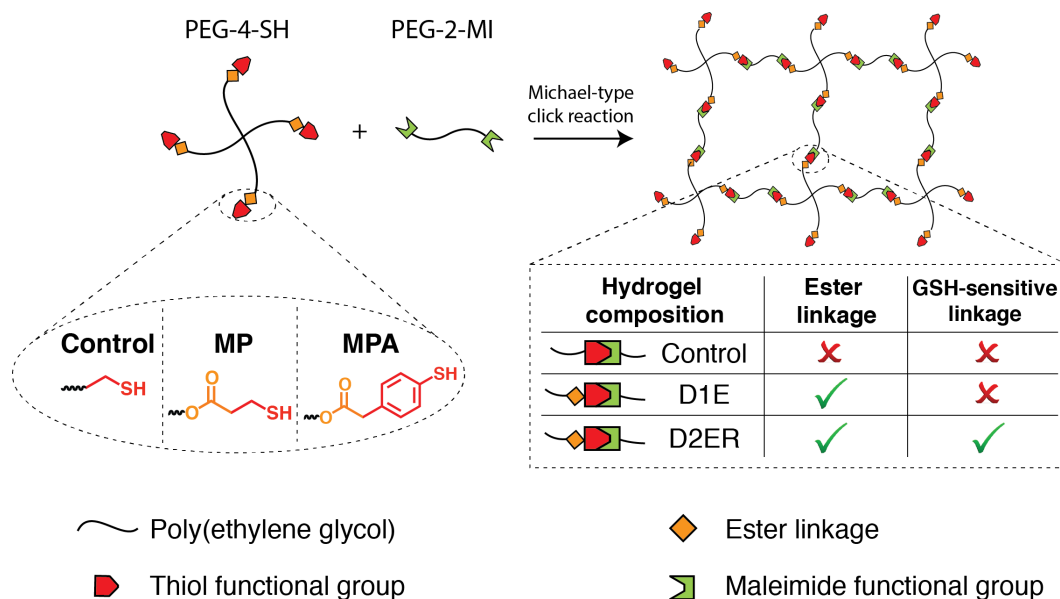


Figure 2.2 Hydrogel formation via click reaction. Degradable PEG hydrogels were synthesized by Michael type addition reaction between thiol functionalized 4-arm PEG (PEG-4-SH) and maleimide functionalized linear PEG (PEG-2-MI). The thiol-functionalized macromers were synthesized by esterification of PEG using two different mercaptoacids (Scheme 1). The identity of the thiol was varied to tune the degradability of the hydrogels (**Control**: no degradable groups; **D1E**: one degradable group per crosslink (i.e., ester linkage); and **D2ER**: two degradable groups per crosslink (i.e., ester and reducing environment susceptible click = linkages)).

2.3.2 Consistent Hydrogel Formation

Dynamic time sweep experiments were conducted to study hydrogel gelation kinetics and final hydrogel moduli. Data were acquired within the linear viscoelastic regime. After vortexing the precursor solutions, the storage and loss moduli were recorded as a function of time. Representative results for the **D2ER** hydrogel formation are shown in **Fig. 2.3A**. The crossover point (i.e., $G'=G''$), which is an indirect measurement of the gel point, was not observed due to the rapid onset of gelation before the first data point was acquired; the gelation time thus was semi-

qualitatively determined by the tube inversion method.³⁶³ Faster gelation was observed for **D2ER** (~20 sec) compared to **D1E** (~35 sec) and **Control** (~40 sec) hydrogels; this rapid gelation is consistent with the reported kinetics of thiol-maleimide reactions.³⁶⁴ The time difference for gelation between **D2ER**, **D1E**, and **Control** can be attributed to the thiol reactivity (**D1E** and **Control**, alkylthiols $pK_a = 10.2$; **D2ER**, arylthiols $pK_a = 6.6$).³⁶⁵⁻³⁶⁶ The difference in thiol reactivity of **Control**, **D1**, and **D2ER** essentially arises from the mesomeric effect provided by the aromatic ring in the case of **D2ER**, making it more nucleophilic than **Control** and **D1E**.

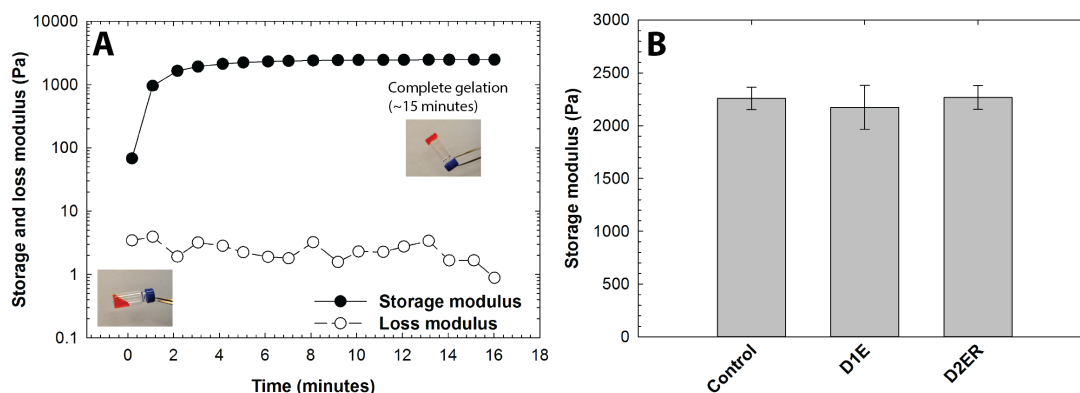


Figure 2.3 Modulus evolution during hydrogel formation. (A) Time-sweep measurements on an oscillatory rheometer were utilized to monitor hydrogel formation (**D2ER** hydrogel shown). Although formation of a gel is clearly observed, samples polymerize too quickly for measurement of the gel point with rheometry. To estimate the time to initial gelation, the tube-tilt method was utilized (inset images), where faster gelation was observed for **D2ER** (~20 s) as compared to **Control** (~40 s) and **D1E** (~35 s) hydrogels. For better visual assessment, Allura Red AC dye was added to the precursor solution (0.5 mg/ml) for tube-tilt measurements. (B) Irrespective of the identity of the thiol used for the hydrogel formation, the storage moduli for all three hydrogels post-gelation were statistically similar, indicating similar structural and mechanical properties. The data shown illustrate the mean ($n = 3$), with error bars showing the standard error.

Presence of aromatic ring in **D2ER** results in higher nucleophilicity due to mesomeric effect, which dictates the thiol reactivity. With increasing time, the storage modulus (G') increases rapidly without a significant increase in loss modulus (G''). These data highlight the elastic nature of the network. Time to achieve final storage moduli varied depending upon the identity of thiol groups, which again can be attributed to the thiol reactivity (**D2ER**: ~15 minutes; **D1E**: ~30 min; and **Control**: ~34 min). Although the experiments were performed at the room temperature (25 °C), the gelation time and time to achieve the final storage moduli can be further decreased by forming hydrogels at elevated temperatures.

Material modulus is directly correlated with the crosslink density as per the theory of rubber elasticity.³⁶⁷ The final storage moduli, which is defined as the value of G' after reaching plateau, for **Control**, **D1E**, and **D2ER** hydrogels were examined to compare the consistency in crosslink density between the different compositions (**Fig. 2.3B**). The final post-gelation, equilibrium-swollen G' were recorded after complete gelation for **Control**, **D1E**, and **D2ER**. As indicated in the figure, the post gelation equilibrium G' was ~2.3 kPa for all three compositions. There were no statistically significant differences between the final plateau moduli of the various gels (one-way ANOVA, $p = 0.88$), indicating that the use of different thiols did not affect the final crosslink density substantially. Side reactions such as disulfide formation and maleimide ring hydrolysis alter the reactivity of the thiol and maleimide groups and thus could affect the number of functional groups available for hydrogel formation (**Figure 2.9**), potentially decreasing the final moduli for a particular composition. The lack of a statistically significant difference between the final equilibrium G' values thus also suggests that there were no significant differences in the extent of these side

reactions for the various hydrogel compositions. These results suggest that differences in gelation for **Control**, **D1E**, and **D2ER** did not significantly contribute to network defects due to strict 1:1 stoichiometry and relative rate of Michael-type addition as compared to other defect forming side reactions. Further, the molecular weight of the PEG chains for the gel compositions investigated here was selected to minimize any looping, unreacted functionalities, and other related network defects based on studies of related PEG hydrogels in the literature.³⁶⁰ The similarity of the initial crosslink densities between the **Control**, **D1E**, and **D2ER** hydrogels allow the study of the degradation kinetics by direct monitoring of changes in G' as a function of time.

2.3.3 Degradation in a Reducing Microenvironment

In order to evaluate the most rapid hydrogel degradation that might be observed in physiologically relevant reducing microenvironments, as well as to evaluate the associated degradation mechanism, the higher GSH of 10 mM first was examined. Potential degradation mechanisms for each hydrogel composition are described in **Fig. 2.4**. Thioether succinimide linkages formed using arylthiols (**D2ER** hydrogels) can undergo thiol exchange in the presence of exogenous thiols (a GSH-rich microenvironment) in contrast to alkylthiols (**Control** and **D1E**), which are stable within the experimental time frame (stable at $t < 6$ days).²⁷⁵ The presence of ester linkages in the **D1E** and **D2ER** hydrogels allows degradation by ester hydrolysis over longer time scales (stable at $t > 1$ month to 2 years depending upon neighboring groups).³⁶⁸ A potential hindrance to degradation by the thiol exchange mechanism is possible hydrolysis of the maleimide ring, which leads to ring opening and the formation of an irreversible crosslink. However, the rate of maleimide ring hydrolysis is significantly slower (by one order of magnitude) than the competing click cleavage

and thiol exchange reaction ($k = 3.7 \times 10^{-2} \text{ h}^{-1}$ for click cleavage and thiol exchange, $k = 3.3 \times 10^{-3} \text{ h}^{-1}$ for maleimide ring hydrolysis).²⁷⁵ Consequently, we assume that changes in G' for **D2ER** hydrogels are dominated by mainly thiol-exchange reactions in reducing microenvironments and by ester hydrolysis in non-reducing microenvironments.

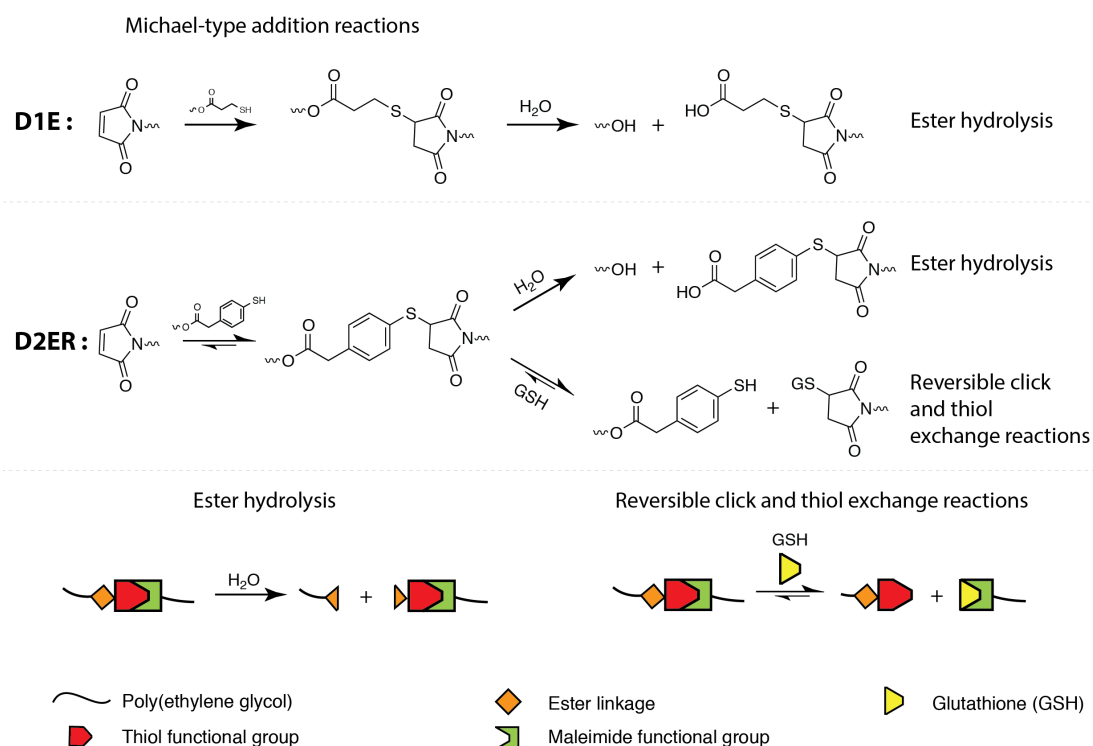


Figure 2.4 Multimode hydrogel degradation. Schematic of the click bond cleavage and thiol exchange reaction of thioether succinimide linkages under a glutathione (GSH) reducing microenvironment and by ester hydrolysis. The **D1E** hydrogels can only undergo degradation by ester hydrolysis. **D2ER** hydrogels can undergo degradation by ester hydrolysis and by thiol exchange reactions, owing to the presence of arylthiol-based thioether succinimide linkages. Owing to the lack of degradable functional groups, control hydrogels do not degrade in aqueous reducing microenvironments. The rate and extent of the click bond cleavage depends on the Michael donor reactivity and thiol pK_a .

Oscillatory rheometry and volumetric swelling measurements were used to study the degradation of the hydrogels (defined here as the scission of network crosslinks) under thiol-rich reducing conditions. Degradation kinetics were assessed by measuring the storage moduli of hydrogel discs that were suspended in solutions containing 10 mM GSH (**Fig. 2.5A**). The storage moduli at each time point were normalized to the initial modulus for that gel composition directly after formation (day 0 before equilibrating with PBS), where the initial gel has a normalized modulus of 100%. As illustrated in the figure, the **Control** and **D1E** samples exhibited an initial decrease in G' to approximately 80% of the normalized value within 24 hours, but did not exhibit any further rapid decrease in moduli after this point. The initial decrease can be attributed to the equilibrium swelling that occurs after hydrogel formation. No significant change was observed in G' post-equilibrium swelling for **Control** hydrogels, which was expected since no degradable functional groups are present within these hydrogels. A slight decrease in modulus over time was observed for **D1E** hydrogels, which can be attributed to ester hydrolysis (calculated first-order rate constant, $k = 3.33 \times 10^{-5} \text{ min}^{-1}$). This rate constant compares well with the typical ester linkage hydrolysis rate constant in hydrophilic polymer networks (1.33×10^{-5} to $7.33 \times 10^{-6} \text{ min}^{-1}$) corresponding to half lives of 6 to 32 days.³⁶⁹ The degradation rate constant for **D1E** was found to be statistically different from the **Control** (two-tailed P value = 0.005), highlighting the role of ester linkages in the degradation of **D1E** (**Fig. S2.4 and S2.5**). In contrast, a rapid decrease in G' was observed for **D2ER** hydrogels, and the reverse gel point, defined as complete hydrogel dissolution, was observed after approximately 4 days (at 5700 minutes). The rapid decrease in G' indicates a substantial decrease in crosslink density and can be attributed to the reversibility of the

thiol-maleimide reaction and the consequent thiol exchange reactions that occur in the presence of GSH. As the rates of ester hydrolysis and maleimide ring hydrolysis are slow, the rapid rate of degradation of **D2ER** highlights the role of click bond cleavage and thiol exchange reaction as leading cause of hydrogel degradation.

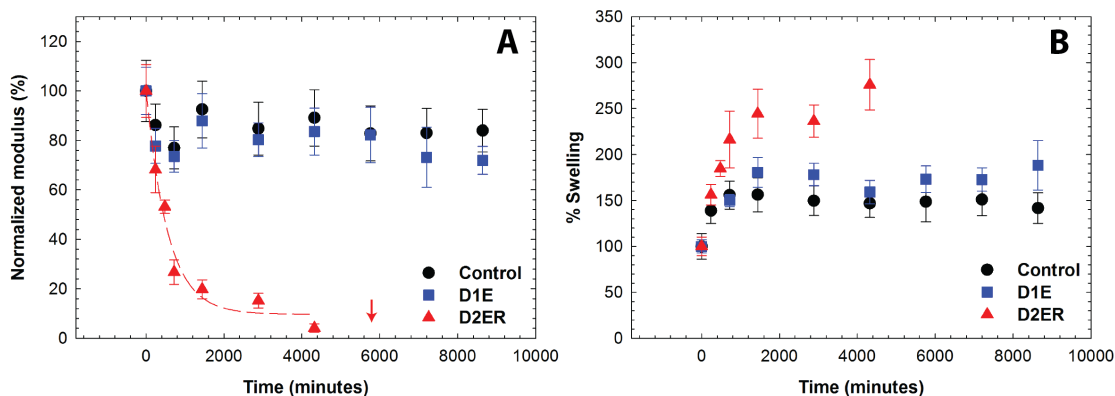


Figure 2.5 Hydrogel degradation in reducing microenvironment by cleavage of click bonds. Degradation of the hydrogel in a thiol-rich reducing microenvironment (10 mM GSH) was studied by monitoring **(A)** the storage modulus and **(B)** % volumetric swelling at discrete time points. All compositions exhibit an initial change in properties over 24 h as equilibrium swelling occurs. Due to the presence of the arylthiol-based thioether succinimide crosslinks, D2ER hydrogels exhibited rapid bulk degradation by click cleavage and thiol exchange reactions. The arrow indicates the time point when reverse gelation was observed. D1E and Control hydrogels were relatively stable during the experimental time frame due to the absence of GSH-sensitive crosslinks. The data shown illustrate the mean ($n = 6$), with error bars showing the standard error.

Temporal changes in the volumetric swelling also were examined for the **Control**, **D1E**, and **D2ER** hydrogels that were suspended in 10 mM GSH (**Fig. 2.5B**). All three hydrogel compositions showed an initial increase in the swelling as the

hydrogels achieved equilibrium swelling. The **Control** and **D1E** hydrogels remained stable after this initial swelling event ($t > \sim 24$ hours), whereas the volumetric swelling for **D2ER** hydrogels continued increasing until complete degradation (gel dissolution) occurred at 5700 minutes. The continuous increase in the swelling before complete degradation for **D2ER** is consistent with a bulk degradation mechanism, as well as with the rheometric measurements where the increases in swelling are commensurate with observed decreases in modulus. Overall, these results indicate that well-defined hydrogels can be designed to degrade in a reducing microenvironment with selection of arylthiol-based thioether succinimide linkages. Such a system could prove useful in the design of hydrogels for controlled and local delivery of anti-cancer drugs.

2.3.4 Influence of GSH Concentration on Hydrogel Degradation

To reject the possibility that the degradation of **D2ER** hydrogels under high [GSH] conditions was substantially affected by ester hydrolysis, the mechanical properties of **D2ER** hydrogels were monitored in solutions lacking GSH (0 mM GSH). In addition, since thiol exchange reactions are dependent on GSH concentration, we investigated an additional condition (0.01 mM GSH, **D2ER** hydrogel), which mimics the extracellular GSH concentration. The storage moduli (G') of hydrogels were measured at predetermined time points. The **Control** hydrogel exhibited an initial decrease in G' over the first 24 hours, after which G' did not change, irrespective of GSH concentration (0 and 10 mM, **Fig. S2.4**). As discussed in Section 3.3, the initial changes in G' can be attributed to equilibrium swelling. The constant moduli observed for timepoints after 24 hours indicate that the polymeric crosslinks are stable within the experimental timeframe and do not undergo any significant degradation. For **D1E** hydrogels, the storage moduli initially decreased,

which again can be attributed to equilibrium swelling (**Fig. S2.5**). However, for the **D1E** hydrogel, the decrease in storage moduli continued past 24 hours, which would be consistent with degradation via ester hydrolysis as discussed above.

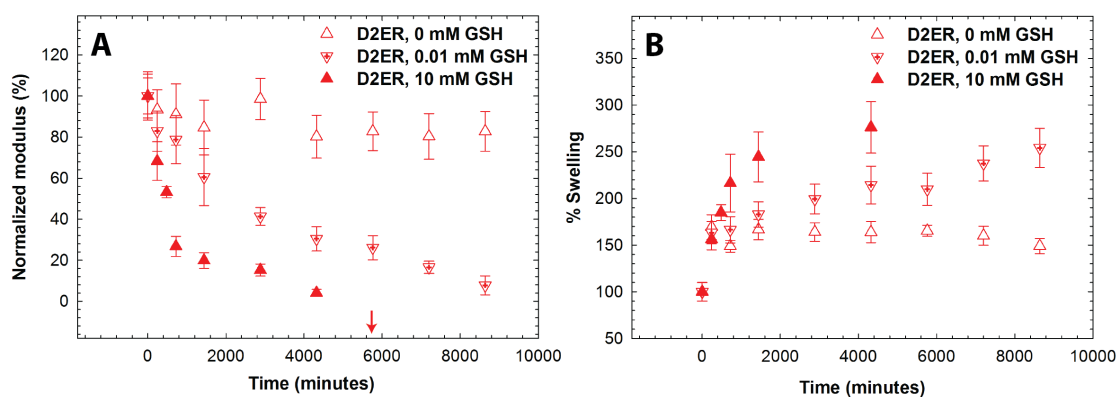


Figure 2.6 Influence of GSH concentration on hydrogel degradation. The effect of GSH concentration (0, 0.01, and 10 mM) on D2ER hydrogel degradation was studied by analyzing A) the decrease in the storage modulus, and B) the % volumetric swelling. The dependence of the decrease in moduli on GSH concentration indicates that the click cleavage and thiol exchange reaction is the dominant degradation mechanism for the D2ER hydrogels. The increase in volumetric swelling as a function of time before the reverse gel point confirms bulk degradation of hydrogels. The arrow indicates the time point when reverse gelation was observed for the 10 mM GSH condition. The data shown illustrate the mean ($n = 6$), with error bars showing the standard error.

As shown in **Fig. 2.6**, the storage moduli varied as a function of GSH concentration for **D2ER** hydrogels. For the 0 mM GSH condition, G' initially decreased during the first 24 hours, owing to equilibrium swelling, followed by a slow decrease in G' to 81% of its initial normalized value. The decrease after 24 h can be attributed to ester hydrolysis ($k = 1.35 \times 10^{-5} \text{ min}^{-1}$, $t_{1/2} = 35 \text{ days}$). For 0.01 mM GSH,

G' decreases rapidly and complete gel degradation was observed at approximately 8 days ($t \sim 200$ h), indicating that the degradation mechanism in the presence of glutathione is dominated by the reversibility of the thiol-maleimide reaction and the resulting thiol exchange that is possible in the presence of GSH. Further, in comparison with solutions containing 10 mM GSH, these data highlight the dependence of the rate of **D2ER** hydrogel degradation on GSH concentration. At lower GSH concentration, the free thiol groups ($\sim 14 \mu\text{M}$) generated due to the click bond cleavage compete with the free GSH thiols ($\sim 10 \mu\text{M}$), since the concentration is comparable. In this case, the GSH concentration is a limiting factor, and the rate of degradation is significantly slower for 0.01 mM compared to the 10 mM GSH condition, in which GSH is present in a large excess. Overall, these results indicate that the **D2ER** hydrogels can undergo ester hydrolysis, but the rate of ester hydrolysis is very slow (under 0 mM GSH $k \sim 10^{-5} \text{ min}^{-1}$). As rapid degradation of **D2ER** hydrogels is observed under reducing conditions (10 mM GSH $k \sim 10^{-3} \text{ min}^{-1}$), the data clearly indicate that the click bond cleavage and thiol exchange reaction is the primary mechanism for gel degradation. Further, to verify that **D2ER** hydrogels can undergo complete degradation via ester hydrolysis, **D2ER** hydrogels were subjected to basic conditions to accelerate ester bond hydrolysis (0.1 M sodium carbonate buffer, pH 11.5) and exhibited complete degradation within 24 hours in the absence of a reducing microenvironment, confirming the dual degradability of the hydrogels.

To further investigate the mode of degradation, temporal changes in the volumetric swelling were monitored for **D2ER** hydrogels suspended in various reducing microenvironments (**Fig. 2.6B**). During the first 24 hours, the volumetric swelling increases for all three conditions, which can be attributed to initial hydrogel

equilibrium swelling. After 24 hours, the volumetric swelling continuously increases for the 0.01 mM and 10 mM condition over the course of degradation, which is consistent with rheometric measurements. A bulk degradation mechanism is indicated by this continuous increase in the swelling as a function of time.^{164, 279}

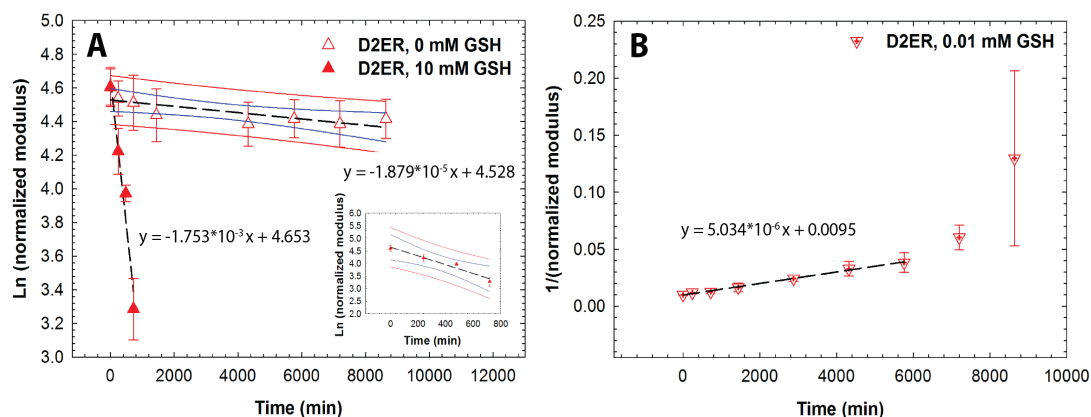


Figure 2.7 Reducing environment-dependent degradation kinetics. (A) D2ER hydrogels exhibited first order degradation kinetics in a strong reducing microenvironment (10 mM GSH), whereas limited degradation is observed in a thiol-lacking microenvironment (0 mM GSH), owing to the slow rate of ester hydrolysis. Data point for 0 mM GSH at 2880 minutes was identified as a significant outlier (Grubb's test, $p < 0.05$) and hence omitted during regression analysis. (B) D2ER hydrogels followed second order reaction kinetics in a weak reducing microenvironment (0.01 mM GSH). Later time points were omitted during the regression analysis, due to large standard error, which can be attributed to experimental limitations when handling soft, more liquid-like degraded gels. As a whole, this study highlights the dependence of hydrogel degradation on GSH concentration. The data shown illustrate the mean ($n = 6$), with error bars showing the standard error. Black line indicates the linear fit using regression analysis. Blue and red lines indicate 95% confidence and prediction bands.

2.3.5 Degradation Kinetics

Regression analysis was conducted to obtain further insight into the degradation mechanism of **D2ER** hydrogels and the kinetics of associated degradation reactions (**Fig. 2.7**). When exposed to 0 mM GSH, the decrease in storage moduli can be attributed to ester hydrolysis. Owing to the highly swollen nature of the hydrogels, and since the buffer is present in large excess, the water concentration during the degradation time period can be assumed to be relatively constant. Hence, the reaction kinetics was observed to be pseudo-first order with a rate constant $1.87 \times 10^{-5} \pm 5.83 \times 10^{-6} \text{ min}^{-1}$. The differences in the rate of ester hydrolysis calculated for the **D2ER** (here) and **D1E** hydrogels (above) can be attributed to local hydrophobic domains associated with aryl thiols in the **D2ER** gels, consistent with a previously reported study by Schoenmakers *et al.* in which the rate of ester hydrolysis varied with local hydrophobicity.³⁷⁰ When **D2ER** gels were exposed to 0.01 mM GSH, a rapid decrease in G' was observed, consistent with the occurrence of both thiol exchange reactions and ester hydrolysis. Because the theoretical concentration of thiol groups from PEG is comparable to that of the thiol groups from GSH (see above), the rate of hydrogel degradation is dependent both on the concentration of degradable functional groups (which correlate with the crosslink density with 2 degradable groups per crosslink) and the concentration of GSH. Consistent with this, the hydrogel degradation kinetics were observed to be second order, with a rate constant $5.03 \times 10^{-6} \pm 0.16 \times 10^{-6} \text{ mM}^{-1} \text{ min}^{-1}$. With a higher concentration of GSH, the **D2ER** hydrogel rapidly degrades. At 10 mM GSH, the GSH is present in large excess (~ 3 orders of magnitude as compared to thiols present in the hydrogel), and thus the concentration of GSH can be assumed to be constant during the experimental time frame. Thus, the rate of degradation is dependent on only the crosslink density, and first order degradation kinetics regression

analysis yields a rate constant of $1.75 \times 10^{-3} \pm 0.26 \times 10^{-3} \text{ min}^{-1}$. The degradation rate constants for the **Control**, **D1E**, and **D2ER** hydrogels are been summarized in **Table 2**.

2.3.6 Controlled Release of a Model Protein

The ability to tune the rate of degradation by varying crosslink chemistry offers opportunities to utilize these hydrogels for the controlled release of therapeutics in response to the reducing microenvironment or at a preprogrammed rate by ester hydrolysis. To study the applicability of these hydrogels for controlled release applications, a fluorescently-tagged model protein, bovine serum albumin (BSA-488), was encapsulated during hydrogel formation. BSA-488 was chosen as a model protein for release studies since the hydrodynamic diameter ($\sim 7.2 \text{ nm}$)²⁶¹ is comparable to the estimated hydrogel mesh size ($\sim 9 \text{ nm}$). The size of the BSA and mesh size calculated for the hydrogels suggest that these materials would be useful for tailored release by hydrogel degradation, upon which the mesh size becomes large enough to facilitate protein release. Similarly, bioactive proteins (e.g., growth factors), therapeutic-laden nanoparticles, or even cells could be released by this mechanism.

The release of BSA-488 was monitored by measuring fluorescence as a function of time. The percent cumulative release was plotted as a function of time for all three compositions (**Fig. 2.8A**). Approximately 40 % of BSA-488 was initially released from all hydrogel compositions (**Control**, **D1E**, and **D2ER** hydrogels). This release may be attributed to the increase in mesh size associated with initial equilibrium swelling. The effective diffusion coefficient (D_e) was calculated using a modified form of Fick's law³⁷¹⁻³⁷² and the value was found to be $\sim 1.56 \times 10^{-8} \text{ cm}^2 \text{ sec}^{-1}$ (see Supporting Information). This value of D_e is in agreement with previously

reported D_e values for BSA release from PEG hydrogels.³¹⁹ **D2ER** hydrogels, which undergo rapid degradation in reducing microenvironments owing to thiol exchange reactions, exhibited degradation-dependent release, with ~95 % of the cargo released after approximately 4 days, commensurate with when complete hydrogel degradation was observed. This result suggests that the degradation reaction broadly modulates the release of the cargo molecule. Here, the D_e was found to be $5.70 \times 10^{-8} \text{ cm}^2 \text{ sec}^{-1}$. The difference between the effective diffusion coefficients for the hydrogel compositions correlates with the degradation profile of these hydrogels.

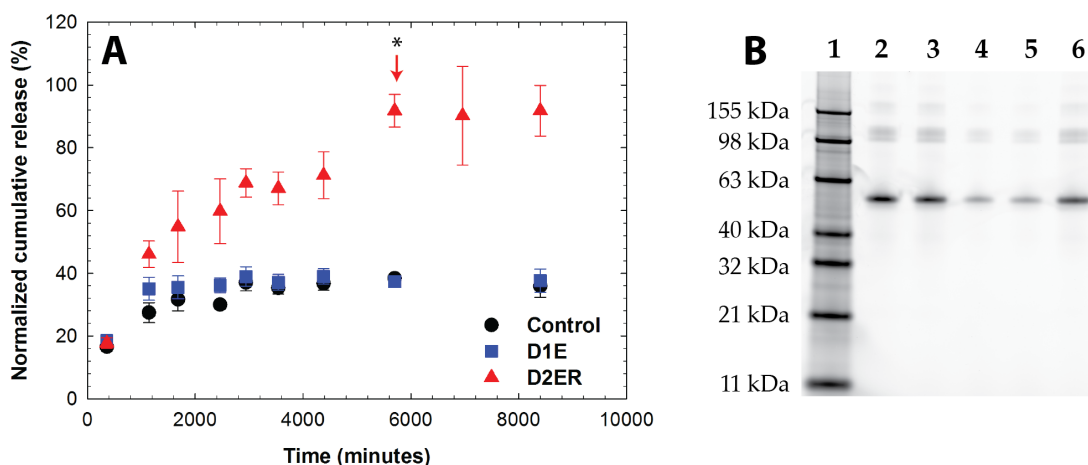


Figure 2.8 Protein release in a reducing microenvironment. (A) Release of a fluorescently-labeled model cargo protein, bovine serum albumin (BSA-488), was monitored using fluorometry. The arrow indicates the time point when reverse gelation (complete gel dissolution) was observed for the **D2ER** hydrogel. While some protein is initially released from all compositions upon gel equilibrium swelling, release from the **Control** and **D1E** hydrogels after this is minimal, owing to no or slow hydrolytic degradation, respectively, over the time course of the experiment. Substantial, statistical differences ($p < 0.05$ for time points after complete hydrogel degradation) in protein release are observed as the **D2ER** hydrogel rapidly degrades by the click cleavage and thiol-mediated exchange mechanism in addition to hydrolytic degradation. Differences in the release profile of BSA-488 from **D2ER**, **D1E**, and **Control** hydrogels highlight that the delivery of cargo molecules is controlled by hydrogel degradation. The data shown illustrate the mean ($n = 6$), with error bars showing the standard error. (B) SDS-PAGE analysis of released protein. Lane 1: protein ladder; Lane 2: free BSA-488; Lane 3: free BSA-488 suspended in reducing microenvironment (10 mM GSH/PBS) with hydrogel precursor solution; Lane 4, 5, 6: supernatant after protein release from **Control**, **D1E**, and **D2ER** hydrogel, respectively. No major differences in the locations of the free BSA and released BSA band are observed, confirming that the protein remained intact during encapsulation and release. Further, analysis of the band intensity by densitometry further supports the relative amounts of protein released from each gel composition as determined by fluorescence (**Control**: ~33%; **D1E**: ~36%; and **D2ER**: ~90%).

SDS PAGE was employed to assess the molecular mass of the released BSA as an indirect measure of its stability during encapsulation and release from the various hydrogel compositions (**Fig. 2.8B**). Lanes 2 and 3 in the figure, which served as controls, were loaded with BSA-488 in PBS buffer containing 10 mM GSH prepared at two different time points (i.e., just before electrophoresis and before starting the release experiment for BSA-488, respectively). Lane 4, 5, and 6 were loaded with sink solution containing released BSA-488 from the **Control**, **D1E**, and **D2ER** hydrogels, respectively. No major differences were observed between the band locations. These results suggest that there were no substantial changes in the overall hydrodynamic volume or molecular weight of the protein during encapsulation and release. Densitometry analysis was carried out using NIH Image J software. The band intensity from lane 3 was normalized to 100%, and compared with the band intensity of released BSA from the **Control** (~33%), **D1E** (~36%), and **D2ER** (~90%) hydrogels. The results correlated well with the protein release data obtained using fluorescence measurements. Taken together, these results suggest the utility of GSH-responsive hydrogels as a drug carrier for controlled cargo release applications. However, for applications where rapid release (~1 to 3 hours) of cargo is desired in response to reducing microenvironment, disulfide linkages still may be more appropriate.

Few studies have reported the use of dually degradable hydrogels for tissue engineering and cell encapsulation applications,^{274, 373} and the use of dually degradable hydrogels for controlled release applications has been limited. Recently, Wang and co-workers investigated use of dually degradable hydrogels for protein release studies by incorporating an enzymatically degradable hyaluronic acid based backbone and chemically cleavable disulfide linkages.³⁷⁴ Depending on concentration of

hyaluronidase and GSH, the hydrogel exhibited significant degradation within the first ~1.5 to 5 hours, and complete release of a cargo molecule (stromal cell-derived factor 1 α , 100 ng) was achieved within approximately 8 hours. The click cleavage and subsequent thiol exchange system presented here undergoes degradation on a significantly longer timescale (~ 4 days) offering advantages for controlled drug delivery, where wider control over degradation can help transition to clinical applications. In addition, incorporation of ester linkages affords long term clearance of these hydrogels from *in vivo* microenvironments due to ester hydrolysis and subsequent degradation.

2.4 Conclusion

In this work, we report dually degradable PEG hydrogels in which degradation can be tailored, without affecting hydrogel formation, by the Michael-type addition of select functional groups that yield crosslinks with tunable, and previously unexplored, degradation mechanisms. This facile approach enables hydrogel formation by broadly useful thiol-maleimide click chemistry employing arylthiols, while eliminating the need for the additional incorporation of more complex and potentially costly labile chemistries within the crosslinker to facilitate degradation, such as enzyme-labile peptides. The rate of hydrogel degradation was found to be dependent upon the chemistry of linker, the number of degradable crosslinks, and the concentration of the reducing microenvironment. The release of a model protein from these hydrogels demonstrates the potential of these matrices and approaches for controlled release applications in thiol-rich reducing microenvironments. Control of degradation rates permitted a 2.5-fold difference in protein release for the dually degradable (**D2ER**) as compared to the non-degradable (**Control**) or single-mode degradable (**D1E**)

hydrogels. In principle, this strategy could easily be employed for controlled release over different time frames using combinations of these thiol functional groups within a single hydrogel or utilized in conjunction with more elaborate degradable chemistries when desired for more complex degradation and release profiles. The degradation of hydrogels by cleavage of click linkages presents considerable opportunities in the design of materials for controlled drug delivery and soft tissue engineering applications.

2.5 Acknowledgements

Research reported in this publication was supported by Institutional Development Award (IDeA) from the National Institute of General Medical Sciences of the National Institutes of Health under grant number P20GM103541 and the University of Delaware Research Foundation. The authors thank Dr. Wilfred Chen for use of the plate reader. The authors thank Rachel Kennel for technical help with precursor solution and hydrogel preparation. Additionally, the authors would like to thank Matthew Rehmann, Megan Smithmyer, Lisa Sawicki, and Kelsi Skeens for feedback on earlier versions of this manuscript.

2.6 Supporting Information

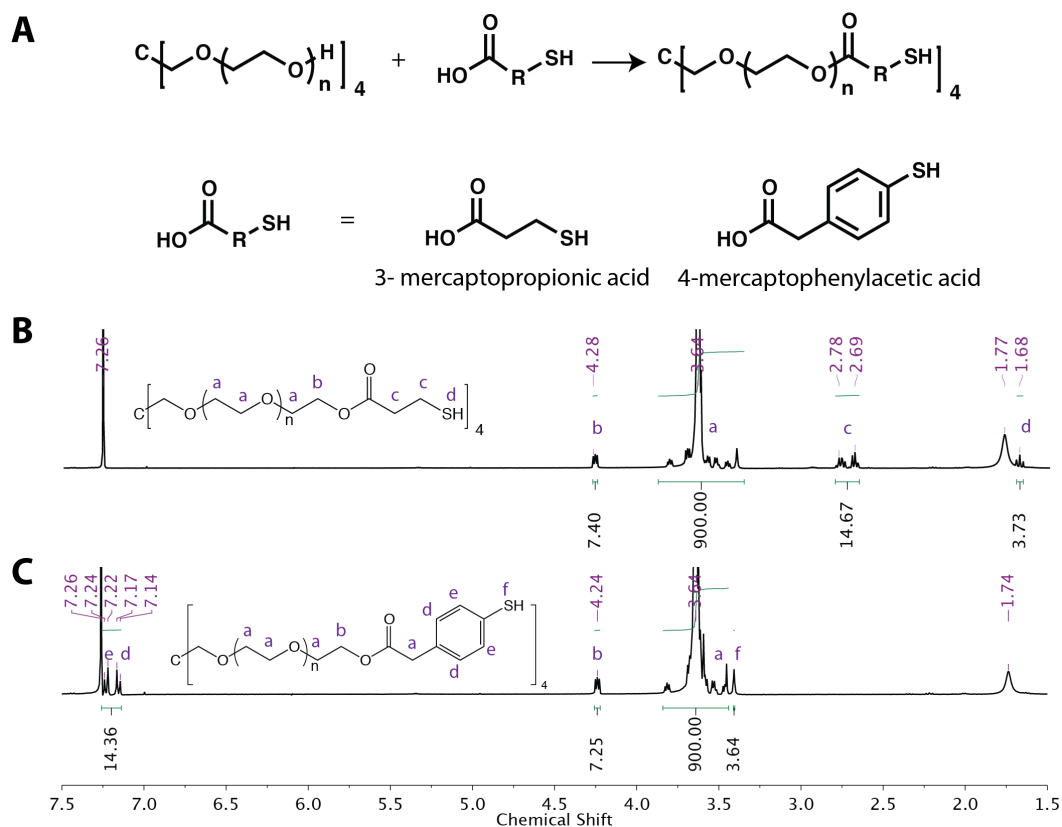


Figure 2.9 Functionalization of PEG. A) Reaction schematic for mercaptoacid esterification of PEG. ¹H NMR spectra for 4-arm PEG functionalized with B) 3-mercaptopropionic acid and C) 4-mercaptophenylacetic acid. The functionality was calculated using the integration area of the proton (labeled b) neighboring the ester linkage (functionality: MP = 92%, MPA = 90%).

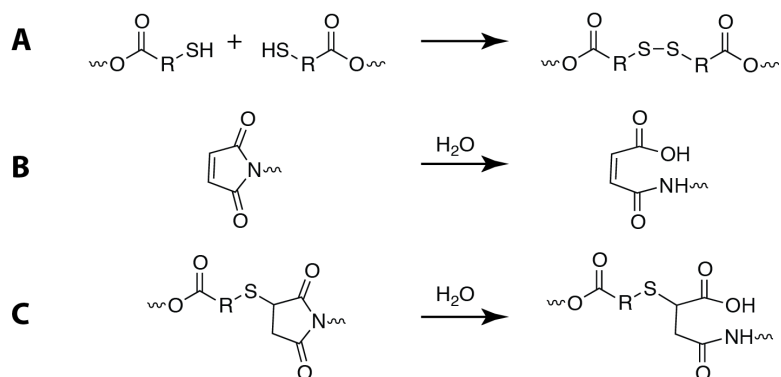


Figure 2.10 Potential side reactions. Hydrogel precursor solutions can undergo **(A)** disulfide formation and **(B)** maleimide ring hydrolysis, which can impact the effective stoichiometry of available SH:MI groups for hydrogel formation. **(C)** Thioether succinimides can undergo ring hydrolysis, making the thioether succinimide linkage unavailable for thiol exchange reactions. However, the rate of ring opening is significantly slower as compared the thiol exchange (order of magnitude different). In addition, ring hydrolysis does not result in breaking of crosslinks and subsequent hydrogel degradation.

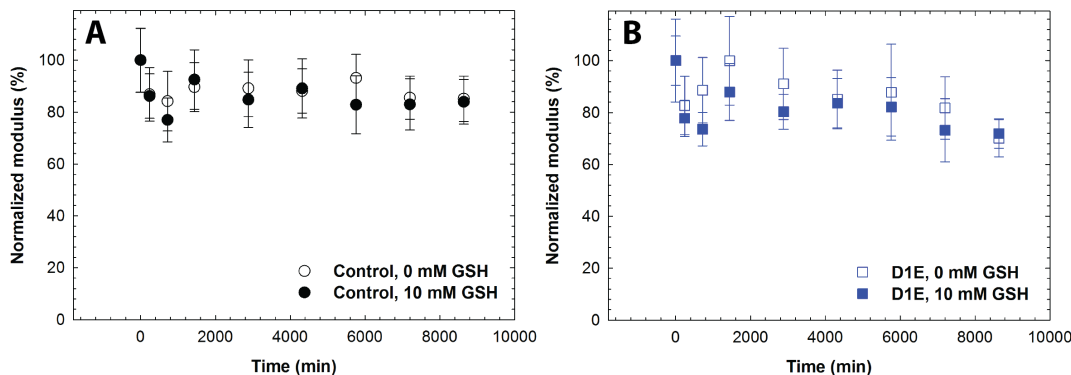


Figure 2.11 Stability of Control and D1E hydrogels under non-reducing and reducing microenvironment. The effect of local microenvironment (0 and 10 mM GSH) on (A) Control and (B) D1E hydrogel was studied by monitoring the decrease in storage modulus at discrete time points. The initial decrease in moduli for Control and D1E in 0 mM GSH and 10 mM GSH can be attributed to equilibrium swelling. D1E hydrogels, compared to the Control, show a relatively larger decrease in moduli, confirming their slow degradation due to hydrolysis. Overall, these data indicate that there were no significant changes in moduli for reducing vs. non-reducing conditions for Control and D1E hydrogels at respective time points. The data shown illustrate the mean ($n = 6$), with error bars showing the standard error.

2.6.1 Degradation Kinetics

The rate of degradation for D2ER hydrogels was evaluated by monitoring storage modulus (G) as a function of time. D2ER hydrogels degraded in 10 mM GSH microenvironment are discussed here as an example of the approach used for this analysis. According to the theory of rubber elasticity,³⁶⁷ material modulus is defined by the following equation:

$$G = \frac{\rho RT}{M_c} Q^{-1/3}$$

...(S4)

where ρ is the density of the polymer, R is the universal gas constant, T is the temperature, M_c is the molecular weight between the crosslinks for the equilibrium swollen gel, and Q is the volumetric swelling ratio. Since we define the degradation of the hydrogel as the scission of network crosslinks (NC), the rate of hydrogel degradation can be described by the following differential equation:

$$-\frac{d[NC]}{dt} = k [NC][GSH][H_2O] \quad \dots(S5)$$

However, since the concentration of thiols from GSH is more than 2 orders of magnitude greater than that of the thiols from the **D2ER** hydrogels, the concentration of GSH in the sink can be assumed to be constant throughout the experiment time period. Similarly, the amount of water in the sink during the experiment timeframe can be assumed as constant. Consequently, the rate expression can be simplified to describe this pseudo first order reaction as shown below.

$$-\frac{d[NC]}{dt} = k_{eff} [NC] \quad \dots(S6)$$

The rate law was obtained by integrating this differential equation (S6) for time from 0 to t and a concentration of network crosslinks from $[NC]_0$ to $[NC]$, arriving at equation S7.

$$[NC] = e^{-k_{eff}t} [NC]_0 \quad \dots(S7)$$

The network crosslinks are directly proportional to hydrogel crosslink density (ρ_x), and hence from equation S4 and S7, we obtain direct correlation between storage modulus and hydrogel degradation rate constant.

$$G \propto \rho_x \propto e^{-k_{eff}t} \dots(S8)$$

Following this method, similar generalizations were made for other sink conditions and are summarized in Table 1. The rate constant for each reaction, k_{eff} , was determined by linear regression using initial parameter estimate functions (SigmaPlot v11, total number of fits = 2000, maximum number of iterations = 200, and stepsize = 1). The results of these regressions are shown in Figures S2.4 and S2.5. **Control** hydrogels under non-reducing as well as reducing conditions exhibited limited changes in G' highlighting their non-degradability. **D1E** hydrogels exhibited degradation via ester hydrolysis as indicated by decrease in G' in both non-reducing and reducing conditions (**Fig. S2.5**).

Table 2.1: D2ER hydrogel degradation kinetics

Sink condition	Limiting parameters influencing rate of degradation	Rate law	k_{eff}
0 mM GSH	Number of crosslinks	$-\frac{d[NC]}{dt} = k_{eff} [NC]$	$1.37 \times 10^{-5} / \text{min}$
0.01 mM GSH	Number of crosslinks, GSH concentration	$-\frac{d[NC]}{dt} = k_{eff} [NC][GSH]$	$5.03 \times 10^{-6} / \text{mM min}$
10 mM GSH	Number of crosslinks	$-\frac{d[NC]}{dt} = k_{eff} [NC]$	$1.75 \times 10^{-3} / \text{min}$

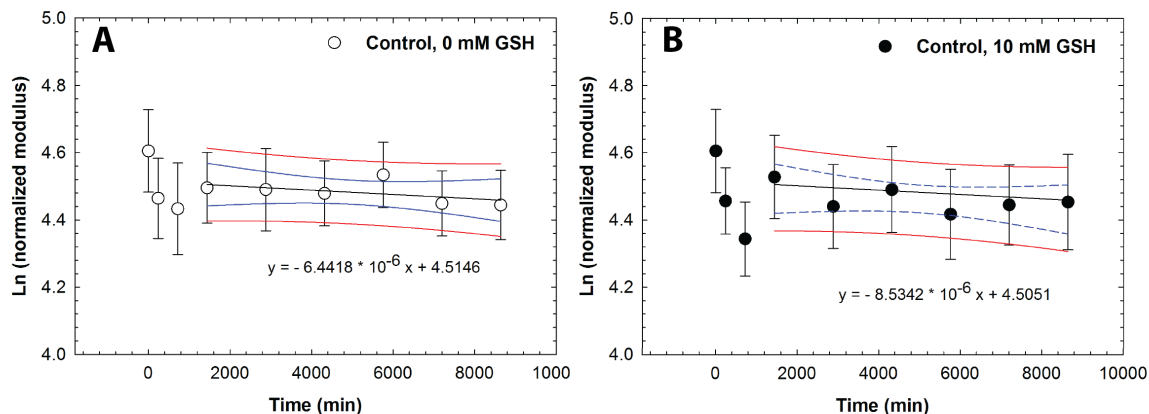


Figure 2.12 Regression analysis for Control hydrogel. Changes in mechanical properties were studied by monitoring storage moduli of **Control** hydrogels suspended under A) non-reducing and B) reducing conditions. The initial decrease in normalized moduli can be attributed to equilibrium swelling. The regression analysis was carried out for timepoints after ~24 hours. The linearity of data points with limited slope (slope with standard error for non-reducing condition = $6.64 \times 10^{-6} \pm 5.24 \times 10^{-6}$ and for reducing condition = $8.53 \times 10^{-6} \pm 6.06 \times 10^{-6}$) indicates that the **Control** hydrogels were stable under both conditions (i.e., no degradation). The data shown illustrate the mean ($n = 6$), with error bars showing the standard error. Initial time points till 1440 minutes were excluded in regression analysis due to initial swelling causing decrease in moduli. Black line indicates linear fit. Blue and red lines indicate 95% confidence and prediction bands.

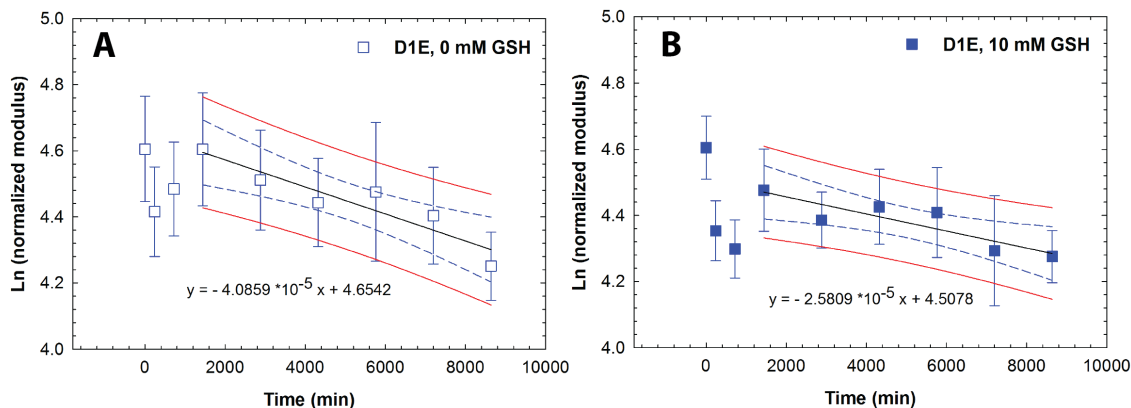


Figure 2.13 Regression analysis for D1E hydrogel. Changes in mechanical properties were studied by monitoring storage moduli of **D1E** hydrogel suspended under A) non-reducing and B) reducing conditions. The initial decrease in normalized moduli can be attributed to equilibrium swelling. The regression analysis was carried out for timepoints after ~24 hours. The linearity of degradation curve with slope indicates that the **D1E** hydrogels showed degradation due to ester hydrolysis (slope with standard error for reducing condition = $4.09 \times 10^{-5} \pm 8.12 \times 10^{-6}$ and non-reducing condition = $2.58 \times 10^{-5} \pm 6.71 \times 10^{-6}$). Comparison of rate of degradation based on regression analysis and slope values for **D1E** and **Control** using Student's t-test indicated statistically significant differences highlighting role of ester linkages in degradation of **D1E** hydrogels. The data shown illustrate the mean ($n = 6$), with error bars showing the standard error. Initial time points till 1440 minutes were excluded in regression analysis due to initial swelling causing decrease in moduli. Black line indicates linear fit. Blue and red lines indicate 95% confidence and prediction bands. Values for coefficient of determination for non-reducing and reducing conditions were found to be 0.86 and 0.79 respectively.

2.6.2 Cumulative Protein Release

The cumulative protein release (R) at each time point was calculated using the following equation:

$$R_t = V_r C_r + \sum_{i=1}^n (V_{m_i} C_i)$$

where V_m and V_r indicate amount of sink solution used for release measurement and remaining volume of sink solution respectively (i.e. total volume of sink, $V = V_r + V_m$) at each time point measurement, C is the concentration of released BSA-488 obtained using fluorometry and calibration curve, and i is the experiment time points.

2.6.3 Mesh Size Calculation

The mesh size was calculated using the Flory-Rehner equation³⁷⁵ as shown below:

$$\frac{1}{\overline{M}_c} = \frac{2}{\overline{M}_n} - \frac{(\bar{v}/V_1)(\ln(1 - v_2) + v_2 + \chi_1 v_2^2)}{v_2^{1/3} - (v_2/2)} \quad \dots(S1)$$

where \overline{M}_c is average molecular weight between crosslinks, \overline{M}_n is the number average molecular weight of the uncrosslinked macromolecular chain, \bar{v} is the specific volume of the polymer, V_1 is the molar volume of the solvent (18 cm³/mol for water), v_2 is the equilibrium volume fraction ($v_2 = Q^{-1}$), and χ_1 is the polymer-solvent interaction parameter (0.45 for PEG-water system).³⁷⁶ The unperturbed root-mean-square end-to-end distance ($(\bar{r}_0^2)^{1/2}$) was calculated by:

$$(\bar{r}_0^2)^{1/2} = lC_n^{1/2} \left(\frac{2\overline{M}_c}{M_r} \right)^{1/2} \quad \dots(S2)$$

where l is the average bond length (1.46 Å), C_n is the characteristic ratio for PEG, taken here as 4, and M_r is the molecular weight of the polymer repeat unit (44 g/mol for PEG). The mesh size was calculated using the following equation,³⁷⁷

$$\xi = v_2^{-1/3} (\bar{r}_0^2)^{1/2} \quad \dots(S3)$$

2.6.4 Effective Diffusion Coefficient Calculation

Effective diffusion coefficient was computed as previously reported.³¹⁹ Briefly, the effective diffusion coefficient (D_e) for the initial time period during which equilibrium swelling occurs was estimated using a modified form of Fick's law as shown below,³⁷¹⁻³⁷² assuming uniform initial drug concentration within the hydrogel:

$$\frac{M_t}{M_\infty} = 4 \left(\frac{D_e t}{\pi \delta^2} \right)^{1/2} = k' \sqrt{t}$$

where M_t and M_∞ are the absolute concentration of released cargo at time t and infinite time, respectively, δ is the thickness of hydrogel, and k' is a constant. The value of k' was obtained by plotting M_t / M_∞ versus \sqrt{t} .

Chapter 3

DESIGN OF THIOL- AND LIGHT-SENSITIVE DEGRADABLE HYDROGELS USING MICHAEL-TYPE ADDITION REACTIONS

3.1 Introduction

Synthetic hydrogels have been widely employed for a range of applications from sensors,³⁷⁸ membranes,³⁷⁹⁻³⁸⁰ and lithography³⁸¹ to sealants,³⁸² adhesives,³⁸³⁻³⁸⁴ and controlled cell culture and drug delivery devices.^{26, 33, 319, 385-386} In particular, hydrogels formed by step growth mechanisms have garnered significant attention owing to their homogenous network structure, robust mechanical properties, and ease of property modulation using responsive and orthogonal chemistries.^{221, 232, 387} For example, nearly ideal step-growth hydrogels have been formed by copper-catalyzed azide-alkyne,^{221, 387} ring strained alkyne-azide,^{219, 226} tetrazine trans-cyclooctene,³⁸⁸⁻³⁸⁹ photoinitiated thiol-ene,^{232, 390} and thiol-maleimide reactions^{159, 391} with stoichiometric amount of reactive functional groups. In biomedical applications, control of mechanical and biochemical properties in time and *in situ* within these materials is key and can be achieved with various combinations of these chemistries for independent control of hydrogel formation and modification³⁹²⁻³⁹³ or by engineering hydrogel degradation.²⁶ Degradation (e.g., ester or enzymatic hydrolysis or other mechanisms) is particularly important for the site-specific delivery of encapsulated therapeutics, including proteins, small molecules, and cells, for administering a desired ‘dose’ with high efficacy while mitigating off-target effects.^{32, 394} Complete degradation of the

material also alleviates the need for implant ‘removal’ as the cleavage products are cleared after matrix dissolution.³⁹⁵⁻³⁹⁶ Further, tunable control over degradation in a noninvasive manner achieved with labile chemistries responsive to endogenous (e.g., hydrolysis, pH, thiol concentration) or exogenous (e.g., light) stimuli, as will be described here, may provide a mechanism for tailoring release profiles for patient-specific treatments.

Control over degradation of hydrogels that are covalently crosslinked often has been achieved by incorporation of degradable groups that can undergo ester hydrolysis or enzymatic degradation.²⁶ Recently, hydrogel degradation using chemistries such as retro Michael-type additions with thiol-exchange,^{249, 275} retro Diels-Alder reactions,^{309, 397} or photocleavable chemistries^{207, 398} has received considerable attention as each provides a responsive synthetic handle for engineering rates of degradation. While these reversible or irreversible cleavage reactions provide control over material degradation and cargo release, a hydrogel system that degrades in response to multiple stimuli would provide a unique tool to create complex cargo release profiles. In recent years, a few groups including ours have developed dually degradable hydrogels for modulating drug release profiles based on degradation kinetics.^{326, 374} While these materials allow microenvironment-responsive release, hydrogel-based drug carriers that degrade in response to multiple triggers, both exogenous (e.g., light) and endogenous (e.g., reducing and aqueous microenvironments), would allow for sustained and complex therapeutic release profiles with spatial and temporal control post fabrication. Several pioneering studies have demonstrated the synthesis of different water-soluble photodegradable macromers with various reactive functionalities, including acrylates, azides, alcohols, amines, halides, and carboxylic

acids.^{277, 349, 399-400} Building upon this, we sought to create injectable, photodegradable and microenvironment-responsive hydrogels that can be crosslinked *in situ* under mild cytocompatible conditions appropriate for *in vitro* and *in vivo* applications.

In this communication, we report a degradable hydrogel, sensitive to multiple stimuli, as an injectable cargo carrier with properties that can be tuned *in situ*. To achieve this, a novel maleimide end-functionalized, photodegradable macromer containing an *o*-nitrobenzyl ether (*o*-NB) group was synthesized and characterized. Thiol-maleimide click reactions were utilized for hydrogel formation, as they are highly efficient, occur under mild conditions, and do not require a catalyst,^{159, 401-402} additionally, selection of the thiol-containing functional group imparts degradability in response to specific stimuli found in cellular microenvironments (e.g., reducing conditions and water). The *o*-NB photolabile group was selected for its susceptibility to degradation over a wide range of cytocompatible irradiation conditions, including long wavelength UV, visible, and two-photon IR light, for user-controlled degradation.^{207, 403} Taken together, the resulting hydrogel undergoes ester hydrolysis in response to an aqueous microenvironment, retro Michael-type reaction with thiol-exchange in response to a reducing microenvironment, and photocleavage in response to externally applied light. This approach provides spatiotemporal control of the properties of cytocompatible hydrogels formed using a catalyst-free Michael-type reaction. Degradation in response to light or aqueous and reducing microenvironments was characterized by monitoring temporal evolution of hydrogel mechanical properties. For proof-of-concept, we also demonstrate how the mode of degradation mediates the release of a model cargo by the incorporation and responsive release of polymeric nanobeads.

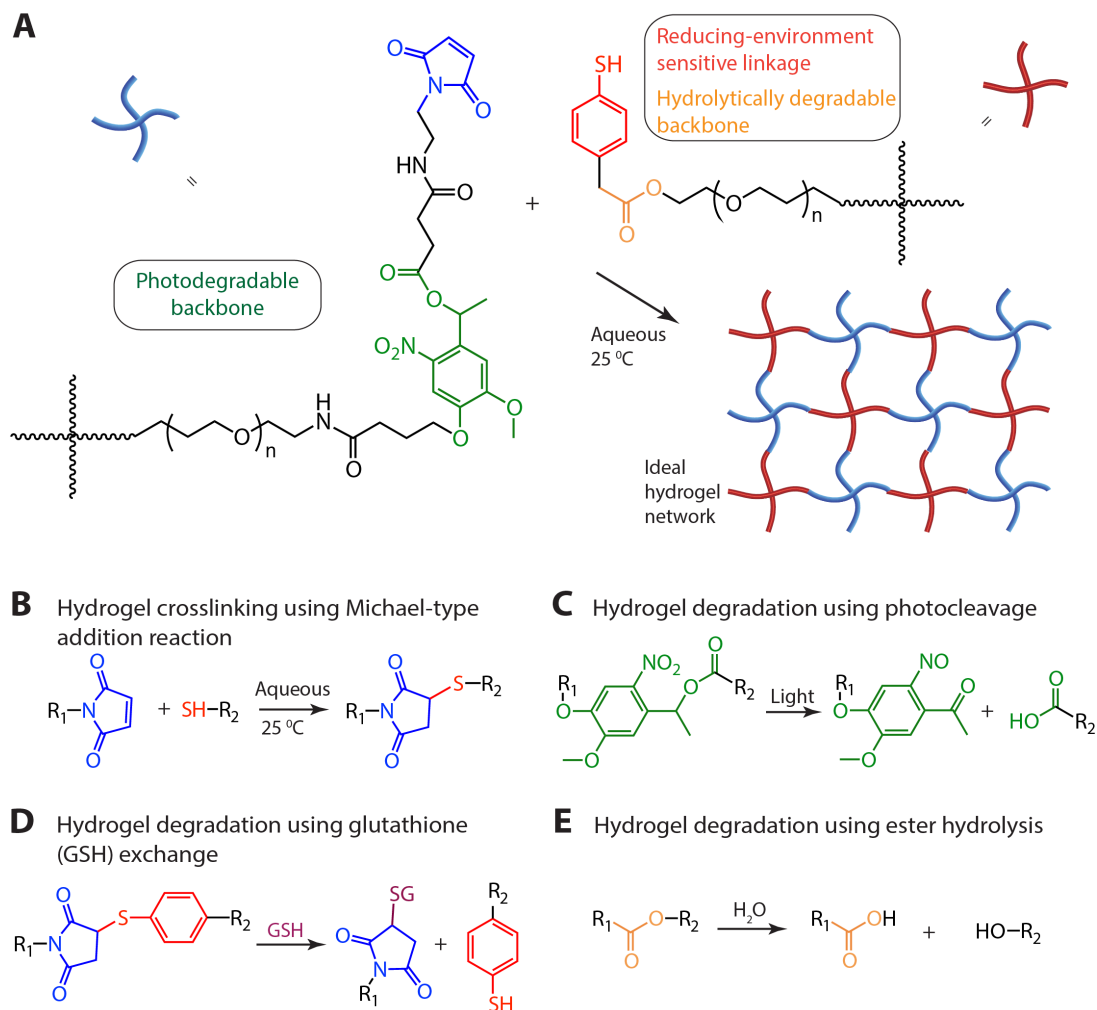


Figure 3.1 Multimodal degradable hydrogel formation and degradation. (A) Multimodal degradable hydrogels were formed by reacting maleimide and thiol end functionalized four-arm poly(ethylene glycol) macromolecular precursors using (B) a Michael-type addition reaction. (C) An *o*-nitrobenzyl ether based photodegradable functional group that undergoes irreversible cleavage upon irradiation with UV, visible, or two-photon IR light were incorporated into the backbone of the network, providing externally-triggered, rapid degradation of thick hydrogels by surface erosion. (D) Presence of arylthiol based thioether succinimide linkages allowed responsive, bulk degradation by retro Michael-type reaction, where thiol exchange with exogenous glutathione (GSH) present in a reducing microenvironment leads to irreversible cleavage. (E) Ester linkages were incorporated within both macromolecular precursors for bulk degradation of hydrogels by hydrolysis over longer timescales.

3.2 Design and Synthesis of Building Blocks with Different Degradable Functional Groups

Several multiarm poly(ethylene glycol) (PEG)-based macromers with different reactive functionalities were created for the rational design of biocompatible, responsive hydrogels with distinct modes of controlled degradation, from preprogrammed and responsive to externally tunable. Specifically, four-arm (PEG) end functionalized with aryl thiols (PEG-4-arylSH) was reacted with four-arm photodegradable PEG end-functionalized with maleimides (PEG-4-PD-MI) by a Michael-type addition reaction (**Fig. 3.1**). PEG, a hydrophilic polymer FDA-approved for various applications, is easily modified with appropriate reactive functional groups for tailoring of the hydrogel properties while limiting any non-specific protein-material interaction.³²⁶ Crosslinking of the photodegradable and thiol-sensitive PEG macromers produces a hydrogel whose main degradable functional units are *o*-NB and mercaptophenylacetic acid (MPA)-based thioether succinimide linkages, respectively. Upon the application of cytocompatible doses of light, the photolabile *o*-NB linkage undergoes irreversible cleavage due to photochemically induced photoisomerization yielding ketone and carboxylic acid-based cleavage products (**Fig. 3.1C**).⁴⁰⁴ Nitrobenzyl-based photolabile groups have been used in several applications as protective groups for uncaging of proteins,⁴⁰⁵ spatiotemporally controlling hydrogel properties,^{207, 399} and the release of live cells or bioactive proteins.^{277, 337, 406} Aryl-thiol based thioether succinimide linkages are susceptible to thiol exchange in the presence of glutathione (GSH), which provides a reducing microenvironment (**Fig. 3.1D**). The degradation kinetics of mercaptophenyl-based thiols in response to reducing microenvironments have been investigated previously by Kiick and coworkers.^{249, 275,}³²⁶ Since the concentration of glutathione is elevated in carcinoma tissues compared to

surrounding healthy tissues,⁴⁰⁷⁻⁴⁰⁸ the incorporation of aryl-thiol-based linkages that cleave in response to glutathione may provide increased release of therapeutics in carcinoma tissues and thus provide higher therapeutic efficacy. In addition, both macromers (PEG-4-PD-MI and PEG-4-arylSH) contain an ester linkage allowing for hydrolysis of the resulting polymeric network under aqueous conditions ultimately leading to complete degradation of the hydrogel in aqueous environments. Overall, the incorporation of multiple cleavable groups that can degrade in response to endogenous and exogenous stimuli presents an attractive strategy for designing drug delivery systems with complex release profiles that could be tuned for the needs of an individual patient.

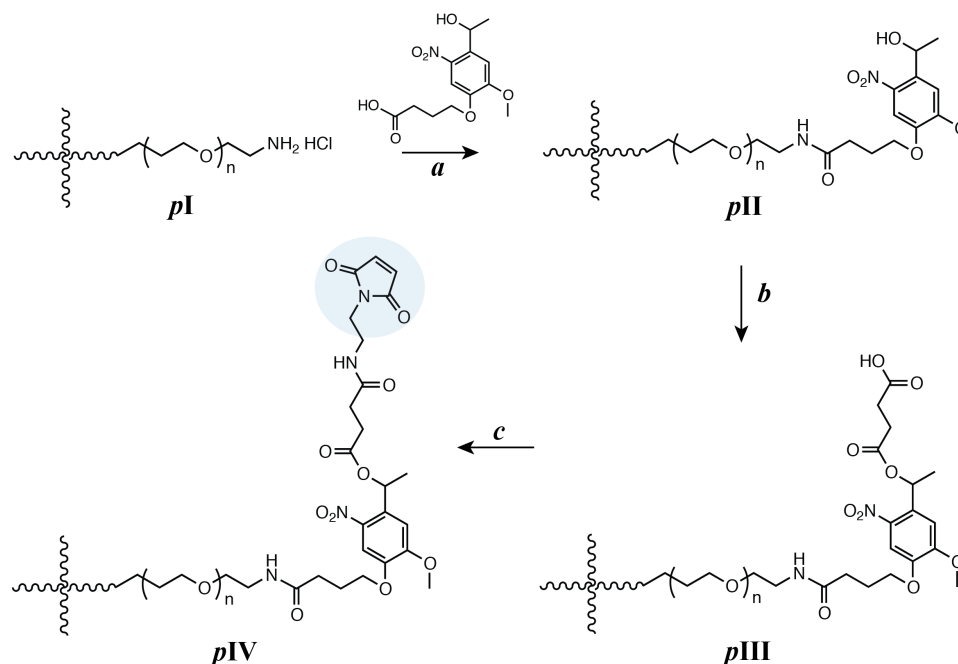


Figure 3.2 Synthetic route for preparing a macromolecular crosslinking agent functionalized with photodegradable maleimide. Reagents and conditions are as follows: *a*) DIPEA, HATU in DMF under Ar; *b*) Succinic anhydride, DMAP in DMF under Ar at 50 °C; and *c*) N-(2-aminoethyl) maleimide, TFA, DIPEA, HATU in DMF under Ar.

PEG-4-arylSH was synthesized via esterification by reacting mercaptophenylacetic acid with the hydroxyl end groups of four-arm PEG (**Fig. 3.2**). Two primary methods can be used for synthesis of the PEG-4-PD-MI: *i*) synthesizing a small photodegradable maleimide monomer for functionalizing the end groups of PEG (or other macromolecules) or *ii*) modifying the end groups of PEG by sequential reactions to conjugate the polymer with the photodegradable maleimide group. Our preliminary efforts focused on the former based on prior successful syntheses of an acrylated photodegradable monomer.⁴⁰⁰ However, conjugation of the photodegradable maleimide monomer to a PEG-*bis*-amine was challenging and led to limited

modification of the amine end groups of the polymer (~ 5-10% modification) [data not shown]. Consequently, we pursued the latter and synthesized a small precursor of the photolabile group, coupled it with the amine end groups of PEG, and subsequently modified the PEG-photolabile precursor with maleimide end groups. This unique approach, as elaborated below, was used to create a PEG crosslinker end-functionalized with a photodegradable maleimide (**Fig. 3.2**). We first synthesized an intermediate, 4-(4-(1-hydroxyethyl)-2-methoxy-5-nitrophenoxy) butanoic acid (**V**, **Figure 3.7**), using a protocol published by Kloxin *et al.* with one modification.⁴⁰⁰ Briefly, the nitration step was carried out continuously on an ice bath to minimize any side reactions (i.e., nitration at multiple positions), and the purification of the nitrated product was carried out using flash chromatography (3:7 ethyl acetate:hexane to 6:4 ethyl acetate:hexane) (see Supporting Information for detailed protocol). The carboxylic acid groups from intermediate **V** were activated with 1-[bis(dimethylamino)methylene]-1H-1,2,3-triazolo[4,5-b]pyridinium 3-oxid hexafluorophosphate (HATU) in the presence of N,N-diisopropylethylamine (DIPEA) to form an amide linkage with four-arm PEG amine (PEG-4-NH₂). This reaction yielded a polymer-photolabile precursor intermediate with hydroxyl end groups (**pII**) with 99% modification as assessed from integration of the area of the aromatic protons in the ¹H NMR spectrum. Multiarm PEG (four-arm) maleimide was employed instead of linear PEG to provide higher functionality per crosslinker and facilitate encapsulation and entrapment of various cargos for delivery applications. The hydroxyl groups from **pII** were subsequently reacted with succinic anhydride to convert them to carboxylic acids and yield the acid-functionalized photodegradable polymer intermediate (**pIII**). The reaction yield was ~79%, and the functionality

(~100%) was quantified by the disappearance of the hydroxyl proton at 5.26 ppm in the ^1H NMR spectrum. The carboxylic acid groups were activated using HATU to form an *o*-acyl(tetramethyl)-active ester that can react with the nucleophilic amine of N-(2-aminoethyl) maleimide (AEM) (or other amine-functionalized reactive groups of interest). This reaction yielded maleimide-functionalized, photodegradable 4-arm PEG (**pIV**, PEG-4-PD-MI) with a reaction yield of 82% and functionality of 79%, as quantified by monitoring the area of the maleimide ring protons (6.97 ppm) in the ^1H NMR spectrum (see Supporting Information). The lower functionalization with maleimide observed here, as compared to the other end group modification reactions, may be attributed to two side reactions: free amines of AEM may react with maleimides on other AEM molecules, and the maleimide ring may undergo hydrolysis during synthesis and purification. Although the synthesis of a water-insoluble nitrobenzyl moiety with maleimide end group recently has been reported,⁴⁰⁹ to the best of our knowledge, this is the first reported synthesis of a water-soluble maleimide end-functionalized photodegradable PEG macromer for controlling hydrogel degradation. These methods in principle could be employed for designing cell compatible hydrogels for tissue engineering and regenerative medicine applications.

3.3 Hydrogel Formation and Tunable Mechanical Properties

The mechanical properties of hydrogels formed using the synthesized multifunctional macromers were investigated to demonstrate the utility of Michael-type addition to form hydrogels sensitive to multiple stimuli. In particular, hydrogel gelation kinetics and mechanical properties play a crucial role in the clinical translation of injectable hydrogels for controlled drug delivery applications. Here, dynamic time sweep rheological experiments were conducted to monitor the gelation

kinetics and to demonstrate the utility of these functionalized macromolecules to form crosslinked networks on timescales appropriate for injection. Hydrogels were formed *in situ* (i.e., on the rheometer stage) by mixing precursor solutions of photodegradable PEG-4-PD-MI and a microenvironment-sensitive PEG-4-arylSH at 1:1 ratio of maleimide to thiol. The mixed precursor solution was added to the rheometer stage before any apparent increase in the solution viscosity, and time sweep measurements were acquired under the viscoelastic regime (**Fig. S3.3**). Representative results for the formation of a 5 wt% hydrogel are shown in **Fig. 3.3A**. Due to rapid gelation, the crossover point of storage and loss moduli, which is an indirect measurement of the gel point, occurred prior to the first measurement on the rheometer. A consistent increase in storage modulus (G' , from ~ 1900 Pa to ~ 4000 Pa) without a significant increase in loss modulus (G'' , values ranging from ~ 50 Pa to ~ 70 Pa) as a function of time was observed, correlating with the crosslinking of the hydrogel ($G \sim \rho_x$). Further, consistent values of storage modulus as a function of frequency highlight the elastic nature of the hydrogels (**Fig. S3.3A**).

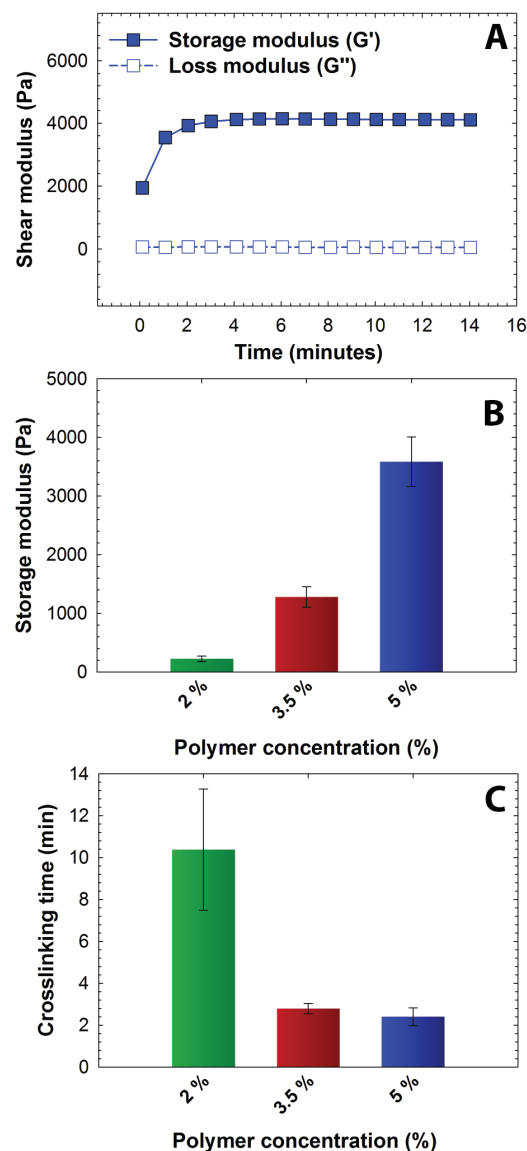


Figure 3.3 Rheological characterization of hydrogels (A) Hydrogel formation was monitored by dynamic time sweep measurements using an oscillatory rheometer, where all measurements were performed within the linear viscoelastic regime (representative data for 5 wt% hydrogel shown). (B) Polymer concentration was varied to achieve a range of moduli and corresponding mesh sizes (see Fig. S3.4), and the impact on crosslinking time was assessed. With increased polymer concentration, the crosslink density increased resulting in increased storage modulus and lowered gelation time. The data shown illustrate the mean ($n \geq 3$) with error bars showing the standard error.

Properties that are critical for the success of injectable hydrogel-based drug carriers, especially mesh size that dictates diffusion of solutes in and out of hydrogel, are dependent on the mechanical properties and vary with the network crosslink density. The impact of crosslink density on the elastic properties of the hydrogel was investigated by varying the polymer concentration (**Fig. 3.3B**). With an increase in the total polymer concentration from 2 to 5 wt%, the storage modulus (G') increased from 0.2 kPa to 3.7 kPa, which correlates to elastic moduli (E) ranging between ~ 0.6 to ~ 11 kPa, where $G \sim E/3$ based on rubber elasticity theory. This range of elastic moduli matches well with that of various soft tissues, from that of neural to muscular tissues.⁴¹⁰⁻⁴¹¹ The corresponding mesh size, calculated from Flory-Rehner theory,⁴¹² varied between 10 nm to 14 nm as a function of polymer concentration, providing a handle to control entrapment, diffusion, and release of cargo molecules (**Fig. S3.4**). The crosslinking time, defined here as the time to reach 90% of the final storage modulus value, ranged from approximately 2 to 10 minutes (**Fig. 3.3C**). The equilibrium mass swelling ratio (q) of resulting hydrogels varied from 17 to 32 (**Table 2**). The gelation kinetics and elastic properties of these novel hydrogels are consistent with the gelation kinetics of similar Michael-type crosslinked PEG hydrogels.^{159, 413-414} Overall, these results indicate that the gelation time and initial elastic properties of the multimodal degradable hydrogels formed using Michael-type reaction of these modified macromers can be tuned over relevant ranges for the end application.

3.4 Degradation in Response to Exogenous and Endogenous Stimuli

We next sought to establish a range of degradation profiles and times that could be achieved with these multifunctional gels in detailed studies of their degradation kinetics in response to light, reducing microenvironments, and aqueous

microenvironments. Changes in the elastic properties of the hydrogels were monitored as a function of time upon application of each stimulus, focusing on the 5-wt% composition with a mesh size (~10 nm) that is appropriate for release of large cargo (e.g., antibodies, nanoparticles, and cells). To study the light-mediated degradation of the multimodal degradable hydrogels, samples formed *in situ* on a photorheometer were irradiated with cytocompatible light conditions (10 mW/cm² at 365 nm [long wavelength UV] or 400-500 nm [visible]).^{207, 210, 276} The hydrogel shear modulus is directly correlated with the crosslink density per the theory of rubber elasticity ($G \sim \rho_x$),³⁶⁷ and a decrease in the storage modulus thus indicates cleavage of crosslinks and degradation of the hydrogel (equation S8). The degradation behavior of the hydrogels was compared with that of a negative control (gels formed using PEG-4-alkylSH and PEG-4-MI that lack the photodegradable group, **Fig. S3.6**), as shown in **Fig. 3.4A**. A significant decrease (approximately 15% reduction) in storage modulus for the multimodal degradable hydrogel was observed with the application of short pulses of light (30-second of 10 mW/cm² at 365 nm), whereas the elastic properties of the control hydrogel remained unchanged. Multimodal degradable hydrogels also degraded with visible irradiation (10 mW/cm² at 400-500 nm, similar to conditions used clinically) as shown in **Fig. 3.4B inset**. These data confirm the triggered degradation of the hydrogels in response to light; the rate of degradation in response to applied light was calculated using continuous degradation data (**Fig. 3.4B**) assuming first-order degradation kinetics based on network connectivity and the kinetics of photocleavage (**Fig. S3.7**).⁴¹⁵ The rate constant (k) for the initial degradation time period was found to be $3.03 \pm 0.13 \times 10^{-1} \text{ min}^{-1}$ ($t_{1/2} = 2.3 \text{ min}$) and compares well with typical rate constants for cleavage of similar *o*-nitrobenzyl ether based moieties ($k \sim$

0.2 - 0.3 min⁻¹).^{276, 416} In addition, a reduction in storage modulus was observed with low doses of visible light with a rate constant of $2.20 \pm 0.03 \times 10^{-2} \text{ min}^{-1}$ (**Fig. 3.4B** inset). The order of magnitude difference in degradation rate constant between 365 nm and 400-500 nm can be attributed to the respective differences in absorbance and quantum yield of the *o*-NB group at these wavelengths (**Fig. S3.5**).^{337, 400}

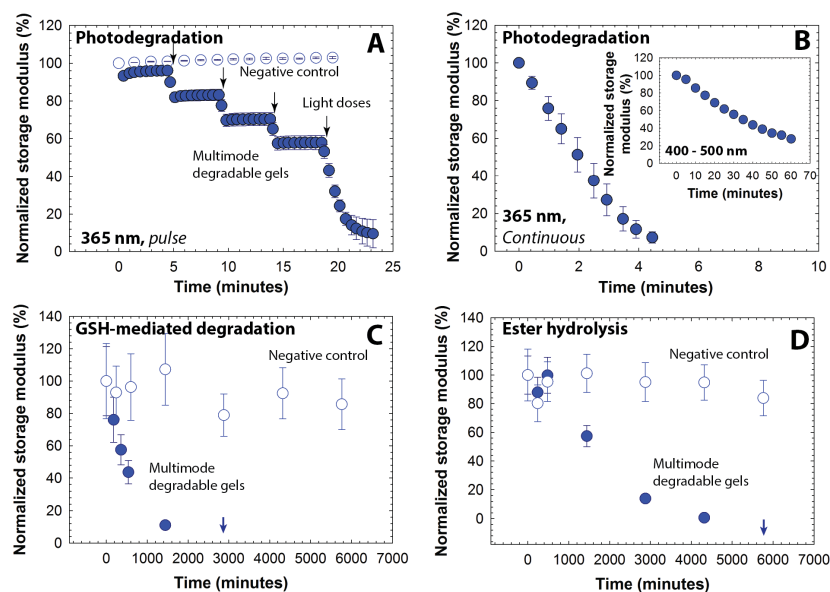


Figure 3.4 Degradation of multimodal degradable hydrogels. Degradation of hydrogels in response to different stimuli was studied by monitoring the storage modulus as a function of time. **(A)** Hydrogels exhibited a rapid decrease in the modulus in response to externally applied, low doses of light (10 mW/cm^2 at 365 nm , 30 sec pulse, closed symbols), and **(B)** complete degradation is observed after ~ 4.5 minutes of continuous exposure. The negative control hydrogels, which lack a photolabile group, show no significant change in modulus over time in response to the same light exposure (open symbols). The hydrogels also were responsive to low intensity visible light (10 mW/cm^2 at 400 to 500 nm , continuous irradiation, inset). **(C)** In a thiol-rich reducing microenvironment like that observed in tumors (ca. 10 mM GSH), a decrease in the modulus of the multimodal degradable hydrogel (closed symbols) was observed, indicating responsive degradation due to reversible click and thiol exchange reactions of aryl thiol based thioether succinimide linkages with GSH under reducing conditions. Complete degradation is observed in approximately 2 days. **(D)** In an aqueous microenvironment (phosphate buffer), the multimodal degradable hydrogel exhibited slower degradation due to hydrolysis of ester linkages with complete degradation in approximately 4 days (closed symbols). The negative control (no degradable groups), after initial swelling, was relatively stable during the experimental time frame (open symbols). The data shown illustrate the mean ($n \geq 3$) with error bars showing the standard error.

Aryl thiol functionalized PEG macromers provide degradability in response to reducing microenvironments within the multimodal degradable hydrogels. GSH is a reducing agent produced at increased levels by highly metabolically active cells, and consequently, is found at elevated concentrations in carcinoma tissues (on the order of 10 mM intracellularly and 10 μ M extracellularly).⁴⁰⁷⁻⁴⁰⁸ To study hydrogel degradation in response to a GSH-rich microenvironment, multimodal degradable hydrogels were suspended in buffer with a physiologically-relevant concentration of GSH (10 mM),³⁵⁸ and the elastic properties of the hydrogels were monitored periodically using oscillatory rheometry (**Fig. 3.4C**). Nondegradable PEG hydrogels without photolabile or reducing environment sensitive linkages (PEG-4-MI and PEG-4-alkylSH) and similar mechanical properties were used as a negative control (**Fig. S6**). As is apparent in Fig. 3C, both control and degradable hydrogels show an initial decrease in storage modulus (approximately 10 to 20% reduction within the first 180 minutes), which can be attributed to initial equilibrium swelling of the hydrogels. Notably, a continuous decrease in modulus for the degradable hydrogels is observed after initial swelling until complete degradation is observed after approximately 2880 minutes (2 days), confirming degradation of these hydrogels in response to the reducing microenvironment. Side reactions, such as maleimide ring hydrolysis that results in a non-degradable crosslink, also can impact the rate and extent of gel degradation; however, our earlier studies indicated that the thiol exchange with the Michael-type adduct occurs on timescales ($k = 1.75 \times 10^{-3} \text{ min}^{-1}$) that are orders of magnitude faster than this side reaction ($k = 5.5 \times 10^{-5} \text{ min}^{-1}$).^{275, 326} Further, ester hydrolysis provides a third mechanism for degradation, where its rate was expected to be slower than that of the thiol-exchange reaction based on prior work ($k = 1.87 \times 10^{-5}$

min^{-1}).³²⁶ Degradation of the multimodal hydrogels in reducing environments without applied light consequently was expected to be dominated by the thiol exchange.^{275, 326} Fits to the data indicated that the observed kinetics for early degradation (first day up to 1440 minutes) were pseudo-first-order with a rate constant of $1.52 \pm 0.003 \times 10^{-3} \text{ min}^{-1}$ ($t_{1/2} = 450 \text{ min}$), which is consistent with earlier reported values for similar hydrogels (**Fig. S3.7**).³²⁶ Complete hydrogel dissolution (i.e., reverse gelation) was observed after approximately 2 days (at 2880 minutes), which is faster than our earlier studies of dually degradable hydrogels that did not contain a photolabile group (complete dissolution at ~ 4 days). We hypothesized that this disparity is due to the elevated rate of hydrolysis of esters present in the PEG-4-PD-MI, since our earlier study indicated that the ester linkage present on the PEG-4-arylSH is relatively stable with a half-life of 14 days. To test this hypothesis, we conducted hydrolytic cleavage studies, characterizing the degradation of multimodal hydrogels over time in an aqueous solution without GSH (**Fig. 3.4D**). The rate of ester hydrolysis was found to be $6.84 \pm 0.91 \times 10^{-4} \text{ min}^{-1}$ ($t_{1/2} = 1013 \text{ min}$, pseudo-first order kinetics, **Fig. S3.7**), which was an order of magnitude larger than that observed for dually degradable hydrogels without the photolabile group ($k = 1.87 \times 10^{-5} \text{ min}^{-1}$).³²⁶ In retrospect, these results are not surprising since neighboring functional groups (here, the photodegradable moiety) have been observed to significantly influence the rate of ester hydrolysis.⁴¹⁷⁻⁴¹⁸ Additional small-molecule studies will shed light on the impact of neighboring groups on the ester hydrolysis of these macromolecules, thus enabling improved design of biomaterials. Nevertheless, the degradation of the multimodal degradable hydrogels can be controlled over minutes to days, with half-lives ranging three orders of magnitude from ~ 2 to ~ 1000 minutes (**Table 3.1**).

Table 3.1 Degradation kinetics of multimodal degradable hydrogels

Degradation Mode	Rate Constant (min^{-1})	Half life ($t_{1/2}$) (min)
Photodegradation (365 nm)	$3.03 \pm 0.13 \times 10^{-1}$	2
Photodegradation (400-500 nm)	$2.20 \pm 0.03 \times 10^{-2}$	32
Thiol exchange	$1.52 \pm 0.003 \times 10^{-3}$	450
Ester hydrolysis	$6.84 \pm 0.91 \times 10^{-4}$	1013

3.5 Degradation Mediated Release of Model Cargo Nanobeads

To demonstrate the utility of this multimodal degradable system for tailored release, fluorescently-labeled nanobeads were entrapped within the hydrogel as a model cargo, where similarly sized beads or particles can be laden with various therapeutics of interest.⁴¹⁹⁻⁴²¹ Since the diameter of these nanobeads ($\varnothing \approx 100$ nm) is ~ 10 -fold larger than the estimated mesh size of the hydrogels ($\xi \approx 10$ nm), the release of cargo was expected to be driven by hydrogel degradation for the proof of concept studies demonstrating control over the time and dose of released cargo. The release of nanobeads in response to appropriate degradation stimuli was monitored in solution using fluorescence spectroscopy. The fractional release, which is defined as the ratio of cargo released at a particular time point (M_t) to the cargo released at complete degradation (M_∞) was plotted as a function of time (**Fig. 3.5**). Hydrogels that were incubated in a thiol-rich microenvironment (10 mM GSH) exhibited limited release of nanobeads ($\leq 1\%$) before complete hydrogel dissolution; release was observed only after reverse gelation after 2 days (2880 minutes). In addition, when incubated in PBS buffer, release was observed only after gel dissolution at 4 days owing to ester hydrolysis (5760 minutes, **Fig. S9**).

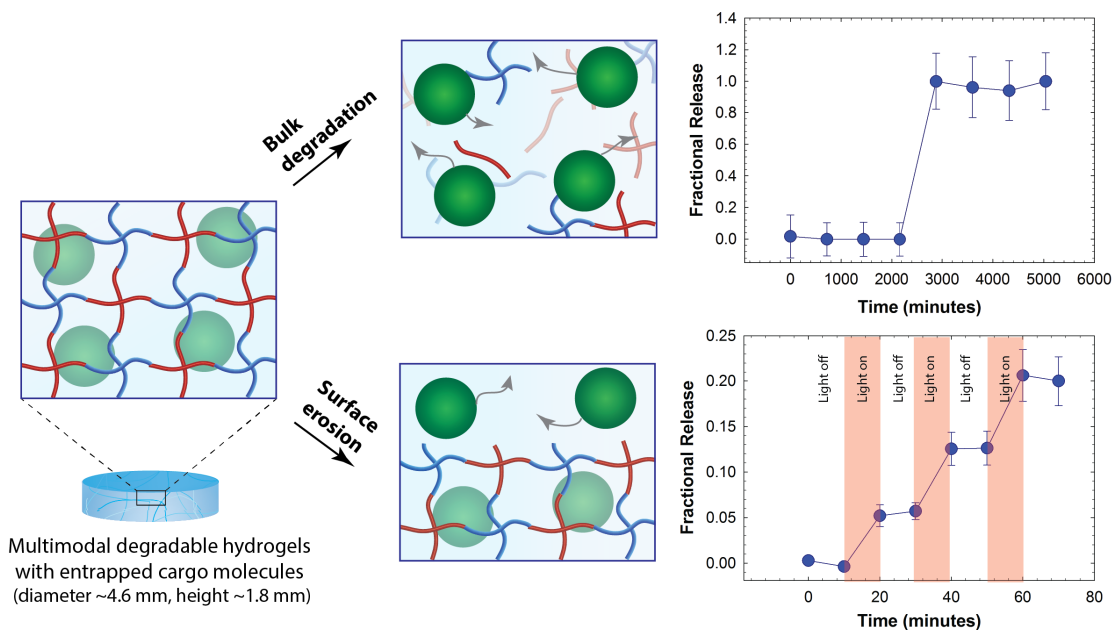


Figure 3.5 Degradation-mediated release of cargo. Fluorescent nanobeads (diameter ~100 nm) were encapsulated as a model cargo within the multimodal degradable hydrogel during formation. Since the diameter of cargo molecules is ~10 times larger than the mesh size, we hypothesized that the release would be controlled by degradation of the hydrogel. Hydrogel samples that were incubated in a reducing microenvironment (10 mM GSH) showed burst release of nanobeads upon hydrogel dissolution (e.g., reverse gelation). When irradiated with pulses of light (10 mW/cm² at 365 nm periodically for 10 minute intervals), the hydrogel exhibited surface erosion (Fig. S6), owing to light attenuation within these thick hydrogels (height ~ 1.8 mm), and the release of nanobeads correlated with this light-mediated surface erosion of the hydrogels. The data shown illustrate the mean ($n \geq 3$) with error bars showing the standard error.

In contrast, hydrogels that were degraded using externally applied light exhibited light-responsive release with approximately 6 to 8% release of the loaded cargo in response to each 10-minute light pulse (10 mW/cm² at 365 nm), without any observable bulk degradation of the hydrogel as elaborated below. These release profiles are consistent with the degradation mechanisms for the related functional

groups, where multimodal hydrogels (height ~ 1.8 mm) should degrade in bulk with reducing and aqueous microenvironments and by surface erosion with applied light.^{276, 415, 422} For photodegradation studies, the height of the hydrogel decreased as a function of time while no significant changes in the diameter of hydrogel discs were observed, further supporting degradation by surface erosion (**Fig. S8**). Surface erosion is expected when using UV and visible light to degrade these *o*-NB-based hydrogels, owing to the strong absorbance of these wavelengths of light by the photolabile group within these thick hydrogel constructs; for example, at 365 nm, the molar absorptivity of the photolabile group is $3840 \text{ L mol}^{-1} \text{ cm}^{-1}$, equating to $\sim 6\%$ transmittance at thickness of $100 \mu\text{m}$ and confining degradation to the top of the surface-eroding gel (see Supplementary Information).^{276, 400, 415} Interestingly, the release of nanobeads (~ 6 to 8%) in response to each applied light pulse was slightly less than expected ($\sim 15\%$ based on the rate of surface erosion in degradation studies, see Supporting Information). We speculate that this disparity likely arises from increased light attenuation in the presence of nanobeads ($\sim 17\%$ by volume of total gel content) that scatter light and may hinder further the light penetration through the hydrogel.

Nanobeads were chosen here for proof of concept where similarly sized particles loaded or decorated with small molecular drugs, proteins, or siRNA can be encapsulated within these hydrogels for localized release for specific applications of interest.⁴²³⁻⁴²⁴ Note, a more continuous release profile upon bulk degradation by thiol exchange or hydrolysis would be expected for biologics (e.g., antibodies and other therapeutic proteins) directly encapsulated within these types of gels; protein release will be driven by diffusion as the mesh size of the hydrogel increases commensurate with degradation, as observed in our earlier work with dually degradable hydrogels.³²⁶

Overall, these results support the hypothesis that the release of cargo can be tuned by controlling the degradation rate and, in principle, such a strategy could be employed for spatiotemporal control over release of cargo molecules in biological systems. For example, we envision that this approach could prove useful for the treatment of various skin cancers, where photodynamic therapies are often employed; with these new materials, therapeutics for the treatment of carcinomas could be released in response to the tumor microenvironment and, as needed, adjusted with light on a patient-specific basis.

3.6 Conclusion

In summary, this work combines three cleavage chemistries to engineer multimodal degradable hydrogels for responsive and triggerable modulation of properties and cargo release. Specifically, a versatile Michael-type addition reaction was employed to synthesize an injectable hydrogel system formed *in situ*, using PEG macromers functionalized with thiols or a photodegradable maleimide, respectively, where incorporation of an aryl thiol imparted degradability in response to reducing microenvironments. The hydrogels exhibited rapid gelation and consistent mechanical properties between samples, which will be helpful for their development as injectable drug delivery vehicles *in vivo*. By incorporating a photodegradable *o*-nitrobenzyl ether group, a thiol-sensitive succinimide thioether linkage, and ester linkages, the hydrogels demonstrated unique controlled degradation via surface erosion or bulk degradation mechanisms, respectively, with degradation rate constants ranging from $\sim 10^{-1} \text{ min}^{-1}$ to $\sim 10^{-4} \text{ min}^{-1}$. As a proof of concept, the controlled release of nanobeads from the hydrogel was demonstrated in a preprogrammed, stimuli-responsive, or spatiotemporal fashion. In principle, such a strategy could be employed for delivery of

multiple therapeutics with precise control over the release and delivery of cargoes, such as drugs, siRNA, drug-loaded nanoparticles, or cells, for creating complex degradation profiles as necessitated by the end application of interest.

3.7 Acknowledgement

Research reported in this publication was supported by an Institutional Development Award (IDeA) from the National Institute of General Medical Sciences (NIGMS) of the National Institutes of Health (NIH) (P20GM103541), an IDeA from NIGMS from the NIH (1 P30 GM110758-01), the Burroughs Wellcome Fund (subcontract from University of California, Davis), and the University of Delaware Research Foundation. Additionally, the authors are deeply grateful to Mr. Srinivasa Chintala and Prof. Joseph Fox for insightful discussions and for supporting an early version of this study in his laboratory. The authors thank Mr. Bassil El-Zaatari, Prof. Christopher Kloxin, and Prof. Wilfred Chen for the training and use of equipment in their respective laboratories. Authors are thankful to Prof. Emanuel Maverakis for helpful discussion regarding material design. Additionally, the authors would like to thank Mr. Matthew Rehmann for feedback on earlier versions of this manuscript.

3.8 Supporting Information

3.8.1 Materials

General organic reagents and solvents were purchased from commercial sources and used as received unless otherwise stated. Four-arm poly(ethylene glycol) (PEG, 10 000 g mol⁻¹) with hydroxyl, thiol, or amine end groups was obtained from JenKem Technology USA (Allen, TX). Deionized water (18 MΩ-cm) was used for experimental procedures.

3.8.2 Organic Synthesis and Polymer Modification

All reactions were conducted in glassware that was oven-dried and cooled under argon. All reactions were performed at least in duplicate and under an inert argon atmosphere using a Schlenk line unless noted otherwise. Chromatography was performed on silica gel (Sorbent Technologies, 40-63 μm , 60 \AA). ^1H spectra were recorded using a Bruker NMR spectrometer (Bruker Daltonics, Billerica, MA) under standard quantitative conditions (600 Hz, 128 scans).

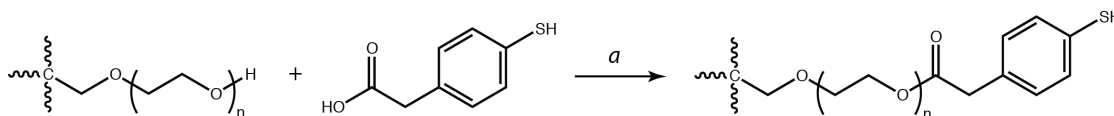


Figure 3.6 Synthesis of PEG-MPA. 4-arm PEG was reacted with 4-mercaptophenylacetic acid (MPA) to yield aryl thiol end-functionalized PEG (a: Toluene, PTSA, $\sim 110\text{ }^{\circ}\text{C}$)

3.8.2.1 Mercaptophenylacetic Acid-based Aryl Thiol-end Functionalized PEG (PEG-MPA)

PEG was modified with 4-mercaptophenylacetic acid (MPA) based on a modified version of a previously published protocol.³²⁶ Briefly, hydroxyl end-functionalized 4-arm PEG (1 g, 0.1 mmol), MPA (0.67 g, 4 mmol), and *p*-toluenesulfonic acid (0.07 g, 0.04 mmol) were dissolved in toluene (20 mL) and refluxed at $110\text{ }^{\circ}\text{C}$ for 48 hours. The reaction was subsequently precipitated in ethyl ether (50 mL, $4\text{ }^{\circ}\text{C}$), and polymer was recovered by filtration. The polymer was washed with isopropanol and hexane and further reduced using dithiothreitol (DTT). The product was dissolved in methanol, filtered through a 0.22- μm filter, and precipitated in isopropanol. The final dried polymer (0.5 g, 66% yield) was obtained by removal of residual solvents under reduced pressure at room temperature. ^1H NMR

(400 MHz, Chloroform) δ : 7.24–7.08(m, 16H), 4.24 (t, 8H), 3.90–3.35 (bs, 900H), 3.42–3.39 (s, 4H).

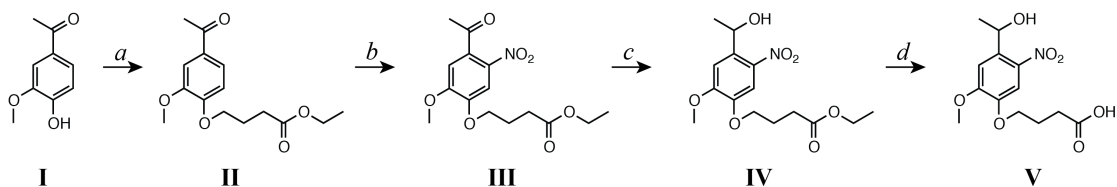


Figure 3.7 Synthetic route for preparing small molecule photolabile precursor.

Reagents and conditions are as follows: *a*) ethyl-4-bromobutyrate, potassium carbonate in DMF; *b*) nitric acid (69.3% w/w); *c*) sodium borohydride in ethanol at 38 °C; and *d*), potassium hydroxide in water:THF (1:1). Each chemical compound is numbered for its identification in experimental procedures.

3.8.2.2 Ethyl 4-(4-acetyl-2-methoxyphenoxy)butanoate (II)

Synthesis of intermediate II to V was based on a modified version of a previously published protocol.⁴⁰⁰ Briefly, 1-(4-hydroxy-3-methoxyphenyl)ethanone (I, 30 g, 180.5 mmol), ethyl-4-bromobutyrate (31 mL, 217 mmol), and potassium carbonate (37.4 g, 271 mmol) were added to DMF (150 mL) and stirred overnight under argon. The reaction mixture was precipitated into DI water (2000 mL), stirred for 2 hours, and stored overnight at 4 °C for maximum precipitation. The resulting precipitant was filtered and washed with a copious amount of water. The product was subsequently dried at room temperature in a vacuum oven, and the final product was collected as a white powder (47.4 g, 94%). ¹H NMR (600 MHz, Chloroform) δ 7.61 – 7.46 (m, 2H), 6.87 (d, 1H), 4.16 – 4.09 (m, 4H), 3.89 (s, 3H), 2.56 – 2.50 (m, 5H), 2.20 – 2.14 (m, 2H), 1.24 (t, 3H).

3.8.2.3 Ethyl 4-(4-acetyl-2-methoxy-5-nitrophenoxy)butanoate (III)

Ethyl 4-(4-acetyl-2-methoxyphenoxy)butanoate (**II**, 25 g, 87.6 mmol) was added slowly to nitric acid (70 mL, 4 °C, ice bath) over the period of 1 hour using small portions while monitoring the reaction temperature to ensure it remained below 30 °C. The reaction was allowed to proceed on an ice bath for approximately 30 minutes until completion as assessed by thin-layer chromatography (TLC) (50:50 ethyl acetate:hexane, product $r_f \sim 0.5$). The reaction mixture was precipitated in DI water (1000 mL), stirred for 2 hours, and stored overnight at 4 °C for maximum precipitation. The yellow solid precipitate that was obtained after filtration was further purified by recrystallization in ethanol (300 mL, 78 °C). Purification using flash chromatography (3:7 ethyl acetate:hexane to 6:4 ethyl acetate:hexane) yielded the yellow solid product (21.2 g, 73%). ¹H NMR (600 MHz, DMSO) δ 7.61 (s, 1H), 7.21 (s, 1H), 4.13 – 4.03 (m, 4H), 3.92 (s, 3H), 2.44 (t, 2H), 1.99 (t, 2H), 1.17 (t, 3H).

3.8.2.4 Ethyl 4-(4-(1-hydroxyethyl)-2-methoxy-5-nitrophenoxy)butanoate (IV)

Ethyl 4-(4-acetyl-2-methoxy-5-nitrophenoxy)butanoate (**III**, 18 g, 55 mmol) was dissolved in ethanol (200 mL), and sodium borohydride (1.3 g, 35 mmol) was slowly added to the reaction mixture. The reaction was allowed to proceed at 38 °C overnight. The reaction mixture was precipitated in DI water (3000 mL), stirred for 2 hours, and stored overnight at 4 °C for maximum precipitation. The resultant precipitant was filtered and washed with water to collect the product (11.6 g, 64%) as a pale yellow powder. ¹H NMR (600 MHz, DMSO) δ 7.52 (s, 1H), 7.36 (s, 1H), 5.47 (s, 1H), 5.25 (d, 1H), 4.06 (q, 4H), 3.90 (s, 3H), 2.45 (t, 2H), 2.08 – 1.91 (m, 2H), 1.36 (d, 3H), 1.18 (t, 3H).

3.8.2.5 4-(4-(1-hydroxyethyl)-2-methoxy-5-nitrophenoxy)butanoic acid (V)

Ethyl 4-(4-(1-hydroxyethyl)-2-methoxy-5-nitrophenoxy)butanoate (**IV**, 10 g, 31 mmol) and potassium hydroxide (2.5 g, 44 mmol) were added to a solution of 1:1 THF (100 mL) and water (100 mL) for ester cleavage. The reaction mixture was stirred at room temperature for 2 hours. The pH of the reaction mixture was dropped to ~4 using hydrochloric acid until precipitant formation. The resulting mixture was stored overnight at 4 °C, and product (7.7 g, 72%) was recovered using filtration and dried using a vacuum oven at 40 °C. ¹H NMR (600 MHz, DMSO) δ 12.16 (s, 1H), 7.53 (s, 1H), 7.36 (s, 1H), 5.56 – 5.38 (m, 1H), 5.25 (q, 1H), 4.05 (t, 2H), 3.90 (s, 3H), 2.39 (t, 2H), 1.95 (p, 2H), 1.37 (d, 3H).

3.8.2.6 Hydroxyl End-functionalized Photodegradable PEG Intermediate (pII)

4-(4-(1-hydroxyethyl)-2-methoxy-5-nitrophenoxy)butanoic acid (**V**, 0.12 g, 0.4 mmol) was dissolved in DMF (10 mL). HATU (0.15 g, 0.4 mmol), DIEA (0.10 g, 0.8 mmol), and amine end-functionalized 4-arm PEG (**pI**, 0.5 g, 0.05 mmol) were added to the reaction, and the reaction was allowed to proceed overnight at room temperature. The reaction was subsequently precipitated in ethyl ether (100 mL, 4 °C), and the polymer was recovered by filtration. The final dried polymer product was obtained by removal of residual solvents under reduced pressure. The dry polymer was dissolved in water (~20 mL), dialyzed (MWCO 2000 g/mol, against 3.5 liter of DI water with a total of 6 changes over 48 hours at room temperature), and then lyophilized to give a yellow solid (0.45 g, 82%). ¹H NMR (600 MHz, DMSO) δ 7.91 (t, 4H), 7.52 (s, 4H), 7.36 (s, 4H), 5.46 (d, 4H), 5.26 (qd, 4H), 4.03 (td, 8H), 3.90 (s, 12H), 3.75 – 3.35 (bs, 900H), 2.25 (t, 8H), 1.94 (p, 8H), 1.36 (d, 12H).

3.8.2.7 Carboxyl End-functionalized Photodegradable PEG Intermediate (pIII)

Hydroxy end-functionalized photodegradable PEG intermediate (pII, 0.5 g, 0.04 mmol), succinic anhydride (0.14 g, 1.4 mmol), and DMAP (0.08 g, 0.71 mmol) were dissolved in DMF (1.5 mL) and heated to 50 °C overnight. The reaction mixture was subsequently precipitated in ethyl ether (50 mL, 4 °C), and the polymer was recovered by filtration. The final dried polymer was obtained by removal of residual solvents under reduced pressure. The filtered polymer was dissolved in water, dialyzed (MWCO 2000 g/mol, against 3.5 liter of DI water with a total of 6 changes over 48 hours at room temperature), and then lyophilized to give a dark orange solid (0.41 g, 79%). ¹H NMR (600 MHz, DMSO) δ 7.92 (t, 4H), 7.55 (s, 4H), 7.10 (d, 4H), 6.17 (q, 4H), 4.04 (t, 8H), 3.95 (d, 12H), 3.75 – 3.35 (bs, 900H), 2.54 (td, 8H), 2.44 (t, 8H), 2.24 (t, 8H), 1.94 (h, 8H), 1.56 (d, 12H).

3.8.2.8 Maleimide End-functionalized Photodegradable PEG (pIV)

Carboxy end-functionalized photodegradable PEG intermediate (pIII, 0.5 g, 0.04 mmol), N-(2-aminoethyl) maleimide (0.08 g, 0.34 mmol), HATU (0.09 g, 0.26 mmol), and DIPEA (0.04 g, 0.34 mmol) were dissolved in DMF (5 mL) and reacted overnight at room temperature. The reaction was subsequently precipitated in ethyl ether (50 mL, 4 °C), and the polymer was recovered by filtration. The final dried polymer was obtained by removal of residual solvents under reduced pressure. The filtered polymer was dissolved in water, dialyzed (MWCO 2000 g/mol, against 3.5 liter of DI water with a total of 6 changes over 48 hours at room temperature), and then lyophilized to give a dark orange solid (0.46 g, 82%). ¹H NMR (600 MHz, DMSO) δ 7.94 (dt, 8H), 7.55 (s, 4H), 7.09 (s, 4H), 6.97 (d, 8H), 6.16 (q, 4H), 4.04 (t, 8H), 3.96 (s, 12H), 3.75 – 3.35 (bs, 900H), 2.25 (t, 12H), 1.94 (h, 8H), 1.54 (d, 12H).

3.8.3 Hydrogel Formation and Rheological Characterization

Thiol and maleimide based PEG precursor solutions were prepared individually in citric acid (pH 3, prepared using citric acid and disodium phosphate) and phosphate buffered saline (pH 7.4), respectively. Hydrogels were formed by vortex mixing the macromolecular precursor solutions at 1:1 stoichiometric ratio (maleimide:aryl thiol). Reaction at acidic pH allowed additional time for vortex mixing before gelation occurred, resulting in homogeneous hydrogels. For rheological and mechanical characterization, oscillatory rheology experiments were conducted on a stress-controlled AR-G2 rheometer (TA Instruments). Hydrogels were formed directly on a Peltier plate pre-cooled to 4 °C. Gelation at reduced temperature allowed sufficient time to lower the parallel plate geometry to the geometry gap (120 μm) before onset of gelation. Time sweep measurements (1% constant strain and 6 rad/s frequency) were obtained under the viscoelastic regime to obtain gelation kinetics and final shear modulus of the hydrogels (**Fig. S3.3**). The final shear modulus was defined as the modulus value after reaching the plateau region. The crosslinking time was defined as the time to reach 90% of the final modulus.

Table 3.2 Mechanical properties of hydrogels

Polymer Concentration	Swelling ratio	Storage modulus (<i>Pa</i>)	Crosslinking time (<i>min</i>)
2 weight %	32.1 ± 2.7	222.9 ± 47.9	10.4 ± 2.9
3.5 weight %	25.9 ± 0.3	1277.0 ± 173.9	2.8 ± 0.2
5 weight %	17.1 ± 0.9	3584.9 ± 421.3	2.4 ± 0.4

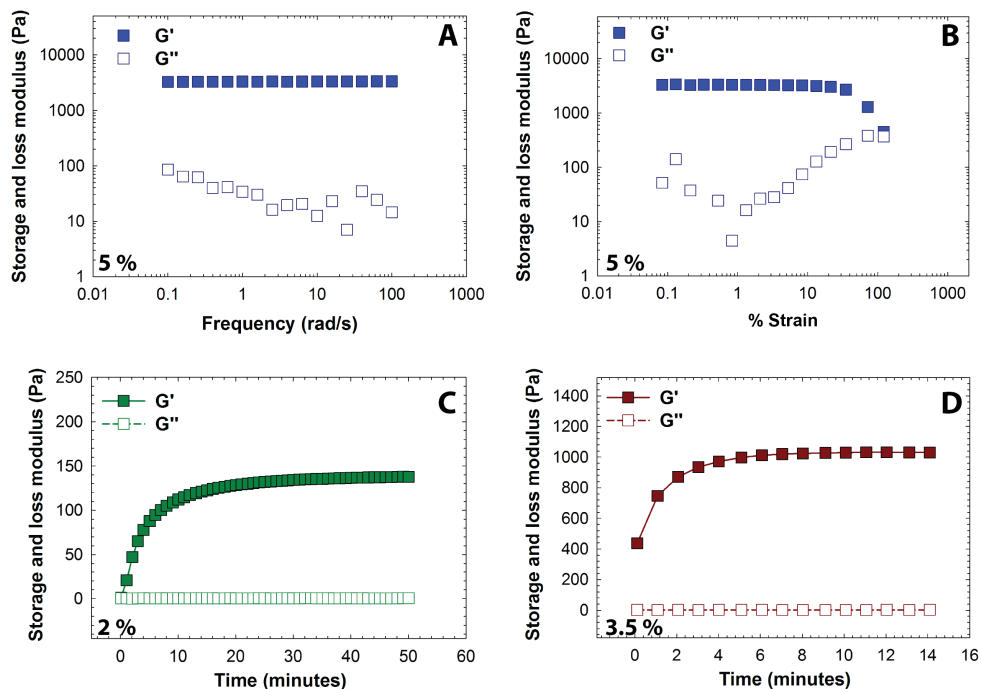


Figure 3.8 **Rheological characterization under the linear viscoelastic regime.** (A) Frequency and (B) strain sweep data was used to determine the linear viscoelastic regime for subsequent rheological characterization (representative data for a 5 wt% gel sample shown). Representative dynamic time sweep measurements for (C) 2 wt% and (D) 3.5 wt% are shown.

3.8.4 Mesh Size Calculations

The mesh size of the hydrogels was calculated based on previously published protocols.^{319, 326} Briefly, the Flory-Rehner equation was used to obtain the average molecular weight between crosslinks (\overline{M}_c) as shown below.^{319, 412}

$$\frac{1}{\overline{M}_c} = \frac{2}{\overline{M}_n} - \frac{(\overline{v}/V_1)(\ln(1 - v_2) + v_2 + \chi_1 v_2^2)}{v_2^{1/3} - (v_2/2)} \quad \dots(SI)$$

where \overline{M}_n is the number average molecular weight of the uncrosslinked macromolecular chain; \overline{v} is the specific volume of the polymer; V_1 is the molar volume

of the solvent (18 cm³/mol for water); v_2 is the equilibrium volume fraction ($v_2 = Q^{-1}$, measured in PBS); and χ_1 is the polymer-solvent interaction parameter (0.45 for PEG-water solutions).³⁷⁶ Subsequently, the unperturbed root-mean-square end-to-end distance ($(\bar{r}_0^2)^{1/2}$) was calculated using following equation:

$$(\bar{r}_0^2)^{1/2} = lC_n^{1/2} \left(\frac{2\bar{M}_c}{M_r} \right)^{1/2} \dots(S2)$$

where l represents the average bond length (1.46 Å); C_n is the characteristic ratio for PEG, taken here as 4; and M_r is the molecular weight of the polymer repeat unit (44 g/mol for PEG). The mesh size was calculated using the following equation for 2%, 3.5% and 5% hydrogel compositions (Fig. S3.4)³⁷⁷

$$\xi = v_2^{-1/3} (\bar{r}_0^2)^{1/2} \dots(S3)$$

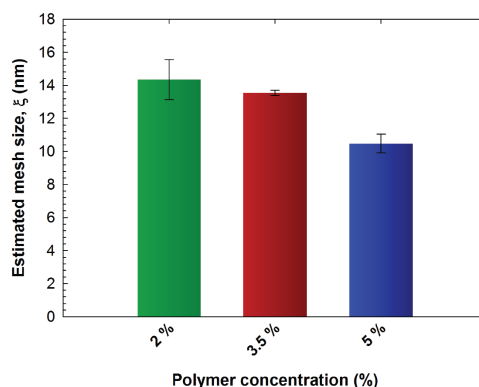


Figure 3.9 Influence of polymer concentration on PEG hydrogel mesh size. Estimated value of the mesh size decreased with increase in the polymer concentration, which can be attributed to the resulting increase in the crosslink density per the theory of rubber elasticity. The data shown illustrate the mean ($n \geq 3$) with error bars showing the standard error.

3.8.5 Absorbance of Photodegradable PEG Macromonomer

The absorbance of maleimide end-functionalized photodegradable PEG (*pIV*) was measured using a UV-visible spectrophotometer (NanoDrop 2000C, Thermo Fisher Scientific) at 10 mg/mL in PBS buffer (**Fig. S3.5**). The molar absorptivity was calculated using the Beer-Lambert law

$$A = abc \quad \dots(S4)$$

where A represents the absorption, a is the molar absorptivity; b is the path length (1 mm); and c is the concentration of photodegradable moiety (2×10^{-3} mol/L).

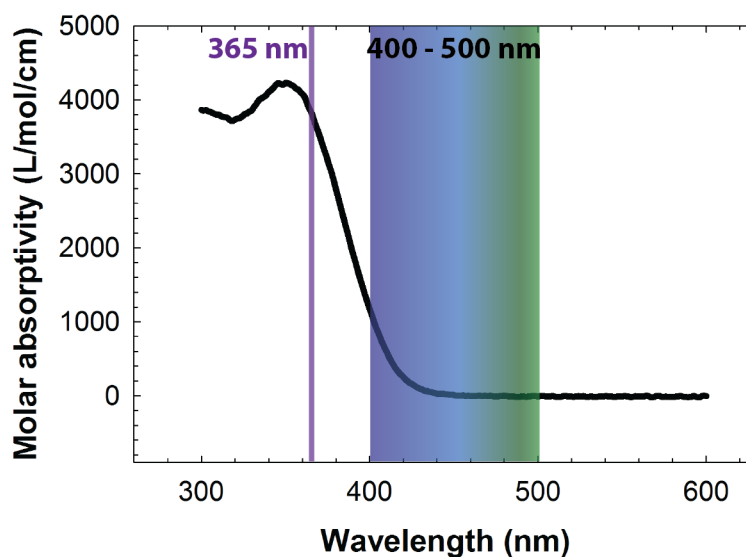


Figure 3.10 Molar absorptivity of the photolabile moiety on the photodegradable macromer. The nitrobenzyl ether based photolabile moiety absorbs 365 nm UV light strongly compared to 400 to 500 nm visible light wavelengths.

3.8.6 Degradation Monitored using Oscillatory Rheometry

For characterization of photodegradation, the hydrogels were directly formed on the rheometer plate; after gelation was complete, low doses of light were applied (10 mW cm^{-2} at 365 nm [long wavelength UV] or 400-500 nm [visible], Exfo Omnicure Series 2000 light source with appropriate bandpass filter, SilverLine UV or International Light Radiometer). For the step-wise degradation study, 30 seconds of light were applied every 5 minutes, whereas for the continuous degradation study, light was constantly applied (<5 minutes for 365 nm and ~60 minutes for 400 to 500 nm wavelength). The degradation was monitored using time sweep measurements in the linear viscoelastic regime (1% constant strain and 6 rad/s frequency). Hydrogels prepared using 4-arm maleimide end-functionalized PEG (without photodegradable groups) and 4-arm PEG-alkylSH served as a negative (nondegradable) control for photodegradation studies (**Fig. S3.6**).

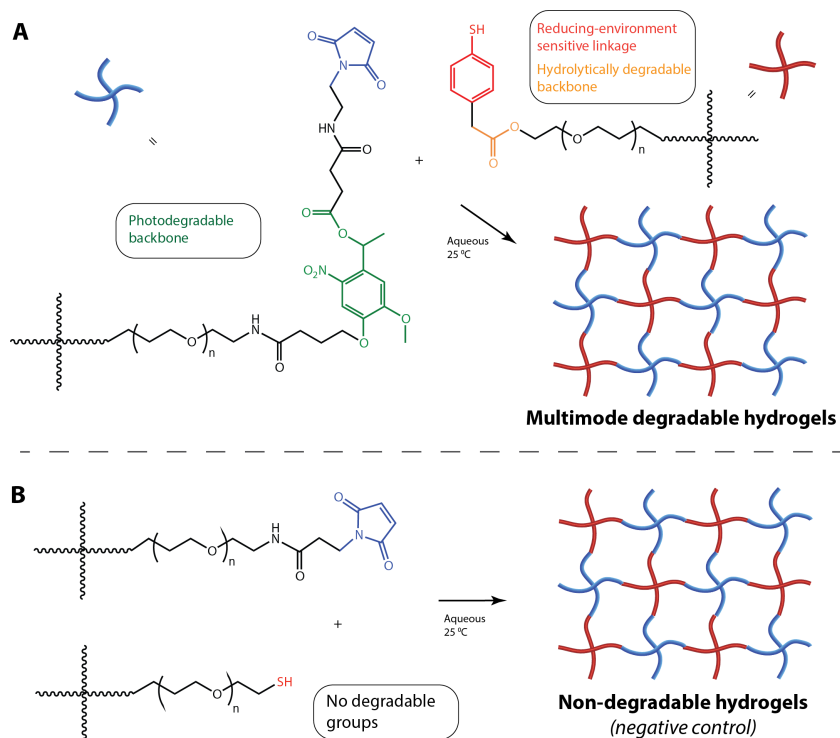


Figure 3.11 Structural differences between the (A) multimode degradable and (B) nondegradable negative control hydrogels. Nondegradable hydrogels (negative control) were prepared by reacting maleimide end functionalized PEG with the alkyl thiol end-functionalized four-arm PEG. The resulting hydrogels thus did not contain any degradable or chemically susceptible functional groups within the backbone structure, as compared with multimode degradable hydrogels.

For GSH-mediated degradation and hydrolytic degradation, hydrogel discs (diameter = 4.6 mm, thickness = 1.8 mm) were prepared by mixing macromolecular precursor solutions (5% w/w) in a 1:1 maleimide:thiol molar ratio and allowing individual hydrogel formation within a cylindrical mold (30 μ L of solution into a 1-mL syringe with tip removed). The resulting hydrogels subsequently were washed with PBS and incubated in appropriate degradation stimuli (10 mM GSH for GSH-mediated degradation and PBS for hydrolytic degradation, pH 7.4) at room

temperature. Degradation was monitored using shear moduli measurements (2 rad/s, 2% strain, and 0.25 N normal force to prevent hydrogel slip). Hydrogels prepared using 4-arm maleimide end-functionalized PEG (without the photodegradable group) and 4-arm alkyl thiol end-functionalized PEG served as a negative (nondegradable) control for GSH-mediated and hydrolytic degradation experiments. The 5 wt% composition was chosen for studying the degradation rates and cargo release of these multimodal hydrogels owing to the ease of handling the higher-modulus formulation relative to the lower moduli 2 and 3 wt% gels.

3.8.7 Degradation Kinetics

For calculating degradation kinetics, hydrogel modulus was monitored as a function of time in response to appropriate degradation stimuli. Hydrogel modulus can be expressed in terms of the molecular weight between the crosslinks for the equilibrium swollen gel (M_c) and the volumetric swelling ratio (Q) per the theory of rubber elasticity, as shown in the following equation.³⁶⁷

$$G = \frac{\rho RT}{M_c} Q^{-1/3} = \rho_x RT Q^{-1/3} \quad \dots(S5)$$

where ρ is the density of the polymer; R is the universal gas constant; T is the temperature; and ρ_x is the crosslink density. Based on the network connectivity, we assume that the cleavage of the labile linkages (DL = degradable linkages) will dictate the rate of degradation of the hydrogel, and consequently, the rate equation can be expressed in first order kinetics as shown below (pseudo-first order for ester hydrolysis and reversible click and thiol exchange where water and GSH, respectively, are in great excess).

$$-\frac{d[DL]}{dt} = k [DL] \quad \dots(S6)$$

where [DL] represents the concentration of degradable linkages within the multimode degradable hydrogels, and k represents the first order degradation rate constant. Integration of equation S6 from time 0 to t and concentration of degradable crosslinks from [DL]₀ to [DL] results in the following equation.

$$[DL] = [DL]_0 e^{-k_{eff}t} \quad \dots(S7)$$

Since the degradable linkages are directly correlated to the crosslink density (ρ_x) for these hydrogels, we arrive at equation S8 based on equation S5 and S7, as shown below.

$$G \propto \rho_x \propto e^{-k_{eff}t} \quad \dots(S8)$$

Using this generalization, the rate constants for various modes of degradation were calculated (**Table 3.1**). The regression analysis for all three modes of degradation for early time points is shown in **Fig. S3.7**.

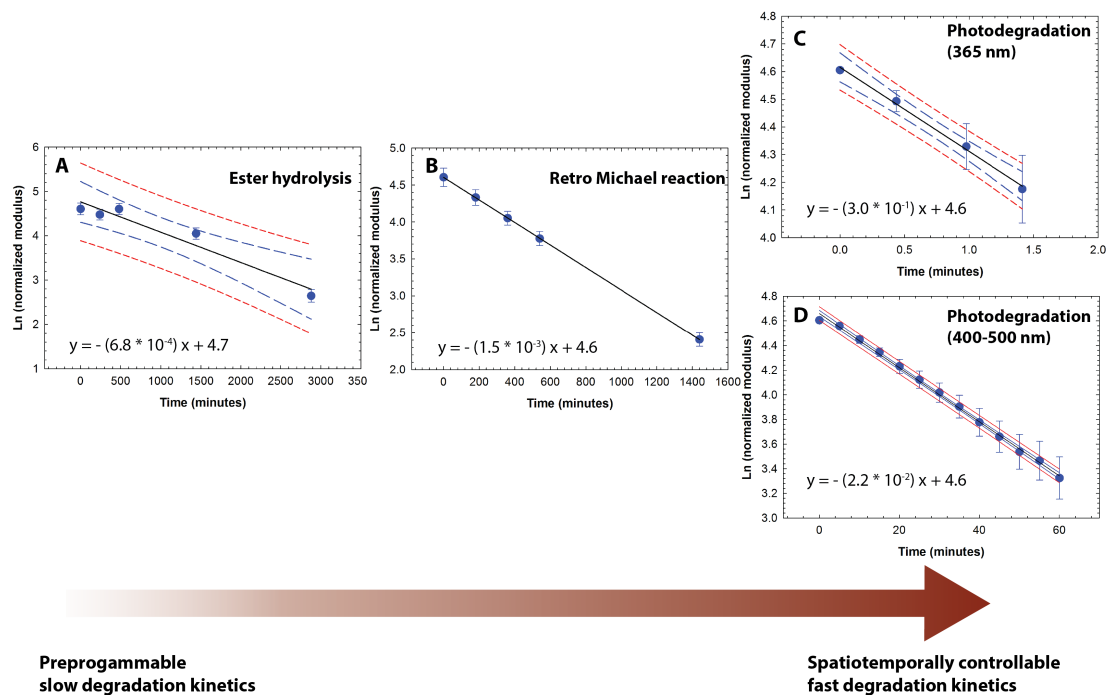


Figure 3.12 Regression analysis for degradation of multimode degradable hydrogels. Multimode degradable hydrogels exhibited first order degradation kinetics in response to the (A) aqueous microenvironment (PBS buffer) with a rate constant of $6.84 \times 10^{-4} \text{ min}^{-1}$, (B) reducing microenvironment (10 mM GSH) with a rate constant of $1.56 \times 10^{-3} \text{ min}^{-1}$, and applied light (10 mW/cm²) at (C) 365 nm with a rate constant of $3.03 \times 10^{-1} \text{ min}^{-1}$ and (D) 400 to 500 nm with a rate constant of $2.20 \times 10^{-2} \text{ min}^{-1}$. The data shown illustrate the mean ($n \geq 3$) with error bars showing the standard error. The black line indicates the linear fit using regression analysis. Blue (long dashes) and red lines (short dashes) indicate 95% confidence and prediction intervals, respectively.

3.8.8 Degradation Monitored Using Hydrogel Volume

Hydrogel discs (diameter ~4.6 mm and thickness ~1.8 mm) were incubated in appropriate degradation microenvironment at room temperature. At predefined time points, the hydrogel discs were removed; the diameter of the sample was measured using a Vernier caliper; and the height of the sample was measured using the rheometer gap values (parallel plate geometry). The volume of the hydrogel was

calculated at each time point assuming an ideal cylindrical geometry. The hydrogel volume at each time point was normalized to the initial volume at time $t = 0$ for that gel composition (**Fig. S3.8**).

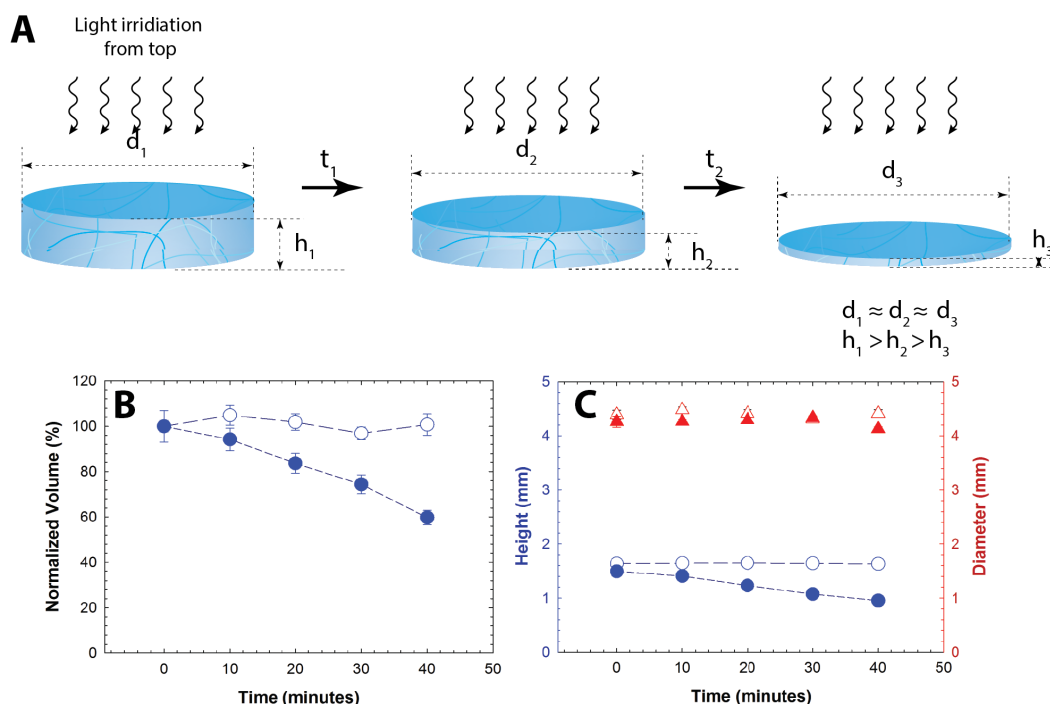


Figure 3.13 Light-mediated surface erosion of hydrogels. (A) Schematic showing surface erosion of the hydrogel upon application of light (10 mW/cm^2 at 365 nm). (B) Multimode degradable hydrogels exhibit a continuous decrease in the normalized volume (closed circle symbols) compared with the negative control (open circle symbols), indicating surface erosion due to degradation of the hydrogel with continuous externally-applied light. The changes in volume are associated with (C) the changes in the height of hydrogel samples, where a continuous decrease in the height with limited changes in diameter are observed, suggesting surface erosion is the prominent mode of degradation of the multimode hydrogel samples upon irradiation (open symbols = negative control and closed symbols = multimode degradable gels; triangle = diameter; circles = height). The data shown illustrate the mean ($n \geq 3$) with error bars showing the standard error.

3.8.9 Calculating Light Attenuation

Percent transmittance was calculated using the Beer-Lambert law as shown below,

$$A = \frac{\log_{10} 100}{\% T} = abc \quad \dots(S9)$$

where A represents absorbance; $\% T$ is the percentage of transmitted light; a is the molar absorptivity of the photolabile group ($3840 \text{ L mol}^{-1} \text{ cm}^{-1}$ at 365 nm); b is the pathlength (depth of penetration); and c is the concentration of photodegradable moiety present in the 5 wt % hydrogel ($8.3 \times 10^{-3} \text{ mol/L}$). With this, approximately 6% of incident light is estimated to penetrate 100- μm deep into these thick hydrogels resulting in surface erosion of the hydrogel.

3.8.10 Cargo Release

Fluorescently labeled polymeric nanobeads (mean particle size = 100 nm, $E_m = 481 \text{ nm}$, $E_x = 644 \text{ nm}$, 16.67 % v/v) were mixed with the maleimide-functionalized macromolecular precursor solution. The photodegradable maleimide and aryl thiol end-functionalized macromolecular precursors were subsequently mixed at 1:1 stoichiometry to yield homogeneous hydrogels with encapsulated nanobeads (one 30- μL hydrogel per each cylindrical mold, diameter = 4.6 mm, thickness = 1.8 mm). The hydrogels were washed with PBS thrice to remove any non-encapsulated nanobeads and then gently rocked at room temperature in 1 mL of PBS buffer for photodegradation studies or PBS with 10 mM GSH for GSH-mediated release. An aliquot of the sink solution (100 μL) was removed for release measurements and replaced by 100 μL of fresh sink solution for cumulative release measurements in bulk degradation experiments. For surface erosion studies, a 100- μL aliquot of the fresh

solution was added back to the sink solution, ensuring a constant sink volume and a detectable concentration of nanobeads in the sink solution. The concentration of nanobeads released at each time point was determined using fluorescence measurements (Synergy H4, BioTek Inc., Winooski, VT), and a calibration curve for the fluorescence of nanobeads as a function of concentration was used to determine the nanobead concentration in the release solution. No significant differences in the slope of the calibration curve were observed due to photobleaching associated with light-mediated degradation experiments ($p = 0.36$, data not shown). The cumulative release (R) at each time point was calculated using the following equation:

$$R_t = V_r C_r + \sum_{i=1}^n (V_{m_i} C_i) \quad \dots(S10)$$

where V_m and V_r indicate amount of sink solution used for release measurement and remaining volume of sink solution, respectively, (i.e., total volume of the sink, $V = V_r + V_m$) at each time point measurement; C is the concentration of released nanobeads obtained using fluorometry and the appropriate calibration curve; and i is the number of experiment time points. For light-mediated release studies, the expected release (~15%) was calculated based on the rate of degradation of hydrogels under similar irradiation conditions: specifically, 120- μm thick hydrogels completely degraded by ~4.5 minutes, consequently, with 10 minutes of irradiation, 267 microns of these thick hydrogel samples (~1.8 mm) and 15 % of beads were estimated to be released, assuming uniform distribution of beads throughout hydrogel samples.

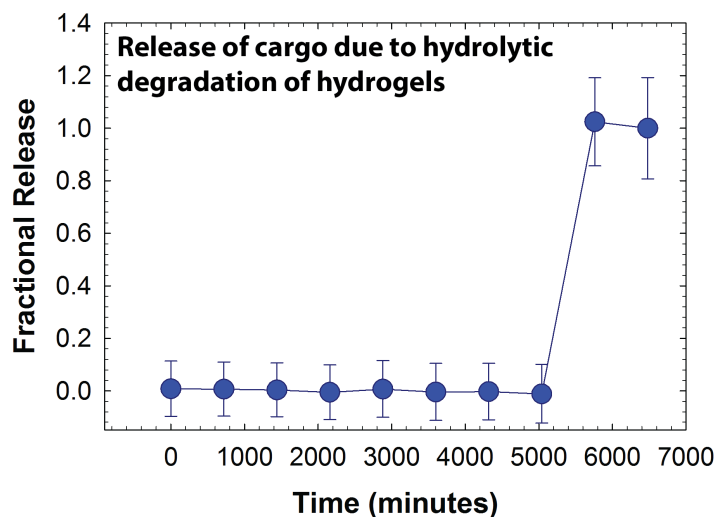


Figure 3.14 **Degradation-mediated release of cargo in response to hydrolytic degradation.** Encapsulated nanobeads were released after 4 days (5760 minutes) upon complete dissolution of the hydrogel owing to bulk degradation by ester hydrolysis. The data shown illustrate the mean ($n \geq 5$) with error bars showing the standard error.

3.8.11 Statistical Analysis

Data are presented as mean \pm standard error. At a minimum three samples were averaged for each data point for all experiments. Statistical comparisons were based on analysis of variance (ANOVA), and $p < 0.05$ was considered statistically significant.

Chapter 4

DEGRADABLE HEPARIN-POLY(ETHYLENE GLYCOL) HYDROGELS FOR BIOLOGICS DELIVERY

4.1 Introduction

Hydrogels have been widely utilized in the area of basic and applied research to study various biological phenomenon^{26, 425} and applications in tissue engineering,^{134, 426} biosensors,⁴²⁷⁻⁴²⁸ protein purification,⁴²⁹⁻⁴³⁰ and drug delivery carriers.^{41, 394, 431} Hydrogels represent crosslinked polymeric networks formed using highly hydrophilic polymers.²⁶ Hydrogels have been prepared using a variety of natural polymers (i.e., hyaluronic acid, chitosan, heparin) and synthetic polymers (i.e., poly(ethylene glycol), poly(vinyl chloride), poly(acrylates)), with polymer selection partly dictated by the intended application.^{13, 432} Natural polymers such as polysaccharides containing glycosaminoglycan provide structural and biological similarities to *in vivo* cellular microenvironment, but may provide challenges due to limited control over mechanical properties of the resulting hydrogels and possible batch-to-batch variation.^{53, 433} In contrast, synthetic polymers provide greater tunability over mechanical properties due to the large scope of chemical modifications available and have minimal batch-to-batch variations.^{31, 434} However, synthetic polymers have limited cell-material interactions and may exhibit limited biocompatibility compared to naturally derived polymers. Hence, a combination of natural and synthetic polymers for hydrogel synthesis not only affords tunable mechanical properties and greater biocompatibility, but also can mimic aspect of native cellular microenvironment.⁴³⁵⁻⁴³⁷

Hydrogels are an attractive candidate as a drug delivery carrier due to their physiochemical similarity to many native soft tissues, ability to maintain bioactivity of cargo molecules, large drug loading capacity, and tunable mechanical properties.^{18, 62} When the cargo molecule of interest, such as drugs, therapeutic proteins, growth factors, or monoclonal antibodies, are physically encapsulated within the hydrogel network, the rate of release is controlled by Fickian diffusion, changes in hydrogel mesh size associated with hydrogel degradation, affinity interactions, or a combination of these mechanisms.¹⁸ In our previous work, we demonstrated degradation-mediated release of cargo (i.e., bovine serum albumin, nanobeads), which was attributed to the mesh size of network being smaller than or comparable with the hydrodynamic diameter of cargo molecules.³²⁶⁻³²⁷ However, several immunomodulatory agents and cytokines that are crucial for mediating cellular processes (e.g., interleukin-2 (IL-2), fibroblast basic growth factor-2 (FGF-2)) have relatively low molecular weight. In such cases, control over rate of cargo release is challenging due to rapid Fickian diffusion-mediated release. For example, Zustiak and Leach compared the release of lysozyme ($M_w = 14.1$ kDa, hydrodynamic diameter ~ 3.2 nm) against bovine- γ -globulins (Ig, $M_w = 150$ kDa, hydrodynamic diameter ~ 9.4 nm) from PEG-based hydrogels.³¹⁹ Release of lysozyme was achieved rapidly (complete release in <24 hours) compared to release of Ig (prolonged release over 7 days) highlighting the role of protein size-associated diffusivity from hydrogels.

In the present work, we hypothesized that a combination of receptor-ligand interactions, along with stimuli-responsive degradation, would afford precise control over the release kinetics of small molecular weight proteins ranging from few days to a week time period. Heparin is heterogeneous glycosaminoglycan which has the

highest negative charge density of any known biological molecules.²¹ The large electronegative charge serves as a multivalent binding site for many proteins including IL-2 (heparin binding constant = 0.5)⁴³⁸ and FGF-2 (heparin binding constant= 0.47 μ M).⁴³⁹ Heparin and heparin-sulfate based polymers have been utilized in numerous drug delivery hydrogels for controlling release of protein via receptor-ligand interactions.^{51, 440-441} For controlling degradation, our group has investigated retro-Michael type and subsequent thiol exchange reaction under high glutathione concentration, which is typically found in intracellular compartment and carcinoma tumor.^{275, 442-443} In addition, our group and others have investigated stability of *o*-nitrobenzyl ether (*o*-NB) moiety under externally applied light leading to irreversible photoisomerization.^{145, 207, 327, 444-445} Ability to control degradation in response to biologically relevant endogenous and exogenous stimuli offers precise control over cargo release.

In the present work, we incorporated aryl-thiol based crosslinker to form succinimide thioether linkages that are susceptible to reducing microenvironment found at higher concentration in intracellular compartments and carcinoma tissue. In addition, we reported synthesis of *o*-NB containing aryl thiol that is responsive to both endogenous (i.e., high reducing microenvironment) and exogenous (i.e., externally applied cytocompatible doses of light) stimuli. Stability of hydrogels, formed via Michael-type reaction, was further investigated in other biologically relevant thiols such as cysteine (CYS) and dithiothreitol (DTT). The rate of degradation was characterized using oscillatory rheometry under varying % degradable content. The release and bioactivity post-encapsulation and -release of small molecular weight protein i.e., FGF-2 was investigated *in vitro*.

4.2 Materials and Methods

4.2.1 Materials

General organic reagents and solvents were purchased from commercial sources and used as received. 4-arm amine-functionalized poly(ethylene glycol) (PEG-4-NH₂, 10,000 g/mol) and linear maleimide-functionalized poly(ethylene glycol) (PEG-MI) was purchased from JenKem Technology USA Inc. (Allen, TX). 4-[4-[1-(9-Fluorenylmethyloxycarbonylamino)ethyl]-2-methoxy-5-nitrophenoxy]butanoic acid (Fmoc-PD) was purchased from Advanced ChemTech (Louisville, KY). Deionized water (18 MΩ-cm) was used for experimental procedures. All reactions were conducted in glassware that was oven-dried and cooled under argon. All reactions were performed in duplicate under an inert argon atmosphere using a Schlenk line unless noted otherwise.

4.2.2 Synthesis of Aryl-thiol End Functionalized PEG

Sulfhydryl groups on 4-mercaptophenylacetic acid (MPA) were oxidized using hydrogen peroxide in the presence of sodium iodide based on previously published protocol.⁴⁴⁶ Briefly, 0.5 g (3 mmol) of MPA was dissolved in 10 mL of ethyl acetate (EtOAc) in the presence sodium iodide (NaI, 4.4 mg, 0.03 mmol) and 30% hydrogen peroxide solution (H₂O₂, 95 mg, 3 mmol). The reaction mixture was stirred at room temperature for 3 hours without inert gas atmosphere. Saturated sodium thiosulfate (Na₂S₂O₃) was subsequently added to reaction mixture (10 mL) and resulting mixture was extracted with EtOAc. The organic phase was isolated and solid residue was further purified using silica gel column chromatography (hexane – EtOAc).

Purified oxidized MPA (100 mg, 0.6 mmol), -[bis(dimethylamino)methylene]-1H-1,2,3-triazolo[4,5-b]pyridinium 3-oxid hexafluorophosphate (HATU, 228 mg, 0.6 mmol), and N,N-diisopropylethylamine (DIPEA, 130 mg, 1 mmol) and amine-end functionalized PEG (500 mg, 0.05 mmol) were subsequently dissolved in DMF (20 mL) and reacted overnight at room temperature. The reaction mixture was precipitated in ethyl ether (10x excess) at 4 °C. The polymer was separated using filtration and dried polymer was obtained by removal of residual solvents under reduced pressure. The polymer was subsequently reduced overnight in the presence tris(2-carboxyethyl)phosphine (TCEP, 470 mg, 1.64 mmol) in DI water (20 mL) at room temperature. The reaction mixture was dialyzed (MWCO 2000 g/mol) against 3.5 liter of acidic DI water (pH 4 adjusted using hydrochloric acid) with total 3 changes over 24 hours at room temperature, and then lyophilized to obtain pale white solid. Degree of thiol functionalization was determined using ¹H NMR spectroscopy using a Bruker AVIII 600 NMR spectrometer (Bruker Daltonics, Billerica, MA) with DMSO as the solvent.

4.2.3 Synthesis of Maleimide Functionalized Heparin

Low molecular weight heparin was modified with maleimide groups based on previously published protocols.^{442, 447} Briefly, 980 mg (0.22 mmol) of heparin was dissolved in 100 mL of 0.1 M 2-(N-morpholino)ethanesulfonic acid buffer (MES, pH = 6.0). Subsequently, 246 mg (1.46 mmol) of 1-hydroxybenzotriazole hydrate (HOBT), 246 mg of N-(3-Dimethylaminopropyl)-N'-ethylcarbodiimide hydrochloride (EDC, 1.28 mmol), and 246 mg (0.96 mmol) of N-(2-Aminoethyl) maleimide, trifluoroacetate salt (AEM) was dissolved and reacted overnight at room temperature under inert atmosphere. The product was subsequently purified using dialysis (MWCO

1000 Da) against 1 M NaCl and deionized water with total 3 changes each over 48 hours. The reaction mixture was subsequently lyophilized to yield solid white product. Degree of functionalization ($f = 2.2$) was determined using maleimide protons in downfield region (6.83 ppm) using ^1H NMR.

4.2.4 Synthesis of Aryl-thiol End Functionalized Photodegradable PEG

Photodegradable aryl-thiol end functionalized PEG was synthesized based on earlier published protocols.^{327, 448} Briefly, Fmoc-PD (200 mg, 0.4 mmol), HATU (152 mg, 0.40 mmol), and DIPEA (104 mg, 0.8 mmol) were dissolved in DMF (10 mL) and amine-end functionalized PEG (500 mg, 1 mmol) was added to the reaction mixture. The reaction mixture was stirred overnight at room temperature and subsequently precipitated in ethyl ether (100 mL). Solid polymer was obtained by filtration and subsequent solvent removal at reduced pressure. Fmoc group was subsequently removed by dissolving solid polymer in DMF (30 mL) containing 20% v/v piperidine. The reaction mixture was stirred overnight at room temperature and product was isolated by precipitation (ethyl ether) and residual solvent removal as described earlier. The photodegradable group containing, amine-end functionalized polymer was subsequently reacted with oxidized MPA and purified as described earlier to obtain aryl-end functionalized photodegradable PEG.

4.2.5 Hydrogel Formation and Rheological Characterization

Thiol-functionalized and Maleimide-functionalized monomers were dissolved individually in citric acid (pH = 3) and phosphate buffered saline (pH = 7) respectively. Maleimide-functionalized heparin was mixed with PEG-MI such that 15% of MI functional groups are contributed by heparin-maleimide. Thiol-

functionalized and maleimide-functionalized monomers were subsequently mixed at 4 °C with 1:1 thiol:maleimide molar ratio to form 7.5 weight % w/w hydrogels. For rheological studies, the hydrogels were formed directly on the rheometer (ARG-2, TA Instruments, USA). Mixed precursor solutions were added directly onto a Peltier plate without apparent increase in the solution viscosity. 20 mm parallel plate geometry was lowered immediately (120 μm gap). Time sweep measurements were carried out under the viscoelastic regime (1% constant strain mode at a frequency of 6 rad s^{-1}) at 25 °C. Three independent samples per time point were analyzed.

4.2.6 Hydrogel Degradation

For hydrogel degradation studies, hydrogels were formed in a cylindrical mold (diameter = 4.6 mm, thickness = 1.8 mm, volume = 30 μL) by mixing 7.5 wt% precursor solutions in a cylindrical mold at 1:1 thiol:maleimide stoichiometry. The solutions were allowed to gel overnight to ensure maximum possible crosslinking density. Resulting hydrogels were washed with PBS (2 mL) and incubated in reducing microenvironment at room temperature over experimental time frame. At predefined time points, mechanical properties of hydrogels were studied using oscillatory rheometry (2 rad/s , 2% strain, 0.25 N force to avoid hydrogel slip) under the viscoelastic regime. For light-mediated degradation studies, hydrogels were formed directly on the quartz plate with slight maleimide excess over thiols (i.e. thiol:maleimide ratio = 1:1.1) to avoid any unreacted thiol functional groups. After complete gelation, a low dose of light was constantly applied (10 mW/cm^2 , 365 nm). Storage and loss modulus were simultaneously measured using parallel plate geometry using time sweep measurements under the linear viscoelastic regime (6 rad/s , 1% strain). Six independent samples per time point were analyzed.

4.2.7 Fibroblast Growth Factor (FGF-2) Release

For growth factor release studies, polymer precursor solutions were mixed and pipetted into a cylindrical mold (diameter = 4.6 mm, thickness = 1.8 mm, volume = 30 μ L). The solutions were allowed to gel at 4°C for 8 hours. Hydrogel discs were immediately washed with PBS thrice to remove any surface-bound FGF-2 and subsequently incubated in 10 mM glutathione in PBS buffer (2 mL volume). The samples were gently rocked on lab shaker and 100 μ L of sink solution was removed at predetermined time points replacing with freshly added 100 μ L GSH in PBS. Amount of released FGF-2 was quantified using ELISA assay (Peprotech, Rocky Hill, NJ). The cumulative release at each time point was calculated using following equation:

$$R_t = V_r C_r + \sum_{i=1}^n (V_{m_i} C_i)$$

where V_m and V_r indicate amount of sink solution used for release measurement and remaining volume of sink solution, respectively, (i.e., total volume of the sink, $V = V_r + V_m$) at each time point measurement; C is the concentration of released FGF-2 obtained using ELISA assay and the appropriate calibration curve; and i is the number of experiment time points. Four samples per time point were analyzed.

4.2.8 Cell Culture

Human aortic adventitial fibroblasts (AF, Lonza) were cultured in stromal cell basal medium (SCBM, Lonza), supplemented with 5% fetal bovine serum (FBS), basic fibroblast growth factor, insulin, and gentamycin/amphotericin-B (all from Lonza). Cells were used between passage numbers 4 and 7 for all assays and maintained at 37°C with 5% CO₂.

4.2.9 Serum Stripping

To ensure that the effects observed in cell culture experiments were attained solely to due FGF-2 released from hydrogels, HiTrap Heparin Affinity Chromatography column (GE Healthcare, Pittsburgh, PA) was used to strip heparin-binding molecules, including FGF-2, contained within FBS, following manufacturer's protocol. The column was equilibrated with 50 mL of binding buffer (10 mM sodium phosphate; pH = 6.9). Next, FBS (5 mL) was then applied to the column and collected, and the column was further washed with 50 mL of binding buffer. Heparin-binding proteins were then eluted with 50 mL of elution buffer (10 mM sodium phosphate and 1.5 M NaCl, pH = 6.9). The serum was run over the column three times using this process to ensure that all heparin-binding molecules were removed. The concentrations of protein in the stripped serum, as well as the wash, binding, and elution solutions, were determined using a Bicinchoninic Acid (BCA) Assay Kit (Pierce, Rockford, IL) performed in triplicate, as described by the manufacturer's instruction.

4.2.10 Proliferation Assay

Hydrogel discs containing FGF-2 were fabricated as described previously, and incubated in 10 mM glutathione in PBS buffer (2 mL volume). After 7 days, 200 μ L of the buffer solution was analyzed via ELISA to determine the amount of FGF-2 released over the culture period. The remainder of the buffer solution was lyophilized to dryness and reconstituted in SCBM containing stripped serum, insulin, and gentamycin/amphotericin-B. Using results obtained from ELISA, the lyophilized proteins collected from the buffer of hydrogels originally incubated in a reducing microenvironment were reconstituted at a concentration of 1 ng/mL FGF-2.

Lyophilized proteins collected from buffer solutions of hydrogels incubated in a non-reducing environment were set to 0.3 ng/mL to account for the differences in the FGF-2 release profile.

AFs were seeded on TCPS surfaces in a 24-well plate format at density of 10,000 cells per well in 500 μ L of medium containing stripped serum with FGF-2 released from hydrogels, at concentrations described above. AFs cultured in SCBM containing 1 ng/mL FGF-2 was utilized as a positive control, while AFs cultures in the absence of FGF-2 served as a negative control. After 48 hrs of culture at 37°C, 5-ethynyl-2-deoxyuridine (EdU) was added to the growth medium to achieve a final concentration of 10 μ M. AFs were incubated for an additional 24 hours and the subsequently, fixed in 4% paraformaldehyde (Electron Microscopy Sciences, Halfield, PA), permeabilized in 0.5% Triton-X 100 (Sigma, St. Louis, MO), and blocked with 1% BSA in PBS. To detect proliferating cells, azide-labeled Alexa Fluor 555 (AF-555, Invitrogen) was selectively bound via copper-catalyzed azide-alkyne ligation of EdU-labeled nuclei; cell nuclei were counter-stained using Hoescht 33342. Proliferating cells were visualized using an EVOS FL Auto Cell Imaging System (Life Technologies) with 10x objective. The percentage of proliferating cells was calculated from the total number of nuclei and the number of nuclei with incorporated EdU from five different spots per well.

4.2.11 Statistical Analysis

Results are expressed as mean \pm standard error of mean unless otherwise specified. For statistical comparison, $p < 0.05$ was considered significant.

4.3 Results and Discussion

4.3.1 Synthesis of Monomers

Various naturally derived polymers and synthetic polymers have been utilized for hydrogel preparation.^{13, 26} Due to the excellent biocompatibility, tunable mechanical properties, and control over chemical modifications, PEG-based hydrogels are well suited for drug delivery applications.^{18, 449} In addition, lack of any protein binding sites makes PEG-based hydrogels attractive candidate for biomedical applications where a blank-slate material is preferred.⁴⁵⁰⁻⁴⁵¹ For drug delivery applications, the release of cargo from PEG-based hydrogels is generally controlled by Fickian diffusion, material degradation, or combination of both. The incorporation of natural polymers (e.g., polysaccharides such as heparin) within hydrogels allows for non-covalent interactions with biological cargo, which both improve the stability of cargo molecules during encapsulation process and control cargo release kinetics.⁴⁵²⁻⁴⁵⁴ Specifically, heparin is a heterogeneous glycosaminoglycan with highest negative charge density among naturally occurring polymers providing ionic interactions with various proteins, growth factors, cytokines.²¹ Hence, we hypothesized that a combination of PEG and heparin containing degradable groups will afford control over release of small molecular weight protein cargo via heparin-mediated interaction and degradation-mediated mesh size changes (**Fig. 4.1**). Owing to presence of aryl-thiol end groups, resulting hydrogels undergo degradation in reducing microenvironment due to retro Michael type and subsequent thiol exchange reactions.

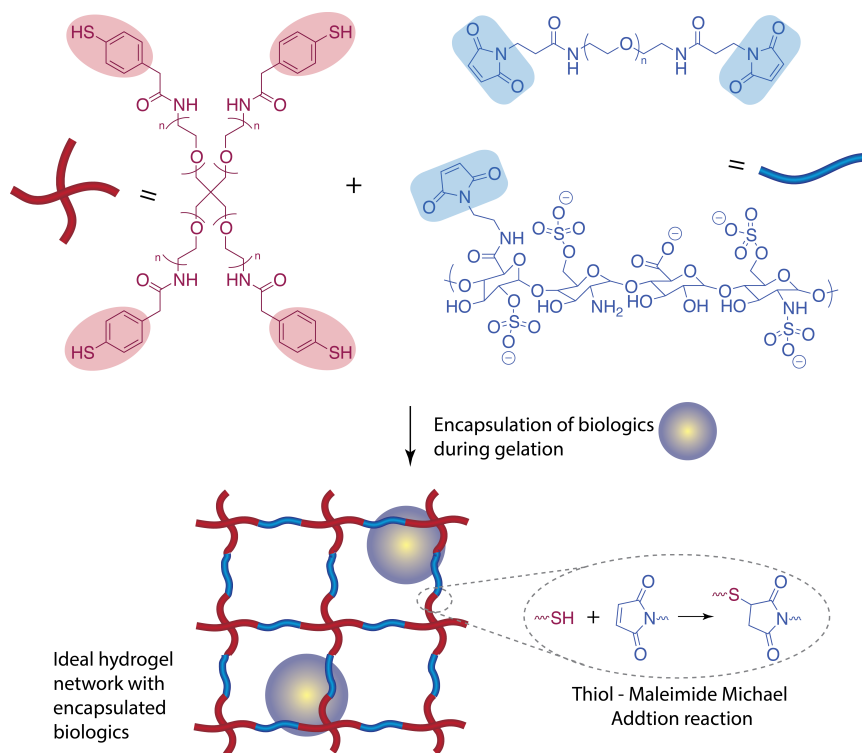


Figure 4.1 Polymeric building blocks for hydrogel formation. Reducing microenvironment sensitive hydrogels were formed by reacting aryl-thiol end functionalized poly(ethylene glycol) macromolecular precursor (PEG-4-MPA) with maleimide-end functionalized PEG (PEG-2-MI) and maleimide functionalized low molecular heparin (Heparin-MI) via Michael-type reaction under aqueous microenvironment. Low molecular weight proteins such as growth factors, cytokine, and immunomodulatory agents can be incorporated within hydrogel network during the hydrogel formation.

To control degradation of the hydrogels exclusively via retro Michael type reactions, we modified earlier version of aryl-thiol end functionalized PEG by removal of ester linkages.³²⁶⁻³²⁷ An amide linkage, which has better stability in aqueous microenvironment compared to ester linkages, was utilized to conjugate small molecular aryl thiol to amine-end functionalized PEG via carbodiimide chemistry (**Fig. 4.2**). Direct addition of MPA to PEG-4-NH₂ was challenging due to formation of

thioester linkages (i.e., reaction of sulfhydryl groups with the carboxylic acids), which are unstable in aqueous microenvironment. Hence, MPA was first oxidized using H_2O_2 in the presence of NaI as a catalyst to protect sulfhydryl groups from participating in subsequent reactions with carboxylic acids. Subsequently, carboxylic groups on oxidized MPA were activated with HATU in the presence of DIPEA to form an amide linkage with PEG-4-NH₂. Successively, the polymer was reduced in the presence of TCEP-HCl to generate reactive sulfhydryl groups in acidic conditions (pH 4). The reaction yielded aryl-thiol end functionalized polymers with 88% modification as assessed from integration of aromatic protons in ¹H NMR (**Fig. S4.1**).

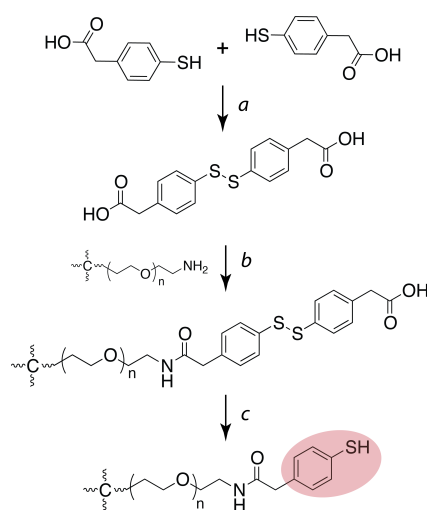


Figure 4.2 Synthesis of aryl-thiol (PEG-4-MPA). Reagents and conditions are as follows: (a) NaI, H_2O_2 in EtOAc; (b) DIPEA, HATU in DMF under Ar; (c) TCEP in DI water followed by dialysis against acidified water.

In order to covalently incorporate heparin within hydrogels, carboxylic acid groups on uronic acid residue on heparin were modified with heterofunctional AEM

crosslinker via carbodiimide coupling (**Fig. 4.3**). The number of maleimide groups conjugated to heparin was controlled to be around 2 in order to incorporate heparin as a crosslinking molecule within hydrogels. The carbodiimide reaction yielded maleimide end-functionalized heparin with 2.2 functionality, as characterized using integration of maleimide ring protons compared to anomeric protons of heparin in ^1H NMR (**Fig. S4.2**).

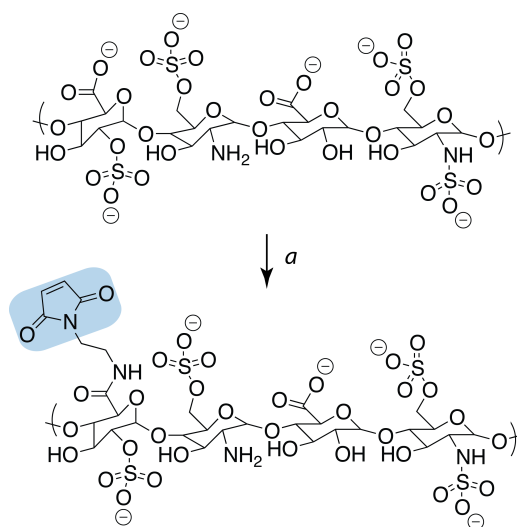


Figure 4.3 Synthesis of maleimide-functionalized heparin (heparin-MI). (a) EDC, HOBT, AEM in AEM buffer

In order to study light-mediated degradation of the hydrogels, *o*-nitrobenzyl ether (*o*-NB) moiety was incorporated within PEG-4-MPA. The *o*-NB moiety undergoes irreversible photoisomerization in response to externally applied cytocompatible light.²⁰⁷ In our previous work, we incorporated *o*-NB moiety on a maleimide end-functionalized PEG macromer via ester linkage.³²⁷ Since the maleimide ring hydrolysis was challenging in addition to the rapid ester hydrolysis (k

= $6.84 \times 10^{-4} \text{ min}^{-1}$), in the present work we sought to incorporate o-NB on PEG-4-MPA along with amide conjugation (**Fig. 4.4**). Amine-end functionalized PEG (**I**) was reacted with carboxylic acid of Fmoc-PD group (**II**) via carbodiimide chemistry. Subsequently, the Fmoc protective group on photodegradable PEG (**III**) was cleaved in the presence of piperidine to generate amine-end functionalized photodegradable PEG (**IV**). Intermediate polymer **IV** was reacted with oxidized MPA in a similar manner as described earlier to obtain aryl-thiol end functionalized PEG (PEG-4-PD-MPA) with 78% modification characterized using ^1H NMR (**Fig. S4.3**). To best of our knowledge, this is the first reported synthesis of aryl-thiol end functionalized photodegradable PEG macromer for controlling hydrogel degradation.

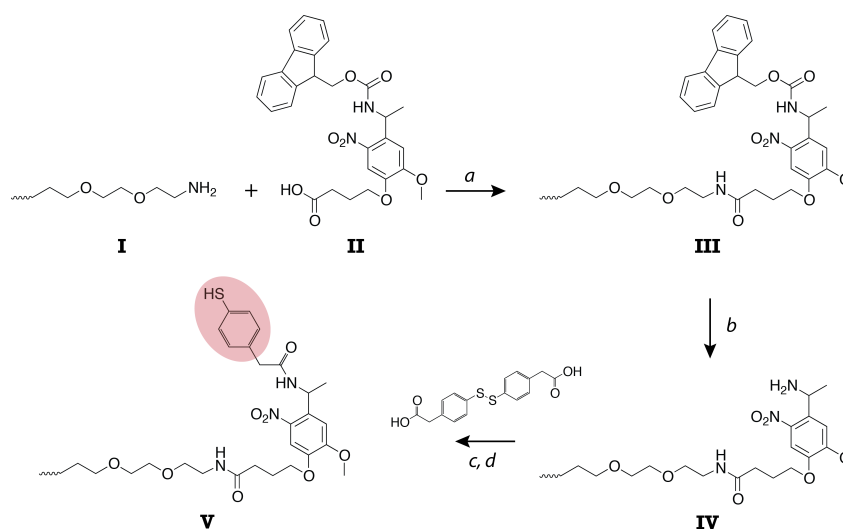


Figure 4.4 Synthesis of photodegradable aryl thiol. Reagents and conditions are as follows: (a) DIPEA, HATU in DMF under Ar; (b) 20% (v/v) piperidine in DMF; (c) DIPEA, HATU in DMF under Ar; (d) TCEP in DI water followed by dialysis against acidified water.

4.3.2 Michael-type Crosslinking to Form Hydrogels

The hydrogels were formed using Michael-type addition reaction between sulfhydryl groups of PEG-4-MPA and maleimide groups of PEG-Mal and heparin. Michael type reaction is versatile reaction that occurs readily in aqueous conditions at room temperature.⁴⁵⁵⁻⁴⁵⁶ In addition, the reaction does not generate any byproducts and hence have been used to design cell-compatible hydrogels.⁴⁵⁷⁻⁴⁵⁹ In chemically crosslinked hydrogels, the crosslinking reaction plays crucial role in hydrogel formation and subsequent mechanical properties. Dynamic time sweep experiments were conducted to study hydrogel formation and gelation kinetics. The storage (G') and loss modulus (G'') were recorded for 7.5 wt% composition using a parallel plate geometry under the linear viscoelastic regime (1% strain, 6 rad/s angular frequency) as a function of time. As indicated in the **Fig. 4.5A**, storage modulus rapidly increased within initial ~2 minutes from 16 Pa to ~2000 Pa, while no significant change was observed in loss modulus. While crossover point between G' and G'' was not observed before the first data point was acquired, this data suggest rapid hydrogel gelation and it's utility for local injection at site of interest. For injectable hydrogels, liquid precursor solutions need to be rapidly polymerized at the site of interest to avoid uncontrolled diffusion of polymers and cargo molecules into the surrounding tissues.

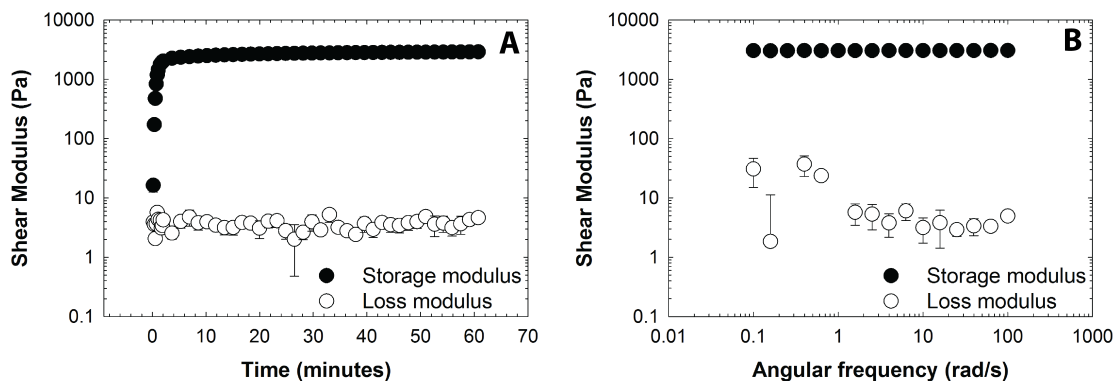


Figure 4.5 Rheological characterization during hydrogel formation. Oscillatory rheology (A) time sweep and (B) frequency sweep data for 7.5 wt% PEG-heparin hydrogels. Crossover point between storage and loss modulus was not observed in time sweep measurement due to rapid hydrogel formation. The data shown illustrate the mean ($n \geq 3$) with error bars showing the standard error.

After the plateau region, no significant change was observed within G' , indicating maximum possible crosslinking was achieved. Post-formation, the storage modulus was significantly higher compared to G'' , under 0.1 to 100 rad/s frequency (Fig. 4.5B), demonstrating elastic nature of the network. While the modulus observed in this experiment is comparable to our earlier studies at lower polymer concentration (i.e., 5 weight % composition, ~ 2300 Pa)³²⁶, this disparity can be attributed to additional network defects associated with incorporation of heparin containing maleimide on the side chains. In general, looping, entanglements, or unreacted functional groups significantly impact the crosslinking density and subsequent mechanical properties of the hydrogels.^{367, 460} Regardless, our results indicate reproducible and robust hydrogel formation via Michael-type addition reaction with gelation time < 30 seconds.

4.3.3 Stimuli-responsive Hydrogel Degradation

In order to study stimuli-responsive degradation, we first incorporated the aryl-thiol based thioether succinimide linkages within the hydrogel backbone. Under the non-reducing conditions, the reaction between aryl-thiol and maleimide yields thioether succinimide linkage with the reaction equilibrium directing towards to the product side, as shown in **Fig. 4.6**. Under reducing conditions, while the equilibrium still lays toward the product side, during the backward reaction, a thiol from the reducing agents, such as glutathione, can react with the maleimide to form relatively stable alkyl-thiol based succinimide thioether linkage, which is dependent on the pK_a of both the aryl-thiol and the thiol of the reducing agent. The formation of relatively stable alkyl-thiol based succinimide thioether results in breakage of the original hydrogel crosslink leading to network degradation. Our previous studies have demonstrated degradation of aryl-thiol based succinimide thioether linkages in the presence of glutathione.³²⁶⁻³²⁷

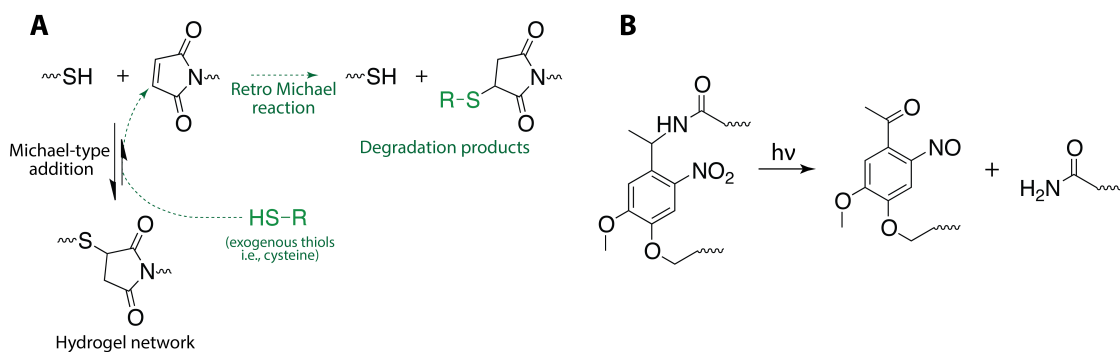


Figure 4.6 Hydrogel degradation pathways (A) Aryl-thiol based succinimide thioether linkage can exchange thiol in solution to form a relatively stable alkyl-thiol (i.e., cysteine) based succinimide thioether linkage resulting in hydrogel degradation. (B) *o*-nitrobenzyl ether moiety undergoes irreversible photoisomerization yielding respective ketone and amide under cytocompatible light doses.

In the present work, we hypothesized that the aryl-thiol based succinimide thioether can undergo cleavage in the presence of biologically relevant thiols such as cysteine (CYS) and dithiothreitol (DTT) besides glutathione (GSH). The retro and subsequent exchange reaction is essentially driven by the differences in pK_a of aryl thiol ($pK_{a(\text{MPA})} = 6.6$) and alkyl thiols ($pK_{a(\text{GSH})} = 9.3$, $pK_{a(\text{DTT})} = 9.0$, $pK_{a(\text{CYS})} = 8.9$).⁴⁶¹⁻⁴⁶² To study hydrogel degradation in response to various reducing agents, we monitored mechanical properties of hydrogels as a function of time using oscillatory rheometry. Specifically, hydrogels were incubated under high reducing microenvironment at 10 mM thiol concentration, similar to the concentration of thiol found in intracellular compartments and tumor microenvironment.^{356, 443} The storage moduli at each time point were measured and the degradation rate was obtained by plotting normalized storage modulus as a function of time (first-order degradation kinetics since the rate of degradation is proportional to number of degradable linkages). The degradation rate constants for aryl-thiol based hydrogels were found to be $1.46 \times 10^{-3} \text{ min}^{-1}$, $1.43 \times 10^{-3} \text{ min}^{-1}$, and $1.88 \times 10^{-3} \text{ min}^{-1}$ for GSH, DTT, and CYS respectively (**Fig 4.7A**). As the rate constants are not statistically different ($p = 1$, one way ANOVA), the experimental results indicate that GSH, DTT, and CYS at a similar thiol concentration results in the degradation of hydrogels at similar rate via retro-Michael type and subsequent thiol exchange reaction. Further, the rate constant in the presence of GSH correlates well with our previous studies ($k = 1.52 \times 10^{-3} \text{ min}^{-1}$).³²⁷ To our knowledge, this is the first study exploring effect of other biologically relevant thiols besides glutathione on the stability of aryl-thiol based thioether succinimide bond. Responsiveness to alkyl thiols can be explored for future biomaterial, biosensor, and biomedical imaging applications.

Next, we sought to study effect of reducing microenvironment concentration on the rate of degradation of the hydrogels. In human body, the concentration of glutathione varies significantly from micromolar to millimolar range.⁴⁶³ In particular, for carcinoma tissue, the concentration of thiols varies from 1 to 1.5 mM.⁴⁶³ Hence, we studied the degradation under lowed GSH concentration of 1 mM. The rate of degradation was calculated by monitoring storage modulus as a function of time (**Fig. 4.7B**). The decrease in storage modulus indicates decrease in crosslinking density due to retro-Michael and subsequent thiol exchange reaction. Under 10 mM GSH condition, degradation rate constant was found to be $1.46 \times 10^{-3} \text{ min}^{-1}$ ($t_{1/2} = 474 \text{ min}$) with complete erosion, or reverse gelation occurring after 48 hours. At lower glutathione concentration (1 mM GSH), the degradation rate constant was found to be $4.47 \times 10^{-4} \text{ min}^{-1}$ ($t_{1/2} = 1550 \text{ min}$) with complete erosion occurring after 168 hours. Since the glutathione concentration varies significantly within human body, the responsiveness to glutathione concentration offers promising approach to specifically deliver cargo molecules at the site of interest utilizing the reducing concentration gradient.

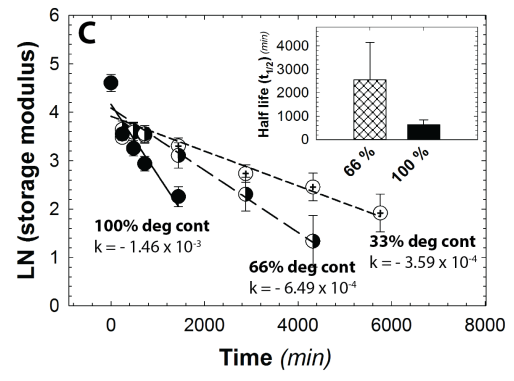
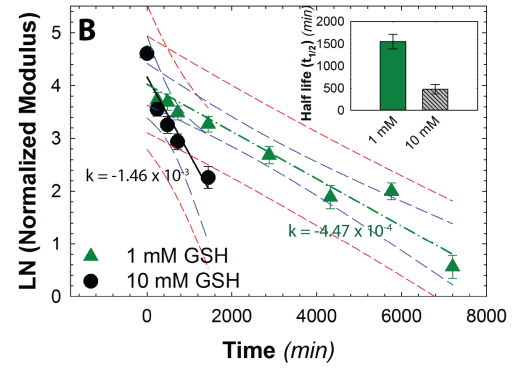
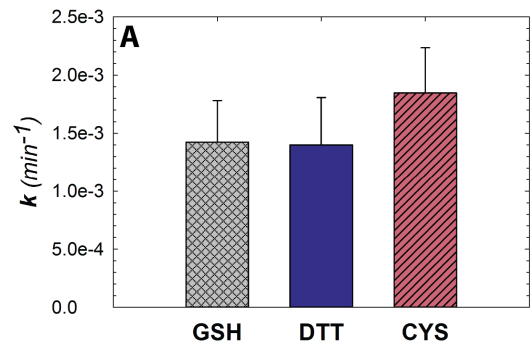


Figure 4.7 Hydrogel degradation in reducing microenvironment. (A) Hydrogels underwent degradation via retro-Michael and subsequent thiol exchange reaction with similar rate constants ($p = 1$) when incubated with biologically relevant alkyl thiols such as glutathione (GSH), dithiothreitol (DTT), and cysteine (CYS). (B) The rate of degradation was found to be dependent on glutathione concentration. At high reducing microenvironment (10 mM) that is found in intracellular compartment and carcinoma tissues, the rate of degradation was an order of magnitude faster compared to lower reducing microenvironment concentration proving promising approach for reducing-microenvironment sensitive drug delivery carriers. (C) By varying ratio of alkyl to aryl thiol, the number of degradable crosslinked was varied between 33% to 100% degradable hydrogels, which in turned controlled the rate of bulk degradation. The degradation half-life was found to be ~ 2550 minutes and ~ 635 minutes for 66% and 100% degradable hydrogels respectively, where as 33% hydrogel did not undergo complete degradation. The data shown illustrate the mean ($n \geq 6$) with error bars showing the standard error.

To further tune the rate of degradation of the hydrogels via retro-Michael and subsequent thiol reactions, we varied the % degradable content. Earlier studies demonstrated the stability of alkyl-thiol based succinimide thioether linkages in the reducing microenvironment.³²⁶ Hence, the ratio of alkyl-thiol and aryl-thiol within precursor solution was varied to obtain 33%, 66%, and 100% degradable hydrogels. Varying the thiol concentration did not affect the final storage modulus post-formation, indicating that similar crosslinking density was achieved irrespective of the alkyl:aryl thiol ratio. Hydrogels were subsequently incubated in PBS buffer containing 10 mM GSH at room temperature and storage modulus was measured at predefined time points. The rate of degradation was calculated by plotting normalized storage modulus as a function time. As is apparent in **Fig. 4.7C**, all conditions showed decrease in modulus indicating hydrogel degradation in the reducing microenvironment. The 100% degradable hydrogels showed rapid degradation under

reducing microenvironment with rate constant of $1.46 \times 10^{-3} \text{ min}^{-1}$, with complete erosion occurring after 48 hours. Hydrogels composed of 66% degradable groups showed relatively slower rate of degradation ($k = 6.49 \times 10^{-4} \text{ min}^{-1}$), where complete erosion was observed after 96 hours. The 33% hydrogels showed slowest degradation among these three conditions, with degradation rate constant of $3.59 \times 10^{-4} \text{ min}^{-1}$. These hydrogels did not undergo complete erosion, but were too soft to handle and measure mechanically after 120 hours. Control over the rate of degradation by varying % degradable content demonstrated a method to provide additional tuning of the hydrogel degradation kinetics.

We further sought to study effect of externally applied light on photodegradation of PEG-heparin hydrogels. In our previous studies, we observed degradation in response to externally applied cytocompatible UV and visible light. However, uncontrolled and rapid ester hydrolysis provided additional challenges for application in drug delivery where long-term (few days to a week) release is needed. Hence, we sought to replace the labile ester linkages within macromers with amide linkages. While the replacement of ester linkage with amide linkage improved the stability in aqueous microenvironment, the rate of photodegradation was 2.5 times slower compared to our previous study ($k_{\text{photodegradation, amide}} = 0.12 \text{ min}^{-1}$, $k_{\text{photodegradation, ester}} = 0.30 \text{ min}^{-1}$, 365 nm, 10 mW/cm²) as shown in **Fig. 4.8** These results are not surprising since typically o-NB groups conjugated with polymer via amide linkages show slower rate of degradation.^{406, 464} For example, Anseth and coworkers demonstrated ~15% degradation in hydrogel containing o-NB amide linkage by ~6 minutes using 10 times higher light intensity (102 mW/cm²).⁴⁶⁴

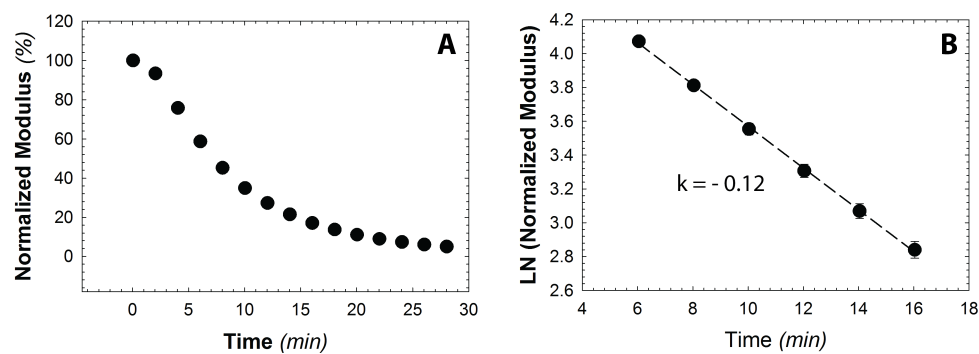


Figure 4.8 Light-mediated degradation. (A) Photodegradable MPA-based hydrogels undergo degradation in response to externally applied light (365 nm, 10 mW/cm²). (B) Photodegradation kinetics were evaluated in a linear region between 6 to 16 minutes yielding photodegradation rate constant of 0.12 min⁻¹. The data shown illustrate the mean (n ≥ 3) with error bars showing the standard error.

4.3.4 Growth Factor Release

Growth factor delivery profiles are of interest in the present work, given our ultimate interest in delivering low molecular weight therapeutic proteins through controlled release mechanisms stemming from degradable hydrogels. Towards these ends, the release of FGF-2 from PEG-heparin hydrogels was investigated *in vitro*. FGF-2 has a comparable molecular weight and heparin-binding affinity similar to that of immune activating cytokine interleukin-2 (IL-2) that is approved for intralesional injectors for melanoma treatment.⁴³⁸⁻⁴³⁹ In initial studies, growth-factor loaded hydrogels were incubated in reducing and non-reducing aqueous microenvironment (i.e., PBS buffer containing 10 mM GSH and 0 mM GSH respectively) and aliquots were removed at pre-determined time points over the course of one week. The concentration of the released FGF-2 was subsequently determined using an immunochemical assay. The cumulative FGF-2 release as was plotted as a function of time as shown in **Fig. 4.9**. Under non-reducing microenvironment, FGF-2 release

shows very little to slight burst release, with approximately ~20 % of total FGF-2 released during experimental time frame. In contrast, under the reducing microenvironment, approximately ~40% of total FGF-2 was released before complete erosion and ~80-90% of the total FGF-2 was released after complete erosion. The difference in release profile clearly shows that the release of small molecular weight protein is controlled by the changes in hydrogel mesh size associated with hydrogel degradation. In addition, the receptor-host mediated interaction prevented free diffusion of small molecular weight proteins from the hydrogels (hydrodynamic size of FGF-2 = 2.8 nm,⁴⁶⁵ estimated mesh size = ~8 nm).

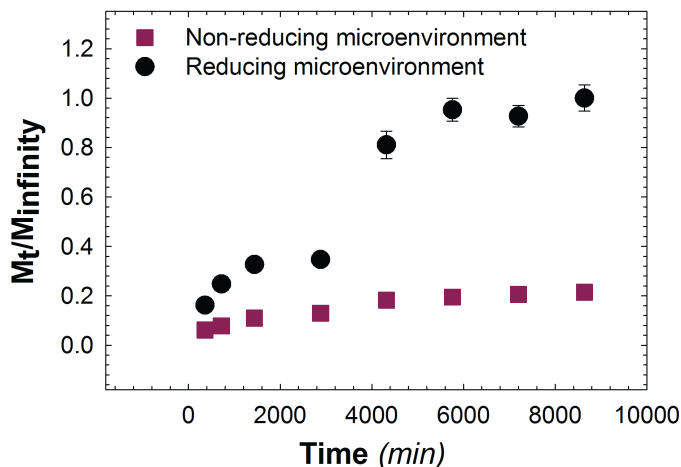


Figure 4.9 Degradation mediated release of biologics. Release of small molecular weight protein, FGF-2 (fibroblast growth factor) was monitored in vitro using immunochemical assay. The release of FGF-2 in reducing microenvironment (PBS buffer containing 10 mM GSH) that is found at carcinoma tissues was compared with non-reducing microenvironment (PBS buffer). Hydrogels show minimal burst release under the non-reducing microenvironment. In contrast, under the reducing microenvironment FGF-2 was released rapidly, with approximately ~40% of cargo getting released before complete erosion, and ~80-95% of cargo getting released once complete hydrogel degradation (i.e. reverse gelation) was observed. The data shown illustrate the mean ($n \geq 4$) with error bars showing the standard error.

4.3.5 Bioactivity of Released Growth Factor

To assess the bioactivity of FGF-2 following encapsulation into and release from growth-factor loaded hydrogels, we examined the bioactivity of released FGF-2. FGF-2 is known to promote proliferation in many cell types, including human aortic adventitial fibroblasts (AF).⁴⁶⁶ Thus, we set out to determine the bioactivity of FGF-2 released from hydrogels on AF proliferation. FGF-2 released from hydrogels cultured in reducing and non-reducing microenvironments was collected after 7 days, lyophilized, and reconstituted in AF medium containing 5% stripped serum. The

lyophilized proteins collected from the buffer of hydrogels originally incubated in a reducing microenvironment were reconstituted at a concentration of 1 ng/mL FGF-2, while proteins collected from hydrogels incubated in a non-reducing environment were set to 0.3 ng/mL to account for the differences in the FGF-2 release profile. After 48 hrs of culture, AFs were treated with 10 μ M EdU for a further 24 hrs. AFs cultured in SCBM containing 1 ng/mL FGF-2 was utilized as a positive control, while AFs cultures in the absence of FGF-2 served as a negative control.

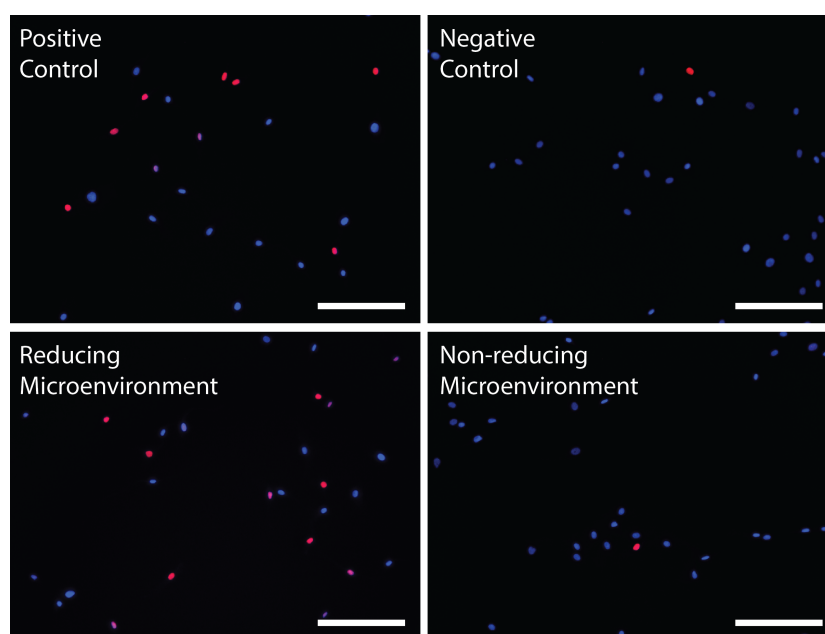


Figure 4.10 Bioactive FGF-2 promotes cell proliferation. Bioactivity of released FGF-2 from PEG-heparin hydrogels was studied using adventitial fibroblast (AFs) proliferation assay since the FGF-2 is known to promote proliferation of AFs. Released FGF-2 from reducing microenvironment and non-reducing microenvironment was added to in vitro cell culture and proliferating cell nuclei were labeled with Alexa Fluor 555 (red) using EdU assay. Released FGF-2 demonstrated similar effect on cell proliferation compared to pristine FGF-2 added at a similar concentration (positive control) indicating that the protein bioactivity was not affected during encapsulation and subsequent release process.

Cell proliferation was quantified by examining the number of EdU-positive AFs after 72 hrs of culture, as demonstrated in **Fig. 4.10**. AFs treated with FGF-2 released in a reducing microenvironment exhibited a proliferation rate of 27%, which was similar to the proliferation rate observed for that of the positive control, which contained pristine FGF-2 (**Fig. 4.11**). These results indicate that encapsulation into and release from hydrogels did not impact the bioactivity of FGF-2. Further, the proliferation of AFs cultured with FGF-2 released in a non-reducing microenvironment was significantly lower, where a proliferation rate of 10% was observed. This was similar to the proliferation rate observed for the negative control, where AFs were cultured in the absence of FGF-2.

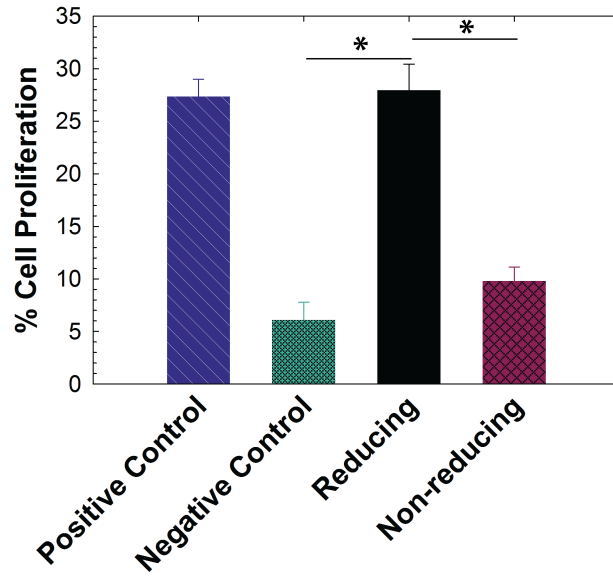


Figure 4.11 Quantification of cell proliferation. FGF-2 released from reducing microenvironment had similar bioactivity as that of the positive control (i.e. pristine FGF-2). However, released FGF-2 from reducing microenvironment showed significant difference compared to negative control (i.e., no FGF-2) and non-reducing condition. The data shown illustrate the mean ($n \geq 4$) with error bars showing the standard error. * indicate p value < 0.05 .

In a separate set of experiments, when the concentration of FGF-2 from released in a non-reducing microenvironment was set to 1 ng/mL FGF-2, similar to the concentration used for the FGF-2 obtained from reducing microenvironment in this experiment, AFs elicited proliferation rate of 25% (data not shown). As such, the low proliferation rate observed in the non-reducing microenvironment cultures is likely attributed to fact that the concentration of FGF-2 is below the threshold required to stimulate proliferation, rather than the released FGF-2 becoming inactive. Regardless, in a non-reducing microenvironment, less AF proliferation would likely be observed

due to the diminished amount of FGF-2 released from the growth factor-loaded hydrogel.

4.4 Conclusion

In this work, we report synthesis of stimuli-responsive hydrogels in which degradation can be tailored by varying degradable chemistries that responsive to reducing microenvironment and externally applied cytocompatible doses of light. Hydrogels were formed rapidly via facile Michael-type reactions without any reaction byproducts. The hydrogels showed controlled degradation in the presence of biologically relevant thiol molecules such glutathione, cysteine, and dithiothreitol via retro-Michael and subsequent exchange reaction. The rate of hydrogel degradation was found to be dependent on degradable crosslink content and reducing microenvironment concentration. Further, we report inclusion of *o*-nitrobenzyl ether moiety that is sensitive to externally applied cytocompatible light. Incorporation of reduction-sensitive linkages resulted in ~2.3 fold differences in the release profile of fibroblast growth factor-2 (FGF-2) in the presence of GSH compared to non-reducing microenvironment. Bioactivity of released FGF-2 was comparable to pristine FGF-2, indicating the ability of the hydrogel to retain bioactivity of cargo molecules during encapsulation and release. Results of this study indicate that incorporation of receptor-host interactions along with degradable linkages are capable of controlling release of small molecular weight proteins in a stimuli-responsive manner.

4.5 Acknowledgement

Research reported in this publication was supported by an Institutional Development Award (IDeA) from the National Institute of General Medical Sciences

(NIGMS) of the National Institutes of Health (NIH) (P20GM103541), an IDeA from NIGMS from the NIH (1 P30 GM110758-01), the Burroughs Wellcome Fund (subcontract from University of California, Davis), and the University of Delaware Research Foundation. Additionally, the authors are grateful to Dr. Robert Akins for providing low molecular weight heparin.

4.6 Supporting Information

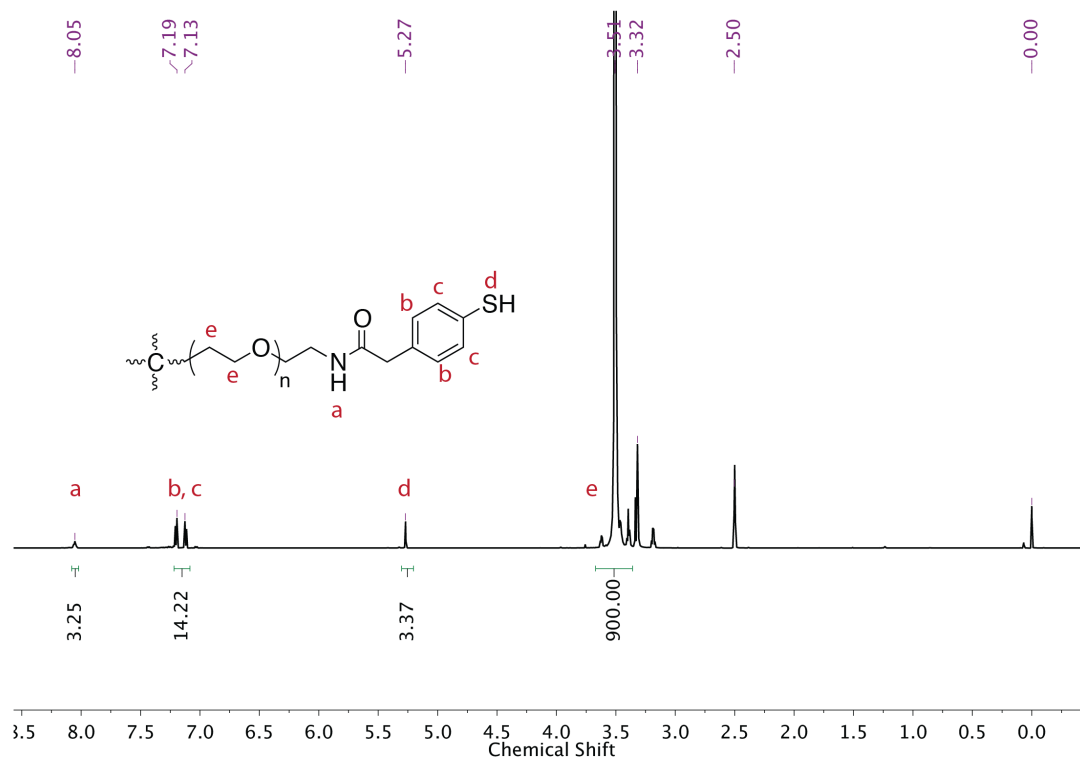


Figure 4.12 ¹H-NMR spectrum for four-arm aryl-thiol functionalized PEG MPA. Functionality was calculated based on the integration of the aromatic proton (labeled as b and c), in this case, 88%.

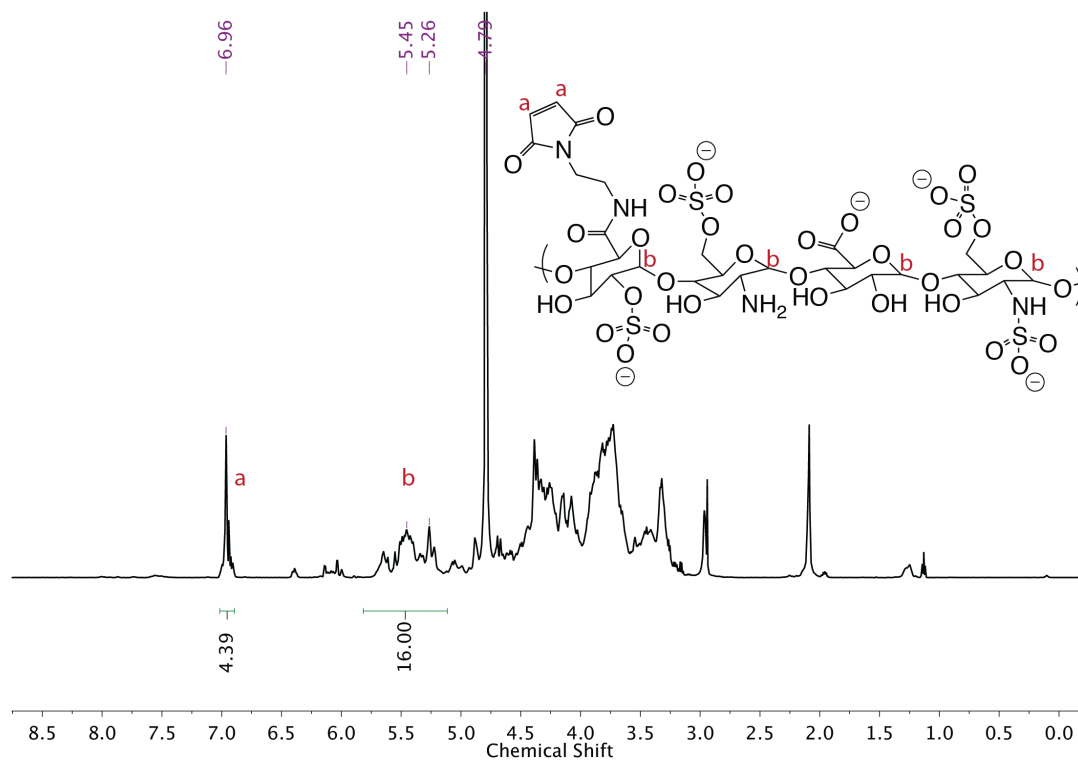


Figure 4.13 $^1\text{H-NMR}$ spectrum for maleimide functionalized heparin. Functionality was calculated based on the integration of the maleimide ring protons, in this case, $f \sim 2.2$.

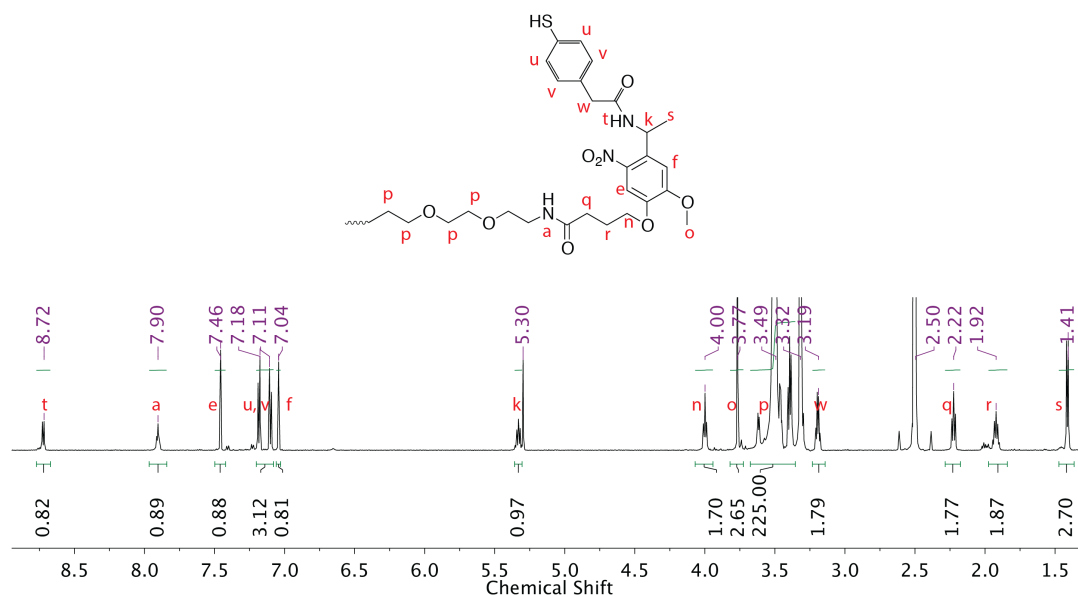


Figure 4.14 ¹H-NMR spectrum for four-arm aryl-thiol functionalized photodegradable PEG MPA. Functionality was calculated based on the integration of the aromatic proton (labeled as u and v), in this case, 78%.

Chapter 5

CONCLUSION AND FUTURE DIRECTIONS

This chapter contains a summary of conclusions discussed in the previous chapters. The goal of this doctoral dissertation was to design multimodal degradable hydrogels that are responsive to multiple biologically relevant stimuli for degradation-mediated controlled drug delivery. We began by studying existing literature about the hydrogel design criteria, polymers for hydrogel formation, crosslinking chemistries, stimuli-responsive degradable moieties, and present hydrogel-based drug delivery technologies. Towards design of injectable hydrogels we considered following parameters: *i*) biocompatibility of polymeric building blocks, *ii*) cytocompatible crosslinking chemistries with appropriate gelation kinetics, *iii*) consistency in mechanical properties *iv*) degradability in response to biologically relevant stimuli, and *v*) mass transport of cargo from hydrogels to desirable site in *in vivo* microenvironment.

We began by developing dually degradable poly(ethylene glycol) (PEG) based hydrogels that are responsive to endogenous stimuli. Rapid hydrogel formation was achieved using Michael-type reaction between thiols and maleimides. Selective incorporation of aryl-thiol based succinimide thioether linkages resulted in controlled degradation in glutathione microenvironment that is found at higher concentration in intracellular compartments and carcinoma tissues. Specifically, the rate of hydrogel degradation was found to be depending on the chemistry of crosslinker, the number of degradable crosslinks, and the concentration of reducing

microenvironment. In addition, ester linkages were incorporated within the polymer backbone to further tune the degradation in response to aqueous microenvironment at a preprogrammed rate. Encapsulation and release of bovine serum albumin (BSA) as a model protein demonstrated potential of these matrices and approaches for controlled release application in glutathione-rich microenvironments.

We next sought to control the hydrogel degradation rate and subsequent release in response to biologically relevant exogenous stimuli. *o*-Nitrobenzyl (*o*-NB) group undergoes irreversible photoisomerization under cytocompatible doses of light. To incorporate *o*-NB group within polymeric monomers, we developed a novel multi-step synthetic route to yield photodegradable maleimide end-functionalized PEG monomers. Subsequent gelation with aryl thiol end-functionalized PEG via versatile Michael-type addition reaction resulted in formation of multimodal degradable hydrogels. The hydrogels exhibited rapid gelation and consistent mechanical properties between samples, which will be helpful for their development as injectable drug delivery vehicles *in vivo*. By incorporation of photodegradable *o*-NB groups, aryl-thiol based succinimide thioether linkage, and ester linkages, degradation in response to externally applied light, glutathione, and aqueous microenvironments was achieved, respectively with degradation rate constants ranging from $\sim 10^{-1}$ to 10^{-4} min^{-1} . As a proof of concept, the controlled release of nanobeads from hydrogels was demonstrated in a preprogrammed or stimuli-responsive manner via bulk degradation and surface erosion. Our preliminary results demonstrated applicability of multimodal hydrogels for delivery of multiple therapeutics using complex material degradation profiles as necessitated by the end application of interest.

Development of multimodal degradable hydrogels presented additional challenges for transitioning towards *in vivo* applications including *i*) relatively faster rate of degradation in aqueous microenvironment due to ester hydrolysis *ii*) need for additional tunability over degradation rate ranging from few days to a week time period, and *iii*) delivery of small molecular weight proteins such as interleukin-2 (IL-2) and fibroblast growth factor-2 (FGF-2). Towards addressing limited stability of ester linkage neighboring *o*-NB group, we modified our synthetic strategy by replacing ester linkage with amide linkage, which is relatively stable in aqueous microenvironment. To incorporate additional tunability over the rate of degradation, we varied the % degradable content resulting in retro-Michael type degradation constant ranging from 10^{-3} to 10^{-4} min^{-1} . Low molecular weight heparin was covalently incorporate within the hydrogel to provide additional control over release of low molecular weight proteins. Incorporation of reduction-sensitive linkages resulted in ~ 2.3 fold differences in the release profile of fibroblast growth factor-2 (FGF-2) in the presence of GSH compared to non-reducing microenvironment. Bioactivity of released FGF-2 was comparable to pristine FGF-2, indicating the ability of the hydrogel to retain bioactivity of cargo molecules during encapsulation and release. Results of this study indicate that incorporation of receptor-host interactions along with degradable linkages are capable of controlling release of small molecular weight proteins in a stimuli-responsive manner.

While improvement of current multimodal hydrogels for drug delivery applications is a on-going process, there are major unexplored areas of research that will significantly improve these systems for drug delivery. While the depth of penetration varies in each patient depending on the type and extent of carcinoma

tumor, incorporation of upconverting nanoparticles within hydrogel formulation will significantly improve the depth of penetration (up to ~5-7 cm). Building upon Zhao and coworkers research, nontoxic nanoparticles that absorb NIR light (900-1050 nm with maximum at 980 nm) and emit long-wavelength UV and blue light (340-450 nm) can be synthesized based on published protocols (core-shell NaYF₄:TmYb; core=NaYF₄:0.5% Tm³⁺:30% Yb³⁺; shell=NaFY₄).⁴⁶⁷⁻⁴⁶⁸ In addition, to achieve better control over the hydrogel formation *in vivo*, injectable formulations can be replaced with preformed microgels and/or nanogels that can be delivered at the site of interest. Micro- and nanogels can be synthesized building on published techniques that incorporate emulsion polymerization, colloidal chemistry, and microfluidics devices.⁴⁶⁹⁻⁴⁷¹ Overall, the investigation of these multimodal hydrogels discussed herein further increases our knowledge of these degradable chemistries to tune the rate of degradation in response to biologically relevant stimuli and application in drug delivery technologies.

REFERENCES

1. Hou, J. J. C., et al., New frontiers in cell line development: challenges for biosimilars. *J Chem Technol Biotechnol*, **2011**, *86* (7), 895-904.
2. Audie, J.; Boyd, C., The Synergistic Use of Computation, Chemistry and Biology to Discover Novel Peptide-Based Drugs: The Time is Right. *Curr Pharm Des*, **2010**, *16* (5), 567-582.
3. Pirogova, E., et al., Advances in methods for therapeutic peptide discovery, design and development. *Curr Pharm Biotechnol*, **2011**, *12* (8), 1117-1127.
4. Li, N., et al., Low molecular weight chitosan-coated liposomes for ocular drug delivery: in vitro and in vivo studies. *Drug Deliv*, **2012**, *19* (1), 28-35.
5. Yang, B., et al., Positively charged cholesterol derivative combined with liposomes as an efficient drug delivery system, in vitro and in vivo study. *Soft Matter*, **2012**, *8* (2), 518-525.
6. Chen, F., et al., In vivo tumor targeting and image-guided drug delivery with antibody-conjugated, radiolabeled mesoporous silica nanoparticles. *ACS Nano*, **2013**, *7* (10), 9027-9039.
7. Liu, Y., et al., Enzyme responsive drug delivery system based on mesoporous silica nanoparticles for tumor therapy in vivo. *Nanotechnology*, **2015**, *26* (14), 145102.
8. Zhang, Q., et al., Biocompatible, Uniform, and Redispersible Mesoporous Silica Nanoparticles for Cancer- Targeted Drug Delivery In Vivo. *Adv Funct Mater*, **2014**, *24* (17), 2450-2461.
9. Anajafi, T.; Mallik, S., Polymersome-based drug-delivery strategies for cancer therapeutics. *Ther Deliv*, **2015**, *6* (4), 521-534.

10. Egli, S., et al., Biocompatible functionalization of polymersome surfaces: a new approach to surface immobilization and cell targeting using polymersomes. *J Am Chem Soc*, **2011**, *133* (12), 4476-4483.
11. Ge, X., et al., PEG-PCL-DEX polymersome-protamine vector as an efficient gene delivery system via PEG-guided self-assembly. *Nanomedicine*, **2014**, *9* (8), 1193-1207.
12. Souza, J. G., et al., Transcorneal iontophoresis of dendrimers: PAMAM corneal penetration and dexamethasone delivery. *J Controlled Release*, **2015**, *200*, 115-124.
13. Tang, Y., et al., Efficient in vitro siRNA delivery and intramuscular gene silencing using PEG-modified PAMAM dendrimers. *Mol Pharm*, **2012**, *9* (6), 1812-1821.
14. Raphael, A. P., et al., Elongate microparticles for enhanced drug delivery to ex vivo and in vivo pig skin. *J Controlled Release*, **2013**, *172* (1), 96-104.
15. Boudou, T., et al., Polyelectrolyte multilayer nanoshells with hydrophobic nanodomains for delivery of Paclitaxel. *J Controlled Release*, **2012**, *159* (3), 403-412.
16. Seib, F. P., et al., Self-assembling doxorubicin silk hydrogels for the focal treatment of primary breast cancer. *Adv Funct Mater*, **2013**, *23* (1), 58-65.
17. Xu, J., et al., Genipin-crosslinked catechol-chitosan mucoadhesive hydrogels for buccal drug delivery. *Biomaterials*, **2015**, *37*, 395-404.
18. Lin, C. C.; Anseth, K. S., PEG hydrogels for the controlled release of biomolecules in regenerative medicine. *Pharm Res*, **2009**, *26* (3), 631-643.
19. Oh, E. J., et al., Target specific and long-acting delivery of protein, peptide, and nucleotide therapeutics using hyaluronic acid derivatives. *J Controlled Release*, **2010**, *141* (1), 2-12.
20. Bhattarai, N., et al., Chitosan-based hydrogels for controlled, localized drug delivery. *Adv Drug Deliv Rev*, **2010**, *62* (1), 83-99.

21. Liang, Y.; Kiick, K. L., Heparin-functionalized polymeric biomaterials in tissue engineering and drug delivery applications. *Acta Biomater*, **2014**, *10* (4), 1588-1600.
22. Yucel, T., et al., Silk-based biomaterials for sustained drug delivery. *J Controlled Release*, **2014**, *190*, 381-397.
23. Gombotz, W. R.; Wee, S. F., Protein release from alginate matrices. *Adv Drug Deliv Rev*, **2012**, *64*, 194-205.
24. Lee, S., et al., The effects of varying poly(ethylene glycol) hydrogel crosslinking density and the crosslinking mechanism on protein accumulation in three-dimensional hydrogels. *Acta Biomater*, **2014**, *10* (10), 4167-4174.
25. Zustiak, S. P.; Leach, J. B., Hydrolytically degradable poly(ethylene glycol) hydrogel scaffolds with tunable degradation and mechanical properties. *Biomacromolecules*, **2010**, *11* (5), 1348-1357.
26. Kharkar, P. M., et al., Designing degradable hydrogels for orthogonal control of cell microenvironments. *Chem Soc Rev*, **2013**, *42* (17), 7335-7372.
27. Appel, E. A., et al., The control of cargo release from physically crosslinked hydrogels by crosslink dynamics. *Biomaterials*, **2014**, *35* (37), 9897-9903.
28. Lin, C. C., Recent advances in crosslinking chemistry of biomimetic poly(ethylene glycol) hydrogels. *RSC Advances*, **2015**, *5* (50), 39844-398583.
29. Kolb, H. C., et al., Click Chemistry: Diverse Chemical Function from a Few Good Reactions. *Angew Chem Int Ed Engl*, **2001**, *40* (11), 2004-2021.
30. Nimmo, C. M., et al., Diels-Alder Click cross-linked hyaluronic acid hydrogels for tissue engineering. *Biomacromolecules*, **2011**, *12* (3), 824-830.
31. Peppas, N. A., et al., Hydrogels in Biology and Medicine: From Molecular Principles to Bionanotechnology. *Adv Mater*, **2006**, *18* (11), 1345-1360.
32. Slaughter, B. V., et al., Hydrogels in regenerative medicine. *Adv Mater*, **2009**, *21* (32-33), 3307-3329.
33. Hoffman, A. S., Hydrogels for biomedical applications. *Adv Drug Deliv Rev*, **2012**, *64*, 18-23.

34. Williams, D. F., On the mechanisms of biocompatibility. *Biomaterials*, **2008**, 29 (20), 2941-2953.
35. Lowe, A. B., Thiol-ene “click” reactions and recent applications in polymer and materials synthesis. *Polym Chem*, **2010**, 1 (1), 17.
36. Liu, V. A.; Bhatia, S. N., Three-dimensional photopatterning of hydrogels containing living cells. *Biomedical Microdevices*, **2002**, 4 (4), 257-266.
37. Kim, K. D.; Wright, N. M., Polyethylene Glycol Hydrogel Spinal Sealant (DuraSeal Spinal Sealant) as an Adjunct to Sutured Dural Repair in the Spine Results of a Prospective, Multicenter, Randomized Controlled Study. *Spine*, **2011**, 36 (23), 1906-1912.
38. Murphy, S. V., et al., Evaluation of hydrogels for bio-printing applications. *J Biomed Mater Res A*, **2013**, 101 (1), 272-284.
39. Fedorovich, N. E., et al., The effect of photopolymerization on stem cells embedded in hydrogels. *Biomaterials*, **2009**, 30 (3), 344-353.
40. Lin, C. C., et al., PEG hydrogels formed by thiol-ene photo-click chemistry and their effect on the formation and recovery of insulin-secreting cell spheroids. *Biomaterials*, **2011**, 32 (36), 9685-9695.
41. Vermonden, T., et al., Hydrogels for protein delivery. *Chem Rev*, **2012**, 112 (5), 2853-2888.
42. Brandl, F., et al., Rational design of hydrogels for tissue engineering: impact of physical factors on cell behavior. *Biomaterials*, **2007**, 28 (2), 134-146.
43. Kraehenbuehl, T. P., et al., Cell-responsive hydrogel for encapsulation of vascular cells. *Biomaterials*, **2009**, 30 (26), 4318-4324.
44. Hunt, N. C.; Grover, L. M., Cell encapsulation using biopolymer gels for regenerative medicine. *Biotechnol Lett*, **2010**, 32 (6), 733-742.
45. Aikawa, T., et al., Spherical phospholipid polymer hydrogels for cell encapsulation prepared with a flow-focusing microfluidic channel device. *Langmuir*, **2012**, 28 (4), 2145-2150.

46. Sundelacruz, S.; Kaplan, D. L., Stem cell- and scaffold-based tissue engineering approaches to osteochondral regenerative medicine. *Semin Cell Dev Biol*, **2009**, *20* (6), 646-655.
47. Martins, A. M., et al., Responsive and in situ-forming chitosan scaffolds for bone tissue engineering applications: an overview of the last decade. *J Mater Chem*, **2010**, *20* (9), 1638-1645.
48. Schmidt, J. J., et al., Hydrogels used for cell-based drug delivery. *J Biomed Mater Res A*, **2008**, *87* (4), 1113-1122.
49. Engler, A. J., et al., Matrix elasticity directs stem cell lineage specification. *Cell*, **2006**, *126* (4), 677-689.
50. Discher, D. E., et al., Tissue cells feel and respond to the stiffness of their substrate. *Science*, **2005**, *310* (5751), 1139-1143.
51. Nie, T., et al., Production of heparin-functionalized hydrogels for the development of responsive and controlled growth factor delivery systems. *J Controlled Release*, **2007**, *122* (3), 287-296.
52. Bencherif, S. A., et al., Influence of the degree of methacrylation on hyaluronic acid hydrogels properties. *Biomaterials*, **2008**, *29* (12), 1739-1749.
53. Patenaude, M.; Hoare, T., Injectable, mixed natural-synthetic polymer hydrogels with modular properties. *Biomacromolecules*, **2012**, *13* (2), 369-378.
54. Kretlow, J. D.; Mikos, A. G., 2007 AIChE Alpha Chi Sigma Award: From Material to Tissue: Biomaterial Development, Scaffold Fabrication, and Tissue Engineering. *AIChE J*, **2008**, *54* (12), 3048-3067.
55. Novosel, E. C., et al., Vascularization is the key challenge in tissue engineering. *Adv Drug Deliv Rev*, **2011**, *63* (4-5), 300-311.
56. Tibbitt, M. W.; Anseth, K. S., Hydrogels as extracellular matrix mimics for 3D cell culture. *Biotechnol Bioeng*, **2009**, *103* (4), 655-663.
57. Van De Manakker, F., et al., Protein-Release Behavior of Self-Assembled PEG- β -Cyclodextrin/PEG-Cholesterol Hydrogels. *Adv Funct Mater*, **2009**, *19* (18), 2992-3001.

58. Weber, L. M., et al., Effects of PEG hydrogel crosslinking density on protein diffusion and encapsulated islet survival and function. *J Biomed Mater Res A*, **2009**, *90* (3), 720-729.
59. Bertz, A., et al., Encapsulation of proteins in hydrogel carrier systems for controlled drug delivery: Influence of network structure and drug size on release rate. *J Biotechnol*, **2013**, *163* (2), 243-249.
60. Du, M. C., et al., Fabrication and biological application of nano-hydroxyapatite (nHA)/alginate (ALG) hydrogel as scaffolds. *J Mater Chem*, **2011**, *21* (7), 2228-2236.
61. Peppas, N. A.; Khare, A. R., Preparation, Structure and Diffusional Behavior of Hydrogels in Controlled-Release. *Adv Drug Deliv Rev*, **1993**, *11* (1-2), 1-35.
62. Lin, C. C.; Metters, A. T., Hydrogels in controlled release formulations: network design and mathematical modeling. *Adv Drug Deliv Rev*, **2006**, *58* (12-13), 1379-1408.
63. Impellitteri, N. A., et al., Specific VEGF sequestering and release using peptide-functionalized hydrogel microspheres. *Biomaterials*, **2012**, *33* (12), 3475-3484.
64. Nelson, D. L., et al., *Lehninger principles of biochemistry*. Macmillan: 2008.
65. Francis Suh, J. K.; Matthew, H. W. T., Application of chitosan-based polysaccharide biomaterials in cartilage tissue engineering: a review. *Biomaterials*, **2000**, *21* (24), 2589-2598.
66. Toole, B. P., Hyaluronan: from extracellular glue to pericellular cue. *Nat Rev Cancer*, **2004**, *4* (7), 528-539.
67. Langer, R.; Tirrell, D. A., Designing materials for biology and medicine. *Nature*, **2004**, *428* (6982), 487-492.
68. Garg, H. G.; Hales, C. A., *Chemistry and biology of hyaluronan*. Elsevier: Amsterdam; Boston, 2004.
69. Laurent, T. C., *The chemistry, biology, and medical applications of hyaluronan and its derivatives*. Portland Press: London; Miami, 1998.

70. Allison, D. D.; Grande-Allen, K. J., Review. Hyaluronan: a powerful tissue engineering tool. *Tissue Eng*, **2006**, *12* (8), 2131-2140.
71. Almond, A., Hyaluronan. *Cell Mol Life Sci*, **2007**, *64* (13), 1591-1596.
72. Liu, L., et al., Microbial production of hyaluronic acid: current state, challenges, and perspectives. *Microb Cell Fact*, **2011**, *10*, 99.
73. Izawa, N., et al., Hyaluronic acid production by recombinant *Streptococcus thermophilus*. *J Biosci Bioeng*, **2011**, *111* (6), 665-670.
74. Stern, R., Hyaluronan catabolism: a new metabolic pathway. *Eur J Cell Biol*, **2004**, *83* (7), 317-325.
75. Burdick, J. A.; Prestwich, G. D., Hyaluronic acid hydrogels for biomedical applications. *Adv Mater*, **2011**, *23* (12), H41-56.
76. Tan, H., et al., Injectable in situ forming biodegradable chitosan-hyaluronic acid based hydrogels for cartilage tissue engineering. *Biomaterials*, **2009**, *30* (13), 2499-2506.
77. Jin, R., et al., Synthesis and characterization of hyaluronic acid-poly(ethylene glycol) hydrogels via Michael addition: An injectable biomaterial for cartilage repair. *Acta Biomater*, **2010**, *6* (6), 1968-1977.
78. Jia, X., et al., Hyaluronic acid-based microgels and microgel networks for vocal fold regeneration. *Biomacromolecules*, **2006**, *7* (12), 3336-3344.
79. Masters, K. S., et al., Crosslinked hyaluronan scaffolds as a biologically active carrier for valvular interstitial cells. *Biomaterials*, **2005**, *26* (15), 2517-2525.
80. Shah, D. N., et al., The effect of bioactive hydrogels on the secretion of extracellular matrix molecules by valvular interstitial cells. *Biomaterials*, **2008**, *29* (13), 2060-2072.
81. Peattie, R. A., et al., Dual growth factor-induced angiogenesis in vivo using hyaluronan hydrogel implants. *Biomaterials*, **2006**, *27* (9), 1868-1875.
82. Patterson, J., et al., Hyaluronic acid hydrogels with controlled degradation properties for oriented bone regeneration. *Biomaterials*, **2010**, *31* (26), 6772-6781.

83. Jha, A. K., et al., Controlling the adhesion and differentiation of mesenchymal stem cells using hyaluronic acid-based, doubly crosslinked networks. *Biomaterials*, **2011**, 32 (10), 2466-2478.
84. Elia, R., et al., Silk-hyaluronan-based composite hydrogels: a novel, securable vehicle for drug delivery. *J Biomater Appl*, **2013**, 27 (6), 749-762.
85. Marklein, R. A.; Burdick, J. A., Spatially controlled hydrogel mechanics to modulate stem cell interactions. *Soft Matter*, **2010**, 6 (1), 136.
86. Lozoya, O. A., et al., Regulation of hepatic stem/progenitor phenotype by microenvironment stiffness in hydrogel models of the human liver stem cell niche. *Biomaterials*, **2011**, 32 (30), 7389-7402.
87. Xu, X., et al., Heparin-decorated, hyaluronic acid-based hydrogel particles for the controlled release of bone morphogenetic protein 2. *Acta Biomater*, **2011**, 7 (8), 3050-3059.
88. Xu, X., et al., Hyaluronic Acid-Based Hydrogels: from a Natural Polysaccharide to Complex Networks. *Soft Matter*, **2012**, 8 (12), 3280-3294.
89. Yao, K., et al., *Chitosan-based hydrogels: functions and applications*. CRC Press: 2012.
90. Zhao, J., Chitosan-based gels for the drug delivery system. In *Chitosan-based hydrogels: functions and applications*, Yao, K., et al., Eds. CRC Press: 2012.
91. Prabakaran, M., Review paper: chitosan derivatives as promising materials for controlled drug delivery. *J Biomater Appl*, **2008**, 23 (1), 5-36.
92. Lü, S., et al., An injectable oxidized carboxymethylcellulose/N-succinyl-chitosan hydrogel system for protein delivery. *Chem Eng J*, **2010**, 160 (2), 779-787.
93. Sukarto, A., et al., Co-delivery of adipose-derived stem cells and growth factor-loaded microspheres in RGD-grafted N-methacrylate glycol chitosan gels for focal chondral repair. *Biomacromolecules*, **2012**, 13 (8), 2490-2502.
94. Park, K. M., et al., Thermosensitive chitosan-Pluronic hydrogel as an injectable cell delivery carrier for cartilage regeneration. *Acta Biomater*, **2009**, 5 (6), 1956-1965.

95. Leipzig, N. D., et al., Differentiation of neural stem cells in three-dimensional growth factor-immobilized chitosan hydrogel scaffolds. *Biomaterials*, **2011**, 32 (1), 57-64.
96. Richardson, S. M., et al., Human mesenchymal stem cell differentiation to NP-like cells in chitosan-glycerophosphate hydrogels. *Biomaterials*, **2008**, 29 (1), 85-93.
97. Wang, L.; Stegemann, J. P., Thermogelling chitosan and collagen composite hydrogels initiated with beta-glycerophosphate for bone tissue engineering. *Biomaterials*, **2010**, 31 (14), 3976-3985.
98. Crompton, K. E., et al., Polylysine-functionalised thermoresponsive chitosan hydrogel for neural tissue engineering. *Biomaterials*, **2007**, 28 (3), 441-449.
99. Zhou, Y., et al., Photopolymerized water-soluble chitosan-based hydrogel as potential use in tissue engineering. *Int J Biol Macromol*, **2011**, 48 (3), 408-413.
100. Valmikinathan, C. M., et al., Photocrosslinkable chitosan based hydrogels for neural tissue engineering. *Soft Matter*, **2012**, 8 (6), 1964.
101. McGann, C.; Kiick, K., Heparin-Functionalized Materials in Tissue Engineering Applications. In *Engineering Biomaterials for Regenerative Medicine: Novel Technologies for Clinical Applications*, Bhatia, S. K., Ed. Springer: 2011.
102. Nelson, D. L.; Cox, M. M., *Lehninger Principles of Biochemistry*. 4th ed.; W.H. Freeman: 2008.
103. Rabenstein, D. L., Heparin and heparan sulfate: structure and function. *Nat Prod Rep*, **2002**, 19 (3), 312-331.
104. Turnbull, J., et al., Heparan sulfate: decoding a dynamic multifunctional cell regulator. *Trends Cell Biol*, **2001**, 11 (2), 75-82.
105. Alban, S., Adverse Effects of Heparin. In *Heparin - A Century of Progress*, Rebecca Lever, B. M. a. C. P. P., Ed. Springer: 2012; Vol. 207. DOI: 10.1007/978-3-642-23056-1.
106. Greinacher, A., Heparin-induced thrombocytopenia: frequency and pathogenesis. *Pathophysiol Haemost Thromb*, **2006**, 35 (1-2), 37-45.

107. Melloni, C., et al., Unfractionated heparin dosing and risk of major bleeding in non-ST-segment elevation acute coronary syndromes. *Am Heart J*, **2008**, *156* (2), 209-215.
108. Nie, T., et al., Production of heparin-containing hydrogels for modulating cell responses. *Acta Biomater*, **2009**, *5* (3), 865-875.
109. Benoit, D. S., et al., Multifunctional hydrogels that promote osteogenic hMSC differentiation through stimulation and sequestering of BMP2. *Adv Funct Mater*, **2007**, *17* (13), 2085-2093.
110. Kim, M., et al., Modulation of cell adhesion of heparin-based hydrogel by efficient physisorption of adhesive proteins. *Macromol Res*, **2012**, *20* (3), 271-276.
111. Freudenberg, U., et al., A star-PEG–heparin hydrogel platform to aid cell replacement therapies for neurodegenerative diseases. *Biomaterials*, **2009**, *30* (28), 5049-5060.
112. Kim, M., et al., Heparin-based hydrogel as a matrix for encapsulation and cultivation of primary hepatocytes. *Biomaterials*, **2010**, *31* (13), 3596-3603.
113. Seto, S. P., et al., Differentiation of mesenchymal stem cells in heparin-containing hydrogels via coculture with osteoblasts. *Cell Tissue Res*, **2012**, *347* (3), 589-601.
114. Wieduwild, R., et al., Minimal Peptide Motif for Non-covalent Peptide-Heparin Hydrogels. *J Am Chem Soc*, **2013**, *135* (8), 2919-2922.
115. Tae, G., et al., Formation of a novel heparin-based hydrogel in the presence of heparin-binding biomolecules. *Biomacromolecules*, **2007**, *8* (6), 1979-1986.
116. Baldwin, A. D., et al., In situ crosslinkable heparin-containing poly(ethylene glycol) hydrogels for sustained anticoagulant release. *J Biomed Mater Res A*, **2012**, *100* (8), 2106-2118.
117. Jeon, O., et al., Affinity-based growth factor delivery using biodegradable, photocrosslinked heparin-alginate hydrogels. *J Controlled Release*, **2011**, *154* (3), 258-266.

118. Bhakta, G., et al., Hyaluronic acid-based hydrogels functionalized with heparin that support controlled release of bioactive BMP-2. *Biomaterials*, **2012**, *33* (26), 6113-6122.
119. Alshamkhani, A.; Duncan, R., Radioiodination of Alginate Via Covalently-Bound Tyrosinamide Allows Monitoring of Its Fate in-Vivo. *J Bioact Compat Polym*, **1995**, *10* (1), 4-13.
120. Gao, C., et al., Preparation and controlled degradation of oxidized sodium alginate hydrogel. *Polym Degrad Stab*, **2009**, *94* (9), 1405-1410.
121. Boonthekul, T., et al., Controlling alginate gel degradation utilizing partial oxidation and bimodal molecular weight distribution. *Biomaterials*, **2005**, *26* (15), 2455-2465.
122. Dai, Y. N., et al., A novel pH sensitive N-succinyl chitosan/alginate hydrogel bead for nifedipine delivery. *Biopharm Drug Dispos*, **2008**, *29* (3), 173-184.
123. Josef, E., et al., Composite alginate hydrogels: An innovative approach for the controlled release of hydrophobic drugs. *Acta Biomater*, **2010**, *6* (12), 4642-4649.
124. Shi, J., et al., Hybrid alginate beads with thermal-responsive gates for smart drug delivery. *Polym Adv Technol*, **2011**, *22* (11), 1539-1546.
125. Zhao, L., et al., An injectable calcium phosphate-alginate hydrogel-umbilical cord mesenchymal stem cell paste for bone tissue engineering. *Biomaterials*, **2010**, *31* (25), 6502-6510.
126. Zhou, H.; Xu, H. H., The fast release of stem cells from alginate-fibrin microbeads in injectable scaffolds for bone tissue engineering. *Biomaterials*, **2011**, *32* (30), 7503-7513.
127. Kim, W. S., et al., Adipose tissue engineering using injectable, oxidized alginate hydrogels. *Tissue Eng Part A*, **2012**, *18* (7-8), 737-743.
128. Murakami, K., et al., Hydrogel blends of chitin/chitosan, fucoidan and alginate as healing-impaired wound dressings. *Biomaterials*, **2010**, *31* (1), 83-90.

129. Kim, J. O., et al., Development of polyvinyl alcohol-sodium alginate gel-matrix-based wound dressing system containing nitrofurazone. *Int J Pharm*, **2008**, 359 (1-2), 79-86.
130. Balakrishnan, B., et al., Evaluation of an in situ forming hydrogel wound dressing based on oxidized alginate and gelatin. *Biomaterials*, **2005**, 26 (32), 6335-6342.
131. Tang, M., et al., Human embryonic stem cell encapsulation in alginate microbeads in macroporous calcium phosphate cement for bone tissue engineering. *Acta Biomater*, **2012**, 8 (9), 3436-3445.
132. Tan, W. H.; Takeuchi, S., Monodisperse alginate hydrogel microbeads for cell encapsulation. *Adv Mater*, **2007**, 19 (18), 2696-2701.
133. Yan, C., et al., Injectable solid peptide hydrogel as a cell carrier: effects of shear flow on hydrogels and cell payload. *Langmuir*, **2012**, 28 (14), 6076-6087.
134. Van Vlierberghe, S., et al., Biopolymer-based hydrogels as scaffolds for tissue engineering applications: a review. *Biomacromolecules*, **2011**, 12 (5), 1387-1408.
135. Perale, G., et al., Hydrogels in spinal cord injury repair strategies. *ACS Chem Neurosci*, **2011**, 2 (7), 336-345.
136. Numata, K.; Kaplan, D. L., Silk-based delivery systems of bioactive molecules. *Adv Drug Deliv Rev*, **2010**, 62 (15), 1497-1508.
137. Pritchard, E. M.; Kaplan, D. L., Silk fibroin biomaterials for controlled release drug delivery. *Expert Opin Drug Deliv*, **2011**, 8 (6), 797-811.
138. Jeon, S. I., et al., Protein—surface interactions in the presence of polyethylene oxide. *J Colloid Interface Sci*, **1991**, 142 (1), 149-158.
139. Cash, B. D.; Lacy, B. E., Systematic review: FDA-approved prescription medications for adults with constipation. *Gastroenterol Hepatol*, **2006**, 2 (10), 736-749.
140. Alconcel, S. N. S., et al., FDA-approved poly(ethylene glycol)—protein conjugate drugs. *Polym Chem*, **2011**, 2 (7), 1442.

141. Pasut, G.; Veronese, F. M., PEG conjugates in clinical development or use as anticancer agents: an overview. *Adv Drug Deliv Rev*, **2009**, *61* (13), 1177-1188.
142. Webster, R., et al., PEGylated proteins: evaluation of their safety in the absence of definitive metabolism studies. *Drug Metab Dispos*, **2007**, *35* (1), 9-16.
143. Fruijtier-Polloth, C., Safety assessment on polyethylene glycols (PEGs) and their derivatives as used in cosmetic products. *Toxicology*, **2005**, *214* (1-2), 1-38.
144. Working, P. K., et al., Safety of poly(ethylene glycol) and poly(ethylene glycol) derivatives. In *Poly(Ethylene Glycol): Chemistry and Biological Applications*, Harris, J. M.; Zalipsky, S., Eds. Amer Chemical Soc: Washington, 1997; Vol. 680, pp 45-57.
145. Fairbanks, B. D., et al., Photodegradable, photoadaptable hydrogels via radical-mediated disulfide fragmentation reaction. *Macromolecules*, **2011**, *44* (8), 2444.
146. Lutolf, M. P.; Hubbell, J. A., Synthesis and physicochemical characterization of end-linked poly(ethylene glycol)-co-peptide hydrogels formed by Michael-type addition. *Biomacromolecules*, **2003**, *4* (3), 713-722.
147. Schultz, K. M., et al., Gelation of Covalently Cross-Linked PEG-Heparin Hydrogels. *Macromolecules*, **2009**, *42* (14), 5310-5316.
148. Metters, A.; Hubbell, J., Network formation and degradation behavior of hydrogels formed by Michael-type addition reactions. *Biomacromolecules*, **2005**, *6* (1), 290-301.
149. Rydholm, A. E., et al., Degradable thiol-acrylate photopolymers: polymerization and degradation behavior of an in situ forming biomaterial. *Biomaterials*, **2005**, *26* (22), 4495-4506.
150. Rydholm, A. E., et al., Development and Characterization of Degradable Thiol-Allyl Ether Photopolymers. *Polymer*, **2007**, *48* (15), 4589-4600.
151. Fairbanks, B. D., et al., A versatile synthetic extracellular matrix mimic via thiol-norbornene photopolymerization. *Adv Mater*, **2009**, *21* (48), 5005-5010.

152. Anderson, S. B., et al., The performance of human mesenchymal stem cells encapsulated in cell-degradable polymer-peptide hydrogels. *Biomaterials*, **2011**, 32 (14), 3564-3574.
153. Hou, Y. P., et al., Photo-Cross-Linked PDMSstar-PEG Hydrogels: Synthesis, Characterization, and Potential Application for Tissue Engineering Scaffolds. *Biomacromolecules*, **2010**, 11 (3), 648-656.
154. Kim, J., et al., Potential of hydrogels based on poly(ethylene glycol) and sebacic acid as orthopedic tissue engineering scaffolds. *Tissue Eng Part A*, **2009**, 15 (8), 2299-2307.
155. Tan, H., et al., Novel multiarm PEG-based hydrogels for tissue engineering. *J Biomed Mater Res A*, **2010**, 92 (3), 979-987.
156. Brandl, F. P., et al., Enzymatically degradable poly(ethylene glycol) based hydrogels for adipose tissue engineering. *Biomaterials*, **2010**, 31 (14), 3957-3966.
157. Perez, C. M., et al., A collagen peptide-based physical hydrogel for cell encapsulation. *Macromol Biosci*, **2011**, 11 (10), 1426-1431.
158. Chan, V., et al., Three-dimensional photopatterning of hydrogels using stereolithography for long-term cell encapsulation. *Lab Chip*, **2010**, 10 (16), 2062-2070.
159. Phelps, E. A., et al., Maleimide cross-linked bioactive PEG hydrogel exhibits improved reaction kinetics and cross-linking for cell encapsulation and in situ delivery. *Adv Mater*, **2012**, 24 (1), 64-70, 62.
160. Benoit, D. S., et al., Small functional groups for controlled differentiation of hydrogel-encapsulated human mesenchymal stem cells. *Nat Mater*, **2008**, 7 (10), 816-823.
161. Park, H., et al., Effect of Swelling Ratio of Injectable Hydrogel Composites on Chondrogenic Differentiation of Encapsulated Rabbit Marrow Mesenchymal Stem Cells In Vitro. *Biomacromolecules*, **2009**, 10 (3), 541-546.

162. Hudalla, G. A., et al., An Approach to Modulate Degradation and Mesenchymal Stem Cell Behavior in Poly(ethylene glycol) Networks. *Biomacromolecules*, **2008**, *9* (3), 842-849.
163. Huynh, C. T., et al., Sustained delivery of doxorubicin using biodegradable pH/temperature-sensitive poly(ethylene glycol)-poly(β -amino ester urethane) multiblock copolymer hydrogels. *Soft Matter*, **2011**, *7* (10), 4974.
164. Aimetti, A. A., et al., Poly(ethylene glycol) hydrogels formed by thiol-ene photopolymerization for enzyme-responsive protein delivery. *Biomaterials*, **2009**, *30* (30), 6048-6054.
165. Andreopoulos, F. M.; Persaud, I., Delivery of basic fibroblast growth factor (bFGF) from photoresponsive hydrogel scaffolds. *Biomaterials*, **2006**, *27* (11), 2468-2476.
166. Papavasiliou, G., et al., *Synthetic PEG Hydrogels as Extracellular Matrix Mimics for Tissue Engineering Applications*. 2012.
167. Chang, G., et al., Enhancement of the fraction of the active form of an antitumor drug topotecan via an injectable hydrogel. *J Controlled Release*, **2011**, *156* (1), 21-27.
168. Baker, M. I., et al., A review of polyvinyl alcohol and its uses in cartilage and orthopedic applications. *J Biomed Mater Res B Appl Biomater*, **2012**, *100* (5), 1451-1457.
169. Alves, M. H., et al., Poly(vinyl alcohol) physical hydrogels: new vista on a long serving biomaterial. *Macromol Biosci*, **2011**, *11* (10), 1293-1313.
170. Alves, M. H., et al., Degradable, click poly(vinyl alcohol) hydrogels: characterization of degradation and cellular compatibility. *Biomed Mater*, **2012**, *7* (2), 024106.
171. Ossipov, D. A.; Hilborn, J., Poly(vinyl alcohol)-Based Hydrogels Formed by "Click Chemistry". *Macromolecules*, **2006**, *39* (5), 1709-1718.

172. Vidović, E., et al., Synthesis and characterization of poly(vinyl alcohol)-graft-[poly(D,L-lactide)/poly(D,L-lactide-co-glycolide)] hydrogels. *J Polym Sci A Polym Chem*, **2007**, *45* (19), 4536-4544.
173. Zhang, N., et al., Synthesis and characterization of thermo- and pH-sensitive poly(vinyl alcohol)/poly(N, N-diethylacrylamide-co-itaconic acid) semi-IPN hydrogels. *Biomed Mater*, **2012**, *7* (3), 035014.
174. Nilasaroya, A., et al., Structural and functional characterisation of poly(vinyl alcohol) and heparin hydrogels. *Biomaterials*, **2008**, *29* (35), 4658-4664.
175. Juntanon, K., et al., Electrically controlled release of sulfosalicylic acid from crosslinked poly(vinyl alcohol) hydrogel. *Int J Pharm*, **2008**, *356* (1-2), 1-11.
176. Wu, L.; Brazel, C. S., Modifying the release of proxiphylline from PVA hydrogels using surface crosslinking. *Int J Pharm*, **2008**, *349* (1-2), 144-151.
177. Lozinsky, V. I., et al., Study of cryostructuring of polymer systems: 27. Physicochemical properties of poly(vinyl alcohol) cryogels and specific features of their macroporous morphology. *Colloid J*, **2007**, *69* (6), 747-764.
178. Samal, S., et al., Hybrid Hydrogels Based on Poly(vinylalcohol)-Chitosan Blends and Relevant CNT Composites. In *Hydrogels: Biological Properties and Applications*, Barbucci, R., Ed. Springer: Milan, 2009; pp 67-78.
179. Otsuka, E.; Suzuki, A., A simple method to obtain a swollen PVA gel crosslinked by hydrogen bonds. *J Appl Polym Sci*, **2009**, *114* (1), 10-16.
180. Bonakdar, S., et al., Preparation and characterization of polyvinyl alcohol hydrogels crosslinked by biodegradable polyurethane for tissue engineering of cartilage. *Mater Sci Eng C Mater Biol Appl*, **2010**, *30* (4), 636-643.
181. Spiller, K. L., et al., Design of semi-degradable hydrogels based on poly(vinyl alcohol) and poly(lactic-co-glycolic acid) for cartilage tissue engineering. *J Tissue Eng Regen Med*, **2011**, *5* (8), 636-647.
182. Peng, Z. Y.; Shen, Y. Q., Study on Biological Safety of Polyvinyl Alcohol/Collagen Hydrogel as Tissue Substitute (I). *Polym Plast Technol Eng*, **2011**, *50* (3), 245-250.

183. Michalek, J., et al., Hydrogels Contact Lenses. In *Biomedical Applications of Hydrogels Handbook*, Ottenbrite, R. M., et al., Eds. Springer New York: 2010; pp 303-315.
184. Atzet, S., et al., Degradable poly (2-hydroxyethyl methacrylate)-copolycaprolactone hydrogels for tissue engineering scaffolds. *Biomacromolecules*, **2008**, *9* (12), 3370-3377.
185. Bryant, S. J., et al., Photo-patterning of porous hydrogels for tissue engineering. *Biomaterials*, **2007**, *28* (19), 2978.
186. Paterson, S. M., et al., The synthesis and degradation of collagenase-degradable poly(2-hydroxyethyl methacrylate)-based hydrogels and sponges for potential applications as scaffolds in tissue engineering. *Mater Sci Eng C Mater Biol Appl*, **2012**, *32* (8), 2536-2544.
187. Casadio, Y. S., et al., Biodegradation of Poly(2-hydroxyethyl methacrylate) (PHEMA) and Poly{(2-hydroxyethyl methacrylate)-co-[poly(ethylene glycol) methyl ether methacrylate]} Hydrogels Containing Peptide-Based Cross-Linking Agents. *Biomacromolecules*, **2010**, *11* (11), 2949-2959.
188. Zhang, J. T., et al., Temperature-sensitive PVA/PNIPAAm semi-IPN hydrogels with enhanced responsive properties. *Acta Biomater*, **2009**, *5* (1), 488-497.
189. Varaprasad, K., et al., Design and development of temperature sensitive porous poly (NIPAAm-AMPS) hydrogels for drug release of doxorubicin-a cancer chemotherapy drug. *J Appl Polym Sci*, **2010**, *116* (6), 3593-3602.
190. Santos, J. R., et al., New Thermo-responsive Hydrogels Based on Poly (N-isopropylacrylamide)/Hyaluronic Acid Semi-interpenetrated Polymer Networks: Swelling Properties and Drug Release Studies. *J Bioact Compat Polym*, **2010**, *25* (2), 169-184.
191. Zhang, X.-Z., et al., Strategies to improve the response rate of thermosensitive PNIPAAm hydrogels. *Soft Matter*, **2008**, *4* (3), 385.

192. Andrianov, A. K.; Langer, R., Polyphosphazenes for Biology and Medicine: Current Status and Future Prospects. In *Polyphosphazenes for Biomedical Applications*, John Wiley and Sons: 2009.
193. Lee, K. Y.; Mooney, D. J., Hydrogels for tissue engineering. *Chem Rev*, **2001**, *101* (7), 1869-1880.
194. Allcock, H. R., Polyphosphazene elastomers, gels, and other soft materials. *Soft Matter*, **2012**, *8* (29), 7521-7532.
195. Chun, C., et al., Doxorubicin-polyphosphazene conjugate hydrogels for locally controlled delivery of cancer therapeutics. *Biomaterials*, **2009**, *30* (27), 4752-4762.
196. Potta, T., et al., Injectable, dual cross-linkable polyphosphazene blend hydrogels. *Biomaterials*, **2010**, *31* (32), 8107-8120.
197. Li, Y., et al., Injectable and biodegradable hydrogels: gelation, biodegradation and biomedical applications. *Chem Soc Rev*, **2012**, *41* (6), 2193-2221.
198. Odian, G. G., *Principles of polymerization*. Wiley-Interscience: Hoboken, N.J., 2004.
199. Salinas, C. N.; Anseth, K. S., Mixed Mode Thiol– Acrylate Photopolymerizations for the Synthesis of PEG– Peptide Hydrogels. *Macromolecules*, **2008**, *41* (16), 6019-6026.
200. Ifkovits, J. L.; Burdick, J. A., Review: photopolymerizable and degradable biomaterials for tissue engineering applications. *Tissue Eng*, **2007**, *13* (10), 2369-2385.
201. Rouillard, A. D., et al., Methods for photocrosslinking alginate hydrogel scaffolds with high cell viability. *Tissue Eng Part C Methods*, **2011**, *17* (2), 173-179.
202. Burdick, J. A., et al., Conversion and temperature profiles during the photoinitiated polymerization of thick orthopaedic biomaterials. *Biomaterials*, **2001**, *22* (13), 1779-1786.
203. Malkoch, M., et al., Synthesis of well-defined hydrogel networks using Click chemistry. *Chem Comm*, **2006**, (26), 2774-2776.

204. Brigham, M. D., et al., Mechanically robust and bioadhesive collagen and photocrosslinkable hyaluronic acid semi-interpenetrating networks. *Tissue Eng Part A*, **2008**, *15* (7), 1645-1653.
205. Khetan, S., et al., Sequential crosslinking to control cellular spreading in 3-dimensional hydrogels. *Soft Matter*, **2009**, *5* (8), 1601-1606.
206. Ekici, S., et al., Hyaluronic acid hydrogel particles with tunable charges as potential drug delivery devices. *Carbohydrate Polymers*, **2011**, *84* (4), 1306-1313.
207. Kloxin, A. M., et al., Photodegradable hydrogels for dynamic tuning of physical and chemical properties. *Science*, **2009**, *324* (5923), 59-63.
208. Dai, X., et al., Free radical polymerization of poly(ethylene glycol) diacrylate macromers: impact of macromer hydrophobicity and initiator chemistry on polymerization efficiency. *Acta Biomater*, **2011**, *7* (5), 1965-1972.
209. Morelli, A.; Chiellini, F., Ulvan as a New Type of Biomaterial from Renewable Resources: Functionalization and Hydrogel Preparation. *Macromol Chem Phys*, **2010**, *211* (7), 821-832.
210. Guvendiren, M.; Burdick, J. A., Stiffening hydrogels to probe short- and long-term cellular responses to dynamic mechanics. *Nat Commun*, **2012**, *3*, 792.
211. Matyjaszewski, K., et al., Hydrogels by atom transfer radical polymerization. I. Poly(N-vinylpyrrolidinone-g-styrene) via the macromonomer method. *J Polym Sci A Polym Chem*, **1998**, *36* (5), 823-830.
212. Yoon, J. A., et al., Thermoresponsive hydrogel scaffolds with tailored hydrophilic pores. *Chem Asian J*, **2011**, *6* (1), 128-136.
213. Yoon, J. A., et al., ATRP: A Versatile Tool toward Uniformly Crosslinked Hydrogels with Controlled Architecture and Multifunctionality. In *Hydrogel Micro and Nanoparticles*, Wiley-VCH Verlag GmbH & Co. KGaA: 2012; pp 169-186. DOI: 10.1002/9783527646425.ch7.
214. Fairbanks, B. D., et al., A Versatile Synthetic Extracellular Matrix Mimic via Thiol-Norbornene Photopolymerization. *Adv Mater*, **2009**, *21* (48), 5005-5010.

215. Moses, J. E.; Moorhouse, A. D., The growing applications of click chemistry. *Chem Soc Rev*, **2007**, *36* (8), 1249-1262.
216. Becer, C. R., et al., Click chemistry beyond metal-catalyzed cycloaddition. *Angew Chem Int Ed Engl*, **2009**, *48* (27), 4900-4908.
217. Deforest, C. A., et al., Peptide-Functionalized Click Hydrogels with Independently Tunable Mechanics and Chemical Functionality for 3D Cell Culture. *Chem Mater*, **2010**, *22* (16), 4783-4790.
218. Liu, S. Q., et al., Biodegradable poly(ethylene glycol)-peptide hydrogels with well-defined structure and properties for cell delivery. *Biomaterials*, **2009**, *30* (8), 1453-1461.
219. Deforest, C. A., et al., Sequential click reactions for synthesizing and patterning three-dimensional cell microenvironments. *Nat Mater*, **2009**, *8* (8), 659-664.
220. Lutz, J. F.; Zarafshani, Z., Efficient construction of therapeutics, bioconjugates, biomaterials and bioactive surfaces using azide-alkyne "click" chemistry. *Adv Drug Deliv Rev*, **2008**, *60* (9), 958-970.
221. Malkoch, M., et al., Synthesis of well-defined hydrogel networks using click chemistry. *Chem Comm*, **2006**, (26), 2774-2776.
222. Nimmo, C. M.; Shoichet, M. S., Regenerative biomaterials that "click": simple, aqueous-based protocols for hydrogel synthesis, surface immobilization, and 3D patterning. *Bioconjug Chem*, **2011**, *22* (11), 2199-2209.
223. Crescenzi, V., et al., Novel hydrogels via click chemistry: synthesis and potential biomedical applications. *Biomacromolecules*, **2007**, *8* (6), 1844-1850.
224. Testa, G., et al., Influence of dialkyne structure on the properties of new click-gels based on hyaluronic acid. *Int J Pharm*, **2009**, *378* (1-2), 86-92.
225. Piluso, S., et al., Hyaluronic acid-based hydrogels crosslinked by copper-catalyzed azide-alkyne cycloaddition with tailorable mechanical properties. *Int J Artif Organs*, **2011**, *34* (2), 192-197.

226. Zheng, J., et al., Strain-Promoted Crosslinking of PEG-based Hydrogels via Copper-Free Cycloaddition. *ACS Macro Lett*, **2012**, *1* (8), 1071-1073.
227. Xu, J., et al., Cytocompatible poly(ethylene glycol)-co-polycarbonate hydrogels cross-linked by copper-free, strain-promoted click chemistry. *Chem Asian J*, **2011**, *6* (10), 2730-2737.
228. Tan, H., et al., Direct synthesis of biodegradable polysaccharide derivative hydrogels through aqueous Diels-Alder chemistry. *Macromol Rapid Commun*, **2011**, *32* (12), 905-911.
229. Devaraj, N. K., et al., Tetrazine-based cycloadditions: application to pretargeted live cell imaging. *Bioconjug Chem*, **2008**, *19* (12), 2297-2299.
230. Pipkorn, R., et al., Inverse-electron-demand Diels-Alder reaction as a highly efficient chemoselective ligation procedure: Synthesis and function of a BioShuttle for temozolomide transport into prostate cancer cells. *J Pept Sci*, **2009**, *15* (3), 235-241.
231. Liu, D. S., et al., Diels–Alder cycloaddition for fluorophore targeting to specific proteins inside living cells. *J Am Chem Soc*, **2012**, *134* (2), 792-795.
232. Shih, H.; Lin, C. C., Cross-linking and degradation of step-growth hydrogels formed by thiol-ene photoclick chemistry. *Biomacromolecules*, **2012**, *13* (7), 2003-2012.
233. McGann, C. L., et al., Resilin-Based Hybrid Hydrogels for Cardiovascular Tissue Engineering. *Macromol Chem Phys*, **2013**, *214* (2), 203-213.
234. Lei, Y.; Segura, T., DNA delivery from matrix metalloproteinase degradable poly(ethylene glycol) hydrogels to mouse cloned mesenchymal stem cells. *Biomaterials*, **2009**, *30* (2), 254-265.
235. Grover, G. N., et al., Biocompatible hydrogels by oxime Click chemistry. *Biomacromolecules*, **2012**, *13* (10), 3013-3017.
236. Broyer, R. M., et al., Dual Click reactions to micropattern proteins. *Soft Matter*, **2011**, *7* (21), 9972-9977.

237. Rostovtsev, V. V., et al., A stepwise Huisgen cycloaddition process: copper(I)-catalyzed regioselective "ligation" of azides and terminal alkynes. *Angew Chem Int Ed Engl*, **2002**, *41* (14), 2596-2599.
238. Van Dijk, M., et al., Synthesis and characterization of enzymatically biodegradable PEG and peptide-based hydrogels prepared by click chemistry. *Biomacromolecules*, **2010**, *11* (6), 1608-1614.
239. Finn, M. G.; Fokin, V. V., Click chemistry: function follows form. *Chem Soc Rev*, **2010**, *39* (4), 1231-1232.
240. Codelli, J. A., et al., Second-generation difluorinated cyclooctynes for copper-free click chemistry. *J Am Chem Soc*, **2008**, *130* (34), 11486-11493.
241. Jewett, J. C.; Bertozzi, C. R., Cu-free click cycloaddition reactions in chemical biology. *Chem Soc Rev*, **2010**, *39* (4), 1272-1279.
242. Sanyal, A., Diels–Alder Cycloaddition-Cycloreversion: A Powerful Combo in Materials Design. *Macromol Chem Phys*, **2010**, *211* (13), 1417-1425.
243. Wei, H.-L., et al., Facile preparation of poly(N-isopropylacrylamide)-based hydrogels via aqueous Diels–Alder click reaction. *Polymer*, **2010**, *51* (8), 1694-1702.
244. Blackman, M. L., et al., Tetrazine ligation: fast bioconjugation based on inverse-electron-demand Diels-Alder reactivity. *J Am Chem Soc*, **2008**, *130* (41), 13518-13519.
245. Hoyle, C. E.; Bowman, C. N., Thiol-ene click chemistry. *Angew Chem Int Ed Engl*, **2010**, *49* (9), 1540-1573.
246. Kade, M. J., et al., The power of thiol-ene chemistry. *J Polym Sci A Polym Chem*, **2010**, *48* (4), 743-750.
247. Gress, A., et al., Thio-click modification of poly [2-(3-butenyl)-2-oxazoline]. *Macromolecules*, **2007**, *40* (22), 7928-7933.
248. Dondoni, A., The emergence of thiol-ene coupling as a click process for materials and bioorganic chemistry. *Angew Chem Int Ed Engl*, **2008**, *47* (47), 8995-8997.

249. Baldwin, A. D.; Kiick, K. L., Reversible maleimide-thiol adducts yield glutathione-sensitive poly(ethylene glycol)-heparin hydrogels. *Polym Chem*, **2013**, *4* (1), 133-143.
250. Migneault, I., et al., Glutaraldehyde: behavior in aqueous solution, reaction with proteins, and application to enzyme crosslinking. *BioTechniques*, **2004**, *37* (5), 790-806.
251. Zhao, L., et al., pH triggered injectable amphiphilic hydrogel containing doxorubicin and paclitaxel. *Int J Pharm*, **2011**, *410* (1-2), 83-91.
252. Abdel-Mottaleb, M. M., et al., Physically cross-linked polyvinyl alcohol for the topical delivery of fluconazole. *Drug Dev Ind Pharm*, **2009**, *35* (3), 311-320.
253. Hosseinkhani, H., et al., Bone regeneration through controlled release of bone morphogenetic protein-2 from 3-D tissue engineered nano-scaffold. *J Controlled Release*, **2007**, *117* (3), 380-386.
254. Hunt, J. N., et al., Tunable, high modulus hydrogels driven by ionic coacervation. *Adv Mater*, **2011**, *23* (20), 2327-2331.
255. Ji, D.-Y., et al., A novel injectable chitosan/polyglutamate polyelectrolyte complex hydrogel with hydroxyapatite for soft-tissue augmentation. *Carbohydrate Polymers*, **2012**, *89* (4), 1123-1130.
256. Lin, Y. H., et al., Physically crosslinked alginate/N,O-carboxymethyl chitosan hydrogels with calcium for oral delivery of protein drugs. *Biomaterials*, **2005**, *26* (14), 2105-2113.
257. Matyash, M., et al., Novel soft alginate hydrogel strongly supports neurite growth and protects neurons against oxidative stress. *Tissue Eng Part A*, **2012**, *18* (1-2), 55-66.
258. Aguado, B. A., et al., Improving viability of stem cells during syringe needle flow through the design of hydrogel cell carriers. *Tissue Eng Part A*, **2012**, *18* (7-8), 806-815.

259. Nugent, M. J.; Higginbotham, C. L., Preparation of a novel freeze thawed poly(vinyl alcohol) composite hydrogel for drug delivery applications. *Eur J Pharm Biopharm*, **2007**, *67* (2), 377-386.
260. Rajagopal, K., et al., Tuning the pH Responsiveness of β -Hairpin Peptide Folding, Self-Assembly, and Hydrogel Material Formation. *Biomacromolecules*, **2009**, *10* (9), 2619-2625.
261. Branco, M. C., et al., The effect of protein structure on their controlled release from an injectable peptide hydrogel. *Biomaterials*, **2010**, *31* (36), 9527-9534.
262. Li, Z.; Deming, T. J., Tunable hydrogel morphology via self-assembly of amphiphilic pentablock copolypeptides. *Soft Matter*, **2010**, *6* (11), 2546.
263. Glassman, M. J., et al., Reinforcement of Shear Thinning Protein Hydrogels by Responsive Block Copolymer Self-Assembly. *Adv Funct Mater*, **2012**, *23* (9), 1182-1193.
264. Koutsopoulos, S., et al., Controlled release of functional proteins through designer self-assembling peptide nanofiber hydrogel scaffold. *Proc Natl Acad Sci U S A*, **2009**, *106* (12), 4623-4628.
265. Nagai, Y., et al., Slow release of molecules in self-assembling peptide nanofiber scaffold. *J Controlled Release*, **2006**, *115* (1), 18-25.
266. Foo, C. T. S. W. P., et al., Two-component protein-engineered physical hydrogels for cell encapsulation. *Proc Natl Acad Sci U S A*, **2009**, *106* (52), 22067-22072.
267. Liu, Y., et al., In Situ Forming Physical Hydrogels for Three-dimensional Tissue Morphogenesis. *Macromol Biosci*, **2011**, *11* (10), 1325-1330.
268. Kiick, K. L., Peptide- and protein-mediated assembly of heparinized hydrogels. *Soft Matter*, **2008**, *4*, 29-37.
269. Yamaguchi, N., et al., Growth factor mediated assembly of cell receptor-responsive hydrogels. *J Am Chem Soc*, **2007**, *129* (11), 3040-3041.

270. Kim, S. H.; Kiick, K. L., Cell-mediated Delivery and Targeted Erosion of Vascular Endothelial Growth Factor-Crosslinked Hydrogels. *Macromol Rapid Commun*, **2010**, *31* (14), 1231-1240.
271. Benoit, D. S., et al., Manipulations in hydrogel degradation behavior enhance osteoblast function and mineralized tissue formation. *Tissue Eng*, **2006**, *12* (6), 1663-1673.
272. Zhang, Z., et al., Biodegradable and thermoreversible PCLA-PEG-PCLA hydrogel as a barrier for prevention of post-operative adhesion. *Biomaterials*, **2011**, *32* (21), 4725-4736.
273. Nuttelman, C. R., et al., Temporal changes in peg hydrogel structure influence human mesenchymal stem cell proliferation and matrix mineralization. In *Tissue Eng*, Fisher, J. P., Ed. Springer-Verlag Berlin: Berlin, 2006; Vol. 585, pp 135-149.
274. Sahoo, S., et al., Hydrolytically Degradable Hyaluronic Acid Hydrogels with Controlled Temporal Structures. *Biomacromolecules*, **2008**, *9* (4), 1088-1092.
275. Baldwin, A. D.; Kiick, K. L., Tunable degradation of maleimide-thiol adducts in reducing environments. *Bioconjug Chem*, **2011**, *22* (10), 1946-1953.
276. Kloxin, A. M., et al., Tunable hydrogels for external manipulation of cellular microenvironments through controlled photodegradation. *Adv Mater*, **2010**, *22* (1), 61-66.
277. Griffin, D. R.; Kasko, A. M., Photodegradable Macromers and Hydrogels for Live Cell Encapsulation and Release. *J Am Chem Soc*, **2012**, *134* (31), 13103-13107.
278. Jo, Y. S., et al., Tailoring hydrogel degradation and drug release via neighboring amino acid controlled ester hydrolysis. *Soft Matter*, **2008**, *5* (2), 440-446.
279. Martens, P. J., et al., Tailoring the Degradation of Hydrogels Formed from Multivinyl Poly(ethylene glycol) and Poly(vinyl alcohol) Macromers for Cartilage Tissue Engineering. *Biomacromolecules*, **2003**, *4* (2), 283-292.
280. Hunt, N. C., et al., Encapsulation of fibroblasts causes accelerated alginate hydrogel degradation. *Acta Biomater*, **2010**, *6* (9), 3649-3656.

281. Lampe, K. J., et al., Impact of degradable macromer content in a poly(ethylene glycol) hydrogel on neural cell metabolic activity, redox state, proliferation, and differentiation. *Tissue Eng Part A*, **2010**, *16* (6), 1857-1866.
282. Lee, F., et al., An injectable hyaluronic acid-tyramine hydrogel system for protein delivery. *J Controlled Release*, **2009**, *134* (3), 186-193.
283. Buwalda, S. J., et al., Stereocomplexed 8-armed poly(ethylene glycol)-poly(lactide) star block copolymer hydrogels: Gelation mechanism, mechanical properties and degradation behavior. *Polymer*, **2012**, *53* (14), 2809-2817.
284. Ashton, R. S., et al., Scaffolds based on degradable alginate hydrogels and poly(lactide-co-glycolide) microspheres for stem cell culture. *Biomaterials*, **2007**, *28* (36), 5518-5525.
285. Tan, J. X., et al., HYAL1 overexpression is correlated with the malignant behavior of human breast cancer. *Int J Cancer*, **2011**, *128* (6), 1303-1315.
286. Patterson, J.; Hubbell, J. A., Enhanced proteolytic degradation of molecularly engineered PEG hydrogels in response to MMP-1 and MMP-2. *Biomaterials*, **2010**, *31* (30), 7836-7845.
287. Giano, M. C., et al., Controlled biodegradation of self-assembling beta-hairpin peptide hydrogels by proteolysis with matrix metalloproteinase-13. *Biomaterials*, **2011**, *32* (27), 6471-6477.
288. Li, L., et al., Resilin-like polypeptide hydrogels engineered for versatile biological function. *Soft Matter*, **2013**, *9* (3), 665-673.
289. Seliktar, D., et al., MMP-2 sensitive, VEGF-bearing bioactive hydrogels for promotion of vascular healing. *J Biomed Mater Res A*, **2004**, *68* (4), 704-716.
290. Wong, V. W., et al., Engineered pullulan–collagen composite dermal hydrogels improve early cutaneous wound healing. *Tissue Eng Part A*, **2010**, *17* (5-6), 631-644.
291. Yang, C., et al., A green fabrication approach of gelatin/CM-chitosan hybrid hydrogel for wound healing. *Carbohydrate Polymers*, **2010**, *82* (4), 1297-1305.

292. Kim, J., et al., Bone regeneration using hyaluronic acid-based hydrogel with bone morphogenic protein-2 and human mesenchymal stem cells. *Biomaterials*, **2007**, 28 (10), 1830-1837.
293. Patenaude, M.; Hoare, T., Injectable, Degradable Thermoresponsive Poly (N-isopropylacrylamide) Hydrogels. *ACS Macro Lett*, **2012**, 1 (3), 409-413.
294. Jones, D. P., et al., Glutathione measurement in human plasma. Evaluation of sample collection, storage and derivatization conditions for analysis of dansyl derivatives by HPLC. *Clin Chim Acta*, **1998**, 275 (2), 175-184.
295. Estrela, J. M., et al., Glutathione in cancer biology and therapy. *Crit Rev Clin Lab Sci*, **2006**, 43 (2), 143-181.
296. Franco, R., et al., The central role of glutathione in the pathophysiology of human diseases. *Arch Physiol Biochem*, **2007**, 113 (4-5), 234-258.
297. Wei, H. L., et al., Diels–Alder reaction in water for the straightforward preparation of thermoresponsive hydrogels. *J Appl Polym Sci*, **2011**, 120 (2), 974-980.
298. Koehler, K. C., et al., A Diels-Alder modulated approach to control and sustain the release of dexamethasone and induce osteogenic differentiation of human mesenchymal stem cells. *Biomaterials*, **2013**, 34 (16), 4150-4158.
299. Pasparakis, G., et al., Photodegradable polymers for biotechnological applications. *Macromol Rapid Commun*, **2012**, 33 (3), 183-198.
300. Skardal, A., et al., The generation of 3-D tissue models based on hyaluronan hydrogel-coated microcarriers within a rotating wall vessel bioreactor. *Biomaterials*, **2010**, 31 (32), 8426-8435.
301. Fomina, N., et al., Low power, biologically benign NIR light triggers polymer disassembly. *Macromolecules*, **2011**, 44 (21), 8590-8597.
302. Pritchard, C. D., et al., An injectable thiol-acrylate poly(ethylene glycol) hydrogel for sustained release of methylprednisolone sodium succinate. *Biomaterials*, **2011**, 32 (2), 587-597.
303. Stevens, D. M., et al., Semibranched polyglycidols as “fillers” in polycarbonate hydrogels to tune hydrophobic drug release. *Polym Chem*, **2015**.

304. Yang, C., et al., Cell-mediated delivery of glucocorticoids from thiol-ene hydrogels. *J Controlled Release*, **2012**, *162* (3), 612-618.
305. Chun, C., et al., Doxorubicin-polyphosphazene conjugate hydrogels for locally controlled delivery of cancer therapeutics. *Biomaterials*, **2009**, *30* (27), 4752-4762.
306. Cuggino, J. C., et al., Novel poly(NIPA-co-AAc) functional hydrogels with potential application in drug controlled release. *Mol Pharm*, **2014**, *11* (7), 2239-2249.
307. Atmani, H., et al., Proliferation and differentiation of osteoblasts and adipocytes in rat bone marrow stromal cell cultures: effects of dexamethasone and calcitriol. *J Cell Biochem*, **2003**, *89* (2), 364-372.
308. Testa, B., Prodrugs: bridging pharmacodynamic/pharmacokinetic gaps. *Curr Opin Chem Biol*, **2009**, *13* (3), 338-344.
309. Koehler, K. C., et al., Diels-Alder mediated controlled release from a poly(ethylene glycol) based hydrogel. *Biomacromolecules*, **2013**, *14* (2), 538-547.
310. Van Hove, A. H., et al., Temporally Tunable, Enzymatically Responsive Delivery of Proangiogenic Peptides from Poly(ethylene glycol) Hydrogels. *Adv Healthc Mater*, **2015**.
311. Lu, Y., et al., Issues related to targeted delivery of proteins and peptides. *AAPS J*, **2006**, *8* (3), E466-478.
312. Bruno, B. J., et al., Basics and recent advances in peptide and protein drug delivery. *Ther Deliv*, **2013**, *4* (11), 1443-1467.
313. Vlieghe, P., et al., Synthetic therapeutic peptides: science and market. *Drug Discov Today*, **2010**, *15* (1-2), 40-56.
314. Wang, H., et al., Multifunctional biohybrid hydrogels for cell culture and controlled drug release. *Chem Comm*, **2013**, *49* (67), 7448-7450.
315. Kontos, S.; Hubbell, J. A., Drug development: longer-lived proteins. *Chem Soc Rev*, **2012**, *41* (7), 2686-2695.
316. Smith, M. R., Rituximab (monoclonal anti-CD20 antibody): mechanisms of action and resistance. *Oncogene*, **2003**, *22* (47), 7359-7368.

317. Siegel, R. A.; Rathbone, M. J., Overview of controlled release mechanisms. In *Fundamentals and Applications of Controlled Release Drug Delivery*, Springer: 2012; pp 19-43.
318. Buwalda, S. J., et al., In Situ Forming Poly(ethylene glycol)- Poly(L-lactide) Hydrogels via Michael Addition: Mechanical Properties, Degradation, and Protein Release. *Macromol Chem Phys*, **2012**, *213* (7), 766-775.
319. Zustiak, S. P.; Leach, J. B., Characterization of protein release from hydrolytically degradable poly(ethylene glycol) hydrogels. *Biotechnol Bioeng*, **2011**, *108* (1), 197-206.
320. Chung, B. G., et al., Microfluidic fabrication of microengineered hydrogels and their application in tissue engineering. *Lab Chip*, **2012**, *12* (1), 45-59.
321. Impellitteri, N. A., et al., Specific VEGF sequestering and release using peptide-functionalized hydrogel microspheres. *Biomaterials*, **2012**, *33* (12), 3475-3484.
322. Piossek, C., et al., Vascular endothelial growth factor (VEGF) receptor II-derived peptides inhibit VEGF. *J Biol Chem*, **1999**, *274* (9), 5612-5619.
323. Mccall, J. D.; Anseth, K. S., Thiol-Ene Photopolymerizations Provide a Facile Method To Encapsulate Proteins and Maintain Their Bioactivity. *Biomacromolecules*, **2012**, *13* (8), 2410-2417.
324. O'shea, T. M., et al., Synthesis and characterization of a library of in-situ curing, nonswelling ethoxylated polyol thiol-ene hydrogels for tailorable macromolecule delivery. *Adv Mater*, **2015**, *27* (1), 65-72.
325. Aimetti, A. A., et al., Human neutrophil elastase responsive delivery from poly(ethylene glycol) hydrogels. *Biomacromolecules*, **2009**, *10* (6), 1484-1489.
326. Kharkar, P. M., et al., Dually degradable click hydrogels for controlled degradation and protein release. *J Mater Chem B*, **2014**, *2* (34), 5511-5521.
327. Kharkar, P. M., et al., Design of thiol-and light-sensitive degradable hydrogels using Michael-type addition reactions. *Polym Chem*, **2015**, *6* (31), 5565-5574.

328. Alconcel, S. N., et al., FDA-approved poly (ethylene glycol)–protein conjugate drugs. *Polym Chem*, **2011**, *2* (7), 1442-1448.
329. O'shea, T. M., et al., Covalent Incorporation of Trehalose within Hydrogels for Enhanced Long-Term Functional Stability and Controlled Release of Biomacromolecules. *Adv Healthc Mater*, **2015**.
330. Jain, N. K.; Roy, I., Effect of trehalose on protein structure. *Protein Sci*, **2009**, *18* (1), 24-36.
331. Peng, K., et al., Light controlled protein release from a supramolecular hydrogel. *Chem Comm*, **2010**, *46* (23), 4094-4096.
332. Holloway, J. L., et al., Synergistic Effects of SDF-1alpha and BMP-2 Delivery from Proteolytically Degradable Hyaluronic Acid Hydrogels for Bone Repair. *Macromol Biosci*, **2015**.
333. Purcell, B. P., et al., Injectable and bioresponsive hydrogels for on-demand matrix metalloproteinase inhibition. *Nat Mater*, **2014**, *13* (6), 653-661.
334. Manetsch, R., et al., In situ click chemistry: enzyme inhibitors made to their own specifications. *J Am Chem Soc*, **2004**, *126* (40), 12809-12818.
335. Pounder, R. J., et al., Metal free thiol–maleimide ‘Click’ reaction as a mild functionalisation strategy for degradable polymers. *Chem Comm*, **2008**, (41), 5158-5160.
336. Azagarsamy, M. A.; Anseth, K. S., Bioorthogonal Click Chemistry: An Indispensable Tool to Create Multifaceted Cell Culture Scaffolds. *ACS Macro Lett*, **2013**, *2* (1), 5-9.
337. Tibbitt, M. W., et al., Student award for outstanding research winner in the Ph.D. category for the 9th World Biomaterials Congress, Chengdu, China, June 1-5, 2012: synthesis and application of photodegradable microspheres for spatiotemporal control of protein delivery. *J Biomed Mater Res A*, **2012**, *100* (7), 1647-1654.
338. Adelow, C., et al., The effect of enzymatically degradable poly(ethylene glycol) hydrogels on smooth muscle cell phenotype. *Biomaterials*, **2008**, *29* (3), 314-326.

339. Brantley, J. N., et al., Unclicking the click: mechanically facilitated 1,3-dipolar cycloreversions. *Science*, **2011**, 333 (6049), 1606-1609.
340. Wiggins, K. M., et al., Polymer Mechanochemistry: Force Enabled Transformations. *ACS Macro Lett*, **2012**, 1 (5), 623-626.
341. Dispinar, T., et al., A Diels-Alder/retro Diels-Alder strategy to synthesize polymers bearing maleimide side chains. *J Polym Sci A Polym Chem*, **2007**, 45 (20), 4545-4551.
342. Dimitrov, D. S., Therapeutic proteins. *Methods Mol Biol*, **2012**, 899, 1-26.
343. Jain, K. K., Role of Biotechnology in Drug Delivery for Cancer. In *Applications of Biotechnology in Oncology*, Springer: 2014; pp 617-669.
344. Hoare, T. R.; Kohane, D. S., Hydrogels in drug delivery: Progress and challenges. *Polymer*, **2008**, 49 (8), 1993-2007.
345. Li, Y., et al., Injectable and biodegradable hydrogels: gelation, biodegradation and biomedical applications. *Chem Soc Rev*, **2012**, 41 (6), 2193-2221.
346. Fu, Y.; Kao, W. J., Drug release kinetics and transport mechanisms of non-degradable and degradable polymeric delivery systems. *Expert Opin Drug Deliv*, **2010**, 7 (4), 429-444.
347. Diab, T., et al., A silk hydrogel-based delivery system of bone morphogenetic protein for the treatment of large bone defects. *J Mech Behav Biomed Mater*, **2012**, 11, 123-131.
348. Rehmann, M. S., et al., Hydrolytically Degradable Thiol-ene Hydrogels for Protein Release. *Macromol Symp*, **2013**, 329 (1), 58-65.
349. Griffin, D. R., et al., Synthesis of photodegradable macromers for conjugation and release of bioactive molecules. *Biomacromolecules*, **2013**, 14 (4), 1199-1207.
350. Balendiran, G. K., et al., The role of glutathione in cancer. *Cell Biochem Funct*, **2004**, 22 (6), 343-352.
351. Meng, F., et al., Reduction-sensitive polymers and bioconjugates for biomedical applications. *Biomaterials*, **2009**, 30 (12), 2180-2198.

352. Cheng, R., et al., Glutathione-responsive nano-vehicles as a promising platform for targeted intracellular drug and gene delivery. *J Controlled Release*, **2011**, *152* (1), 2-12.
353. Cai, X. J., et al., Glutathione-mediated shedding of PEG layers based on disulfide-linked cationomers for DNA delivery. *J Mater Chem*, **2011**, *21* (38), 14639-14645.
354. Liu, J., et al., Bioreducible micelles self-assembled from amphiphilic hyperbranched multiarm copolymer for glutathione-mediated intracellular drug delivery. *Biomacromolecules*, **2011**, *12* (5), 1567-1577.
355. Wen, H. Y., et al., Rapidly disassembling nanomicelles with disulfide-linked PEG shells for glutathione-mediated intracellular drug delivery. *Chem Comm*, **2011**, *47* (12), 3550-3552.
356. Ferruzzi, E., et al., Blood glutathione as a surrogate marker of cancer tissue glutathione S-transferase activity in non-small cell lung cancer and squamous cell carcinoma of the head and neck. *Eur J Cancer*, **2003**, *39* (7), 1019-1029.
357. Fiaschi, A. I., et al., Glutathione, ascorbic acid and antioxidant enzymes in the tumor tissue and blood of patients with oral squamous cell carcinoma. *Eur Rev Med Pharmacol Sci*, **2005**, *9* (6), 361-367.
358. Wu, G., et al., Glutathione metabolism and its implications for health. *J Nutr*, **2004**, *134* (3), 489-492.
359. Gajewska, J., et al., Glutathione S-transferase isoenzymes and glutathione in renal cell carcinoma and kidney tissue. *Neoplasma*, **1994**, *42* (4), 167-172.
360. Schultz, K. M., et al., Gelation of Covalently Cross-Linked PEG– Heparin Hydrogels. *Macromolecules*, **2009**, *42* (14), 5310-5316.
361. Robinson, K. G., et al., Differential effects of substrate modulus on human vascular endothelial, smooth muscle, and fibroblastic cells. *J Biomed Mater Res A*, **2012**, *100* (5), 1356-1367.
362. McGann, C. L., et al., Resilin-Based Hybrid Hydrogels for Cardiovascular Tissue Engineering. *Macromol Chem Phys*, **2013**, *214* (2), 203-213.

363. Gupta, D., et al., Fast-gelling injectable blend of hyaluronan and methylcellulose for intrathecal, localized delivery to the injured spinal cord. *Biomaterials*, **2006**, *27* (11), 2370-2379.
364. Nguyen, L.-T. T., et al., Kinetic comparison of 13 homogeneous thiol-X reactions. *Polym Chem*, **2013**, *4* (22), 5527-5536.
365. Danehy, J. P.; Paramesw.Kn, Acidic Dissociation Constants of Thiols. *J Chem Eng Data*, **1968**, *13* (3), 386-&.
366. Decollo, T. V.; Lees, W. J., Effects of aromatic thiols on thiol-disulfide interchange reactions that occur during protein folding. *J Org Chem*, **2001**, *66* (12), 4244-4249.
367. Treloar, L. R. G., *The physics of rubber elasticity*. Oxford University Press: 1975.
368. Gschwend, P. M.; Imboden, D. M., *Environmental organic chemistry*. John Wiley & Sons: 2005.
369. Jo, Y. S., et al., Tailoring hydrogel degradation and drug release via neighboring amino acid controlled ester hydrolysis. *Soft Matter*, **2009**, *5* (2), 440-446.
370. Schoenmakers, R. G., et al., The effect of the linker on the hydrolysis rate of drug-linked ester bonds. *J Controlled Release*, **2004**, *95* (2), 291-300.
371. Siepmann, J.; Peppas, N. A., Modeling of drug release from delivery systems based on hydroxypropyl methylcellulose (HPMC). *Adv Drug Deliv Rev*, **2012**, *64*, 163-174.
372. Siepmann, J.; Siepmann, F., Mathematical modeling of drug delivery. *Int J Pharm*, **2008**, *364* (2), 328-343.
373. Raza, A.; Lin, C. C., The influence of matrix degradation and functionality on cell survival and morphogenesis in PEG-based hydrogels. *Macromol Biosci*, **2013**, *13* (8), 1048-1058.
374. Choh, S. Y., et al., Facile synthesis and characterization of disulfide-cross-linked hyaluronic acid hydrogels for protein delivery and cell encapsulation. *Biomacromolecules*, **2011**, *12* (4), 1126-1136.

375. Flory, J. P., *Principles of polymer chemistry*. Cornell University Press: 1953.
376. Brandrup, J.; Immergut, E. H., *Polymer Handbook*. Wiley-Interscience: New York, 1975.
377. Canal, T.; Peppas, N. A., Correlation between mesh size and equilibrium degree of swelling of polymeric networks. *J Biomed Mater Res*, **1989**, *23* (10), 1183-1193.
378. Buenger, D., et al., Hydrogels in sensing applications. *Prog. Polym. Sci.*, **2012**, *37* (12), 1678-1719.
379. Tokarev, I.; Minko, S., Stimuli-responsive porous hydrogels at interfaces for molecular filtration, separation, controlled release, and gating in capsules and membranes. *Adv Mater*, **2010**, *22* (31), 3446-3462.
380. Yang, Q., et al., Composites of functional polymeric hydrogels and porous membranes. *J Mater Chem*, **2011**, *21* (9), 2783-2811.
381. Chen, J. K.; Chang, C. J., Fabrications and Applications of Stimulus-Responsive Polymer Films and Patterns on Surfaces: A Review. *Materials*, **2014**, *7* (2), 805-875.
382. Cho, E., et al., Formulation and characterization of poloxamine-based hydrogels as tissue sealants. *Acta Biomater*, **2012**, *8* (6), 2223-2232.
383. Chawla, P., et al., Hydrogels: a journey from diapers to gene delivery. *Mini Rev Med Chem*, **2014**, *14* (2), 154-167.
384. Peak, C. W., et al., A review on tough and sticky hydrogels. *Colloid and Polymer Science*, **2013**, *291* (9), 2031-2047.
385. Patenaude, M., et al., Designing injectable, covalently cross-linked hydrogels for biomedical applications. *Macromol Rapid Commun*, **2014**, *35* (6), 598-617.
386. Guvendiren, M.; Burdick, J. A., Engineering synthetic hydrogel microenvironments to instruct stem cells. *Curr Opin Biotechnol*, **2013**, *24* (5), 841-846.
387. Adzima, B. J., et al., Spatial and temporal control of the alkyne-azide cycloaddition by photoinitiated Cu(II) reduction. *Nat Chem*, **2011**, *3* (3), 256-259.

388. Zhang, H., et al., Interfacial Bioorthogonal Cross-Linking. *ACS Macro Lett*, **2014**, *3* (8), 727-731.
389. Alge, D. L., et al., Synthetically tractable click hydrogels for three-dimensional cell culture formed using tetrazine–norbornene chemistry. *Biomacromolecules*, **2013**, *14* (4), 949-953.
390. Mccall, J. D.; Anseth, K. S., Thiol–ene photopolymerizations provide a facile method to encapsulate proteins and maintain their bioactivity. *Biomacromolecules*, **2012**, *13* (8), 2410-2417.
391. Liang, Y. K.; Kiick, K. L., Multifunctional lipid-coated polymer nanogels crosslinked by photo-triggered Michael-type addition. *Polym Chem*, **2014**, *5* (5), 1728-1736.
392. Xi, W. X., et al., Click Chemistry in Materials Science. *Adv Funct Mater*, **2014**, *24* (18), 2572-2590.
393. Deforest, C. A.; Tirrell, D. A., A photoreversible protein-patterning approach for guiding stem cell fate in three-dimensional gels. *Nat Mater*, **2015**, *14* (5), 523-531.
394. Qiu, Y.; Park, K., Environment-sensitive hydrogels for drug delivery. *Adv Drug Deliv Rev*, **2012**, *64*, 49-60.
395. Angelova, N.; Hunkeler, D., Rationalizing the design of polymeric biomaterials. *Trends Biotechnol*, **1999**, *17* (10), 409-421.
396. Lu, S. X.; Anseth, K. S., Release behavior of high molecular weight solutes from poly(ethylene glycol)-based degradable networks. *Macromolecules*, **2000**, *33* (7), 2509-2515.
397. Kislukhin, A. A., et al., Degradable conjugates from oxanorbornadiene reagents. *J Am Chem Soc*, **2012**, *134* (14), 6491-6497.
398. Tomatsu, I., et al., Photoresponsive hydrogels for biomedical applications. *Adv Drug Deliv Rev*, **2011**, *63* (14-15), 1257-1266.
399. Deforest, C. A.; Anseth, K. S., Cytocompatible click-based hydrogels with dynamically tunable properties through orthogonal photoconjugation and photocleavage reactions. *Nat Chem*, **2011**, *3* (12), 925-931.

400. Kloxin, A. M., et al., Synthesis of photodegradable hydrogels as dynamically tunable cell culture platforms. *Nat Protoc*, **2010**, *5* (12), 1867-1887.
401. Nair, D. P., et al., The Thiol-Michael Addition Click Reaction: A Powerful and Widely Used Tool in Materials Chemistry. *Chem Mater*, **2013**, *26* (1), 724-744.
402. Zhou, Y., et al., Rapidly in situ forming adhesive hydrogel based on a PEG-maleimide modified polypeptide through Michael addition. *J Mater Sci Mater Med*, **2013**, *24* (10), 2277-2286.
403. Holmes, C. P., Model studies for new o-nitrobenzyl photolabile linkers: Substituent effects on the rates of photochemical cleavage. *J Org Chem*, **1997**, *62* (8), 2370-2380.
404. Bochet, C. G., Photolabile protecting groups and linkers. *J Am Chem Soc*, **2002**, (2), 125-142.
405. Deiters, A., Principles and applications of the photochemical control of cellular processes. *Chembiochem*, **2010**, *11* (1), 47-53.
406. Shin, D. S., et al., Photodegradable Hydrogels for Capture, Detection, and Release of Live Cells. *Angew Chem Int Ed Engl*, **2014**, *53* (31), 8221-8224.
407. Chang, T. C., et al., Glutathione concentration and distribution in cervical cancers and adjacent normal tissues. *Gynecol Obstet Invest*, **1993**, *36* (1), 52-55.
408. Wong, D. Y., et al., Glutathione concentration in oral cancer tissues. *Cancer Lett*, **1994**, *81* (2), 111-116.
409. Azagarsamy, M. A.; Anseth, K. S., Wavelength-controlled photocleavage for the orthogonal and sequential release of multiple proteins. *Angew Chem Int Ed Engl*, **2013**, *52* (51), 13803-13807.
410. Swift, J., et al., Nuclear lamin-A scales with tissue stiffness and enhances matrix-directed differentiation. *Science*, **2013**, *341* (6149), 1240104.
411. Levental, I., et al., Soft biological materials and their impact on cell function. *Soft Matter*, **2007**, *3* (3), 299-306.
412. Flory, P. J., *Principles of polymer chemistry*. Cornell University Press: 1953.

413. Arslan, M., et al., Cyclodextrin mediated polymer coupling via thiol-maleimide conjugation: facile access to functionalizable hydrogels. *RSC Advances*, **2014**, *4* (101), 57834-57841.
414. Mahadevaiah, S., et al., Decreasing matrix modulus of PEG hydrogels induces a vascular phenotype in human cord blood stem cells. *Biomaterials*, **2015**, *62*, 24-34.
415. Tibbitt, M. W., et al., Mechanical Properties and Degradation of Chain and Step Polymerized Photodegradable Hydrogels. *Macromolecules*, **2013**, *46* (7), 2785-2792.
416. Griffin, D. R., et al., Photodegradation as a mechanism for controlled drug delivery. *Biotechnol Bioeng*, **2010**, *107* (6), 1012-1019.
417. Maniar, M. L., et al., Alkaline hydrolysis of oligomers of tartrate esters: Effect of a neighboring carboxyl on the reactivity of ester groups. *J Pharm Sci*, **1992**, *81* (7), 705-709.
418. Shalitin, Y.; Bernhard, S. A., Neighboring group effects on ester hydrolysis. I. Neighboring hydroxyl groups [5]. *J Am Chem Soc*, **1964**, *86* (11), 2291-2292.
419. Davis, M. E., et al., Nanoparticle therapeutics: an emerging treatment modality for cancer. *Nat Rev Drug Discov*, **2008**, *7* (9), 771-782.
420. Probst, C. E., et al., Quantum dots as a platform for nanoparticle drug delivery vehicle design. *Adv Drug Deliv Rev*, **2013**, *65* (5), 703-718.
421. Wang, A. Z., et al., Nanoparticle delivery of cancer drugs. In *Annual Review of Medicine*, 2012; Vol. 63, pp 185-198.
422. Tibbitt, M. W., et al., Modeling Controlled Photodegradation in Optically Thick Hydrogels. *J Polym Sci A Polym Chem*, **2013**, *51* (9), 1899-1911.
423. Dou, S., et al., ScFv-decorated PEG-PLA-based nanoparticles for enhanced siRNA delivery to Her2+ breast cancer. *Adv Healthc Mater*, **2014**.
424. El-Dakdouki, M. H., et al., Development of drug loaded nanoparticles for tumor targeting. Part 1: Synthesis, characterization, and biological evaluation in 2D cell cultures. *Nanoscale*, **2013**, *5* (9), 3895-3903.

425. Murphy, N. P.; Lampe, K. J., Mimicking biological phenomena in hydrogel-based biomaterials to promote dynamic cellular responses. *J Mater Chem B*, **2015**, *3* (40), 7867-7880.
426. Jabbari, E., Bioconjugation of hydrogels for tissue engineering. *Curr Opin Biotechnol*, **2011**, *22* (5), 655-660.
427. Le Goff, G. C., et al., Hydrogel microparticles for biosensing. *Eur Polym J*, **2015**, *72*, 386-412.
428. Mateescu, A., et al., Thin hydrogel films for optical biosensor applications. *Membranes*, **2012**, *2* (1), 49-69.
429. Buhrman, J. S., et al., In-house preparation of hydrogels for batch affinity purification of glutathione S-transferase tagged recombinant proteins. *BMC Biotechnology*, **2012**, *12*.
430. Ha, E. J., et al., Site-specific reversible immobilization and purification of His-tagged protein on poly(2-acetamidoacrylic acid) hydrogel beads. *Polym Adv Technol*, **2013**, *24* (1), 75-80.
431. Seliktar, D., Designing cell-compatible hydrogels for biomedical applications. *Science*, **2012**, *336* (6085), 1124-1128.
432. Kim, J. K., et al., Natural and synthetic biomaterials for controlled drug delivery. *Archives of Pharmacal Research*, **2014**, *37* (1), 60-68.
433. Zhao, W., et al., Degradable natural polymer hydrogels for articular cartilage tissue engineering. *J Chem Technol Biotechnol*, **2013**, *88* (3), 327-339.
434. Thiele, J., et al., Designer hydrogels for cell cultures: A materials selection guide. *Adv Mater*, **2014**, *26* (1), 125-148.
435. Finosh, G. T., et al., Hybrid alginate-polyester bimodal network hydrogel for tissue engineering - Influence of structured water on long-term cellular growth. *Colloids Surf B*, **2014**.
436. Tan, H., et al., Covalently crosslinked chitosan-poly(ethylene glycol) hybrid hydrogels to deliver insulin for adipose-derived stem cells encapsulation. *Macromol Res*, **2013**, *21* (4), 392-399.

437. Zhu, J.; Marchant, R. E., Design properties of hydrogel tissue-engineering scaffolds. *Expert Rev of Med Devic*, **2011**, *8* (5), 607-626.
438. Najjam, S., et al., Characterization of human recombinant interleukin 2 binding to heparin and heparan sulfate using an ELISA approach. *Cytokine*, **1997**, *9* (12), 1013-1022.
439. Thompson, L. D., et al., Energetic characterization of the basic fibroblast growth factor-heparin interaction: identification of the heparin binding domain. *Biochemistry*, **1994**, *33* (13), 3831-3840.
440. Yamaguchi, N., et al., Growth factor mediated assembly of cell receptor-responsive hydrogels. *J Am Chem Soc*, **2007**, *129* (11), 3040-3041.
441. Zieris, A., et al., FGF-2 and VEGF functionalization of starPEG-heparin hydrogels to modulate biomolecular and physical cues of angiogenesis. *Biomaterials*, **2010**, *31* (31), 7985-7994.
442. Baldwin, A. D.; Kiick, K. L., Reversible maleimide–thiol adducts yield glutathione-sensitive poly (ethylene glycol)–heparin hydrogels. *Polym Chem*, **2013**, *4* (1), 133-143.
443. Fiaschi, A., et al., Glutathione, ascorbic acid and antioxidant enzymes in the tumor tissue and blood of patients with oral squamous cell carcinoma. *Eur Rev Med Pharmacol Sci*, **2005**, *9* (6), 361.
444. Wong, D. Y., et al., Photodegradable hydrogels to generate positive and negative features over multiple length scales. *Macromolecules*, **2010**, *43* (6), 2824-2831.
445. Zhao, H., et al., O-Nitrobenzyl alcohol derivatives: Opportunities in polymer and materials science. *Macromolecules*, **2012**, *45* (4), 1723-1736.
446. Masayuki Kiriara, et al., A Mild and Environmentally Benign Oxidation of Thiols to Disulfides. *Synthesis*, **2007**, *21*, 3286 - 3289.
447. Baldwin, A. D., et al., In situ crosslinkable heparin-containing poly (ethylene glycol) hydrogels for sustained anticoagulant release. *J Biomed Mater Res A*, **2012**, *100* (8), 2106-2118.

448. Siltanen, C., et al., Micropatterned Photodegradable Hydrogels for the Sorting of Microbeads and Cells. *Angew Chem Int Ed Engl*, **2013**, *125* (35), 9394-9398.
449. Bakaic, E., et al., Injectable hydrogels based on poly(ethylene glycol) and derivatives as functional biomaterials. *RSC Advances*, **2015**, *5* (45), 35469-35486.
450. Bonora, G. M.; Drioli, S., Recent advances on patents in poly(ethylene glycol)-based drug delivery. *Recent Patents on Drug Delivery and Formulation*, **2008**, *2* (2), 189-195.
451. Zhu, J., Bioactive modification of poly(ethylene glycol) hydrogels for tissue engineering. *Biomaterials*, **2010**, *31* (17), 4639-4656.
452. Vulic, K.; Shoichet, M. S., Affinity-based drug delivery systems for tissue repair and regeneration. *Biomacromolecules*, **2014**, *15* (11), 3867-3880.
453. Yamaguchi, N.; Kiick, K. L., Polysaccharide-poly(ethylene glycol) star copolymer as a scaffold for the production of bioactive hydrogels. *Biomacromolecules*, **2005**, *6* (4), 1921-1930.
454. Zhang, L., et al., Manipulation of hydrogel assembly and growth factor delivery via the use of peptide-polysaccharide interactions. *J Controlled Release*, **2006**, *114* (2), 130-142.
455. Mather, B. D., et al., Michael addition reactions in macromolecular design for emerging technologies. *Prog. Polym. Sci.*, **2006**, *31* (5), 487-531.
456. Nair, D. P., et al., The Thiol-Michael addition click reaction: A powerful and widely used tool in materials chemistry. *Chem Mater*, **2014**, *26* (1), 724-744.
457. Fu, Y.; Kao, W. J., In situ forming poly(ethylene glycol)-based hydrogels via thiol-maleimide Michael-type addition. *J Biomed Mater Res A*, **2011**, *98 A* (2), 201-211.
458. Liu, Z. Q., et al., Dextran-based hydrogel formed by thiol-Michael addition reaction for 3D cell encapsulation. *Colloids Surf B*, **2015**, *128*, 140-148.
459. Yu, Y., et al., Novel injectable biodegradable glycol chitosan-based hydrogels crosslinked by Michael-type addition reaction with oligo(acryloyl carbonate)-b-

- poly(ethylene glycol)-b-oligo(acryloyl carbonate) copolymers. *J Biomed Mater Res A*, **2011**, *99 A* (2), 316-326.
460. Shibayama, M., Structure-mechanical property relationship of tough hydrogels. *Soft Matter*, **2012**, *8* (31), 8030-8038.
461. Danehy, J. P.; Parameswaran, K., Acidic dissociation constants of thiols. *J Chem Eng Data*, **1968**, *13* (3), 386-389.
462. Keire, D. A., et al., Kinetics and equilibria of thiol/disulfide interchange reactions of selected biological thiols and related molecules with oxidized glutathione. *J Org Chem*, **1992**, *57* (1), 123-127.
463. Rossi, R., et al., Blood glutathione disulfide: in vivo factor or in vitro artifact? *Clin Chem*, **2002**, *48* (5), 742-753.
464. Mckinnon, D. D., et al., Design and characterization of a synthetically accessible, photodegradable hydrogel for user-directed formation of neural networks. *Biomacromolecules*, **2014**, *15* (7), 2808-2816.
465. Onuma, K., et al., Association of Calcium Phosphate and Fibroblast Growth Factor-2: a Dynamic Light Scattering Study. *Macromol Biosci*, **2004**, *4* (1), 39-46.
466. Boilly, B., et al., FGF signals for cell proliferation and migration through different pathways. *Cytokine Growth Factor Rev*, **2000**, *11* (4), 295-302.
467. Yan, B., et al., Near infrared light triggered release of biomacromolecules from hydrogels loaded with upconversion nanoparticles. *J Am Chem Soc*, **2012**, *134* (40), 16558-16561.
468. Viger, M. L., et al., Low Power Upconverted Near-IR Light for Efficient Polymeric Nanoparticle Degradation and Cargo Release. *Adv Mater*, **2013**, *25* (27), 3733-3738.
469. Jiang, Y., et al., Click hydrogels, microgels and nanogels: Emerging platforms for drug delivery and tissue engineering. *Biomaterials*, **2014**, *35* (18), 4969-4985.
470. Li, Y., et al., Biodegradable polymer nanogels for drug/nucleic acid delivery. *Chem Rev*, **2015**, *115* (16), 8564-8608.

471. Mavuso, S., et al., A review of polymeric colloidal nanogels in transdermal drug delivery. *Curr Pharm Des*, **2015**, *21* (20), 2801-2813.

Appendix

LICENSES FOR COPYRIGHTED MATERIAL

Chapter 1: Reproduced from following article:

Designing degradable hydrogels for orthogonal control of cell microenvironments

P. M. Kharkar, K. L. Kiick and A. M. Kloxin, *Chem. Soc. Rev.*, 2013, 42, 7335

DOI: 10.1039/C3CS60040H

This article is licensed under a Creative Commons Attribution Non-Commercial 3.0 Unported Licence. Material from this article can be used in other publications provided that the correct acknowledgement is given with the reproduced material and it is not used for commercial purposes.

Chapter 2: Reproduced from following article:

Dually degradable click hydrogels for controlled degradation and protein release

P. M. Kharkar, K. L. Kiick and A. M. Kloxin, *J. Mater. Chem. B*, 2014, 2, 5511-5521

DOI: 10.1039/C4TB00496E

You do not need to request permission to reuse your own figures, diagrams, etc, that were originally published in a Royal Society of Chemistry publication. However, permission should be requested for use of the whole article or chapter except if reusing it in a thesis. If you are including an article or book chapter published by us in your thesis please ensure that your co-authors are aware of this.

Chapter 3: Reproduced from following article:

Design of thiol- and light-sensitive degradable hydrogels using Michael-type addition reactions

P. M. Kharkar, K. L. Kiick and A. M. Kloxin, *Polym. Chem.*, 2015, 6, 5565 DOI: 10.1039/C5PY00750J

This article is licensed under a Creative Commons Attribution Non-Commercial 3.0 Unported Licence. Material from this article can be used in other publications provided that the correct acknowledgement is given with the reproduced material and it is not used for commercial purposes.